

**NEW LUBRICITY ADDITIVES FOR ULTRA LOW SULPHUR DIESEL:
SYNTHESIS, CHARACTERIZATION AND EVALUATION OF
LUBRICITY PROPERTIES**

Thesis

Submitted in partial fulfilment of the requirements for the degree of
DOCTOR OF PHILOSOPHY

BY

SRUTHI H

(REG. NO. 187096CY006)



DEPARTMENT OF CHEMISTRY

NATIONAL INSTITUTE OF TECHNOLOGY KARNATAKA,

SURATHKAL, MANGALORE - 575 025

May, 2023

DECLARATION

By the Ph.D. Research Scholar

I hereby declare that the Research Thesis entitled “**New lubricity additives for ultra-low sulphur diesel: synthesis, characterization and evaluation of lubricity properties**” which is being submitted to the **National Institute of Technology Karnataka, Surathkal** in partial fulfillment of the requirements for the award of the Degree of **Doctor of Philosophy in Chemistry** is a *bonafide report of the research work carried out by me*. The material contained in this Research Thesis has not been submitted to any University or Institution for the award of any degree.



Sruthi H

Reg. No. 187096CY006

Department of Chemistry

Place: NITK - Surathkal

Date: 04/05/2023

CERTIFICATE

This is to certify that the Research Thesis entitled "New lubricity additives for ultra-low sulphur diesel: synthesis, characterization and evaluation of lubricity properties" submitted by Ms. Sruthi H (Register Number: 187096CY006) as the record of the research work carried out by her *is accepted as the Research Thesis submission* in partial fulfillment of the requirements for the award of degree of Doctor of Philosophy.



Dr. Udaya Kumar D

Research Guide

Date: 09/05/2023

HEAD, DEPARTMENT OF CHEMISTRY
National Institute of Technology Karnataka
Surathkal, Srinivasnagar
MANGALORE- 575 025, D.K.



Chairman, DRBC

Date: 09/05/2023

HEAD, DEPARTMENT OF CHEMISTRY
National Institute of Technology Karnataka
Surathkal, Srinivasnagar
MANGALORE- 575 025, D.K.

DEDICATED TO
ALMIGHTY GOD
AND MY BELOVED
FAMILY

ACKNOWLEDGEMENTS

I would like to express my deep sense of gratitude to my research supervisor **Dr. Udaya Kumar D**, Associate Professor, Department of Chemistry. His invaluable guidance and support were always with me despite his busy schedule, without which I would not have completed this endeavor successfully. The directions he gave and the knowledge he shared in each and every single step of this work made it all possible. I am extremely thankful to him for all his support during my research work.

I sincerely thank NITK for providing necessary facilities to carry out this research work. I am thankful to **Dr. Airody Vasudeva Adhikari** former Professor, Department of Chemistry, NITK for his invaluable guidance and supports. I express my earnest thanks to the RPAC members, **Dr. P. B. Beneesh**, Chemistry Department and **Dr. Suresha S.N.**, Civil Engineering Department, NITK for insightful comments and constructive criticism towards the improvement of research quality.

I thank **Mangalore Refinery and Petrochemicals Ltd (MRPL)**, Mangalore for providing project fellowship.

My special thanks to **Mr. Nandakumar V**, **Dr. Manjunatha M.G**, **Dr. Pramod Hegde** and Mr. Karthick. R., Research and Development (R&D) Division, MRPL, Mangalore for providing the lab facilities and instrumental facilities. I am also thankful to Mr. Uday B and Dr. Sampath Kumar, MRPL for their support.

I am also thankful to Prof. A. N. Shetty, Prof. A. C. Hegde, Prof. B. R. Bhat, Prof. D. K. Bhat, Dr. A. M. Isloor, Dr. D. R. Trivedi, Dr. Sib Sankar Mal, Dr. Saikat Dutta, Dr. Debashree Chakraborty, Dr. Vijayendra S. Shetti and Dr. Lakshmi Vellanki Department of Chemistry for their constant support and encouragement. I also wish to extend my gratitude to all non-teaching staff in the Department of Chemistry.

I thank Mangalore University Konaje, Mangalagangothri for providing NMR spectral facilities.

I also thank my colleagues Dr. Rajalakshmi K., Dr. Kavya S. Keremane, Ms. Vishrutha K.S, and Mr. Sudhanva prasad S.S for their constant support, encouragement and company.

I am grateful to my friends Dr. Chitra, Mrs. Megha ., Ms. Sundari., Mrs. Athira., Mrs. Revathy., Ms. Jain., Ms. Ekta., Mr. Akash and Ms. Royline for their supports and help during my research work. I extend my sincere thanks to all the research scholars in the Department of Chemistry for their constant help and support.

Mere words are not enough to express my gratitude to my family, father Mr. Purushothama H, mother Mrs. Vimalakshi H, brother Mr. Roopesh H, sister Ms. Divya H, elder uncle Mr. Kamalaksha H, younger uncle Mr. Pushpangada H, fiancée Mr. Roopesh P for their constant support, encouragement and prayers. Finally, I thank the God almighty for strengthening me during hardships to successfully complete this endeavor.

SRUTHI H

ABSTRACT

In order to limit the emission of polluting elements such as sulphur and polar trace components from fossil fuels, standard norms and regulations have been formulated throughout the world. The maximum permitted sulphur concentration in diesel fuel is 10 ppm, according to the most recent European 6 standard (Euro 6, since 2014 to present). The fuel with less than 15 ppm of sulphur is called as ultra-low sulphur diesel (ULSD). Most of the refineries prefer hydrodesulphurization (HDS) process to produce ULSD, which removes sulphur from the fuel along with nitrogen and oxygen-based polar trace compounds. The loss of sulphur and other polar trace compounds makes the fuel harder. As a result, the direct use of ULSD produces a lot of friction between the moving parts of the fuel injection system. Therefore, diesel fuel needs external lubricating agents to balance its lubricity qualities. Blending of lubricity improvers with ULSD is one of the solutions to increase its lubricity property.

Based on a detailed literature survey, more than 100 new lubricity enhancers were designed in the present study. New additives were synthesized using low-cost raw materials such as methyl oleate, light cracked naphtha, glycidyl methacrylate, methacrylic acid, fatty acid and maleic anhydride by following simple reaction protocols. The tribological study was carried out for all the molecule using high frequency reciprocating rig (HFRR). The wear scar diameter was measured through optical microscope. Interestingly, the lubricity additive derived from oleic acid and stearic acid -based esters showed the best lubrication enhancing property at low (below 200 ppm) dosage level. Further, studies on physiochemical properties of blend fuel revealed that blending of these additives do not alter the key parameters of the diesel fuel. The mechanism of lubricity action of newly synthesised molecules on metal surface were studied using scanning electron microscopy (SEM) and energy dispersive X-ray spectroscopy (EDS) techniques. Conspicuously, the formation of defensive thin layer of the additive between the metal surfaces reduces the direct contact between the metal surfaces and hence protects the metal surfaces from wear and tear.

Keywords: ultra-low sulphur diesel, wear scar diameter lubricity improver, friction, high frequency reciprocating rig

CONTENTS	Page No
CHAPTER 1	01
INTRODUCTION	01
1.1 PETROLEUM-BASED FUELS	01
1.1.1 Environmental issues	01
1.1.2 Classification of fuels	02
1.2 EMISSION STANDARDS OF INDIA	03
1.3 DIESEL FROM CRUDE OIL (PETROLEUM)	05
1.3.1 Production of diesel	05
1.3.2 Diesel blending components	06
1.4 DIESEL ADDITIVES	07
1.4.1 Lubricity improvers	07
1.4.2 Cetane improvers	07
1.4.3 Anti-foam additives	07
1.4.4 Cloud point additives and pour point depressants	07
1.4.5 Ultra low sulphur diesel	08
1.5 TESTING OF BLENDED ULSD	08
1.5.1. Acidity	08
1.5.2. Cetane index	08
1.5.3. Pour point	08
1.5.4. Copper strip corrosion test	09
1.5.5. Distillation	09
1.5.6. Flash point	09
1.5.7. Kinematic viscosity	09
1.5.8. Density	10
1.5.9. Total sulphur	10
1.5.10. Oxidation stability	10
1.5.11. Lubricity corrected wear and scar diameter	10
1.5.12. Cold filter plugging point	10
1.6 THESIS STRUCTURE	10

CHAPTER 2	13
LITERATURE REVIEW, SCOPE AND OBJECTIVES	13
2.1 INTRODUCTION	13
2.2 STRATEGIES TO DEVELOP LUBRICITY ADDITIVES	14
2.3 TYPES OF ADDITIVES	15
2.3.1 Synthetic additives	15
2.3.2 Bio-oil additives	19
2.4 MECHANISM OF ACTION OF LUBRICITY ADDITIVES	23
2.5 FACTORS INFLUENCING THE LUBRICITY OF ADDITIVES	24
2.5.1 Impact of temperature on lubricity	24
2.5.2 Influence of the ester group on lubricity	24
2.5.3 Role of polar groups on lubricity	25
2.6 MOTIVATIONS FOR CURRENT RESEARCH WORK	26
2.7 SCOPE AND OBJECTIVES OF THE WORK	27
CHAPTER 3	29
EFFICIENT LUBRICITY IMPROVERS DERIVED FROM METHYL	29
OLEATE FOR ULTRA-LOW SULPHUR DIESEL	
3.1 INTRODUCTION	29
3.2 EXPERIMENTAL PART	29
3.2.1 Materials	29
3.2.2 Instruments	30
3.2.3 Methods	30
3.2.4 Tribological tests	32
3.2.5 Surface analysis of wear scar	33
3.2.6 Test methods of physical and chemical parameters of diesel	33
3.3 RESULTS AND DISCUSSION	34
3.3.1 Structural characterization of epoxy methyl oleate (EPMO)	34
3.3.2 Structural characterization of lubricity improvers (LAMOR)	36
3.4 MEASUREMENT OF LUBRICITY	40
3.5 STUDY OF PHYSIOCHEMICAL PARAMETERS	45
3.5.1 Effect of new lubricity improvers on fuel properties of the diesel	45

3.6 LUBRICITY MECHANISM	47
3.6.1 SEM analysis of wear scar	47
3.6.2 EDS analysis of the wear scar	48
3.7 CONCLUSIONS	50
CHAPTER 4	51
SIMPLE METHOD FOR THE CONVERSION OF LIGHT CRACKED NAPHTHA INTO EFFICIENT LUBRICITY IMPROVERS FOR ULTRA-LOW SULPHUR DIESEL	51
4.1 INTRODUCTION	51
4.2 EXPERIMENTAL PART	53
4.2.1 Materials and Instruments	53
4.2.2 Epoxidation method	53
4.2.3 Hydroboration method	58
4.2.4 Tribological study	61
4.3 RESULTS AND DISCUSSION	61
4.3.1 Structural characterization of epoxy hexane (EPHX) to corresponding esters (3a-c)	61
4.3.2 Structural characterization of hexanol and corresponding esters (8a-c)	66
4.3.3 Structural characterization of hydroxy LCN (HLLCN) and LCN esters (ELCN) (10a-j)	72
4.4 LUBRICITY ANALYSIS	75
4.5 PHYSIOCHEMICAL PARAMETERS STUDY	78
4.5.1 Evaluation of diesel property in ULSD blend	78
4.6 MECHANISM OF TRIBOLOGICAL BEHAVIOUR OF ADDITIVES	79
4.6.1 Analysis of wear scar using SEM	79
4.6.2 Analysis of wear scar using EDS	80
4.7 CONCLUSIONS	82

CHAPTER 5	83
CONVERSION OF LCN INTO LUBRICITY ADDITIVES FOR ULTRA-LOW SULPHUR DIESEL THROUGH A TWO-STEP PROCESS	83
5.1 INTRODUCTION	83
5.2 EXPERIMENTAL PART	83
5.2.1 Materials and instruments	83
5.2.2 Synthesis of LCN esters (15a-h)	83
5.2.3 Test for friction	87
5.3 RESULTS AND DISCUSSION	87
5.3.1 Structural characterization of 2-hexen-1-ylsuccinic anhydride (HSA) and corresponding diesters (13a-c)	87
5.3.2 Structural characterization of alkenyl succinic anhydride (ASA) and LCN diesters, LCNDE (15a-h)	93
5.4 LUBRICITY MEASUREMENT	99
5.5 PHYSIOCHEMICAL PROPERTIES OF THE BLEND FUEL	103
5.5.1 Impact of new lubricity enhancers on the diesel fuel's characteristics	103
5.6 MECHANISM OF LUBRICITY ACTION	104
5.6.1 Study of scar through SEM and EDS technique	104
5.7 CONCLUSIONS	106
CHAPTER 6	109
GLYCIDYL METHACRYLATE, METHACRYLIC ACID AND FATTY ACID DERIVATIVES AS LUBRICITY IMPROVER FOR ULTRA- LOW SULPHUR DIESEL	109
6.1 INTRODUCTION	109
6.2. EXPERIMENTAL PART	109
6.2.1 Materials	109

6.2.2 Instruments	110
6.2.3 Esterification of glycidyl methacrylate (GMA) with organic acids/fatty acids (R)	110
6.2.4 Esterification of methacrylic acid (MAA) with fatty alcohols (FAL)	110
6.2.5 Esterification of oleic acid (OLA) with polyols (POL).	111
6.2.6 Esterification of oleic acid (OLA) with fatty alcohol (FAL).	111
6.3.7 Study of friction	112
6.4 RESULTS AND DISCUSSION	112
6.4.1 Structural characterization of (17a-e), (19a-c) (21a-c) and (22a-c)	112
6.5 MEASUREMENT OF WEAR SCAR	125
6.6 PHYSIOCHEMICAL PROPERTIES EVALUATION	128
6.6.1. Effect of new lubricity improvers on fuel properties of the diesel.	128
6.7 LUBRICITY MECHANISM	128
6.8 CONCLUSIONS	130
CHAPTER 7	131
COST EFFECTIVE LUBRICITY IMPROVER DERIVED FROM NATURALLY ABUNDANT SUBSTANCES FOR ULTRA LOW SULPHUR DIESEL	131
7.1 INTRODUCTION	131
7.2 EXPERIMENTAL SECTION	131
7.2.1 Materials and Instruments	131
7.2.2 General procedure for the synthesis of lubricity improver starting from an anhydride, triol, fatty acid and amine	132
7.2.3 General procedure for the synthesis of LI starting from an anhydride triol and fatty acid (Scheme 7.2)	138
7.2.4 Test for friction	140
7.3 RESULTS AND DISCUSSION	140
7.3.1 Measurement and analysis of wear scar	140
7.4 PHYSIOCHEMICAL PARAMETERS INVESTIGATION	145

7.4.1 Impact of new lubricity enhancers on the characteristics of diesel fuel	145
7.5 MECHANISM OF LUBRICITY ACTION	147
7.5.1 Study of wear scar using SEM	147
7.5.2 Study of wear scar through EDS	147
7.6 CONCLUSIONS	148
CHAPTER 8	149
SUMMARY AND CONCLUSIONS	149
8.1 SUMMARY	149
8.1.1 The summary of best lubricity value obtained in each series	153
8.2 CONCLUSIONS	153
8.3 SCOPE FOR FUTURE WORK	154
REFERENCES	155
LIST OF PUBLICATIONS	161
PAPERS PRESENTED IN CONFERENCE	162
BIODATA	

LIST OF FIGURES		Page No
Fig.1.1	Graphical representation of Indian emission standards (four-wheel vehicles).	04
Fig.1.2	Basic scheme of modern crude oil refinery used for motor gasoline and diesel fuel production.	05
Fig.2.1	Removal of sulphur atoms via HDS process.	14
Fig.2.2	Different types of synthetic additives as lubricity improvers for ULSD.	15
Fig.2.3	Structure of carbonate	16
Fig.2.4	Structure of succinic acid half ester	16
Fig.2.5	Structure of branched-chain alkyl ester	17
Fig.2.6	Structure of TOFA diethanolamide	17
Fig.2.7	Structure of Tung oil based fatty acid ester	18
Fig.2.8	Structure of dilauryl carbonate	18
Fig.2.9	WSD (μm) values of blends of ULSD with different types of synthetic additives.	18
Fig.2.10	Natural sources of bio lubricity additives.	20
Fig.2.11	Adsorption of lubricity additives on metal surfaces through chemisorption.	24
Fig.3.1	Schematic diagram of HFRR instrumentation.	32
Fig.3.2	The working principle of high-frequency reciprocating rig.	33
Fig.3.3	Gas chromatogram of a) MO and b) EPMO.	34
Fig.3.4	Mass spectrum of MO.	34
Fig.3.5	Mass spectrum of EPMO.	35
Fig.3.6	2D gas chromatogram of a) neat ULSD, b) blended ULSD (LAMOSA 200ppm), c) MO and d) EPMO.	36
Fig.3.7	FTIR spectrum of LAMOPEA.	37
Fig.3.8	FTIR spectrum of LAMOCA.	38
Fig.3.9	FTIR spectrum of LAMOSA.	38

Fig.3.10	¹³ C NMR spectra of LAMOSA, LAMOCA and LAMOPEA.	39
Fig.3.11	¹ H NMR spectra of LAMOSA, LAMOCA and LAMOPEA.	39
Fig.3.12	The optical microscopic images of wear and scar for samples neat ULSD and LAMOR.	41
Fig.3.13	Graphical representation of WSD values obtained for neat ULSD, neat MO and LAMOR.	42
Fig.3.14	Graphical representation of a) film % vs coefficient of friction (CoF) and b) WSD for ULSD blends with LAMOSA at different blend concentrations.	43
Fig.3.15	The optical microscopic images of wear and scar for samples neat MO and LAMOSA.	43
Fig.3.16	Friction coefficient and film % graph obtained from HFRR for neat ULSD and LAMOSA-ULSD blends.	45
Fig.3.17	SEM images of neat ULSD and blended LAMOSA.	48
Fig.3.18	EDS graphs of neat ULSD and blended LAMOSA.	49
Fig.3.19	Schematic representation of interactions between the metal surface and LAMOR.	50
Fig.4.1	Graphical representation of LCN composition and Graphical representation of compositions of olefin in LCN.	53
Fig.4.2	Graphical representation of reaction time vs olefin conversion.	56
Fig.4.3	a)1D gas chromatogram of EPHX, b)2D gas chromatogram of EPHX, c) 2D density distribution spectrum of EPHX and d) mass spectrum obtained for EPHX.	62
Fig.4.4	2D gas chromatogram of a) 3a, b) 3b and c) 3c.	63
Fig.4.5	2D density distribution spectra of a) 3a, b) 3b and c) 3c.	64
Fig.4.6	Mass spectra obtained for a) 3a, b) 3b and c) 3c.	65
Fig.4.7	FTIR spectra of a) 3a, b) 3b and c) 3c.	66
Fig.4.8	FTIR spectra of a) 6a and b) 6j.	66
Fig.4.9	Gas chromatogram obtained for a) HL, b) 8a, c) 8b and d) 8c.	67
Fig.4.10	2D gas chromatogram of a) HL, b) 8a, c) 8b and d) 8c.	68
Fig.4.11	Mass spectra obtained for a) HL, b) 8a, c) 8b and d) 8c.	70

Fig.4.12	2D density distribution spectra of a) HL, b)8a, c)8b and d)8c.	71
Fig.4.13	FTIR spectra of a) HL, b) 8a, c) 8b and d) 8c.	72
Fig.4.14	Gas chromatogram of HLCN and b) 2D density distribution spectrum of HLCN.	74
Fig.4.15	2D gas chromatogram of a) HLCN and b) ELCN.	74
Fig.4.16	FTIR spectra of a) HLCN and b) ELCN (10e).	74
Fig.4.17	Mass spectrum of major peak identified in ELCN (10e).	75
Fig.4.18	Graphical representation of WSD value obtained for (3a-c)-ULSD, (6a-j)- ULSD, (8a-c)- ULSD and (10a-j)- ULSD blends.	76
Fig.4.19	The optical microscopic images of wear and scar for neat ULSD, ULSD- additive blends (300 ppm).	78
Fig.4.20	SEM images of the wear scars on balls of the friction couples with neat ULSD and blended ULSD.	80
Fig.4.21	EDS graphs of the metal surfaces with neat ULSD and blended ULSD.	81
Fig.5.1	a) Gas chromatogram, b)2D gas chromatogram of HSA and c) Mass spectrum of HSA.	88
Fig.5.2	a)2D density distribution spectrum and b) FTIR spectrum of HSA.	89
Fig.5.3	Gas chromatogram obtained for a) 13a, b) 13b and c) 13c.	89
Fig.5.4	2D gas chromatogram of a) 13a, b) 13b and c) 13c.	90
Fig.5.5	2D density distribution spectra of a) 13a, b) 13b and c) 13c.	90
Fig.5.6	Mass spectra obtained for a)13a, b)13b and c)13c.	92
Fig.5.7	FTIR spectra of HSA diesters a) 13a, b) 13b and c) 13c.	92
Fig.5.8	Gas chromatogram of ASA and 2D gas chromatogram of ASA.	94
Fig.5.9	2D density distribution spectrum of ASA.	94
Fig.5.10	Mass spectrum of the major peak identified in ASA of C5.	95
Fig.5.11	Mass spectrum of the major peak identified in ASA of C6.	95
Fig.5.12	Mass spectrum of the major peak identified in ASA of C7.	96

Fig.5.13	FTIR spectrum of ASA.	96
Fig.5.14	Gas chromatogram of LCNDE (15a) and 2D chromatogram of LCNDE (15a).	96
Fig.5.15	2D density distribution spectrum of LCNDE (15a).	97
Fig.5.16	2D density distribution spectrum of LCNDE (15a).	97
Fig.5.17	Mass spectrum of the major peak identified in LCNDE (15a) of C6.	97
Fig.5.18	Mass spectrum of the major peak identified in LCNDE (15a) of C7.	98
Fig.5.19	FTIR spectra of LCNDE a)15a, b)15c, c)15d, d)15e, e)15f and f)15h.	99
Fig.5.20	The optical microscopic images of wear and scar neat ULSD, ULSD-13c and ULSD-(15d-h) blends.	101
Fig.5.21	Friction coefficient and film % data obtained from HFRR for neat ULSD, 15f-ULSD and 15h-ULSD blends.	102
Fig.5.22	SEM images of the wear scars on balls of the friction couples with a) neat ULSD b) ULSD- 15h (150ppm) and ULSD- 15h (300ppm).	105
Fig.5.23	Energy dispersive x-ray spectra of the metal surfaces with a) neat ULSD b) blended ULSD (15h 150 ppm) and c) blended ULSD (15h 300 ppm)	106
Fig.5.24	Schematic representation of interactions between the metal surface and LCN diester through oxygen-containing functional groups.	106
Fig.6.1	1D gas chromatogram of GMA and 1D gas chromatogram of 17a	113
Fig.6.2	2D gas chromatogram of GMA and d) 2D gas chromatogram of 17a	113
Fig.6.3	Mass spectrum of GMA.	113
Fig.6.4	Mass spectrum of 17a.	114
Fig.6.5	2D density distribution spectra of a) GMA and b) 17a.	114

Fig.6.6	FTIR spectra of a) 17a, b) 17b, c) 17c, d) 17d and e) 17e.	115
Fig.6.7	2D gas chromatogram of a) 19a, b)19b and b) 19c.	116
Fig.6.8	a) 1D gas chromatogram of 19a, 2D density distribution spectra of b) 19a and c) 19b.	116
Fig.6.9	Mass spectra of a) 19a, b) 19b and b) 19c.	118
Fig.6.10	IR spectra of a) MAA, b) 19a, c) 19b and d) 19c.	118
Fig.6.11	a) 1D gas chromatogram of 21a, b) 2D gas chromatogram of 21a and c) 2D density distribution spectrum of 21a.	120
Fig.6.12	Mass spectra of a) 21a, b) 21b and c) 21c.	121
Fig.6.13	IR spectra of a) OLA, b) 21a, c) 21b and d) 21c.	122
Fig.6.14	2D gas chromatogram of a) 22a.	122
Fig.6.15	Mass spectra of a) 22a, b) 22b and c) 22c.	124
Fig.6.16	IR spectra of a) 22a, b) 22b and c) 22c.	124
Fig.6.17	The optical microscopic images of scars obtained for neat ULSD and blended ULSD.	126
Fig.6.18	Real time graph obtained from HFRR instrument for neat ULSD, 21c-ULSD blends.	127
Fig.6.19	SEM images of the wear scars on balls of the friction couples with neat ULSD and ULSD-21c blends.	129
Fig.6.20	EDS graphs of the metal surfaces with neat ULSD and ULSD-21c blends.	130
Fig.7.1	The optical microscopic images of wear and scar for samples neat ULSD and blended MAGLOLA (1B).	143
Fig.7.2	Friction coefficient and film % data obtained from HFRR and the optical microscopic images of wear and scar for neat ULSD and ULSD blends (1B).	145
Fig.7.3	SEM images of the wear scars on balls of the friction couples with a) neat ULSD and b) ULSD- 1B (100ppm) blend.	147
Fig.7.4	EDS graphs of the worn surfaces with a) neat ULSD b) blended ULSD (1B150 ppm).	148

Fig.8.1 The summary of the reaction schemes and the general structure of all the LIs synthesized in the present study. 152

LIST OF TABLES		Page No
Table 1.1	Indian emission standards (four-wheel vehicles).	04
Table 2.1	List of important synthetic lubricity additives and their lubricity characteristics.	19
Table 2.2	List of important bio lubricity additives.	22
Table 3.1	The lubricity data of neat ULSD and LAMOR blended ULSD at 300 ppm dosage concentration.	41
Table 3.2	Lubricity data of LAMOSA at different blended concentrations.	42
Table 3.3	The test report summary of neat and blended (200 ppm of LAMOSA) ULSD.	46
Table 4.1	Composition of light cracked naphtha (vol %).	52
Table 4.2	The olefin conversion data for the epoxidation reaction.	56
Table 4.3	The chemical structures of LCN hydroxy esters (6a-j).	57
Table 4.4	The chemical structures of LCN esters (10-j).	60
Table 4.5	The composition of HLCN identified through 2D-GCMS.	72
Table 4.6	The lubricity data of neat ULSD and blended ULSD.	75
Table 4.7	The key parameters of blended ULSD (150 ppm).	78
Table 5.1	The chemical structures of LCN diesters (15a-h).	86
Table 5.2	The lubricity data of neat ULSD and blended ULSD.	99
Table 5.3	The test report summary of blended (150 ppm of 15h) ULSD.	103
Table 6.1	The lubricity data of neat ULSD and blended ULSD.	125
Table 6.2	The test report summary of neat ULSD and blended ULSD (100 ppm of 21c).	128
Table 7.1	The summary of yield (%) obtained for MAGLR2EHA at different reactant ratio (trial- 1).	133
Table 7.2	The summary of yield (%) obtained for MAGLR2EHA at	134

	different reactant ratio (trial- 2).	
Table 7.3	The summary of yield (%) obtained for MAGLR2EHA at different reactant ratio (trail-3).	134
Table 7.4	The summary of yield (%) obtained for MAEGLR2EHA at different reactant ratio (trail-4).	135
Table 7.5	The summary of yield (%) obtained for MAGLROLA and MAGLROA at different reactant ratio (trail-4).	135
Table 7.6	The summary of yield (%) obtained for MAEGLROLA and MAEGLROA at different reactant ratio (trial -5).	136
Table 7.7	The summary of yield (%) obtained for MAGLDEAR ¹ at different reactant ratio (trail-6).	137
Table 7.8	The summary of yield (%) obtained for MAGLR at different reactant ratio (trail-6).	140
Table 7.9	Lubricity data of MAGL2EHARNH ₂ at dosage level of 150 ppm	141
Table 7.10	Lubricity data of MAGL2EHADEA at dosage level of 150 ppm	141
Table 7.11	Lubricity data of MAEGL2EHA RNH ₂ at dosage level of 150 ppm	141
Table 7.12	Lubricity data of MAGLOA at dosage level of 150 ppm.	141
Table 7.13	Lubricity data of MAGLOLA RNH ₂ at dosage level of 150 ppm.	142
Table 7.14	Lubricity data of MAEGL2EHADEA at dosage level of 150 ppm.	142
Table 7.15	Lubricity data of mixture of MAGLOLA at different ratio.	142
Table 7.16	The test report summary of neat and blended MAGLOLA (1B) ULSD.	146
Table 8.1	The comparison of WSD of LAMOSA,10a, 6a ,15h, 21c and 1B with commercial LA	153

ABBREVIATIONS

ATF: Aviation turbine fuel
BS: Barth stage
CFPP: Cold filter plugging point
CN: Cetane number
CoF: Coefficient of friction
CP: Cloud point
1D: One-dimensional
2D: Two-dimensional
EAME: Eleostearic acid methyl ester
EDS: Energy dispersive X-ray spectroscopy
EGL: Ethylene glycol
FAME: Fatty acid methyl esters
FPEE: Field pennycress seed oil ethyl esters
FPME: Field pennycress seed oil methyl esters
FTIR: Fourier-transform infra-red
GCMS: Gas chromatography mass spectra
GL: Glycerol
GMA: Glycidyl methacrylate
HDS: Hydro-desulphurization
HFRR: High frequency reciprocating rig.
HSD: High-speed diesel
LCN: Light cracked naphtha
LPG: Liquefied petroleum gas
LI: Lubricity improver
MAA: Methacrylic acid
 μm : Micrometer
MS: Motor spirit
NMR: Nuclear magnetic resonance

OECD: Organization for economic co-operation and development

OLA: Oleic acid

PM: Particulate matter

PME: Palm oil methyl ester

PP: Pour point

Ppm: Parts per million

PTSA: p-toluenesulfonic acid

SEM: Scanning electron microscopy

SME: Soybean oil methyl ester

TEA: Triethylamine

THC: Total hydrocarbon

TMP: Trimethylolpropane

TOFA: Tall oil fatty acid

ULSD: Ultra low sulphur diesel

WASA: Wax anti-settling additives

WD: Wax dispersants

WSD: Wear scar diameter

YOME: Yellow oleander methyl ester

CHAPTER 1

INTRODUCTION

1.1. PETROLEUM-BASED FUELS

Petroleum-based fuels have been in use to power automotive vehicles and industrial production for well over 100 years. Based on the high economic growth trends in India and China, the demand for energy in South East Asia alone will increase by roughly 75% by 2030. According to the reports, [Tanveer et al.2020] the energy consumption derived from fossil fuels is approximately 80% of the total consumption. The industrial sector consumes more energy than any other end-user sector does, and at this time, it accounts for nearly half of all delivered energy globally. It is relevant fact that the enormous amount of energy is consumed in manufacturing, mining, and construction, largely by processing and assembly equipment but also by air conditioning and lighting. Global industrial energy consumption is expected to grow by 1.75×10^9 tons from 2010 to 2030, while transportation by about 0.6×10^9 tons and other energy consumption by about 0.8×10^9 tons during the same time period [Tanveer et al.]. The energy demand of industry varies across countries based on the level and mixes of economic activity and technological development. The countries like Brazil, Russia, India, and China will account for more than two-thirds of the growth of non-organization for economic co-operation and development (non-OECD) industrial energy use by 2030. To comply with climate change regulations, the energy sector is required to limit the long-term concentration of greenhouse gases to 450 ppm (mg/kg) of carbon dioxide equivalent in the atmosphere so that the global temperature rise can be contained.

1.1.1 Environmental issues

The usage of fossil fuels results in environmental contamination through the production of carbon dioxide, carbon monoxide, unburned hydrocarbons, NO_x, SO_x, soot, and particulate matter while burning. In 2010, it is projected that 620,000 premature deaths were caused by respiratory and cardiovascular conditions brought on by exposure to dirty air. To overcome this situation Indian government implemented new norms related to pollution control, Bharat stage emission standards (BSES) is one

CHAPTER 1

of them. The production of air pollutants from internal combustion engines and spark-ignition engines, including motor vehicles, is regulated by the emission control board of the Indian government. The Central pollution control board, ministry of environment, forests, and climate change, establishes the timeline for standard implementation. In our country (on 2000) the pollution control norms have been implemented by referring European standard norms. Bharat Stage (BS) III rules came into effect throughout the country in October 2010. The implementation of Bharat Stage IV emission norms began in 13 major cities in April 2010 and has been in effect nationwide since April 2017. The Indian government applied BS VI standards in 2020 directly from BS IV norms.

In the last two decades, refiners have been forced by increasingly strict international fuel emission rules to drastically reduce the amount of sulphur in fuels in an effort to produce greener, more ecologically friendly fuels. Diesel engine technology keeps developing and getting better as automakers work to comply with stringent government car emissions requirements. In response, the oil sector changed its refining procedures to accommodate the demands of contemporary engine designs. Today, refineries take steps to reduce the amount of sulphur in the fuel. Compared to typical high-sulfur diesel fuel, hydro-desulphurization produces fuels with lower viscosities and lower concentrations of sulphur, nitrogen, and other polar and polycyclic aromatic molecules. These ultra-low sulphur diesel (ULSD) fuels have diminished lubricity characteristics, which can lead to metal wear, fuel pump seizures and mechanical problems. To overcome this loss in lubrication and to meet specification, lubricity-improving additives are used.

1.1.2 Classification of fuels

Fuel is categorized based on its composition. The majority of hydrocarbon fuels for engines are liquid or gaseous. The fuel industry divides fuels into the following groups.

Gasoline: This is a volatile mixture of liquid hydrocarbons commonly containing small amount of additives suitable for use as a fuel in a spark-ignition internal combustion engine.

CHAPTER 1

Unleaded gasoline: Lead free gasoline, that is no lead have been intentionally added and which contains not more than 0.013 g lead per liter (0.05 g lead/US gal).

E85 fuel: Ethanol and hydrocarbon blended in gasoline with 75–85% of ethanol.

M85 fuel: Methanol and hydrocarbon blend, where the methanol is nominally 70- 85%.

Racing gasoline: A remarkable automotive gasoline that is typically of lower volatility, has a narrower boiling range, a higher antiknock index, and is free of significant amounts of oxygenates. It is designed for use in racing vehicles, which have high compression engines.

Aviation gasoline: This fuel used in an aviation spark-ignition internal combustion engine.

Petroleum gases (LPG): This is one of the gas phase hydrocarbons, mainly C₃ and in low quantity C₄ fractions.

Compressed natural gas (CNG): Mostly methane compressed at high pressures suitable as fuel in internal combustion engine.

Aviation turbine fuel: A refined middle distillate suitable for use as a fuel in an aviation gas turbine engine.

Diesel fuel A: Middle distillate from crude oil commonly used in internal combustion engines where ignition occurs by pressure and not by electric spark.

Low or ultra-low sulphur diesel: Diesel fuel with less than 15 mg/kg Sulphur content.

Biodiesel A: Special category of fuel derived from vegetable oils or animal fats and it contains mono-alkyl esters of long-chain fatty acids.

Ethanol/gasoil (biodiesel) emulsions: A fuel that which contains a minimum of 80% diesel gas oil.

1.2 EMISSION STANDARDS OF INDIA

Since 1986, smoke test for diesel vehicles has been enforced in various states of India. The first Indian emission regulations were idle emission limits that became effective in 1989. India has begun implementing European fuel and pollution standards for four-wheeled light- and heavy-duty vehicles. For two- and three-wheeled vehicles, India's own emission laws are still in effect. The national car fuel policy, which was unveiled on October 6, 2003, calls for a staggered implementation of Euro 2, 3, and 4 fuel and emission rules by 2010.

CHAPTER 1

Indian emission norms

The implementation schedule of emission standards in India is summarized in Table 1.1. The graphical representation of Indian emission standards is given in Fig 1.1.

Table 1.1: Indian emission standards (four-wheel vehicles)

Standard	Allowed Sulphur content in diesel fuel (ppm)	Reference	Date	Region
India 2000	2,500	Euro 1	2000	Nationwide
Bharat stage II	500	Euro 2	2001 2003 2005	NCR, Mumbai, Kolkata, Chennai NCR, 10 cities * Nationwide
Bharat stage III	350	Euro 3	2005 2010	NCR, 10 cities* Nationwide
Bharat stage IV	50	Euro 4	2010	NCR, 10 cities*
Bharat stage VI	10	Euro 6	2020	Nationwide

Note: NCR (national capital region) refers to delhi, * indicates Mumbai, Kolkata, Chennai, Bengaluru, Hyderabad, Ahmedabad, Pune, Surat, Kanpur, and Agra.

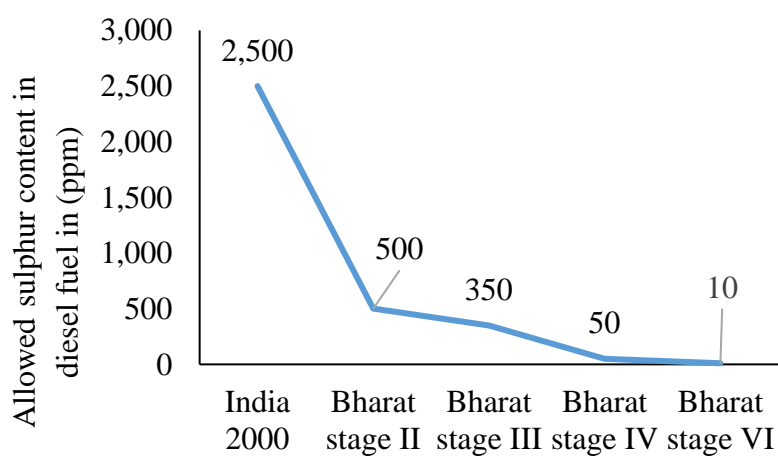


Fig.1.1 Graphical representation of Indian emission standards (four-wheel vehicles Srivastava et al.).

1.3 DIESEL FROM CRUDE OIL (PETROLEUM)

1.3.1 Production of diesel

Crude oil is a hydrocarbon mixture having very wide boiling point range. It is first separated to narrower boiling range fragments, based on the final product demand, mainly by distillation processes (Fig.1.2).

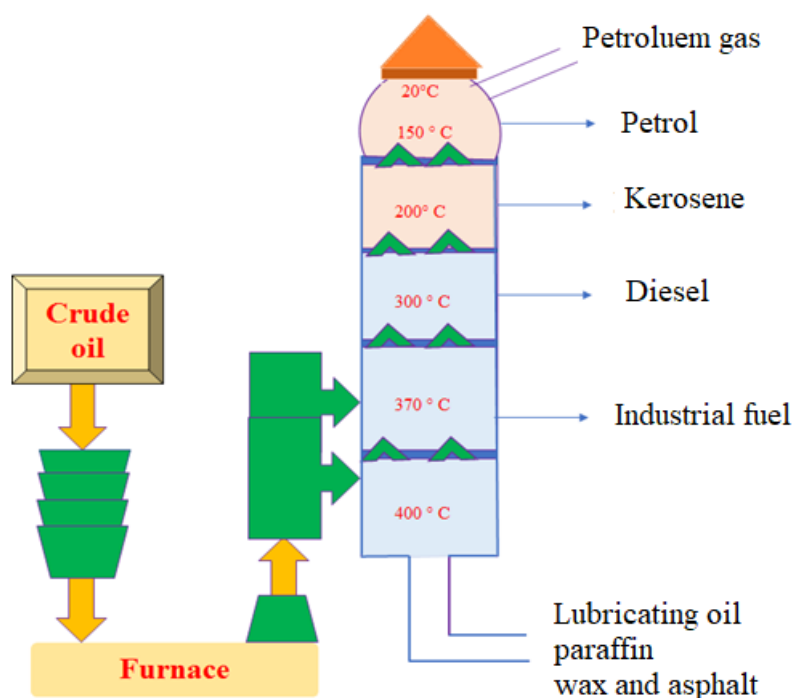


Fig.1.2 Basic scheme of modern crude oil refinery used for motor gasoline and diesel fuel production [Srivastava et al.].

In distillation of the crude oil to fractions, the crude oil refining starts with atmospheric distillation (distillation at atmospheric pressure). Crude oil is separated into distinct fractions with narrow boiling ranges at air pressure. After being partially vaporised in a tube furnace at temperatures between 280 and 340 °C, the crude oil next exchanges heat with product distillates in a heat exchanger train before being supplied to a distillation column with trays or partially structured packing. The distillation column's evaporation zone is where the components of the vapour and liquid phases are separated next. As the cold liquid flows downward, lighter vapour phase constituents rise to the top while those with higher boiling points condense (reflux). The hydrocarbons with the lowest boiling points (below 120–135°C) leave the column near

CHAPTER 1

the top during the vapour phase. After condensation, the overhead product is separated into gas (C₁–C₄ gases) and liquid (light naphtha) products.

1.3.2 Diesel blending components

Diesel fuels are mixtures of traditional (produced from crude oil) and alternative blending components with high energy content and high cetane values, similar to motor gasolines (i.e., ease of ignition). Additionally, additives assist in ensuring that the diesel meets all required standards. In addition to the rising market demand for diesel fuel, the development of refinery technology for making diesel-blending components has mostly been driven by the increasingly strict compliance requirements. The main quality requirements are given in below table.

1. Distillation properties (e.g., 95 vol% of diesels recovered at 360 °C)	2. Ease of blending with alternative components
3. Low sulphur content (≤ 10 –500 mg/kg)	4. Optimized additive content
5. Low polyaromatic content (<0.5–8%)	6. Nontoxicity
7. Low aromatic content (≤ 5 –20)	8. Ease of handling
9. Appropriate density (810–845 kg/m ³)	10. Exhaust products that pollute as little as possible
11. Good cold filter plugging point (CFPP) suitable to various climatic conditions (e.g., from +5 °C to –35 °C), in terms of pour point and viscosity properties	12. Low production costs
13. Good storage stability	14. Consistent quality
15. Low content of olefins and other compounds susceptible to resinification	16. Easy ignition and good combustion (cetane number: 50–58)

CHAPTER 1

1.4 DIESEL ADDITIVES

1.4.1 Lubricity improvers

The lubricity of a fuel can be defined as the ability of the fuel to reduce friction between moving metal parts and consequently to minimize wear. Lubricity improvers are additives that are added to diesel fuels to improve lubricity of diesel fuels e.g. fatty acids esters, epoxide-based esters etc.

1.4.2 Cetane improvers

Cetane number (CN) is a performance rating measuring the combustion quality of diesel *viz.* the time period delay between the start of the injections and the ignition of the fuel. Cetane improvers are additives that are added to diesel fuels to improve cetane number of diesel fuels, e.g. 2-ethylhexyl nitrate and di-*tert* butyl peroxide compounds.

1.4.3 Anti-foam additives

Anti-foam additives are used often as part of a multifunctional package to reduce foam formation in some fuels. Formation of foam can result in underfilling of tanks or in spillages. Organosilicon compounds are mostly used as antifoam additives and used at relatively low concentrations of about 10 ppm or below.

1.4.4 Cloud point additives and pour point depressants

The cloud point is the temperature at which wax crystals first appear. At this temperature, the fuel becomes turbid due to phase separations as the wax crystals are forming. The cloud point depressants are additives that are able to lower this temperature. Cold filter plugging point (CFPP) is the temperature at which wax crystals have continued to grow and eventually plug a standard 45 μm filter. Additives that are added to facilitate independent growth of wax crystals there by preventing formation of an interlocked 3-D network of crystal matrix are referred to as CFPP additives. Cold flow additives are fundamentally polymeric materials that are able to improve the low temperature properties such as the cloud point (CP), pour point (PP) and the CFPP of a fuel. The lowest temperature at which fuel can flow under standard conditions is referred to as its pour point. At this temperature, the fuel gets trapped in the cage-like wax crystal matrix structure. Pour point depressants are additives that enable lowering of pour point temperature resulting in improved flow properties and operability of

CHAPTER 1

diesel fuel at low temperatures. Wax anti-settling additives (WASA) also referred to as wax dispersants (WD) are also one of the cold flow improvers.

1.4.5 Ultra low sulphur diesel

Ultra-low sulphur diesel fuel contains sulphur content is 15 parts per million (ppm) or less. The move toward ULSD is aimed at lowering diesel engines' harmful exhaust emissions and improving air quality.

1.5 TESTING OF BLENDED ULSD

The blended fuel should reach fuel specification criteria, otherwise it is hard to use for motor engines. Such a fuel undergoes several testing to make sure that it meets fuel specifications.

1.5.1. Acidity

The total acidity is a measure of the combined organic and inorganic acidity in petroleum products in the range up to 0.1mg of KOH/g. The sample is dissolved in a mixture of toluene and isopropyl alcohol titrated using p-naphthol benzoic indicator against alcoholic KOH (0.01N). Colour change is from orange to green.

1.5.2. Cetane index

Cetane index is used as a substitute for the cetane number of diesel fuel. The cetane index is calculated based on the fuel's density and distillation range. The test is done for high-speed diesel (HSD) where the minimum requirement is 46. The number gives the ignition quality of diesel fuel.

1.5.3. Pour point

The pour point is the lowest temperature expressed as a multiple of 3°C at which the oil is observed to flow when cooled and examined under standard test conditions. The sample is first heated without stirring at 46°C in a water bath maintained at 48 to 50°C. Then the oil is cooled to 35°C in air or in water bath maintained at 25°C. When the temperature reaches 35°C, the jar is kept for test in the pour bath. The pour point is reported by adding 3°C to the temperature at which the oil shows no movement when kept in horizontal position for exactly five seconds. The pour point is an indication of the lowest temperature at which a fuel can be stored and still be capable of flowing under very low forces. The specification is different for summer and winter.

CHAPTER 1

1.5.4. Copper strip corrosion test

This method is to cover the detection of the corrosiveness of petroleum products to copper. A polished copper strip is immersed in the sample and heated at a specified temperature for a specified time (for liquefied petroleum gas (LPG) 1hr at 38°C, motor spirit (MS) 3h at 50°C, Kerosene 3h at 50°C, aviation turbine fuel (ATF) 2h at 100°C, HSD 3h at 100°C.) After the test, the strip is compared with the standard and the rate of corrosiveness is noted. The various rates are 1a, 1b, 2a, 2b, 2c, 2d, 2e, 3a, 3b, 4a, 4b and 4c based on the coloration of the test strip. The coloration/corrosion is due to the presence of sulphur compounds like H₂S, mercaptans. The maximum allowed rate is 1b. Higher number represent higher corrosion rate.

1.5.5. Distillation

The distillation characteristic (volatility) of hydrocarbon has an important effect on their safety and performance, especially in the case of fuels and solvents. Volatility is the major determinant of the tendency of a hydrocarbon to produce potentially explosive vapours. It is also critically important for both automotive and aviation gasoline, affecting starting, warm up, and tendency to vapour lock at high operating temperature or at high altitude, or both. The presence of high boiling point components in these and other fuels can significantly affect the degree of formation of solid combustion deposits

1.5.6. Flash point

Flash point is the lowest temperature at which the application of a test flame causes the vapour above the sample to ignite. Fire point is the point at which oil ignites and continues to burn for minimum of 5 seconds. Flash point below 70°C are determined by Abel flash point method and for 70°C and above by pensky martins closed cup method. The flash point is used primarily as an index of fire hazards and as criterion to establish labelling requirements for transportation, and to ensure compliance with fire regulations, insurance and other legal requirements.

1.5.7. Kinematic viscosity

Kinematic viscosity is a measure of the resistive flow of liquid under gravity, the pressure head being proportional to the density of the liquid. For any particular viscometer the time for flow of a fixed volume of liquid is directly proportional to its

CHAPTER 1

kinematic viscosity. Kinematic viscosity of petroleum fuels is important for their proper use, e.g. flow of fuels through pipelines, injection nozzles and orifices, and the temperature range for the proper operation of the fuel burners.

1.5.8. Density

The test is done by the hydrometer method and is most accurate when determined at or near the standard reference temperature of 15°C. Depending on the heaviness of the sample, the test can be carried out at any other temperature.

1.5.9. Total sulphur

This test method covers the determination of sulphur in liquid petroleum products like naphtha, kerosene, ATF, MS in concentrations of mg/Kg (ASTM D 5453).

1.5.10. Oxidation stability

This test method covers the measurement of the inherent stability of middle distillate petroleum fuels under specified oxidizing conditions at 95 °C.

1.5.11. Lubricity corrected wear and scar diameter

The lubricity determinations are performed using high frequency reciprocating rig (HFRR) instrument at 60°C according to the standard method ASTM D6079, with a HFRR lubricity tester.

1.5.12. Cold filter plugging point

It is the lowest temperature, at which a given volume of diesel type of fuel still passes through a standardized filtration device in a specified time when cooled under certain conditions. This test gives an estimate for the lowest temperature that a fuel will give trouble free flow in certain fuel systems. This is important as in cold temperature countries, a high cold filter plugging point will clog up vehicle engines more easily.

1.6 THESIS STRUCTURE

The entire thesis has been divided into **eight** chapters. **Chapter 1** outlines a brief introduction to petroleum-based fuels. Further, it explains the emission standards in India and importance of lubricity additives in BS VI fuel. **Chapter 2** includes a review of the literature reports on lubricity improver for ULSD. Further, it includes the

CHAPTER 1

scope and objectives of the present research work, arrived at on the basis of a detailed literature survey. Finally, it describes the design of six series of molecules comprising more than hundred lubricity improvers for ULSD. The synthesis and tribological study of eleven organic lubricity improvers derived from methyl oleate have been elaborated in **Chapter 3**. The synthesis and tribological study of twenty-eight organic lubricity improvers derived from light cracked naphtha are explained in **Chapters 4 and 5**. In addition, the synthesis and tribological study of sixteen organic friction depressive additive derived from fatty acid, fatty alcohol and acrylate derivatives are discussed in **Chapter 6**. **Chapter 7** describes the synthesis of maleic anhydride-based lubricity improver along with tribological studies of the ULSD blends. Finally, **Chapter 8** includes the summary of the entire work and important conclusions as well as the outcome of the research work.

CHAPTER 1

CHAPTER 2

LITERATURE REVIEW, SCOPE AND OBJECTIVES

Abstract

In this chapter, a brief description on strategies to develop new lubricity additives, different types of lubricity additives and their mechanism of action are discussed. The scope and objectives of the present work are included.

2.1 INTRODUCTION

Fossil diesel fuels are miscellaneous mixtures and their composition vary from refinery to refinery depending on the type of crude oil processed. The properties of the diesel fuels are fixed to a standard value so that the fuel could be utilized over a wide range of climatic conditions. In order to lower the environmental contamination, standard rules and regulations have been framed so as to limit the amount of harmful sulphur and nitrogen components in the fuel. As per the latest standard (Euro 6, since 2014 to present) the maximum allowed sulphur content in the diesel fuel is 10 ppm. Such a diesel fuel with very low sulphur content i.e. less than 10 ppm is termed as ULSD.

For the manufacturing of ULSD, the petroleum refineries generally prefer catalytic desulphurization process. In hydro-desulphurization (HDS) process, the sulphur content in the organosulphur compounds is converted to H₂S. This method is considered as a mature process involving a series of reactions that improves the quality of the fuel and removes sulphur and some other undesired impurities. Some of the representative reactions involved in the process are presented in Fig.2.1.

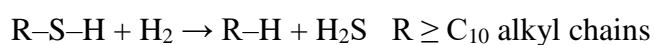
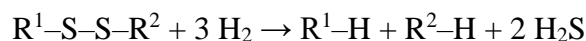
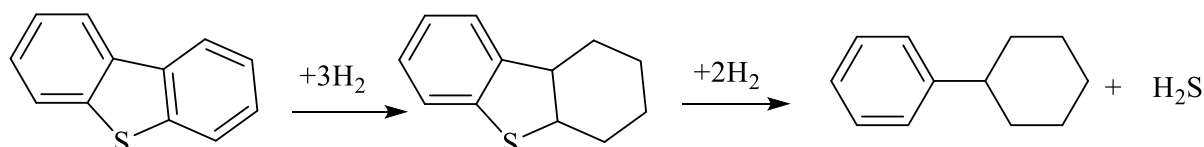
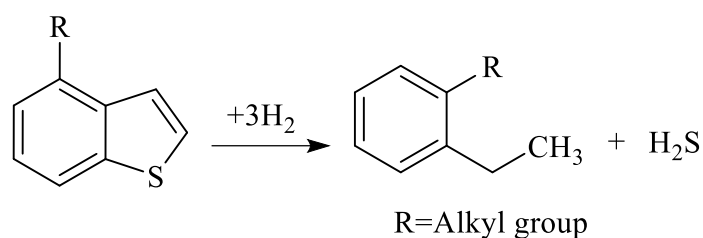
From mercaptans:**From disulfides:****From dibenzothiophens:****From benzothiophens:**

Fig.2.1 Removal of sulphur atoms via HDS process

The HDS process removes not only sulphur atom but also other hetero atoms like oxygen, nitrogen and some polar trace compounds that are responsible for the lubricity characteristics of the fuel. Hence, ULSD loses its lubricity property, experiences enhanced friction between two moving metallic surfaces of the engine components such as fuel injection system. This leads to the breakdown and failure of engine components by wear and tear. The major problem in the direct use of ULSD are engine smoke, accelerated wear, low power, hard starting, injection nozzle corrosion and instability of engine speed. The loss of lubricity property of the fuel is regained by the adding lubricity improver to it. This is the juncture where the development of new lubricity improvers comes into picture.

2.2 STRATEGIES TO DEVELOP LUBRICITY ADDITIVES

Various approaches have been reported in the literature towards the development of lubricity improvers. In 1986 Wei and Spikes reported that, nitrogen compounds in the diesel fuel reduce the wear. Studies revealed that the polar groups of the chemical additive play a vital role in lubricity enhancement. According to James et al., the lubricity of ULSD depended on the number of carbon atoms in the alkyl chain of the additive and the compounds with longer carbon chain show higher lubricity. In

CHAPTER 2

2001, Anastopoulos et al. employed esters of monocarboxylic acids of different structures as lubricity additives for ULSD. In 2007, Burgazli reported that the lubricity can be improved by adding additives like mono acids, amides and natural or synthetic esters to ULSD. The carboxylic acid group enhances the lubricity and the variation in the alkyl chain length affects the lubricity characteristics of the additive as reported by Kim et al. in 2012.

2.3 TYPES OF ADDITIVES

The lubricity additives of ULSD developed over the last two decades by various researchers can be classified mainly into two types, bio and synthetic lubricity additives. A brief description on these two classes of compounds in terms of their synthesis and lubricity characteristics are presented in the following sections.

2.3.1 Synthetic additives

Synthetic additives are prepared by using low-cost raw materials following well known synthetic procedures. There are mainly two methods for the preparation of synthetic additives. First one is through pure chemical synthesis, and another one is through chemical modification of bio oils. The important types of synthetic additives include carbonates, carboxylic acids, amides and long chain fatty acid esters (Fig.2.2).

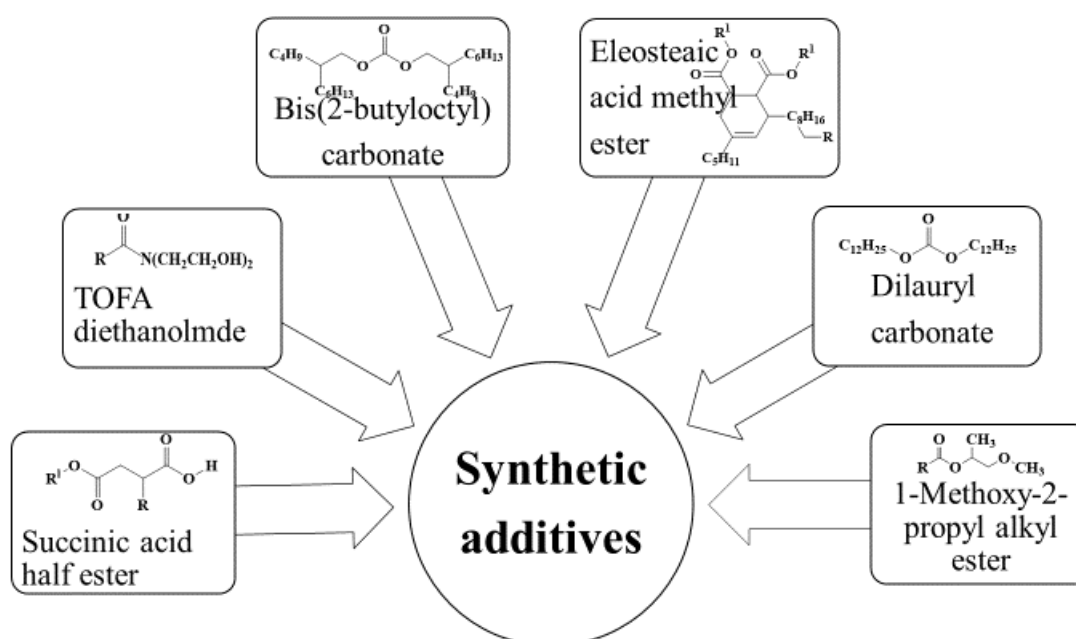


Fig.2.2 Different types of synthetic additives as lubricity improvers for ULSD.

CHAPTER 2

A few synthetic additives were prepared by the structural modification of biofuels through chemical reactions. In 2005, James et al. found that the lubricity of ULSD increased with an increase in the number of carbon atoms in the alkyl chain of a neat carbonate blended with it. Accordingly, the lowest WSD values for dialkyl carbonates (Fig.2.3) at 25 °C are 208, 179, 164, 145, 120 and 126 μm respectively and the lowest WSD values at 60 °C for dialkyl carbonate are 375, 411, 372, 299, 321, 323 and 257 μm respectively.

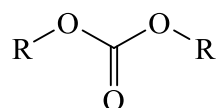


Fig.2.3 Structure of carbonate

Baek et al. in 2012 synthesised succinic acid alkyl half-ester (HSE) derivatives from several alkyl succinic anhydrides and fatty alcohols through the ring opening reaction. The HFRR results indicated a drastic decrease in WSD values from 606 μm (blank fuel) to 300 μm with the addition of HSE-C12-oleyl up to 120 ppm with HSE-C16-C12. The lubricity depended on the length of the alkyl (R') group of the half-esters. The WSD values of succinic acid half esters (which contain a $-\text{COOH}$ group) were compared with those of succinic acid diesters (no $-\text{COOH}$ group) (Fig.2.4 a) and succinic acid half ester with no alkyl group (R) (Fig.2.4 b) to understand the effect of different functional groups on the lubricity. Among these, the half ester showed better lubricity than other two groups of molecules which signifies the contribution of $-\text{COOH}$ and alkyl groups in enhancing the lubricity of the molecules.

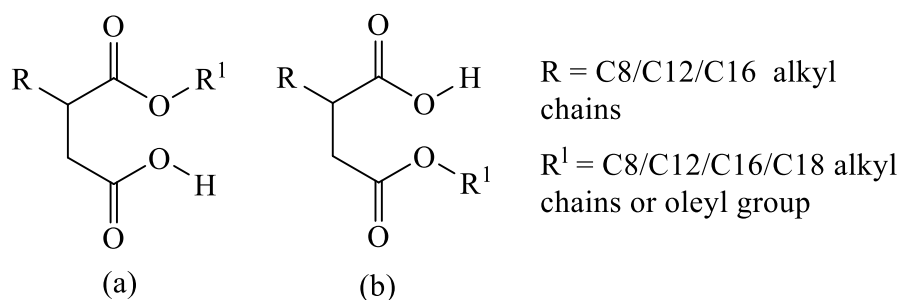


Fig.2.4 Structure of succinic acid half ester

In 2012 Sunmin et al. prepared branched-chain alkyl esters such as 1-methoxy-2-propyl alkyl ester (Fig.2.5) and iso-amyl alkyl ester through transesterification reaction starting with fatty acid methyl esters (FAME). The esters when blended at levels of 0.1 or 0.2 % (v/v) with commercial ULSD substantially improved the lubricity

CHAPTER 2

characteristics of the fuel as observed by increased lubricity numbers and reduced wear scar areas. It was concluded that branched-chain alkyl ester enriched esters are capable in enhancing the lubricity and these esters are suitable to be used as low-temperature fuel additives.

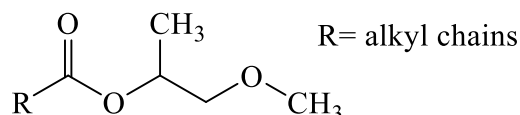


Fig.2.5 Structure of branched-chain alkyl ester

In 2014 Zinina et al. analysed that an amide-based additive derived from stearic acid improves the lubricating properties of fuels (at a concentration of 150 ppm) and increases the thermo oxidative stability. The rate of oxygen absorption by fuel decreases by about fourfold with the addition of this amide-based additive. However, the additive is a solid and hence its practical application in petrochemical industry is limited owing to the complications associated in mixing of a powdered additive with diesel fuels. To address this issue, a liquid additive was synthesized from commercially available and less expensive tall oil fatty acid (TOFA). Tall oil contains both saturated and unsaturated fatty acids (linoleic acid, oleic acid, linolenic acid, stearic acid, myristic acid, palmitic acid, etc.). It was observed that TOFA diethanolamide (Fig.2.6) is an effective antiwear additive which controls both lubricating and thermal-oxidative properties of the fuels.

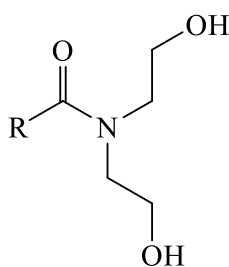


Fig.2.6 Structure of TOFA diethanolamide

Recently, Liu et al. in 2019 synthesised Tung oil based fatty acid esters (Fig. 2.7) as lubricity improvers through chemical modification of the eleostearic acid methyl ester (EAME) derived from the oil. These molecules at a low additive level (500–1000 ppm) significantly improved the lubricity of ULSD. The additives reduced the wear scar values of the ULSD by 40 %.

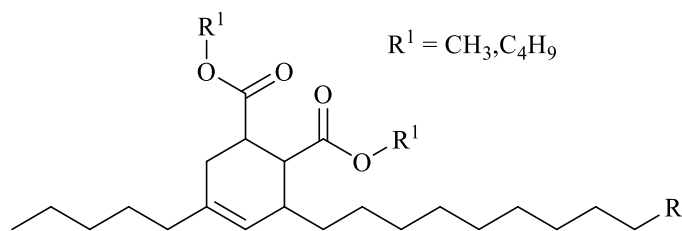


Fig.2.7 Structure of Tung oil based fatty acid ester

In 2019 Krishna et al. synthesized long-chain dialkyl carbonates through ash catalysed carbonyl exchange reaction between long chain alcohols and diethyl carbonate. The base diesel blended with 10 % w/w dialkyl carbonates lowered the WSD of the base fuel from 610 to 430 – 450 μm with ULSD. Accordingly, the ULSD blend with 10% dilauryl carbonate (Fig.2.8) exhibited better lubricity (WSD = 431 μm) as compared to other alkyl carbonates of the series.

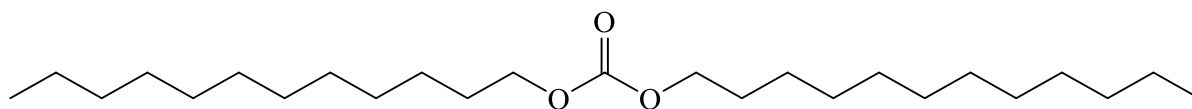


Fig.2.8 Structure of dilauryl carbonate

The lubricity of some of the important synthetic additives is summarised in Fig.2.9 and Table 2.1.

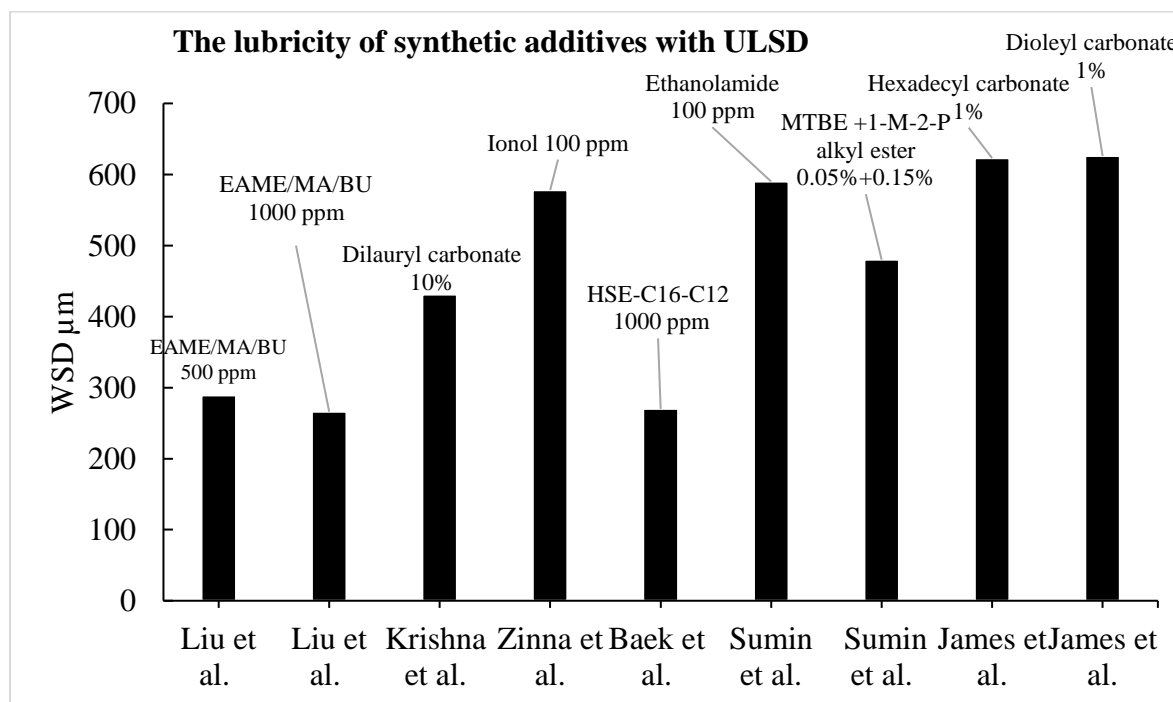


Fig.2.9 WSD (μm) values of blends of ULSD with different types of synthetic lubricity additives.

CHAPTER 2

Table 2.1 List of important synthetic lubricity additives and their lubricity characteristics.

Reference	Name of synthetic additives	Dosage Concentration	WSD (μm) of ULSD blend
James et al. (2005)	Hexadecyl carbonate	1%	623
	Dioleyl carbonate	1%	626
Baek et al. (2012)	HSE-C16-C12	1000 ppm	270
Sumin wang et al. (2012)	Ethanolamides	100 ppm	590
	MTBE +1-M-2-P alkyl ester	0.05% +0.15%	480
Zengshe Liu et al. (2014)	EAME/MA/BU	500 ppm	289
		1000 ppm	266
Zinna et al. (2014)	Ionol	100 ppm	578
Krishna et al. (2019)	Dilauryl carbonate	10%	431

2.3.2 Bio-oil additives

In 2017, Knothe and Razon reported that addition of commercial biodiesel at low levels improved the lubricity of ULSD more than the neat fatty esters. Further, addition of biodiesel as a lubricity improver is advantageous compared with the conventional lubricity-enhancing additives because unlike them, biodiesel characteristically possesses fuel properties identical to those of diesel. Bio additives can be used in neat or blended forms with petroleum diesel. Also, it is perfectly miscible in diesel at any ratios. Bio additives are derived mainly from naturally available resources, such as plants, flower, seeds etc., main resources are listed in Fig.2.10.

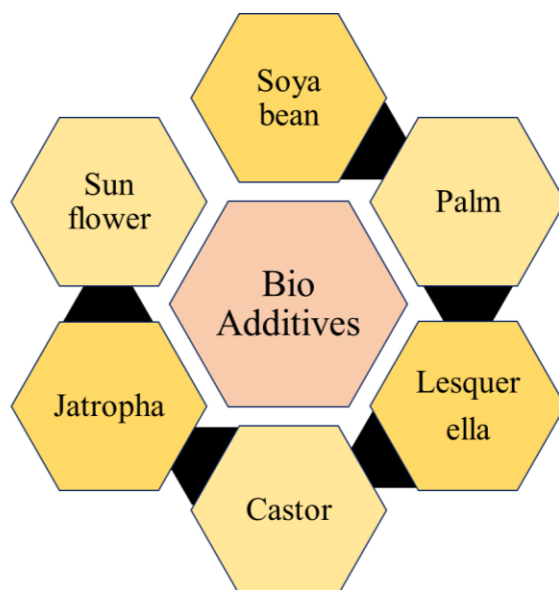


Fig.2.10 Natural sources of bio lubricity additives.

Most of the work on this class of lubricity improvers focus on seed and flower oil-based additives. They inherently possess fuel properties competitive and compatible with conventional petroleum-based diesel fuel, which other additives usually do not have. So, they are being used as diesel fuel substitutes as well as extenders. Also, they are found to be energy efficient and low emission sources for diesel engines. The major components (98%) of biodiesel are methyl esters of long chain fatty acids and minor components include free glycerine, mono-, di-, and triglycerides, antioxidants, sterols, phospholipids and water. Jianbo et al. in 2005 studied lubricity enhancing properties of refined and unrefined biodiesels derived from sunflower, canola and soybean. The lowest WSD values ($351 \mu\text{m}$) were obtained for base diesel blended with 2% w/w canola biodiesel. Refined biodiesels showed lower lubricity properties than unrefined biodiesels. The lubricity of biodiesel was found to be dependent on its composition. Fatty acid methyl esters and monoglycerides were the main compositions affecting the lubricity properties of the biodiesels. The free fatty acid and diglyceride components affected them slightly whereas no significant affect was observed from triglyceride components. Agarwal et al. in 2013 reported that biodiesels are preferred over other additives for enhancing lubricity of the diesel fuel. The presence of minor components such as free glycerine, antioxidants, phospholipids contribute towards the anti-wear property and hence enhance lubricity of biodiesels.

CHAPTER 2

2.3.2.1 Lubricity additives from seed oil

Additives produced from seed oils has been found to be one of the most promising lubricity enhancers. Bryan et al. in 2009 reported that soybean oil methyl ester (SME) imparts superior lubricity to ULSD than palm oil methyl ester (PME). The presence of higher saturated fatty ester with shorter chain lengths of PME in comparison with methyl esters alter the lubricity. The mixture (20 vol.%) of soybean oil methyl esters and partially hydrogenated SME (PHSME) in ULSD fuel improved lubricity which also exhibited higher kinematic viscosity and cetane number. With respect to exhaust emissions, B20 (20% biodiesel by volume in petrodiesel) mixture of PHSME and SME showed less PM (particulate matter) and CO (carbon monoxide) emissions in comparison to those of neat ULSD. The PHSME blend also exhibited a significant reduction in total hydrocarbon (THC) emissions. However, slightly higher NOx emissions were observed with both SME and PHSME B20 blends. Further, in 2010 Topaiboul et al. reported that jatropha oil (at a loading level < 1%) enhances lubricity better than the palm oil. Sulek et al. in 2010 synthesised 5% rape seed methyl ester as a blending agent to fuel oil. In comparison with the fuel oil, the blend fuel reduced the friction and wear about 20 and 50% respectively due to formation of a stable lubricant film in the tribo-contact surfaces. In 2015, Momin et al. prepared a biodiesel (yellow oleander methyl ester, YOME) from yellow oleander seed oil. YOME, despite zero sulphur content, improved the lubricity of ULSD at low blending levels while the neat YOME exhibited better lubricity than the blend fuel. Bryan et al. in 2016 revealed the fact that blends of field pennycress seed oil methyl esters (FPME) and ethyl esters (FPEE) in ULSD are excellent lubricity enhancers for petro diesel, as even small amounts markedly improved the lubricity. Alves et al. (2018) synthesised biodiesel B100 by ethanolysis route under a homogeneous base catalysed trans-esterification reaction of lipids from soybean oil. It was observed that the biodiesel B100 possess strong antifriction property and excellent film formation capability. John et al. (2019) studied the effectiveness of castor and lesqurella oil esters as lubricity enhancers for diesel fuel and compared their performance with that of methyl esters of the other oils. A series of tests were performed using different concentrations of castor and lesquerella oil esters in mixtures with diesel fuel. The results of these tests are compared to those obtained for soybean and rapeseed oil methyl ester. The lubricity was analyzed by

CHAPTER 2

HFRR method. The castor oil methyl ester enhanced lubricity quite well for diesel fuel at concentrations less than 1 % whereas lesquerella oil methyl ester enhanced lubricity to acceptable levels at concentrations as low as 0.25%. Soybean and rapeseed methyl esters do not show such good improvement in diesel lubricity at concentrations less than 1 %. The list of important reports on bio lubricity additives is given in Table 2.2.

Table 2.2 List of important reports on bio lubricity additives.

Reference	Bio lubricity improver*
Jianbo et al. (2005)	Canola biodiesel
John et al. (2005)	Lesquerella oil methyl ester
Bryan et al. (2008)	Soybean oil methyl ester
	Palm oil methyl ester
Topaiboul et al. (2010)	Jatropha oil
Sulek et al. (2010)	Rape seed methyl ester
Momin et al. (2015)	Yellow oleander methyl ester
Bryan et al. (2016)	Pennycress seed oil ethyl esters
	Pennycress seed oil methyl esters
Alves et al. (2018)	Soybean oil
John et al. (2019)	Castor oil methyl ester

* As per the reported literatures these bio additives need to be added in higher concentration (% level) to enhance the lubricity of base fuel.

2.3.2.2 Merits and demerits of bio additives

According to Sulek et al. in 2010, biodiesel can assist in reducing the pollutant emissions from engine combustion and effectively contribute to enhance the lubricity of diesel-biodiesel blend fuel. Hence, it can be considered as a lubricity additive for diesel fuel. However, there are some drawbacks with bio- based additives when used as lubricity improvers for ULSD. In 2015, Li et al. established that compared to pure petroleum diesel, biodiesel produced much lower smoke emissions from a 4-stroke diesel engine. Biodiesel blends can improve the lubricity performance of pure petroleum diesel fuel effectively under all testing conditions. In 2019, Kasumba et al. reported that potentially toxic unregulated combustion products like carbonyls are emitted in higher concentrations in biodiesel exhaust than in petrodiesel exhaust and

CHAPTER 2

hence biodiesel is not a suitable substitute for petrodiesel. At higher temperature, bio fuels are not stable and it effects cold filter plugging point and pour point (Hazrat et al.2020) also it reduces the overall oxidation stability of the fuel. The acidic nature of biodiesel favours to degrade metal surface and the sticking nature of biodiesel impact negative effect on metal surface. The storage of biodiesel is a challenging task, some biodiesels degrade in presence of light, temperature and atmospheric humidity (Madhu Sudan et al. in 2019). Most of the bio additive sources are costly and less abundant (Liu et al. in 2019) and also bio additives make marked changes in lubricity only when it is blended at higher concentrations with ULSD which is not economical (George et al. in 2009).

2.4 MECHANISM OF ACTION OF LUBRICITY ADDITIVES

There are mainly two lubrication mechanisms, namely the hydrodynamic lubrication and the boundary lubrication. In the hydrodynamic lubrication mechanism, a layer of fuel prevents contact between opposing surfaces. The studies of boundary lubricants initiated in 1940s which leads to the development of several additive compounds for lubricants and greases. In boundary lubrication, a compound containing polar functionalities such as nitrogen or oxygen adheres to the metal surface thus providing a protective anti-wear layer. Boundary lubricants avoid direct contact between asperities, thereby lowering friction and wear at the sliding interface of metallic layer. Surface-active compounds are helps to improve lubricity of fuels. Fatty acids and their derivatives readily adhere to metal surfaces to form a protective thin film and are often added to fluids as friction modifiers (Choudhary et al. in 2004). The polar head group of these additive compounds favourably adsorb onto surface oxides, which results to the formation of an organic film composed of nonpolar linear hydrocarbon chains. And also, a linear alkyl polar compounds help to increase lubricity of fuel when they are present in a distillate motor fuel above a minimum concentration of 10–100 ppm. There are various mechanisms reported in the literature to predict the lubricity action on metal surfaces. According to the most accepted mechanism (Homa et al. 2018) the polar head group of the additives strongly adsorb on the metal surfaces through chemisorption (Fig.2.11). The straight hydrocarbon tails align themselves parallel to each other and vertical to the metal surface which results in the formation of

CHAPTER 2

adsorbed molecular films with a hydrocarbon surface and hence the metal surfaces get protected.

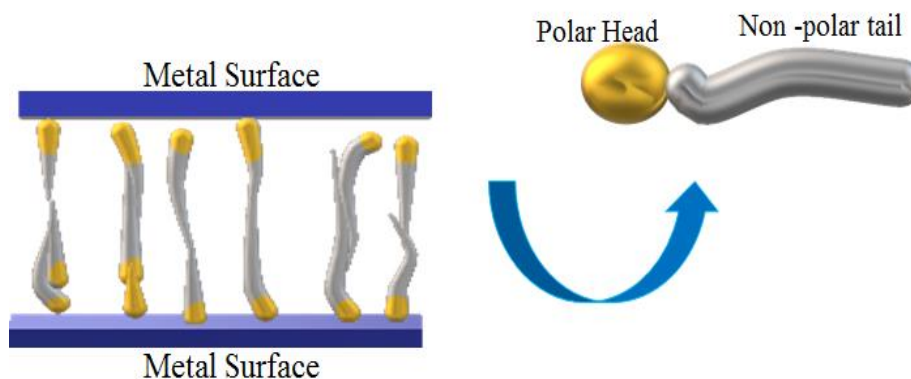


Fig.2.11 Adsorption of lubricity additives on metal surfaces through chemisorption.

2.5 FACTORS INFLUENCING THE LUBRICITY OF ADDITIVES

The impact of temperature and structural factors such as presence of ester and other polar groups on lubricity are summarised in this section.

2.5.1 Impact of temperature on lubricity

Kapila et al. (2009) studied the effect of temperature on lubricity of a ULSD blend with 2 vol % of soybean oil (SBO)-biodiesel. WSD increased with increase in the temperature up to 70 °C and then decreased at 80 and 90°C. At lower temperatures (20-70°C), the adherence of the minor polar phase onto the metal surface is weaker because of poor mixing. Whereas at higher temperature range (80 - 90°C), molecular motion for the polar phase increases which enables the adherence of the polar phase onto the metal surface. As a result, WSD decreases and lubricity increases at higher temperatures. Studies with palm biodiesel blends (B10, B20 and B50) in the temperature range 30-75°C revealed an increase in wear and friction with increasing temperature which could be due to reduced viscosity at higher temperatures.

2.5.2 Influence of the ester group on lubricity

The effect of carboxylic ester group on lubricity properties were investigated by several researchers and the studies revealed that lubricity of additives strongly depended on oxygen moiety which assists improving their lubricity. In 2003 Kenesey and Ecker reported ethyl esters to be possessing better lubricity than methyl esters.

CHAPTER 2

Titipong et al. (2011) analysed different alkyl (methyl, ethyl, propyl and butyl) esters derived from mustard oil as lubricity additive with ULSD. They observed that methyl ester is the most efficient lubricity additive among all alkyl esters, due to the presence of $-\text{COOCH}_3$ moiety. Sunmin et al. (2012) established that branched chain alkyl fatty acid esters are effective lubricity enhancers. A mixture of fatty acid methyl ester (15 %) and branched-chain alkyl esters (85%) showed lower pour point as compared to unmodified methyl ester. The addition of the branched alkyl esters (up to 1%, v/v) to ULSD fuel significantly improved lubricity of the blend fuel. Bryan (2014) reported that blending of branched diesters with ULSD improved both lubricity and cold flow property. The biodiesel components, such as fatty acid methyl esters, free fatty acids and mono-glycerides improve the lubricity, thereby substantially reducing wear tendencies. The ester-based additives are expected to form a protective film on the metal surface which decreases the roughness and hence improves the lubricating action.

2.5.3 Role of polar groups on lubricity

The polar groups on additives play an important role in enhancing the lubricity of ULSD. Gerhard et al. in 2005 reported that presence of a polarity-imparting heteroatom, preferably oxygen, and number and nature of the oxygen-based functional groups as well as a carbon chain of sufficient length significantly affect the lubricity property of the additives. The biodiesel prepared from corn oil, sunflower and olive oil ($\leq 5\%$) improves lubricity of hydrocracking diesel fuel. Oleic acid and mono olein improves the lubricity of hydrocracking diesel fuel better than the methyl oleate and methyl linoleate. Hence it was concluded that biodiesel improves the lubricity of hydrocracking diesel fuel due to the existence of trace amounts of polar impurities such as glycerol, free fatty acids, partially reacted acyl glycerols and the starting material (tri-acyl glycerols). In 2015 Hazrat et al. proposed that unrefined biodiesels which contain small amounts of monoglycerides ($< 0.8\%$) and free fatty acids show better lubricity property with ULSD. The lubricity of ULSD increased by 30% when blended with 1% of the biodiesel. It was concluded that the blend fuel which contain 20% biodiesel can serve in best way as a clean alternative. A correlation between the unsaturation level in the additives and their lubricity characteristics was observed. Methyl linoleate with three conjugated double bonds exhibits better lubricity than its saturated analogue, methyl stearate. Whereas, ricinoleic acid with a hydroxy group

CHAPTER 2

increases lubricity in diesel fuel more effectively than its non-hydroxylated counterpart oleic acid signifying the importance of polar hydroxy group in enhancing the lubricity. Another exclusive work was reported by Hong et al. in 2020, which states that oxygenated compounds do not necessarily improve the lubricity of fuel. However, addition of multiple oxygenated compound reduces lubricity of fuel by forming tribo-film on metal surfaces.

2.6 MOTIVATIONS FOR CURRENT RESEARCH WORK

The public-health issues associated with hazardous diesel engine emissions intensified efforts to develop viable solutions for reducing such emissions. Consequently, it was thought of adopting stringent fuel standards for diesel, particularly to reduce sulphur and aromatics content allowed in the fuel. Accordingly, the national regulators in the countries like the US, Europe, China and India took active steps to reduce diesel emissions and, in this approach, it was decided to fuel diesel vehicles (2007 or later model) with a cleaner-burning fuel that contains total sulphur as low as 10 ppm. This fuel is termed as ULSD, which on use resulted in immediate improvements across the entire diesel on- and off-road fleet, and thereby reducing the negative environmental and health impacts. Now, ULSD is produced by a catalytic hydrodesulphurization process, which removes mainly the sulphur of the fuel along with nitrogen and oxygen-based polar trace compounds. Thus, it facilitates the use of cleaner technology in diesel engines and vehicles with advanced emission control devices, resulting in significantly improved air quality.

However, usage of ULSD in diesel engines causes several unwanted side effects. Loss of lubricity which leads to engine damage is the major problem associated with ULSD. In the absence of lubricity imparting components such as sulphur and other polar components, the diesel fuel must get its lubricity property by an alternative source. Lubricity is critical to fleet performance because it helps to protect the engine from tear and wear. More particularly, diesel fuel lubricates the fuel injection system, which comprises the fuel pump and injectors. These moving parts in the absence of any lubricating agent generate huge heat during the engine operation due to extensive rubbing between the parts, which causes pitting and break down of the engine parts. Hence, it is necessary to use an effective lubricating agent to prevent engine damage due to friction between the moving parts. Adding a lubricity agent helps to decrease

CHAPTER 2

friction between the engine parts thus minimizing the impact of these moving parts, thereby saving the engine components from wear and tear. It can be successfully achieved by mixing lubricity improving additives to it or blending it with another appropriate fuel of sufficient lubricity. In the recent past, several attempts have been made to prepare and develop effective lubricity improving agents for ULSD.

As described in the literature, bio and chemical-based additives are the two common types and are extensively studied lubricants for ULSD. Bio-based additives, directly originated from natural resources are prepared by extraction, and conversion to suitable forms and are directly blended in certain concentrations with ULSD. On the other hand, chemical additives, prepared through simple synthetic routes starting from various types of compounds like fatty acid esters, carbonates, fatty acids are quite interesting lubricants. These agents synthesized from cheaply available natural products are the attractive choice since they possess good lubricity improving behaviour. Hence it is the recommended fact that, cost effective lubricity additives can be developed from immensely available bioorganic substances.

2.7 SCOPE AND OBJECTIVES OF THE WORK

In the past few years, several types of lubricity additives for ULSD were designed and synthesized. But most of the molecules are economically not suitable, because of high cost involved in their development and high quantity dosage level required for enhancing lubricity (BS VI required percentage level). To overcome these limitations, researchers proposed a new strategy for designing lubricity enhancer with cheaply available naturally abundant chemicals. Hence, it has been focused towards the synthesis of inexpensive additives from the abundantly available natural products like glycerol, oleic acid, maleic anhydride, pentaerythritol, *etc.* through simple reaction strategies and utilizing them as effective lubricity improvers for application in ULSD.

Based on the literature reports, it has been thought of designing lubricity improvers with good lubricity enhancing properties, for ULSD. For this, we have contemplated to choose oxygen rich groups in the additive molecules.

The major objectives of the present study are as given below.

CHAPTER 2

- To synthesize lubricity additives from methyl oleate, cracked naphtha available in refinery, glycidyl methacrylate, methacrylic acid, fatty acid and maleic anhydride adopting well-known reaction protocols.
- To characterize newly synthesized molecules by GCXGC MS, FTIR, ^1H NMR and ^{13}C NMR spectroscopic techniques.
- To evaluate all 12 tests for blended ULSD which showed maximum lubricity in individual series.
- To evaluate the lubricity properties of the newly developed additives by standard ASTM methods.
- To study the lubricity action on metal surface of newly synthesized molecules by scanning electron microscopy (SEM) and energy dispersive x-ray spectroscopy (EDS) techniques.

Conclusively, the present systematic investigation is aimed at the synthesis and characterization of new lubricity improvers for ULSD. It has been contemplated to focus our attention on ester-based molecules. Synthetic schemes were planned for their synthesis through simple reaction protocols and the structures of all the new compounds were confirmed by spectral techniques. Further, it was planned to study lubricity of developed molecules using HFRR method and also to study the other parameters of the ULSD blends. The newly developed molecules can be useful for some other applications as well such as pour point depressant, anti-oxidant, etc.

CHAPTER 3

EFFICIENT LUBRICITY IMPROVERS DERIVED FROM METHYL OLEATE FOR ULTRA-LOW SULPHUR DIESEL

Abstract:

This chapter deals with the synthesis of new series of lubricity improvers (LI) for ultra-low sulphur diesel starting from methyl oleate through a simple chemical reaction protocol. Also, it covers details of structural characterisation of the new molecules and study of lubricity property using HFRR method. Further, it includes studies on mechanism of lubricity action of newly synthesised LIs towards the metal surfaces.

3.1 INTRODUCTION

Methyl oleate is a fatty acid methyl ester resulting from the formal condensation of the carboxy group of oleic acid with methanol. It is a clear to amber liquid, insoluble in water with a faint fatty odour. It is used as a lubricant additive. It contains a terminal methyl ester moiety and a C-C double bond (-C=C-) between C-9 and C-10 of the alkyl chain. The double bond offers a reactive functionality for the chemical modification of the molecule and hence it is a promising precursor for the development of lubricity additives. In the present study, the alkene functionality was converted into hydroxy esters through a two-step process involving epoxidation of the alkene followed by esterification of the epoxide with different long chain carboxylic acids. The resulting products which contain polar functional groups (one hydroxy and two ester groups) are expected to show good lubricity properties with ULSD.

3.2 EXPERIMENTAL PART

3.2.1 Materials

Methyl oleate (70%), hydrogen peroxide (30% solution), formic acid (89–91%), hexane (99%), acetone, sodium bicarbonate (99.7%), sodium sulphate anhydrous, p-toluene sulfonic acid (PTSA) and all carboxylic acids were purchased from Sigma Aldrich (USA). All solvents and other chemicals were used as received, without further purification.

CHAPTER 3

3.2.2 Instruments

The gas chromatogram and the mass spectra of the compounds were recorded using a Leco, Pegasus GCXGC time of flight (TOF) mass spectrometer with liquid-N₂ modulation. The evaluation of lubricity property of the fuel was carried out using a high frequency reciprocating rig (HFRR, PCS instruments, USA). The ¹H and ¹³C NMR spectra were recorded using a JEOL NMR spectrometer. A Bruker (Alpha) KBr/ATR Fourier Transform Infrared Spectrophotometer (FTIR) was used to confirm the presence of different functional groups in the compound. The worn surface of the ball was analysed using a JSM-7610F plus field emission scanning electron microscope (SEM, Japan electron optics laboratory Co. Ltd). The composition and chemical states of worn surface of the balls were analysed using a X max^N (80) energy dispersive spectrometer (Oxford EDS, Aztec 4.0 UK). The test of physical and chemical parameters of samples were carried out using mitsubishi-Japan Trace sulfur analyser, diesel oxidation stability bath (Stanhope Seta, UK), automatic distillation unit (Herzog-PAC Optidist, USA), automatic density meter (Rudolph Analytical, USA), automatic flash point tester (Herzog-PAC Optiflash, USA), kinematic viscosity bath (Koehler-USA), automatic CFPP tester (ISL-PAC FPP 5G, USA) and automatic pour point tester (ISL-PAC OptiMPP, USA).

3.2.3 Methods

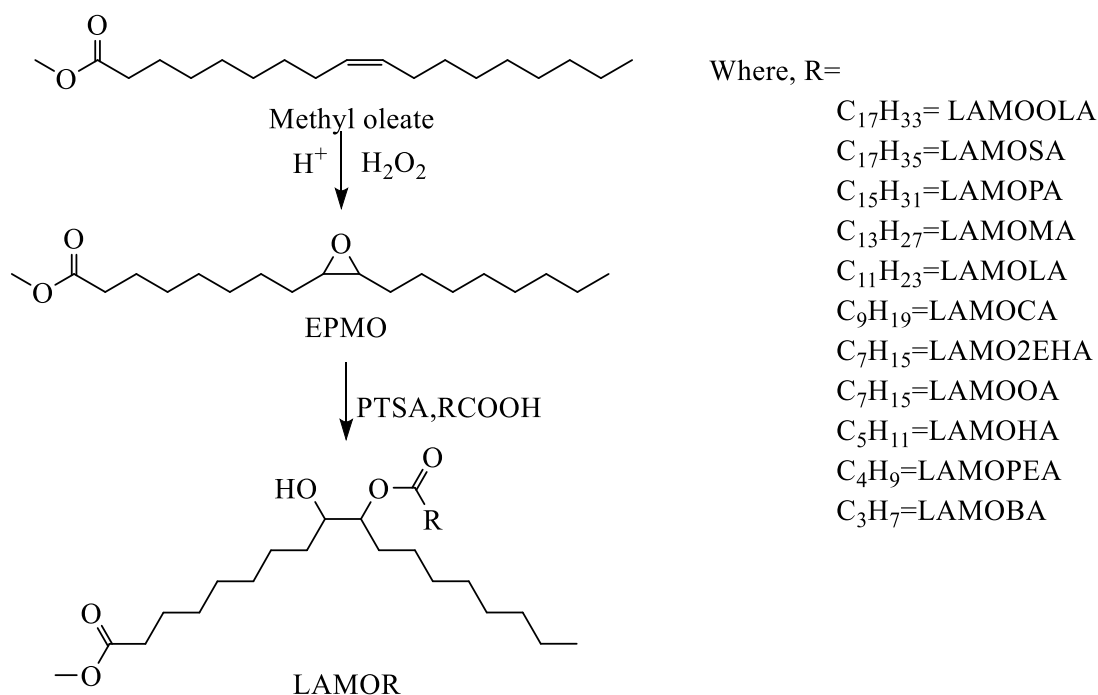
3.2.3.1 Epoxidation of methyl oleate

The epoxidation of methyl-oleate was carried out according to the reported procedure (Bunker et al., Scheme 3.1). Methyl oleate (120.0 g, 0.4 mol) was placed in a 1000 mL RB flask equipped with an overhead stirrer and the flask was cooled in an ice bath. Then, to the ice cooled methyl oleate, formic acid (112 mL, 3 mol) was added. After the addition of the formic acid, 30% hydrogen peroxide (64 mL, 2.7 mol) was added drop wise over about 5 min while the temperature of the solution was monitored continuously. Then, the reaction mixture was stirred at room temperature for 5 h. The thick off-white precipitate formed was filtered through vacuum filtration, washed with excess of demineralised (DM) water followed by n-hexane. The precipitate was dried over vacuum to obtain the product, epoxidized methyl oleate (EPMO) with 90% yield.

CHAPTER 3

3.2.3.2 General procedure for the esterification of EPMO

To a mixture of EPMO (6g, 0.02 mol), PTSA (1g, 0.006 mol) and toluene (10 mL), appropriate amount of the organic acid (0.02 mol) was added. The reaction mixture was refluxed for 8 h (Scheme 3.1). After completion of the reaction, the mixture was cooled to room temperature. Then the mixture was extracted with ethyl acetate and the organic layer was washed with DM water (200 mL) followed by 5 % sodium bicarbonate (200 mL) solution. The organic layer was filtered through sodium sulphate and the solvent was evaporated using rotary evaporator to yield the product. The obtained product was termed as LAMOR (where R corresponds to alkyl chains of different fatty acids).



Scheme 3.1: Synthetic route of methyl oleate-based lubricity improvers (LAMOR) for ULSD [C₁₇H₃₃COOH= oleic acid: C₁₇H₃₅COOH= stearic acid: C₁₅H₃₁COOH= palmitic acid: C₁₃H₂₇COOH= myristic acid: C₁₁H₂₃COOH= lauric acid: C₉H₁₉COOH= capric acid: C₇H₁₅COOH= 2-ethylhexanoic acid: C₇H₁₅COOH= octanoic acid: C₅H₁₁COOH= hexanoic acid: C₄H₉COOH= pentanoic acid and C₃H₇COOH= butyric acid].

3.2.4 Tribological tests

3.2.4.1 Evaluation method of high frequency reciprocating rig (HFRR)

To study the effect of newly synthesized diesters on the lubrication performance of ULSD, high frequency reciprocating rig (Fig.3.1) was used to evaluate the lubricity property on the basis of the ASTM D 6079-18 standard method (A vibrator with 50 Hz frequency, 1 mm stroke length, 200 g weight load, 2 mL sample, temperature of 60°C and test duration of 75 min). By measuring the length (as μm) of the scar in X and Y direction of the wear scar forming on the ball's surface, the wear scar diameter (WSD) can be calculated using the equation $\text{WSD} = (X+Y)/2 \mu\text{m}$. The maximum allowed limit for the lubricity value of BS VI ULSD is 460 μm . Therefore, a WSD less than or equal to 460 μm at 60°C was considered as acceptable for the diester-ULSD blends. The size of the wear scar is directly related to the lubrication property of the sample. The lubricity of the blends was evaluated via a high-frequency reciprocating rig, which is driven by an electromagnetic oscillator. The WSD and coefficient of friction (CoF) were obtained from the HFRR tests for each diesel. Diesel blends with smaller WSD and CoF are considered to have better lubricity. The working principle of HFRR is shown in Fig.3.2.

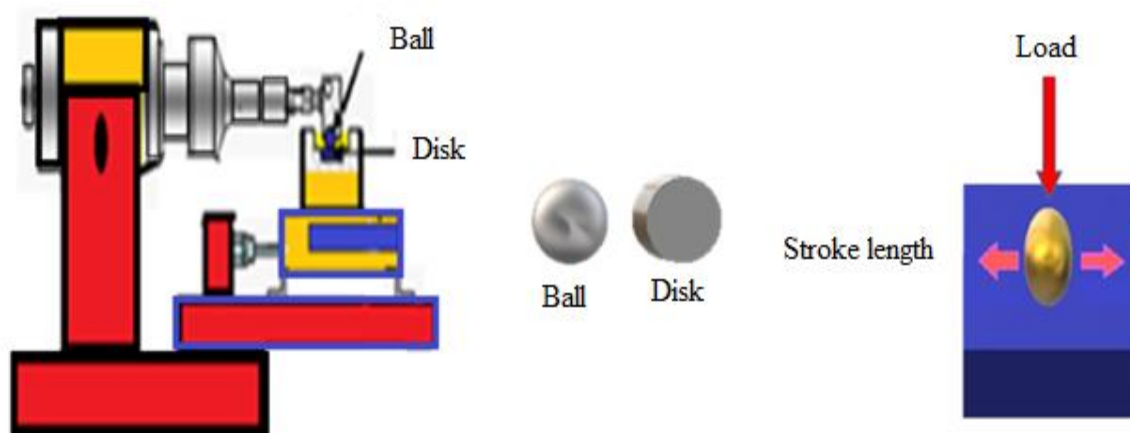


Fig.3.1 Schematic diagram of HFRR instrumentation

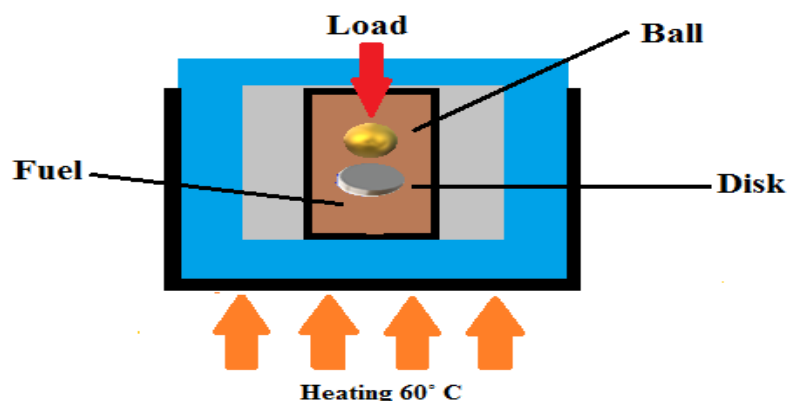


Fig.3.2 The working principle of high-frequency reciprocating rig.

Sample preparation. LAMOR (0.003 g) was weighed into a 10 mL standard flask. 5 mL of ULSD was added to it and the mixture was sonicated for 3 min. Then the solution was made up to the mark with ULSD and the solution was shaken well. This blended stock sample was used for HFRR analysis. LAMOSA and ULSD blend solutions with blending levels of 150, 200 and 600 ppm were prepared according to same procedure by weighing 0.0015, 0.002 and 0.006 g of LAMOSA sample respectively into 10 mL standard flask. At the end of test, the ball was removed from HFRR and washed properly with acetone to remove stains. Then wear scar diameter was measured using optical microscope with magnification of 100. The percent of friction and film percentage were recorded.

3.2.5 Surface analysis of wear scar

To study the mechanism of lubricity action on surface, the worn surface of the ball was analysed using a scanning electron microscope. The microscope was operated at an accelerating voltage of 20 kV, and the micrographs of worn surface of the balls were obtained at 100x magnifications. The composition and chemical states of worn surface of the balls were analysed using EDS technique.

3.2.6 Test methods of physiochemical properties of diesel

In addition to the requirement for lubricant efficiency, the lubricity improver must not affect the main performances of diesel, such as oxidation stability, acid number, kinematic viscosity, pour point, and distillation range. The tests for physical

CHAPTER 3

and chemical parameters of blended samples were carried out according to the Indian standards (IS-1460).

3.3 RESULTS AND DISCUSSION

3.3.1 Structural characterization of epoxy methyl oleate (EPMO)

The conversion of methyl oleate (MO) to EPMO was confirmed by 2D gas chromatography mass spectra (GCXGC-MS). The obtained chromatograms and mass spectra are shown in Figs.3.3-3.5

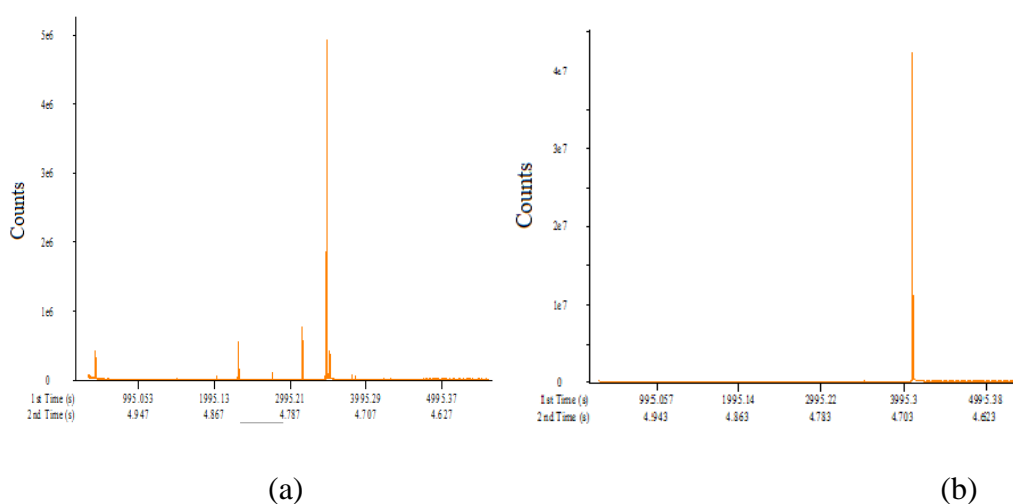


Fig.3.3 Gas chromatograms of a) MO and b) EPMO

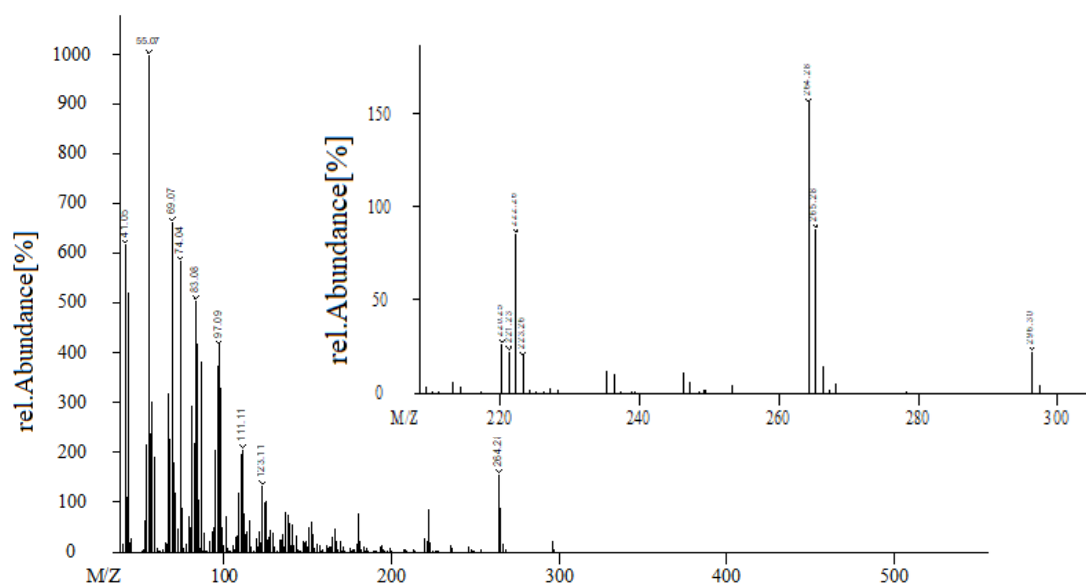


Fig.3.4 Mass spectrum of MO. Inset shows the enlarged spectrum in the region m/z 200-300.

CHAPTER 3

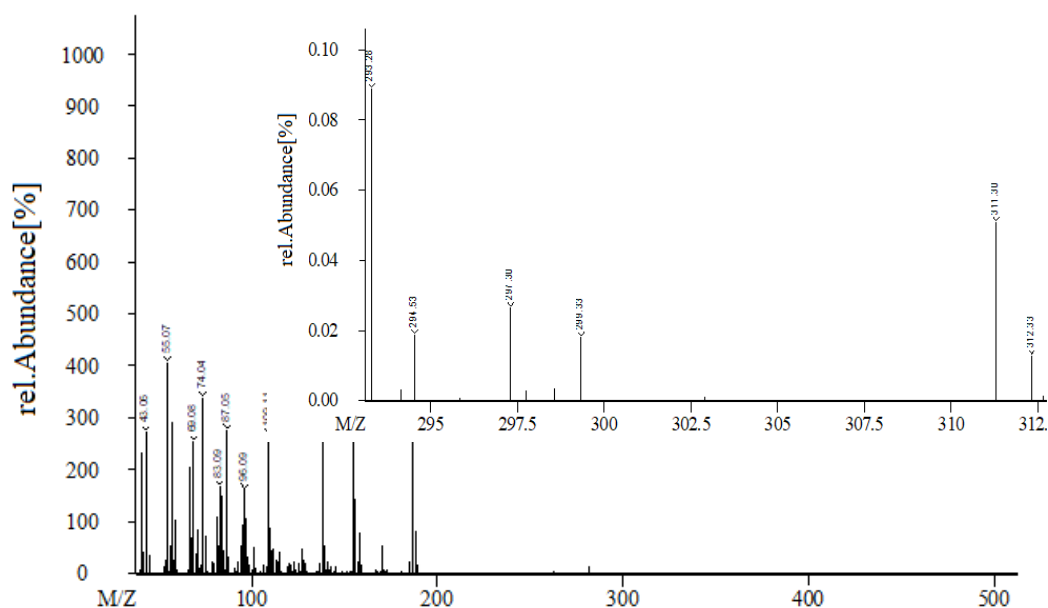


Fig.3.5 Mass spectrum of EPMO. Inset shows the enlarged spectrum in the region m/z 290-313.

The GC purity of MO is 70% and the major impurities are hexadecanoic acid methyl ester, dodecanoic acid methyl ester and methyl stearate (Fig.3.3a). While converting MO to EPMO, these impurities are eliminated during water/hexane wash and hence pure EPMO was obtained as the major product in the epoxidation reaction (Fig.3.3b). The mass spectral data (Figs.3.4 and 3.5) also confirms the successful conversion of MO into EPMO. The peak at (m/z) 313.56 corresponds to the molecular ion of EPMO. The 2D chromatograms obtained for neat ULSD, blended ULSD (LAMOSA 200 ppm), MO and EPMO are shown in Fig.3.6. The ULSD contains paraffins, naphthene and aromatics (Fig.3.6 a) and hence no polar component signals were observed in the chromatogram. No significant changes were observed in the 2D chromatogram of LAMOSA and ULSD blend (Fig.3.6b). In the case of MO, there are multiple peaks due to the presence of impurities as mentioned earlier. Whereas a single sharp chromatogram was observed for EPMO which further confirms the successful conversion of MO to EPMO as well as purity level (98%) of EPMO.

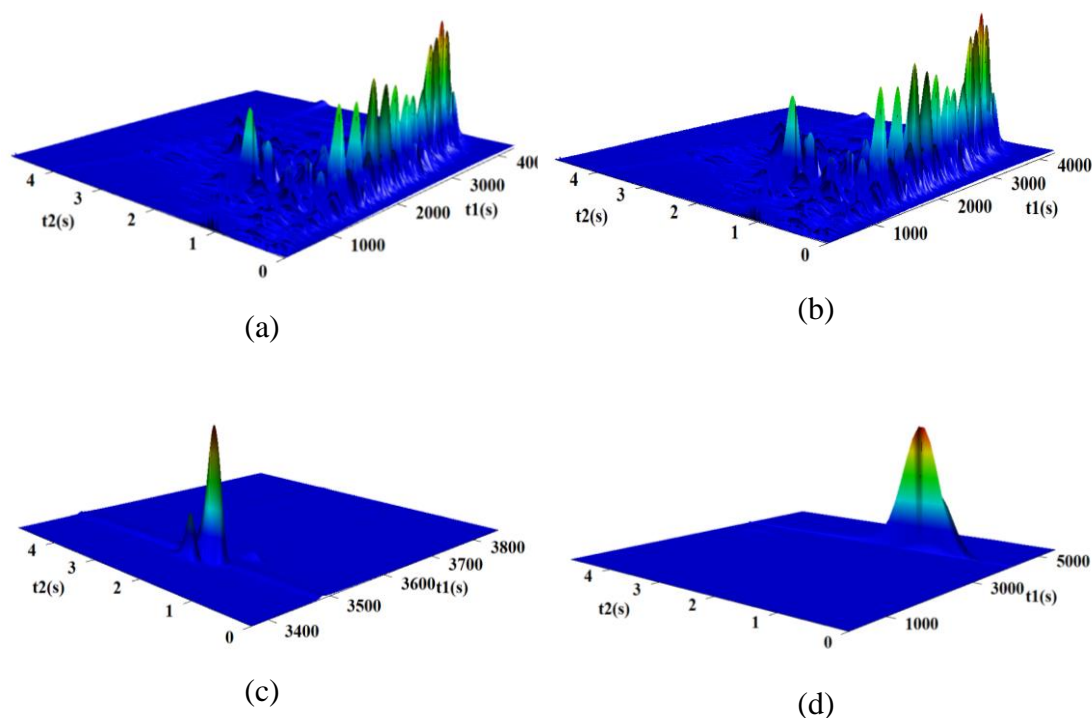


Fig.3.6 2D gas chromatogram of a) neat ULSD, b) blended ULSD -LAMOSA c) MO and d) EPMD (Where, t_1 is the first dimensional retention, t_2 is the second dimensional retention).

3.3.2 Structural characterization of lubricity improvers (LAMOR)

All the prepared lubricity additives were purified through column chromatography using ethyl acetate: hexane (40:60) as mobile phase and silica 100-200 mesh as stationary phase. The purified samples were characterised through FTIR and NMR spectroscopic techniques to confirm their chemical structure. The NMR and FTIR spectral data of purified LAMOPEA, LAMOCA and LAMOSA are given below.

LAMOPEA: Yield: 85%. ^1H NMR (400 MHz, CDCl_3), δ (ppm): 4.99 (s, hydroxyl proton), 4.85-4.81 (t, 1H), 3.66 (t, 1H), 3.58 (s, 3H, OCH_3), 2.34-2.30 (m, 4H), 1.64-1.57 (m, 10H), 1.48-1.34 (m, 20H), 0.94-0.836 (m, 6H). IR (KBr, cm^{-1}): 3507 (OH), 2911, 2845, 1738 ($\text{C}=\text{O}$ from ester), 1450, 1365, 1167, 1130, 1028 and 734. ^{13}C NMR (400MHz, CDCl_3), δ (ppm): 173.71, 173.35, 77.31, 76.99, 74.47, 73.51, 72.56, 34.34, 33.84, 33.67, 31.78, 30.70, 29.63, 29.36, 28.99, 28.88, 27.10, 25.55, 25.36, 25.07, 24.85, 22.2, 14.03 and 13.64.

LAMOCA: Yield: 87%. ^1H NMR (400 MHz, CDCl_3), δ (ppm): 4.96 (s, hydroxyl proton), 4.81-4.78 (t, 1H), 4.12-4.06 (t, 1H), 3.63 (s, 3H, OCH_3), 2.41- 2.25 (m, 4H),

CHAPTER 3

2.05-2.01 (m, 10H), 1.58-1.08 (m, 30H), 0.94-0.83 (m, 6H). IR (KBr, cm^{-1}): 3524 (OH), 2918, 2854, 1738 (C=O from ester), 1463, 1368, 1253, 1177, 1113, 1036 and 717. ^{13}C NMR (400 MHz, CDCl_3), δ (ppm) 174.32, 173.34, 129.11, 126.24, 77.37, 76.72, 73.47, 72.50, 60.10, 51.34, 34.43, 33.51, 33.31, 31.79, 30.68, 29.60, 29.40, 29.19, 25.54, 25.36, 25.08, 25.04, 24.96, 24.89, 24.81, 24.70, 22.59, 14.15 and 14.01.

LAMOS A: Yield: 82%. ^1H NMR (400 MHz, CDCl_3), δ (ppm): 5.25 (s, hydroxyl proton), 4.98-4.81 (t, 1H), 4.11-4.08 (t, 1H), 3.64 (s, 3H, OCH_3), 2.33- 2.05 (m, 4H), 2.07-1.40 (m, 10H), 1.60-1.24 (m, 46H), 0.87- 0.84 (m, 6H). IR (KBr, cm^{-1}): 3473 (OH), 2930, 2860, 1725 (C=O from ester), 1469, 1362, 1253, 1177, 1055 and 729. ^{13}C NMR (400MHz, CDCl_3), δ (ppm) 173.79, 173.39, 77.35, 77.03, 76.71, 76.29, 74.53, 73.58, 72.5, 60.14, 51.40, 34.35, 34.29, 33.98, 33.92, 33.57, 33.48, 31.88, 31.83, 30.69, 29.65, 29.47, 29.41, 29.32, 29.17, 29.10, 29.05, 28.88, 26.01, 25.63, 25.38, 25.06, 24.86, 24.69, 22.62, 14.18 and 14.05.

The FTIR spectra of LAMOPEA, LAMOCA and LAMOS A are shown in Figs. 3.7-3.9 respectively whereas the ^{13}C and ^1H NMR spectra of these lubricity improvers are presented in Figs.3.10 and 3.11 respectively.

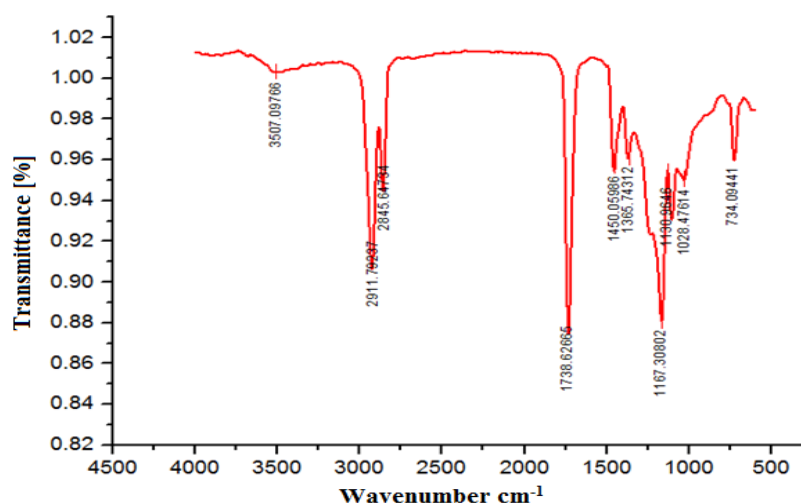


Fig.3.7 FTIR spectra of LAMOPEA. The product displays a sharp carbonyl peak at 1738 cm^{-1} as well as a broad OH band at 3507 cm^{-1} .

CHAPTER 3

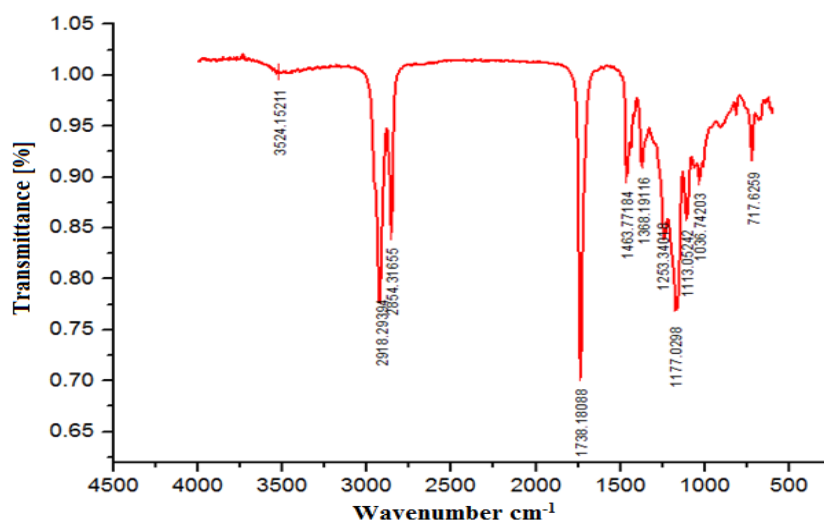


Fig.3.8 FTIR spectra of LAMOCA. The product displays a sharp carbonyl peak at 1738 cm^{-1} as well as a broad OH band at 3524 cm^{-1} .

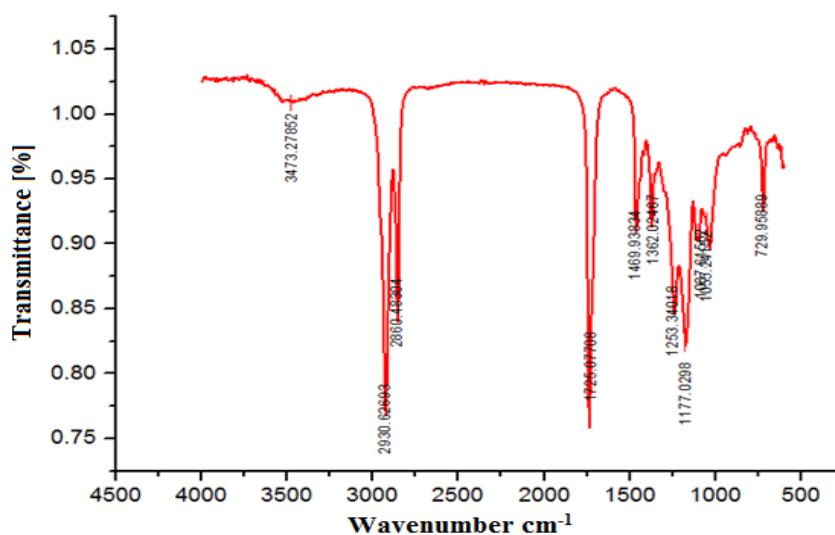


Fig.3.9 FTIR spectra of LAMOSA. The product displays a sharp carbonyl peak at 1725 cm^{-1} as well as a broad OH band at 3473 cm^{-1} .

CHAPTER 3

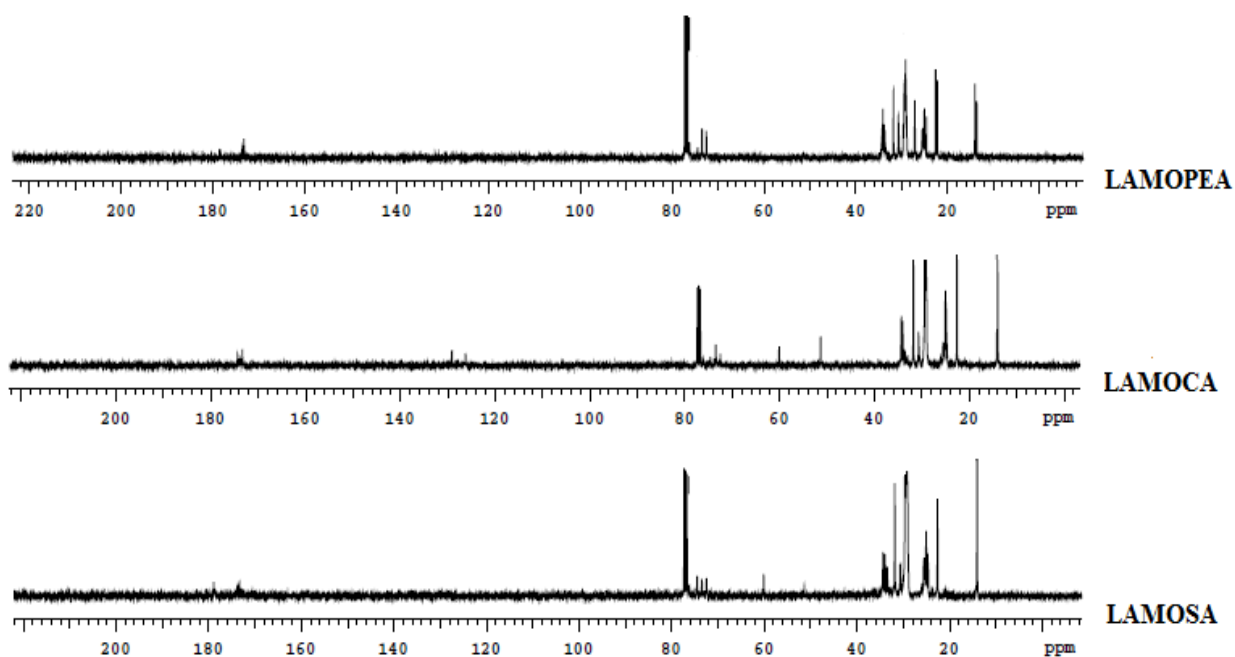


Fig.3.10 ^{13}C NMR spectra of LAMOSA, LAMOCA and LAMOPEA.

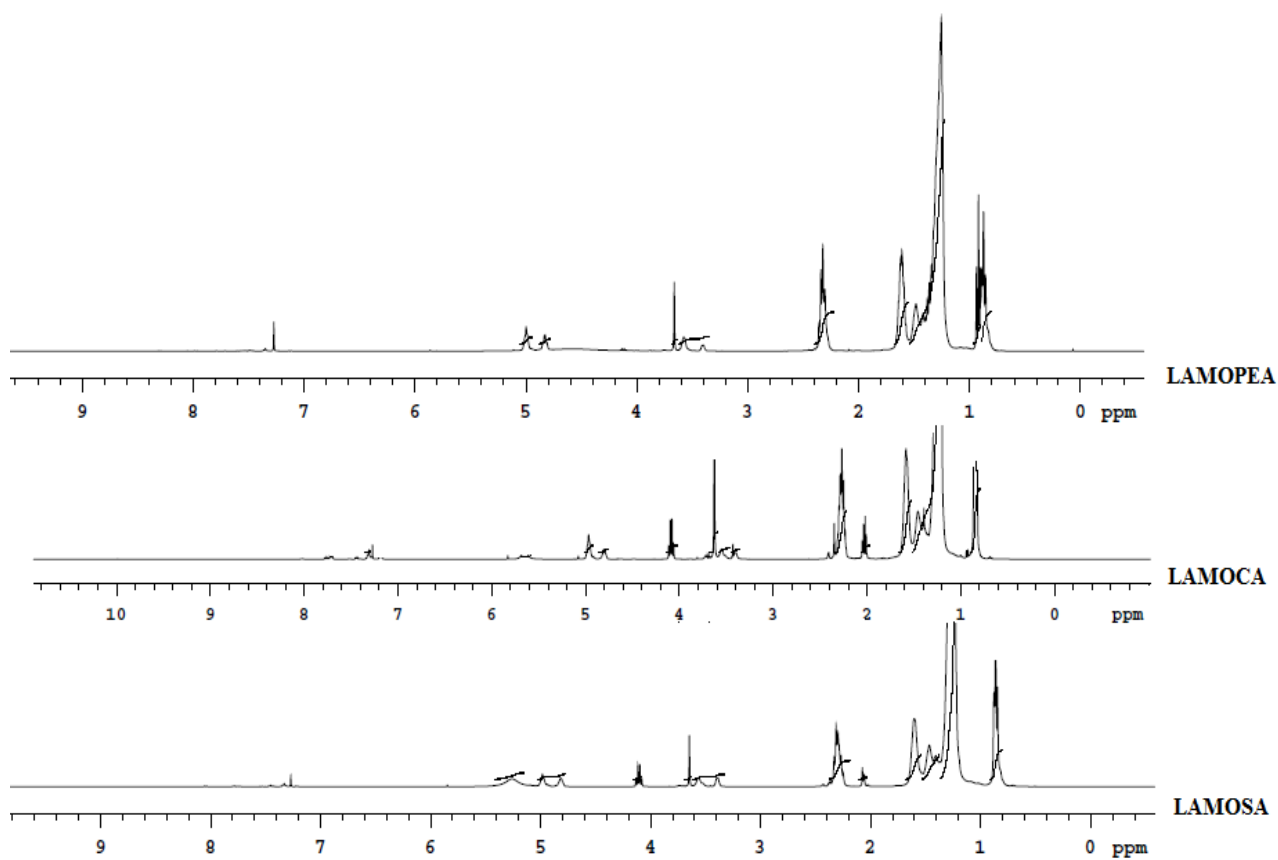


Fig.3.11 ^1H NMR spectra of LAMOSA, LAMOCA and LAMOPEA.

CHAPTER 3

The carboxylic acid (-COOH) signal was not observed in the ^1H NMR spectra of LAMOSA which confirms the absence of any fatty acid impurity in the final product. The singlet peak in the region 4.96-5.25 ppm corresponding to the hydroxyl (-OH) proton indicates mono esterification of the epoxide ring. The $-\text{OCH}_3$ protons of the ester group appeared as a singlet at around 3.6 ppm along with other characteristic peaks of the alkyl chains. The ^{13}C NMR of the purified products further confirmed the formation of the expected reaction products and no free carboxylic acid peaks were observed in the spectra. The peaks in the range 173.7 - 174.3 ppm corresponds to the carbonyl carbons of the ester group. The FTIR spectra of LAMOR displayed a strong band at around 1730 cm^{-1} corresponding to $-\text{C}=\text{O}$ stretching of the ester group as well as a broad OH band at around 3500 cm^{-1} along with other characteristic peaks. There is no absorption band observed for $\text{C}=\text{O}$ of carboxylic acid group which indicates the purity of the final product.

3.4 MEASUREMENT OF LUBRICITY

The lubricity of each blended sample was analysed through HFRR method at 60°C (Table 3.1). Addition of LAMOR lowered the WSD value of the ULSD signifying their lubricity characteristic and the WSD values for the blends are in the range $450 - 388\text{ }\mu\text{m}$ which is lower than the accepted value of $460\text{ }\mu\text{m}$. The optimal microscopic images of the wear scars on the balls employed in lubricity measurement of neat ULSD and LAMOR are shown in Fig.3.12. With the increase of carbon chain length of LAMOR the lubricity of the fuel increases the WSD of metal surface on the ball becomes smaller with minimum scratching marks on the surface. It is interesting to note that all LAMOR derivatives when blended with ULSD (at 300 ppm) imparted lubricity characteristic with minimum wear and scar on the surfaces. Hence, the LAMOR derivatives act as effective anti-wear agents on the metal surface. The WSD values of neat ULSD, neat MO and LAMOR-ULSD blends are given in table 1 and are graphically represented in Fig. 3.13.

CHAPTER 3

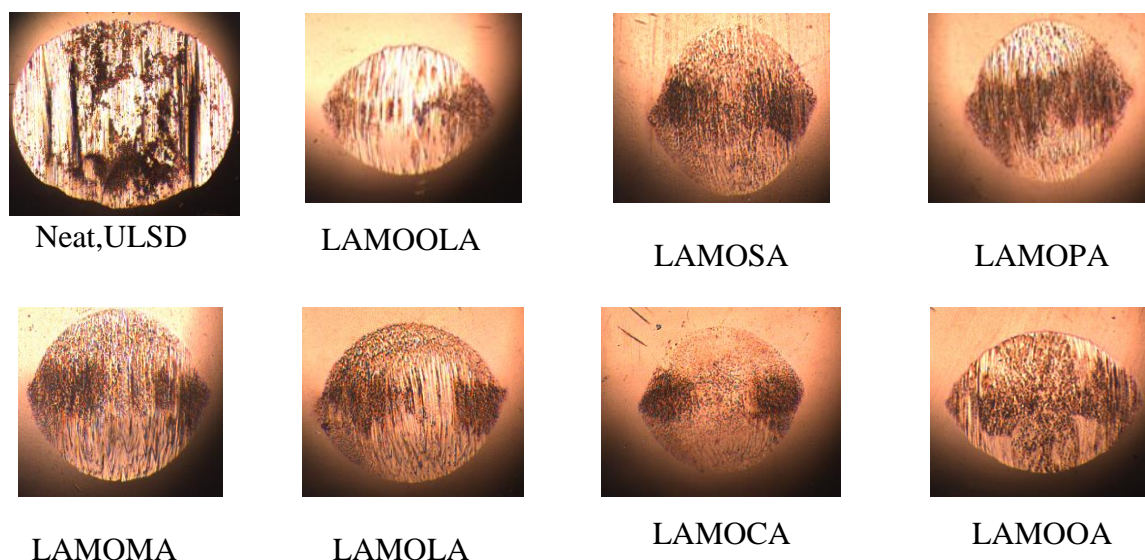


Fig.3.12 The optical microscopic images of wear and scar for samples neat ULSD and LAMOR (300 ppm)

Table 3.1: The lubricity data of neat ULSD and ULSD-LAMOR blend (300 ppm)

Sample ID	HFRR at 60°C				
	Wear scar diameter, μm			Result	
	Ball X	Ball Y	Average	Film, %	Friction coefficient
Neat ULSD	534	470	502	13	0.846
Neat MO	521	449	485	16	0.591
LAMoola	458	382	420	26	0.284
LAMOSA	413	362	388	34	0.253
LAMOPA	436	372	404	29	0.256
LAMOMA	421	405	413	26	0.280
LAMOLA	415	409	412	24	0.286
LAMOCA	480	418	449	22	0.290
LAMOOA	440	392	416	21	0.296
LAMO2EHA	438	400	419	20	0.290
LAMOHA	470	400	435	19	0.294
LAMOPEA	445	429	437	18	0.299
LAMObA	470	382	426	17	0.300

CHAPTER 3

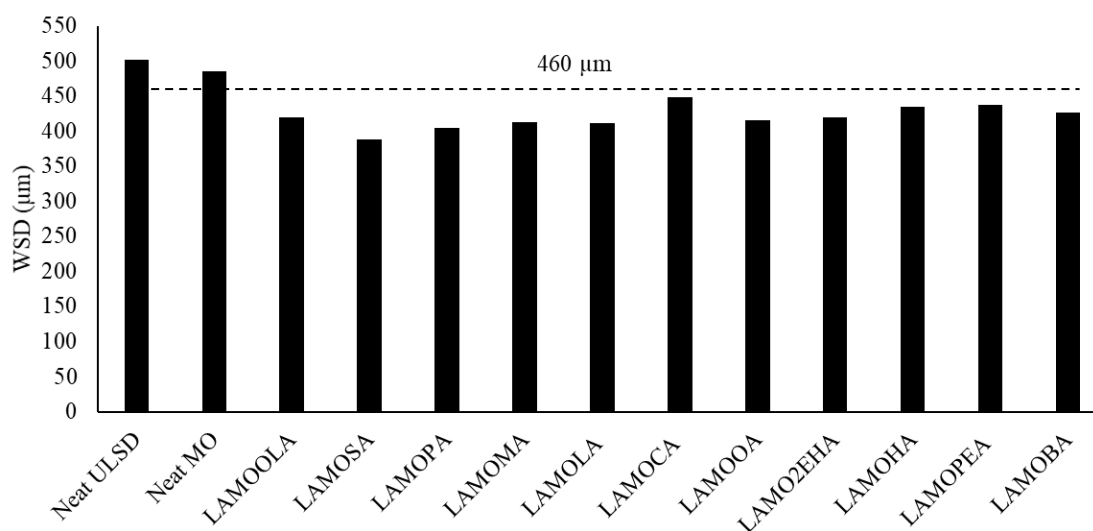


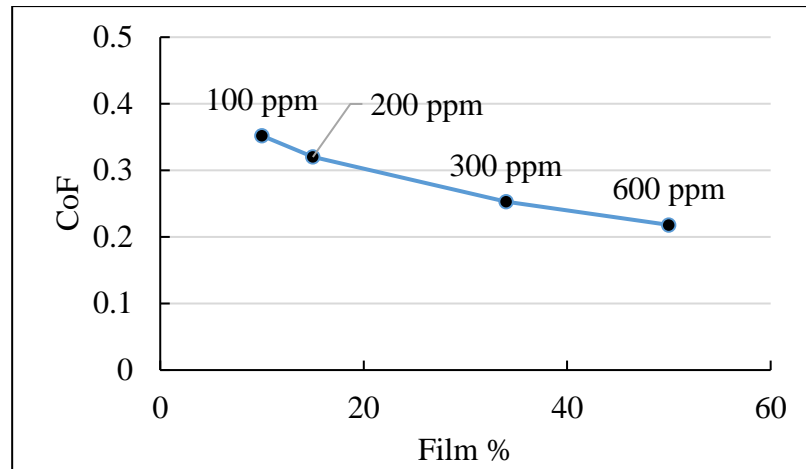
Fig.3.13 Graphical representation of WSD values obtained for neat ULSD, neat MO and LAMOR at 300 ppm (dotted line implies the accepted WSD value of 460 µm according to BS VI norms)

Among different ULSD-LAMOR blends, the best WSD value was observed for the blend with LAMOSASA as the additive. So, LAMOSASA was chosen for further analysis wherein the lubricity was measured with different blending concentrations such as 600, 200 and 100 ppm. The results are tabulated in Table.3.2 and graphically represented in Fig.3.14. The optimal microscopic images of wear and scar for samples, neat MO and LAMOSASA (100, 200 and 600 ppm) are shown in Fig.3.15. The friction and film % graph obtained from HFRR for neat ULSD, neat MO and ULSD-LAMOSASA (600, 300, 200 and 100 ppm) blends is given in Fig.3.16.

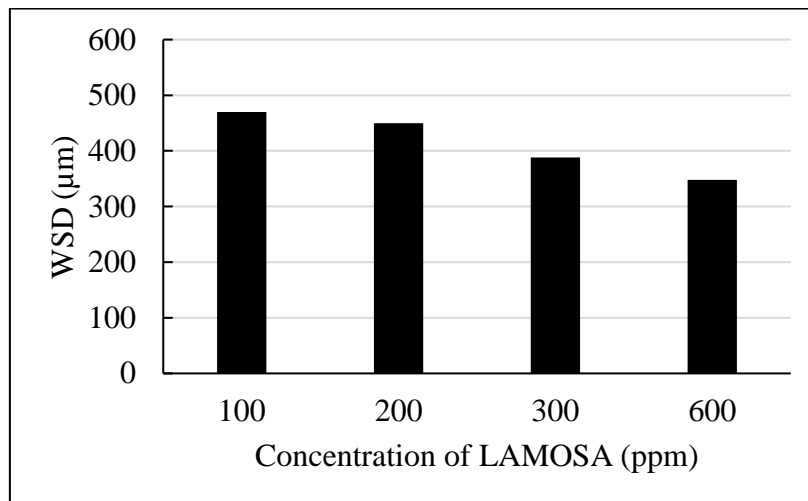
Table 3.2: Lubricity data of LAMOSASA-ULSD at different blended concentrations

HFRR at 60°C					
LAMOSASA- ULSD Blend concentration (ppm)	Wear scar diameter (µm)			Result	
	Ball X	Ball Y	Average	Film %	Friction Coefficient
100	475	464	470	10	0.352
200	460	440	450	15	0.320
300	413	362	388	34	0.253
600	379	317	348	50	0.218

CHAPTER 3



(a)



(b)

Fig.3.14 Graphical representation of a) film % vs coefficient of friction (CoF) and b) WSD for ULSD blends with LAMOSA at different blend concentrations.

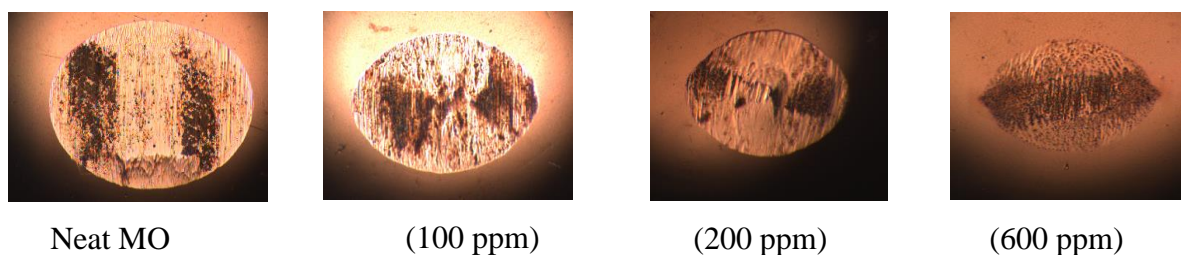
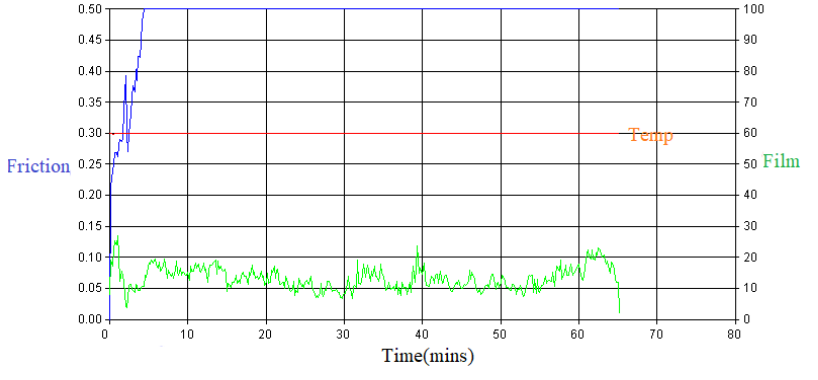
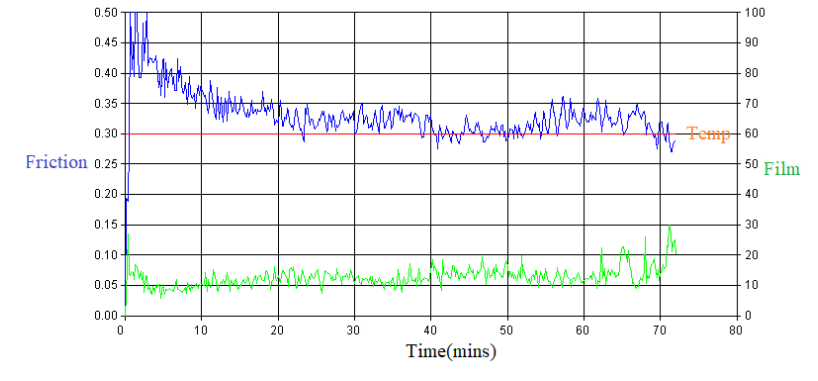
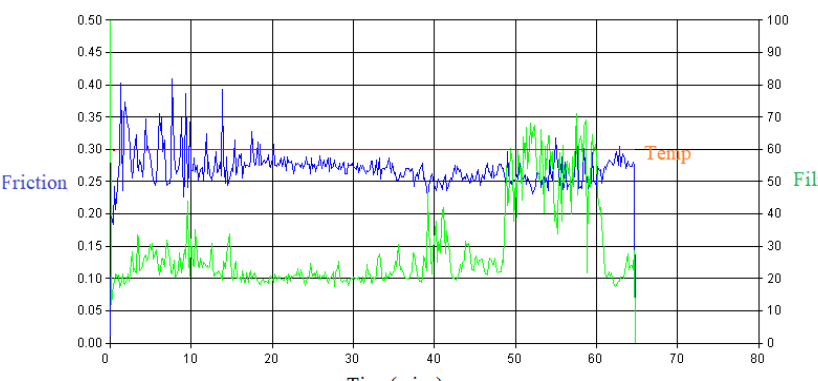


Fig.3.15: The optical microscopic images of wear and scar for samples neat MO and LAMOSA-ULSD blends.

CHAPTER 3

Sample, at 60 °C	Instrumental data
Neat, ULSD	 <p>The graph for Neat ULSD shows three data series over 80 minutes. The Friction (blue line) starts at 0.00, rises sharply to 0.50 by 5 minutes, and remains constant thereafter. The Temperature (orange line) is a constant horizontal line at 0.30. The Film (green line) starts at 0.00, rises to a peak of approximately 0.12 at 5 minutes, and then fluctuates between 0.05 and 0.10 for the remainder of the test.</p>
(100 ppm)	 <p>The graph for 100 ppm shows three data series over 80 minutes. The Friction (blue line) starts at 0.50 and gradually decreases to a steady state of approximately 0.30 after 20 minutes. The Temperature (orange line) is a constant horizontal line at 0.30. The Film (green line) starts at 0.00, rises to a peak of approximately 0.12 at 5 minutes, and then fluctuates between 0.05 and 0.10 for the remainder of the test.</p>
(200 ppm)	 <p>The graph for 200 ppm shows three data series over 80 minutes. The Friction (blue line) starts at 0.50 and gradually decreases to a steady state of approximately 0.30 after 20 minutes. The Temperature (orange line) is a constant horizontal line at 0.30. The Film (green line) starts at 0.00, rises to a peak of approximately 0.12 at 5 minutes, and then fluctuates between 0.05 and 0.10 for the remainder of the test.</p>

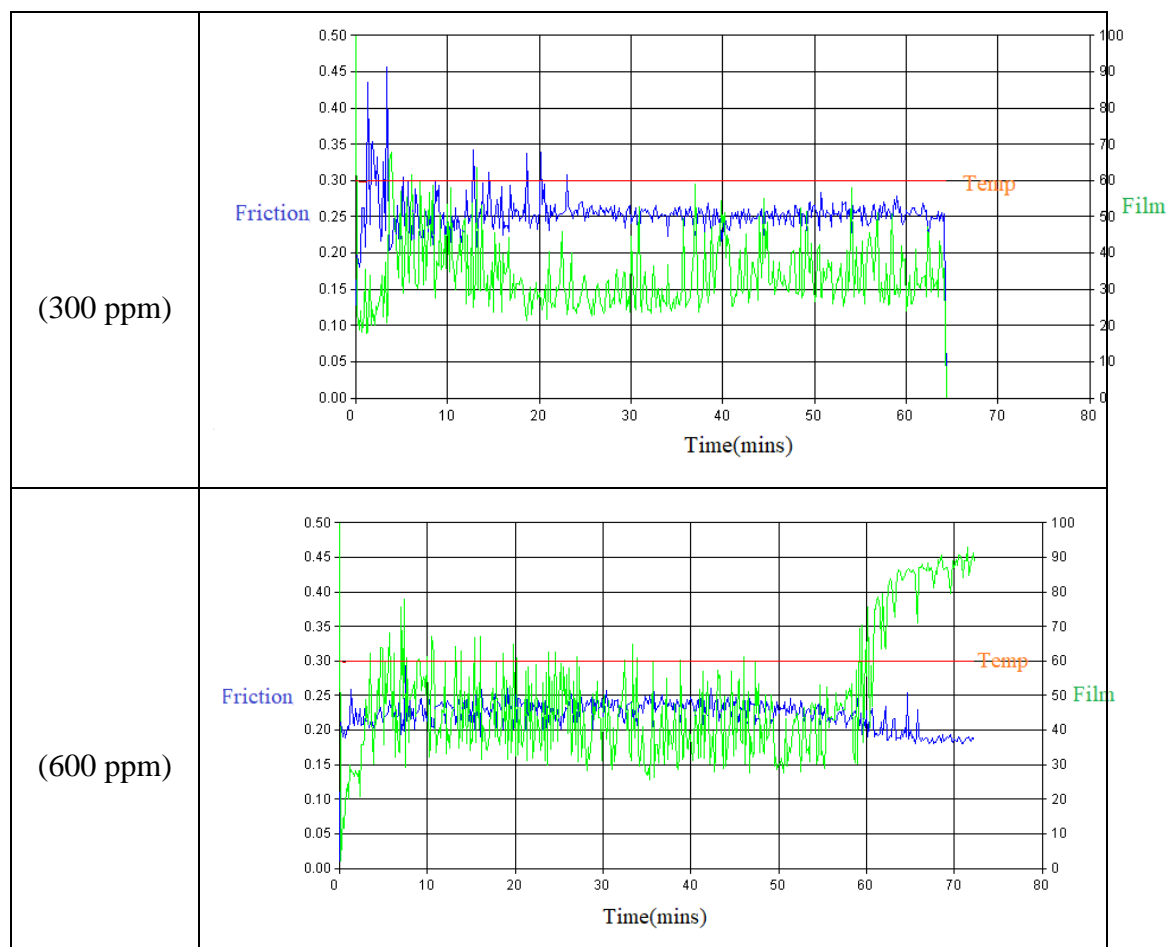


Fig.3.16 Friction coefficient and film % graph obtained from HFRR for neat ULSD and LAMOSA-ULSD blends.

From the above data (Fig.3.16), it is clear that as the concentration of blended LAMOSA increases, the friction experienced between the metallic surface decreases. Due to this WSD decreases indicating that LAMOSA is an efficient lubricity improver for ULSD. It is interesting to note that the WSD value at a low blend concentration of 200 ppm is below the accepted value of $460\mu\text{m}$ which is an added advantage from the commercialisation point of view.

3.5 STUDY OF PHYSIOCHEMICAL PARAMETERS

3.5.1 Effect of new lubricity improvers on fuel properties of the diesel

To study the effect of new lubricity improvers on other fuel properties of the diesel, several key parameters like pour point, copper corrosion, oxidation stability etc. of the blend fuels were determined. The results of these measurements for neat ULSD and the blended fuel (200 ppm of LAMOSA) are given in table 3.3.

CHAPTER 3

Table 3.3: The test report summary of neat and blended (200 ppm of LAMOSA) ULSD

S. No.	Parameter	Test Method	Specification	Result	
				Neat ULSD	Blend fuel
1	Acidity, Total, mg of KOH/g, <i>Max*</i>	ASTM D 974	0.2	0.039	0.13
2	Cetane Index, <i>Min*</i>	IP 380	46	56.1	56.0
3	Pour point, °C, <i>Max*</i>	ASTM D 5950	3 for winter 15 for summer	-33	-33
4	Copper strip corrosion test 3 h at 50° C	ASTM D 130	Not worse than No.1	No.1	No.1
5	Distillation, 95% recovery, v/v, recovery, °C, <i>Max*</i>	ASTM D 86	360	344.5	343.5
6	Flash point, °C, <i>Min*</i>	IP 170	35	>100	>100
7	Kinematic viscosity, cSt at 40° C	ASTM D 445	2.0-4.5	3.051	3.058
8	Density @ 15° C, kg/m ³	ASTM D 4052	810-845	839.7	839.8
9	Total Sulphur, mg/Kg, <i>Max*</i>	ASTM D 5453	10	2.4	3.1
10	Lubricity, WSD at 60° C, microns, <i>Max*</i>	ASTM D 6079-18	460	502	450

CHAPTER 3

11	Oxidation stability, g/m ³ , <i>Max</i> *	ASTM D 2274	25	8.8	12.5
12	Cold Filter Plugging Point (CFPP), °C	ASTM D 6371	6 for winter 18 for summer	-16	-16

Note* *Max* implies maximum allowed value, *Min* implies minimum allowed value

The study clearly indicates that, addition of new lubricity improver does not affect other fuel properties of the diesel. However, the lubricity of the blend fuel is improved which is reflected in terms of its lower WSD value (450 µm) as compared with that of the neat ULSD (502 µm). Hence, the LAMOSA-ULSD blend meets the Euro VI/BS VI fuel specifications.

3.6 LUBRICITY MECHANISM

Examination of tribological behaviour of LAMOR lubricity improver on metal surface is very important part of lubricity study. The metal surfaces of friction couples were analysed by their SEM and EDS morphologies.

3.6.1 SEM analysis of wear scar

The SEM images of the wear scars on balls of the friction couples are shown in Fig.3.17. It is evident from the SEM images that with the increase in the concentration of LAMOSA in the diesel blend, the WSD of metal surface on the ball becomes smaller and the scratching marks also become thinner and shallower. The reason is that the polar components in the LAMOSA lubricity improving agent assist its easy adsorption on the surface of the friction couples which results in the formation of a layer of protective lubricant film. The presence of polar components in the lubricity additive and the formation of a thin film are helpful in reducing the scratching on the surface of the friction couples. In addition, the hydroxy and ester functional groups of LAMOSA offer active oxygen sites that bind to the metal surface to form a thin layer, which can avoid the direct metal to metal contact in friction couples. In other words, the protective layer of LAMOSA reduces the friction on the metallic surfaces.

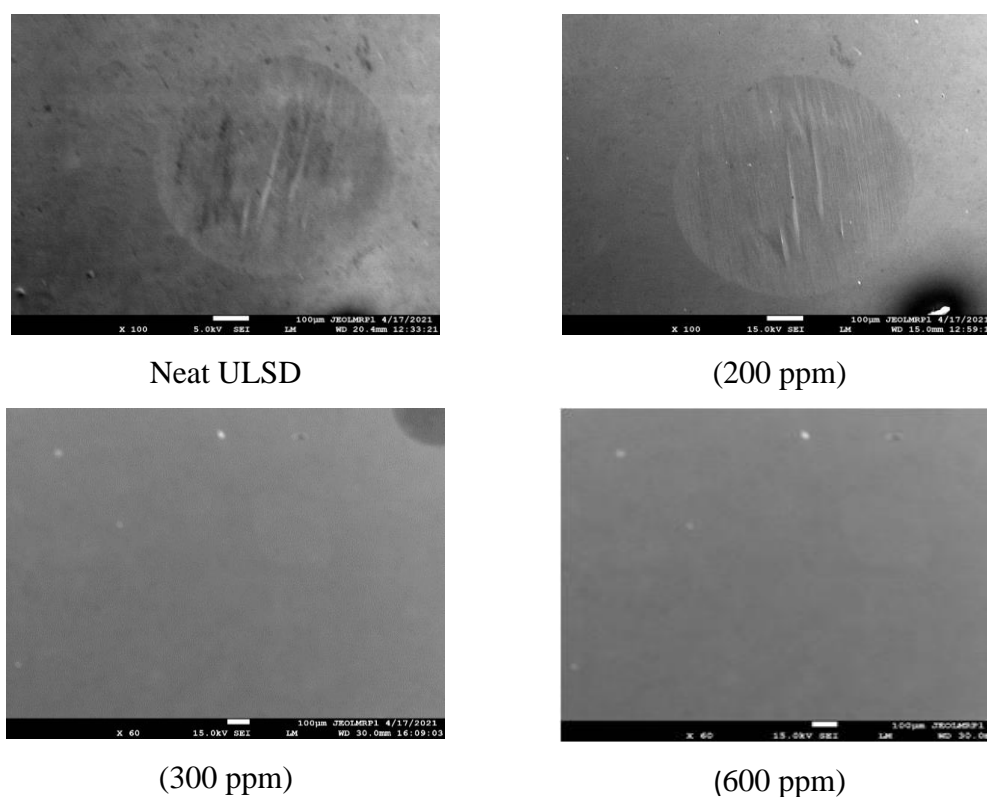


Fig.3.17 SEM images of neat ULSD and blended LAMOSA with ULSD at different concentrations

3.6.2 EDS analysis of the wear scar

In order to recognize the interaction between the additive and the metal surface during the friction process, EDS analysis of the metal surface of the balls was performed after the HFRR test. Three main elements were detected on the metal surface; C from the diesel, O from the lubricity improving agent and air, and Fe from the friction matrix. The EDS graphs are shown in Fig.3.18. The composition of elements C, O, Fe and Cr on the surfaces tested with different LAMOSA-ULSD blends were compared with those of the surface tested with neat ULSD. The oxygen content on the metal surfaces lubricated by the blend fuel was higher than that on the surface lubricated by the neat ULSD. The higher oxygen content in the case of blend fuel could be due to the interaction of the metal surface with the oxygen containing functional groups of the diester which assists in the formation of a protective lubricating layer. The oxygen content on the metal surface increases from 4.3 to 9.1% with an increase in the blend concentration from 100 to 600 ppm which further supports the interaction of the metal

CHAPTER 3

surface with the diester through oxygen containing functional groups. The schematic representation of such interactions of the metal surfaces with the diester is shown in Fig.3.19. Hence, it can be concluded that the polar functionalities such as -COOR and -OH groups in these molecules enhance their absorptivity on the metal surface by the formation of thin protective layer. Due to this, metal to metal interactions decrease and hence the experienced friction on metal surfaces also decreases, which leads to improved lubricating action.

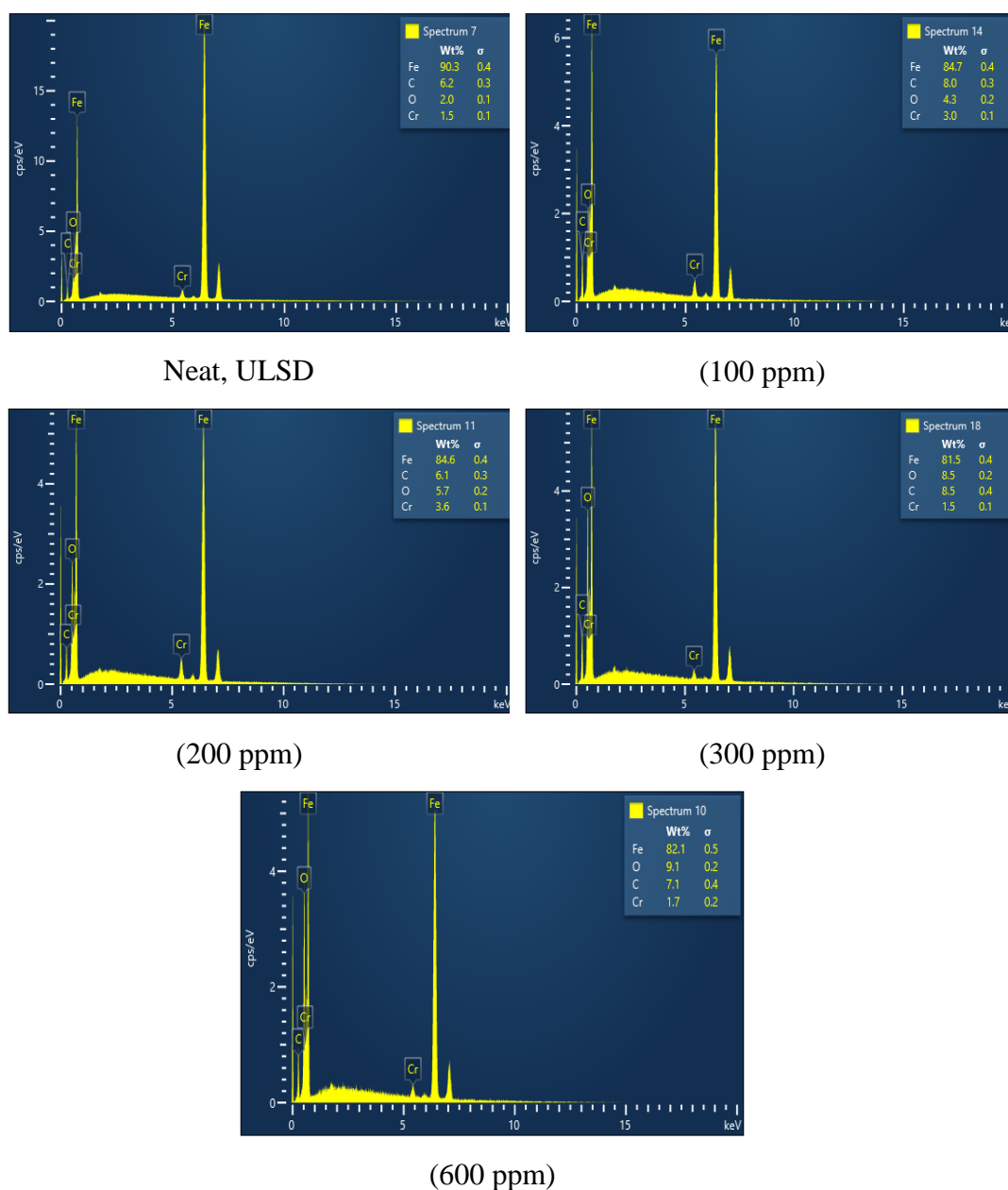


Fig.3.18 EDS graphs of neat ULSD and blended LAMOSA with ULSD at different concentrations

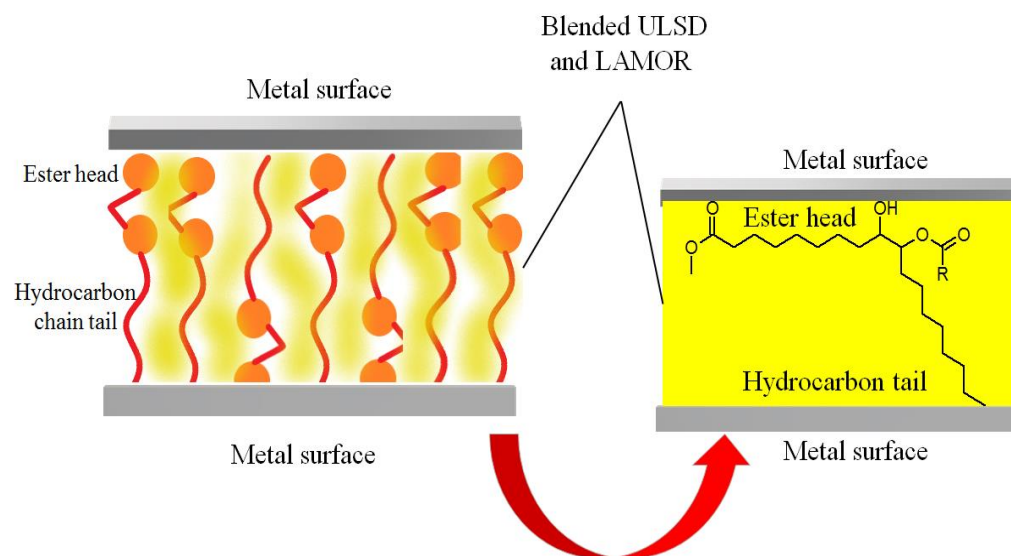


Fig.3.19 Schematic representation of interactions between the metal surface and LAMOR through oxygen-containing functional groups.

3.7 CONCLUSIONS

A new series of methyl oleate –based diesters (LAMOR) were synthesized through a simple two-step process. These diesters effectively improve the lubricity of ultra-low sulphur diesel at a low blend concentration of 300 ppm, by greatly reducing the WSD and CoF of the diesel. Amongst them, diester LAMOSA derived from stearic acid showed the best lubrication enhancing property with a WSD of 388 μm at 300 ppm dosage level. Interestingly, it maintains lubricity characteristics even at a lower blending concentration of 200 ppm with a WSD value of 450 μm which is lower than the than the accepted value (460 μm). Moreover, it has long term antiwear stability when blended with the diesel fuel and do not alter or negatively influence the physical and chemical parameters of the diesel. The adsorption of LAMOR through the oxygen atom of the polar functional groups on the surface of friction couples contributes to the formation of lubricant protective film which improves the lubricity of the blend fuel. Hence, these lubricity improvers (LAMOR) present a promising prospect in the improvement of diesel lubricity and reduction of friction and wear of the diesel engine.

CHAPTER 4

SIMPLE METHOD FOR THE CONVERSION OF LIGHT CRACKED NAPHTHA INTO EFFICIENT LUBRICITY IMPROVERS FOR ULTRA-LOW SULPHUR DIESEL

Abstract:

This chapter deals with the synthesis of new series of LI for ULSD starting from cracked naphtha through an epoxidation esterification and hydroboration esterification reaction protocols. It covers lubricity study of neat ULSD as well as blended ULSD. Also, it discusses the structural characterization followed by mechanism of lubricity action of newly synthesised LI on metal surfaces.

4.1 INTRODUCTION

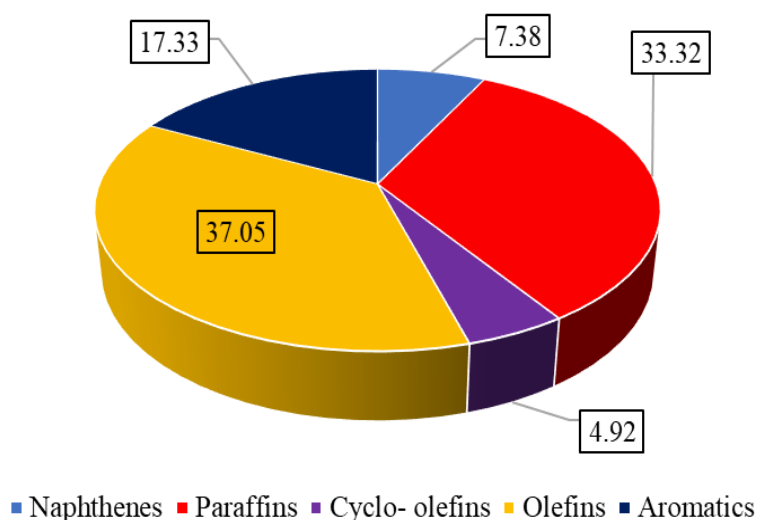
The amount of lubricity improver for BS VI fuel is almost double the amount required for BS IV fuel in order to meet the lubricity specifications of the fuel. Consequently, the blended fuel becomes costlier than the BS IV fuel. Hence, there is a challenge to prepare cost effective lubricity improvers. According to the literature, ester and acid groups are favourable to enhance the fuel lubricity rather than ether and aldehyde groups in the additives. But the direct use of an acid-based additive is not recommended due to its corrosive nature towards metal surfaces. The succinic acid alkyl half-esters and tung oil based fatty acid esters are reported to be a good lubricity enhancer for ULSD. In this work, it was planned to synthesize lubricity additives by utilizing the olefin rich naphtha stream (LCN) of the fluidized catalytic cracker (FCC) unit of the petroleum refinery. The olefin content in the LCN of FCC unit is about 40 - 45 vol% and the detailed composition analysis of the LCN employed in the present study is tabulated in Table 4.1. The LCN composition and compositions of olefin in LCN are graphically represented in Fig4.1. The main objective of the present study was to convert the olefins into a mixture of esters through epoxidation/hydroboration reaction followed by the esterification of the LCN derivative with different carboxylic acids. The mixture of LCN esters comprising of polar functional groups is expected to improve the lubricating property of ULSD when dosed with it in small quantities. To

CHAPTER 4

the best of our knowledge, this is the first report on LCN-based lubricity improvers for ULSD. The synthetic procedure followed in the present study could be a feasible protocol for the oil refineries to develop ULSD additives in a commercial scale by employing the refinery raw material LCN.

Table 4.1. Composition of light cracked naphtha (vol %)

Normalized volume percent result (LCN)						
Carbon number	Naphthenes	Paraffins	Cyclo-olefins	Olefins	Aromatics	Total
4	-	0.39	-	0.18	-	0.57
5	0.73	18.08	0.88	28.61	-	48.30
6	2.39	9.93	2.03	6.33	3.74	24.41
7	2.55	3.33	1.50	1.31	7.70	16.38
8	1.27	1.39	0.37	0.27	4.49	7.80
9	0.25	0.21	0.13	0.31	0.61	1.52
10	0.05	-	-	-	0.79	0.83
11	0.15	-	-	0.04	-	0.19
12+	-	-	-	-	-	-
Poly	-	-	-	-	-	-
Total	7.39	33.33	4.91	37.05	17.33	100



(a)

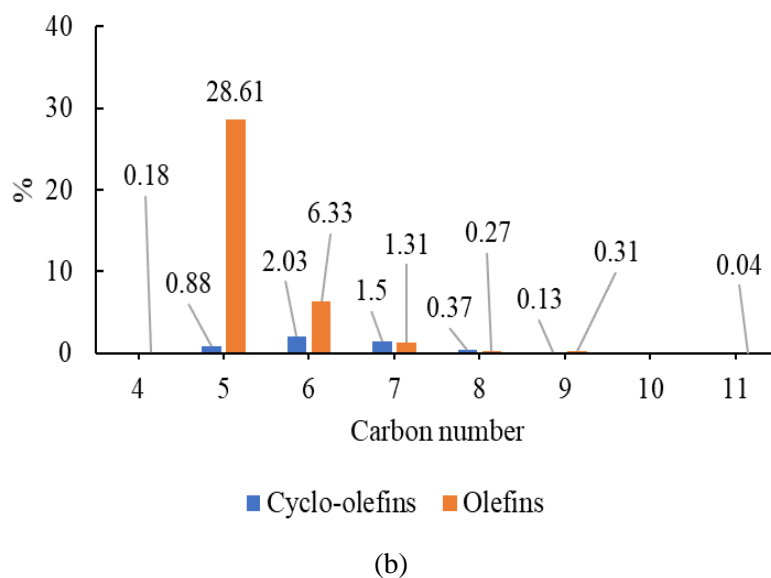


Fig.4.1a) Graphical representation of LCN composition and b) Graphical representation of compositions of olefin in LCN.

4.2. EXPERIMENTAL PART

4.2.1 Materials and Instruments

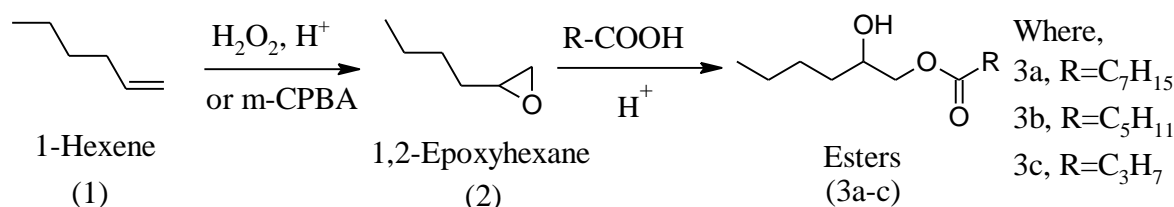
1-Hexene (97%), glacial acetic acid ($\geq 99\%$), hydrogen peroxide (50% solution), meta-chloroperbenzoic acid (m-CPBA), borane-tetrahydrofuran complex solution (1.0 m in THF) (BH_3 in THF), NaOH, methanol, organic/fatty acids, solvents and all the other chemicals were purchased from Sigma Aldrich. The component analysis of the LCN was carried out using a PAC Reformulyzer-M₄ analyser. The details of other instruments are already given in chapter 3 (3.2.2).

4.2.2 Epoxidation method

In this method, the LCN from the PFCC unit was subjected to epoxidation reaction followed by the esterification of the epoxides with different organic acids to get the mixture of hydroxy esters. The epoxidation was carried out following two different approaches viz i) using H_2O_2 / glacial acetic acid and ii) using m-CPBA. A variety of carboxylic acids including some fatty acids were employed for the esterification of the epoxidized LCN to get the corresponding hydroxy ester derivatives. Initially, the overall process was optimized using a neat olefin where in 1-hexene was subjected to epoxidation reaction followed by the esterification of the epoxide with different organic acids. The detailed synthetic procedure for the process is given below.

4.2.2.1 Synthesis of esters from 1-hexene

The conversion of 1-hexene to corresponding hydroxy esters is depicted in scheme 4.1.



Scheme 4.1 Synthetic route for 1-hexene based esters (3a-c)

4.2.2.2 Epoxidation of 1-hexene

i. Hydrogen peroxide route

1-Hexene (160 g, 1.9 mol) was placed in a 1000 mL RB flask equipped with an overhead stirrer and the flask was cooled in an ice bath. To the ice cooled hexene, glacial acetic acid (400 g, 6.6 mol) was added. After the addition of the acetic acid, 50 % hydrogen peroxide (400 g, 11.8 mol) was added drop wise over about 5 mins while the temperature of the solution was monitored continuously. Then, the reaction mixture was allowed to stir at room temperature for 8 h. After the completion of the reaction, distilled water (500 mL) was added to the reaction mixture. The product was extracted using dichloromethane (DCM), washed with excess of water and 1.0 M sodium bicarbonate. The organic phase was dried over anhydrous sodium sulphate and the solvent was removed under vacuum to yield the final product 1,2-epoxyhexane (2) (yield 85-88%).

ii. m-CPBA route

A mixture of 1-hexene (120 g, 1.43 mol) and DCM (200 mL) was taken in a 1000 mL RB flask. The mixture was cooled for 5 mins at 0-5°C with continuous stirring. To the reaction mixture, m-CPBA (140 g, 0.81 mol) in DCM (500 mL) was added drop wise. After the completion of addition, the reaction mixture was stirred for 8 h at room temperature. Progress of the reaction was monitored using gas chromatography. After completion of the reaction, the product was washed with 2% sodium sulphite (200 mL) followed by 2% sodium carbonate solution (200 mL). Then the product was extracted using DCM and washed with excess of water. The organic phase was dried over sodium

CHAPTER 4

sulphate and the solvent was removed under reduced pressure to yield the final product 1,2-epoxyhexane (2) (yield 92-94%).

4.2.2.3 Esterification of 1,2-epoxyhexane

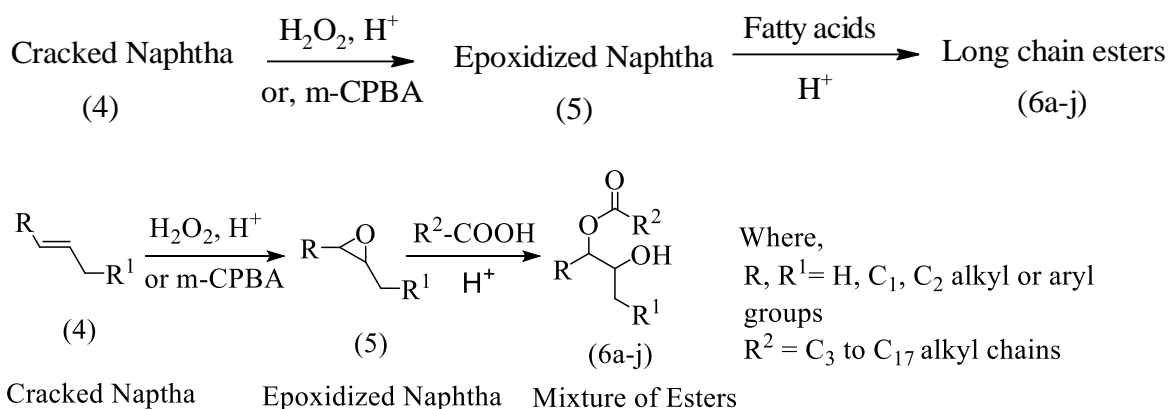
Synthesis of ester 3a from octanoic acid

To a mixture of 1,2-epoxyhexane (5 g, 0.05 mol), p-toluene sulfonic acid (0.2g, 0.001 mol) and toluene (10 mL), octanoic acid 7.2 g (0.05 mol) was added. The reaction mixture was refluxed for 6h in N₂ atm. After completion of the reaction, the mixture was cooled to room temperature and left to stand for 3 h. Then the mixture was extracted with ethyl acetate and the organic layer was washed with DM water (200 mL) followed by 5 % sodium bicarbonate (200 mL) solution. The organic layer was filtered through sodium sulphate and the solvent was evaporated using rotary evaporator to yield the product (3a) as dark yellow liquid (yield 85%).

Similarly, esters **3b** and **3c** were synthesized by using the reactants hexanoic acid and butyric acid respectively.

4.2.2.4 Synthesis of hydroxy esters from LCN

The conversion of LCN into mixture of hydroxy esters is schematically depicted in scheme 4.2, considering a general structure (4) for the olefins present in the LCN.



Scheme.4.2 Synthetic route for hydroxy esters (6a-j) from LCN through epoxidation reaction

4.2.2.5 Epoxidation of LCN

The epoxidation of LCN (400 g batch) was carried out following the same procedure described above for 1-hexene. The reaction was monitored using GC and the

CHAPTER 4

olefin conversion data for both H₂O₂ and m-CPBA methods is presented in Table 4.2 whereas the graphical representation is given in Fig. 4.2. Both the methods were found to be effective for the epoxidation of olefins. However, olefin conversion was slightly higher in m-CPBA method (90.5% at 8 h) than that in H₂O₂ method (85.8% at 8 h). Hence, the epoxide obtained by m-CPBA method was utilized for the esterification reaction.

Table 4.2: The olefin conversion data for the epoxidation reaction.

Method	Sample	Reaction time (h)	Olefin, vol%	Conversion (%)
H ₂ O ₂	Pure LCN	0	41.97	-
	Reaction mixture	2	20.19	51.9
		4	9.56	77.2
		6	6.55	84.4
		8	5.98	85.8
m-CPBA	Pure LCN	0	41.97	-
	Reaction mixture	2	19.45	53.6
		4	8.42	79.9
		6	4.51	89.3
		8	3.98	90.5

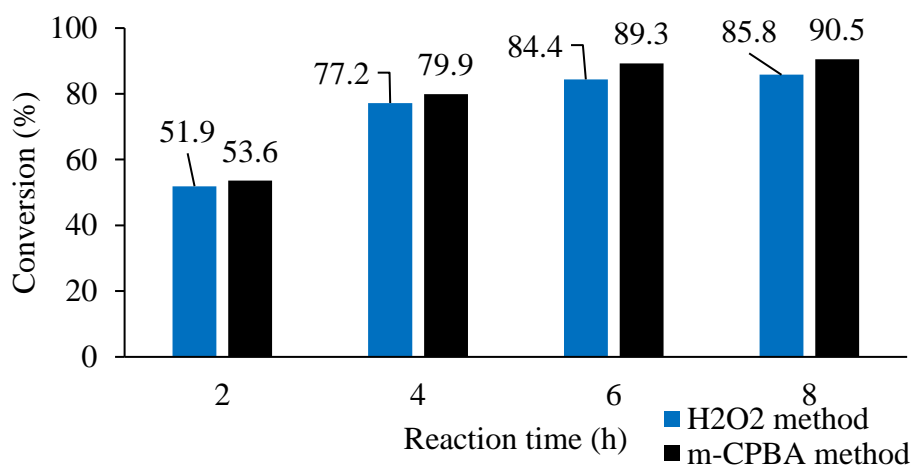


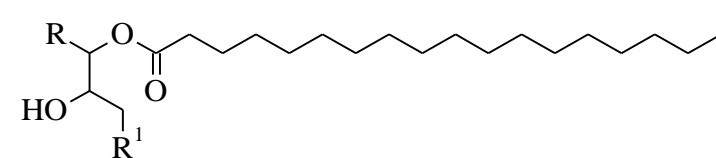
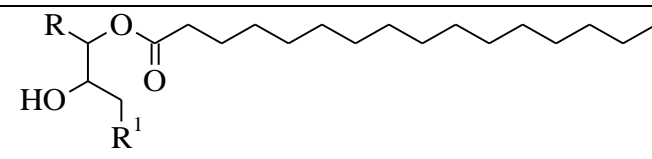
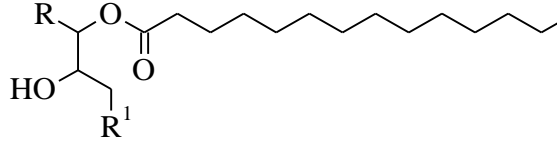
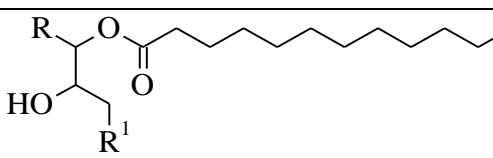
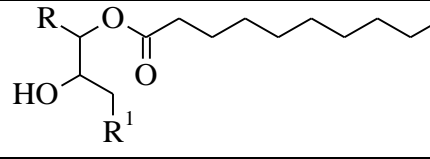
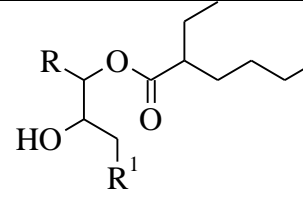
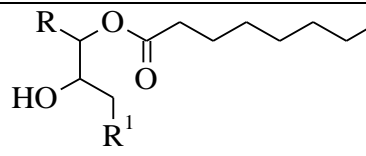
Fig.4.2 Graphical representation of reaction time vs olefin conversion

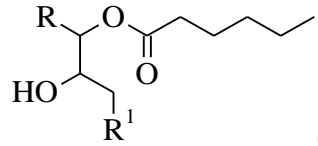
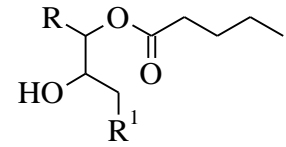
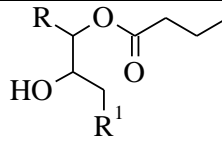
CHAPTER 4

4.2.2.6 Esterification of epoxidized LCN

The epoxidized LCN (synthesized via m-CPBA route) was subjected to esterification reaction with long chain ($C_4 - C_{18}$ alkyl groups) organic acids following the procedure described above for the esterification of epoxy hexane to get the final hydroxy esters (6a-j). The chemical structures of all the hydroxy esters are given in the Table 4.3.

Table 4.3. The chemical structures of LCN hydroxy esters (6a-j)

Acid	Obtained Product
Stearic acid $C_{18}H_{36}O_2$	 6a
Palmitic acid $C_{16}H_{32}O_2$	 6b
Myristic acid $C_{14}H_{28}O_2$	 6c
Lauric acid $C_{12}H_{24}O_2$	 6d
Capric acid $C_{10}H_{20}O_2$	 6e
2-Ethyl hexanoic acid $C_8H_{16}O_2$	 6f
Octanoic acid $C_8H_{16}O_2$	 6g

Hexanoic acid $C_6H_{12}O_2$	 <p style="text-align: right;">6h</p>
Pentanoic acid $C_5H_{10}O_2$	 <p style="text-align: right;">6i</p>
Butyric acid $C_4H_8O_2$	 <p style="text-align: right;">6j</p>

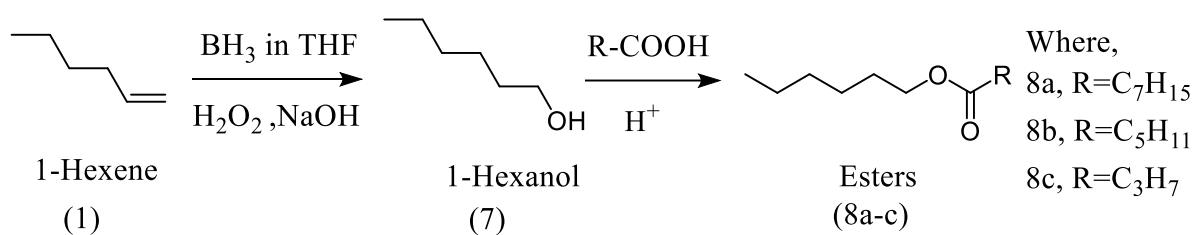
Where, R, R¹ = H, C₁ and C₂ alkyl or aryl groups

4.2.3 Hydroboration method

In this method, the LCN subjected to hydroboration reaction to get hydroxy LCN. Then obtained hydroxy LCN was esterified using different acids to get the mixture of esters. Initially, the overall process was optimized using a neat olefin where in 1-hexene was subjected to hydroboration reaction followed by the esterification of the hexanol with different organic acids. The detailed synthetic procedure for the process is given below.

4.3.3.1 Conversion of 1-hexene to esters

The conversion of 1-hexene to corresponding esters is depicted in scheme 4.3.



Scheme 4.3. Synthetic route for 1-hexene based esters (8a-c)

4.2.3.2 Hydroboration of 1-hexene

A mixture of 1-hexene (8.4 g, 0.10 mol) and THF (20 mL) was taken in a three necked (500 mL) RB flask equipped with dropping funnel, condenser and N₂ purging wall. The mixture was cooled for 5 mins at 0-5°C with continuous stirring. To the reaction mixture, BH₃/THF (40 mL, 0.42 mol) was added drop wise (1 drop/sec) while maintaining the temperature at 0-5°C for 1 hr. After the completion of addition, the

CHAPTER 4

reaction mixture was stirred for 1 hr at room temperature. It was then quenched with 1N of NaOH (20 mL) and 50% of H₂O₂ (20 mL, 0.85 mol) mixture at 0-5^o C with continuous stirring. The mixture was washed with methanol (15 mL) and the product was extracted using ethyl acetate and washed with excess of water. The organic phase was dried over sodium sulphate and the solvent was removed under reduced pressure to yield the final product 1-hexanol as white thick liquid (**7**) (yield 90-95%).

4.2.3.3 Esterification of 1-hexanol

Synthesis of ester (8a) from octanoic acid

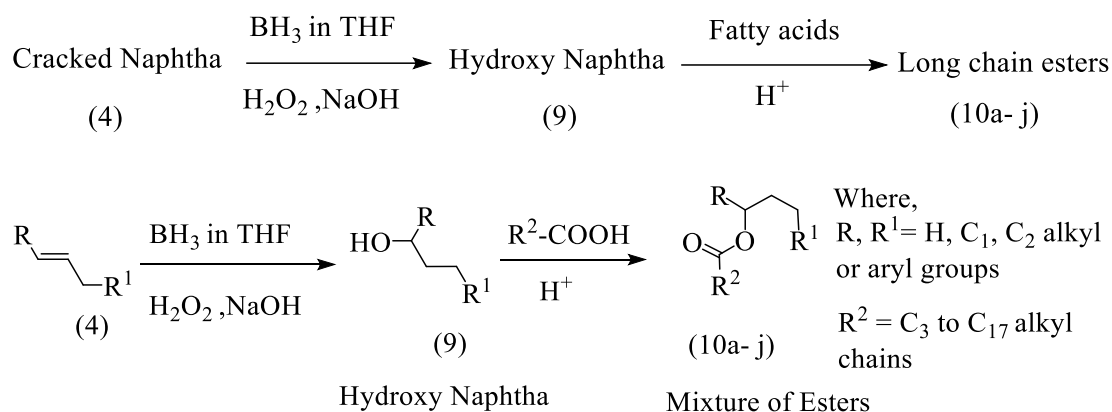
To a mixture of 1-hexanol (2g, 0.02 mol), PTSA (0.1g, 0.0006 mol) and toluene (40 mL), octanoic acid (2.8 g 0.02 mol) was added in a 100 mL RB flask. The flask was connected to dean-stark apparatus and kept in a heating mantle with magnetic stirrer and temperature controller. The reaction mixture was refluxed at 110°C with constant stirring. The water liberated during the reaction was removed using dean-stark apparatus. The progress of the reaction was monitored using thin layer chromatography. After completion of the reaction, the whole reaction mixture was cooled to room temperature. The product was extracted using ethyl acetate and the organic phase was washed with excess of water followed by 5 % sodium bicarbonate (200 mL) solution. The organic layer was filtered through sodium sulphate and the solvent was evaporated using rotary evaporator to get the product (8a) as dark yellow liquid (yield 88.4%).

Similarly, esters 8b and 8c were synthesized using the reactants hexanoic acid and butyric acid respectively.

4.2.3.4 Synthesis of esters from LCN

The conversion of LCN into mixture of esters is schematically depicted in scheme 4.4, considering a general structure (4) for the olefins present in the LCN. The hydroboration of LCN (200 g batch) was carried out following the same procedure described above for 1-hexene. The hydroxy LCN was subjected to esterification reaction with long chain (C₄-C₁₈ alkyl groups) organic acids following the procedure described above for the esterification of hexanol to get the final esters (10a-j). The chemical structures of all the esters are given in the Table 4.4.

CHAPTER 4

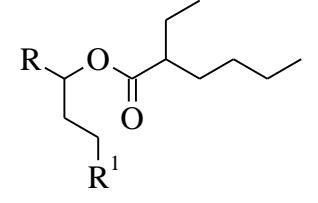
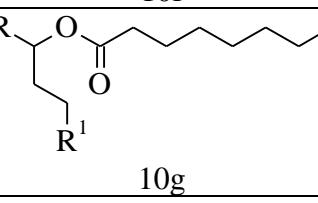
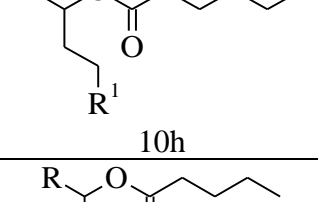
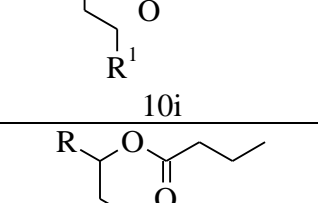
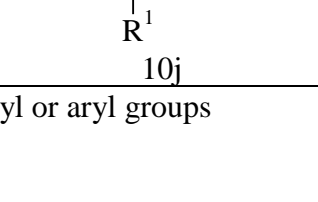


Scheme 4.4 Synthetic route for mixtures of esters (10a-j) from LCN through hydroboration reaction

Table 4.4. The chemical structures of LCN esters (10a-j)

Acid	Obtained Product
Stearic acid C ₁₈ H ₃₆ O ₂	<p style="text-align: center;">10a</p>
Palmitic acid C ₁₆ H ₃₂ O ₂	<p style="text-align: center;">10b</p>
Myristic acid C ₁₄ H ₂₈ O ₂	<p style="text-align: center;">10c</p>
Lauric acid C ₁₂ H ₂₄ O ₂	<p style="text-align: center;">10d</p>
Capric acid C ₁₀ H ₂₀ O ₂	<p style="text-align: center;">10e</p>

CHAPTER 4

2-Ethyl hexanoic acid $C_8H_{16}O_2$	 <p style="text-align: center;">10f</p>
Octanoic acid $C_8H_{16}O_2$	 <p style="text-align: center;">10g</p>
Hexanoic acid $C_6H_{12}O_2$	 <p style="text-align: center;">10h</p>
Pentanoic acid $C_5H_{10}O_2$	 <p style="text-align: center;">10i</p>
Butyric acid $C_4H_8O_2$	 <p style="text-align: center;">10j</p>

Where, R, R^1 = H, C_1 and C_2 alkyl or aryl groups

4.2.4 Tribological study

The lubricity study, analysis of scar and study of physical and chemical parameter of diesel fuel are detailed in chapter 3 (3.2.4).

4.3 RESULTS AND DISCUSSION

4.3.1 Structural characterization of epoxy hexane (EPHX) to corresponding esters (3a-c)

The conversion of 1-hexene (HX) to EPHX was confirmed by 2D gas chromatography mass spectra (GCXGC-MS) (Fig.4.3). The purity of the compound is indicated by the appearance of a sharp peak in both one dimensional and two-dimensional chromatogram (Fig.4.3a-b). Also, there is no unwanted signal in the density distribution spectrum which further confirms the purity of EPHX (Fig.4.3c).

CHAPTER 4

In the mass spectrum (Fig.4.3d), the peak at (m/z) 100.08 corresponds to molecular ion of EPHX.

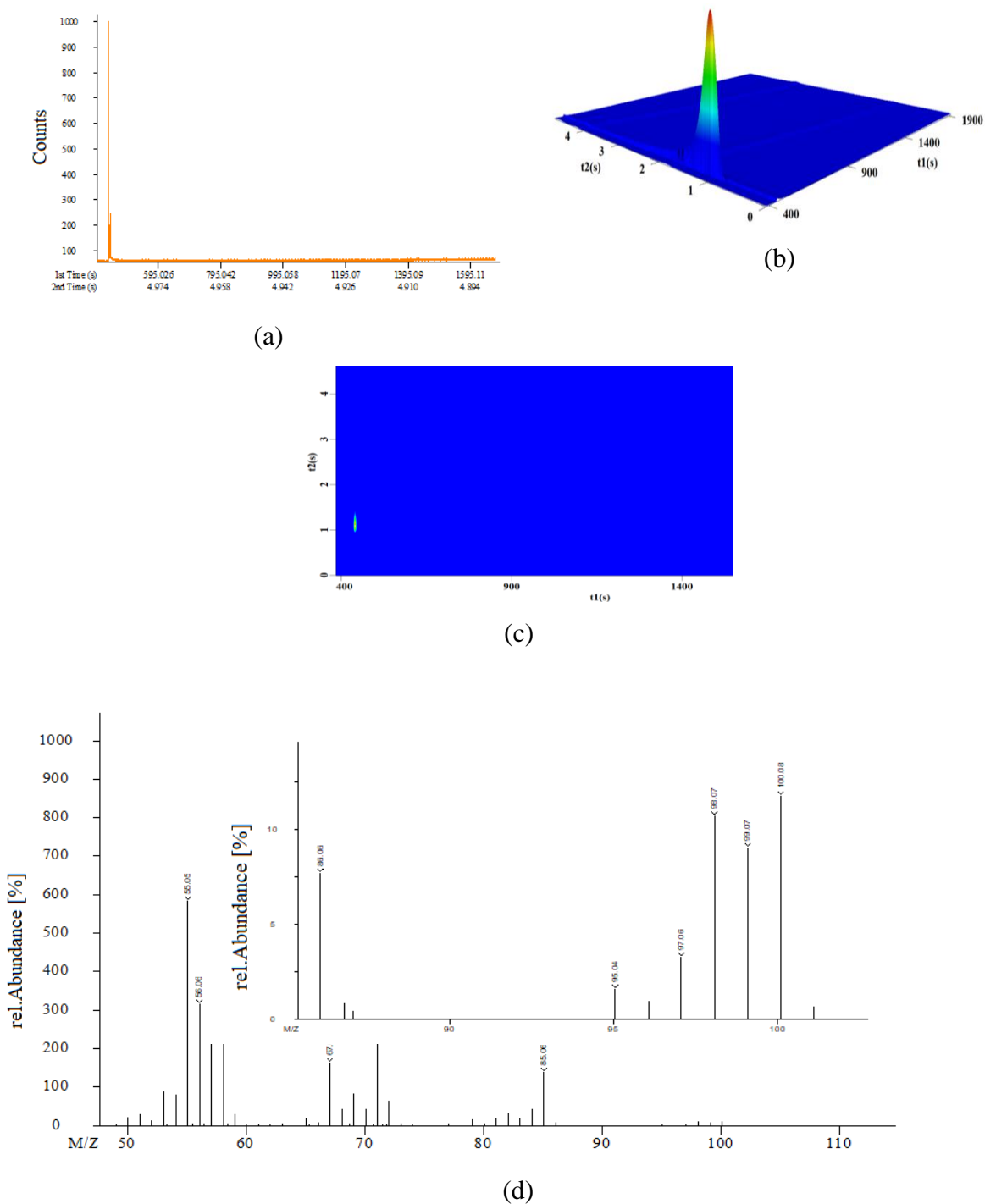


Fig.4.3. a) 1D gas chromatogram of EPHX b) 2D gas chromatogram of EPHX c) 2D density distribution spectrum of EPHX (Where, t_1 is the first dimensional retention, t_2 is the second dimensional retention) and d) mass spectrum obtained for EPHX.

CHAPTER 4

The 2D-gas chromatogram (Fig.4.4) and density distribution spectrum (Fig. 4.5) confirm the formation of the esters (3a-c). The chromatograms of all the esters exhibited single sharp peak with characteristic retention values. The mass spectra of the esters (Fig.4.6) displayed characteristic molecular ion peak corresponding to (m/z) 245.21 for 3a, 217.17 for 3b and 188.13 for 3c. With a decrease in the molecular weight of the product from 3a to 3c, the corresponding density distribution spectrum shifts from higher to lower period (from 3800 s to 2600 s) which further confirms the efficient conversion of EPHX to corresponding esters (3a-c).

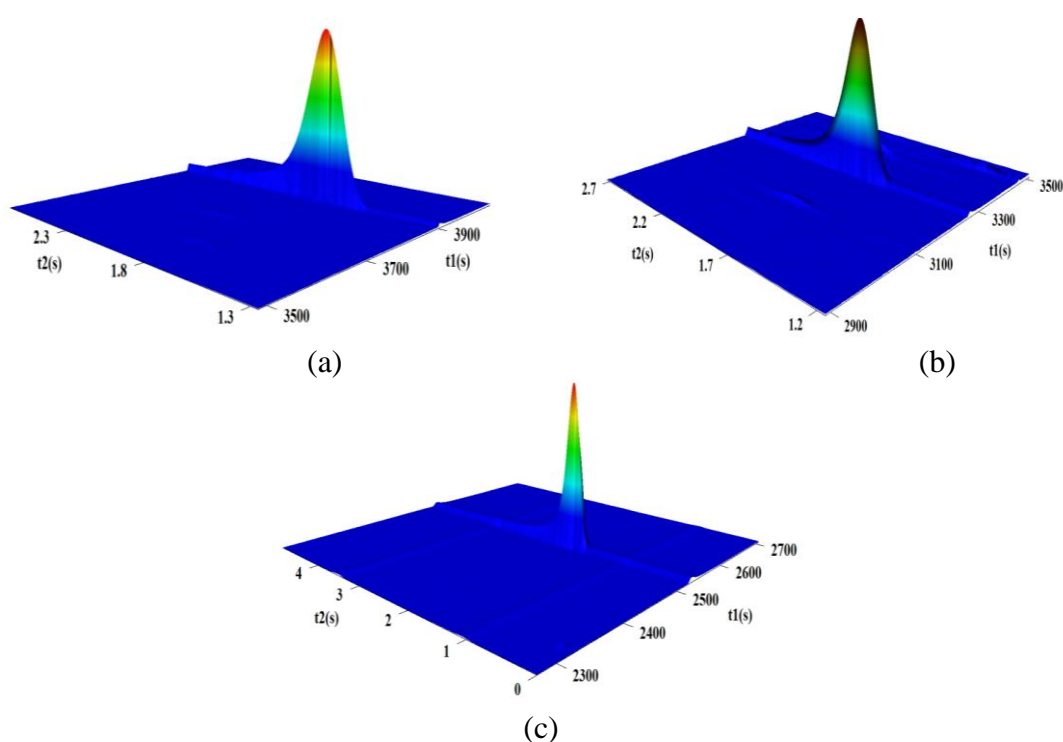
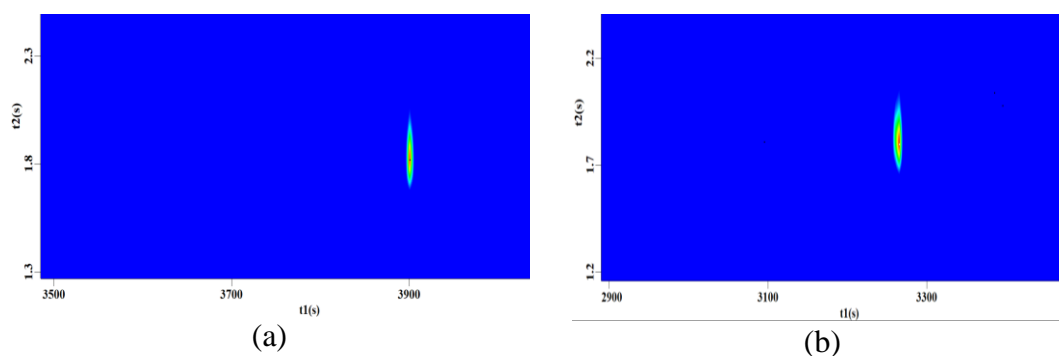
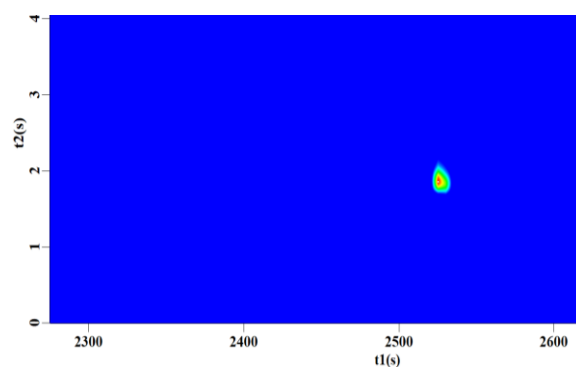


Fig.4.4 2D gas chromatogram of a) 3a, b) 3b and c) 3c (Where, t_1 is the first dimensional retention, t_2 is the second dimensional retention).





(c)

Fig.4.5 2D density distribution spectra of a) 3a, b) 3b and c) 3c (Where, t_1 is the first dimensional retention, t_2 is the second dimensional retention).

Further to confirm chemical structure, esters (3a-c) were purified through column chromatography using ethyl acetate: hexane (40:60) as the mobile phase and silica 100- 200 mesh as the stationary phase and the purified samples were characterised using FTIR spectroscopic technique. The FTIR spectra (Fig.4.7) displayed a strong band at around 1730 cm^{-1} corresponding to -C=O stretching of the ester group as well as a broad OH band in the region $3458\text{-}3523\text{ cm}^{-1}$ along with other characteristic peaks. There is no absorption band corresponding to C=O of carboxylic acid group which indicates the purity of the final products. Similar to hexane hydroxy esters, the LCN hydroxy esters (6a-j) also showed characteristic absorption bands in the FTIR spectra (Fig.4.8). The absorption band for -C=O stretching of the ester group was observed in the region $1713\text{-}1715\text{ cm}^{-1}$ whereas broad O-H bands appeared at $3401\text{-}3443\text{ cm}^{-1}$. The FTIR spectral data are given below.

3a: IR (ATR, cm^{-1}): 3506 (OH), 2932, 2864, 1733 (C=O from ester) 1172 and 1100.

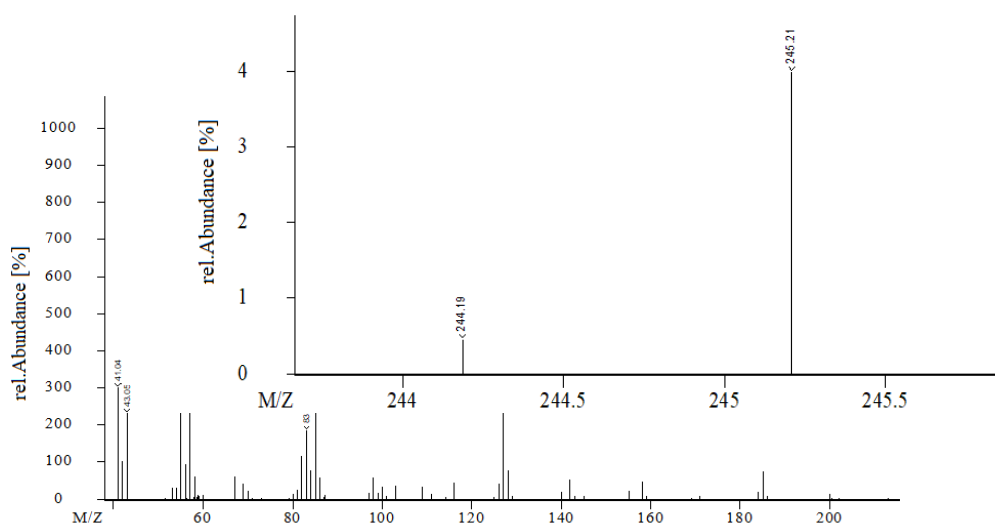
3b: IR (ATR, cm^{-1}): 3458 (OH), 2943, 2867, 1731 (C=O from ester), 1173 and 1100.

3c: IR (ATR, cm^{-1}): 3523 (OH), 2944, 2867, 1731 (C=O from ester), 1173 and 1100.

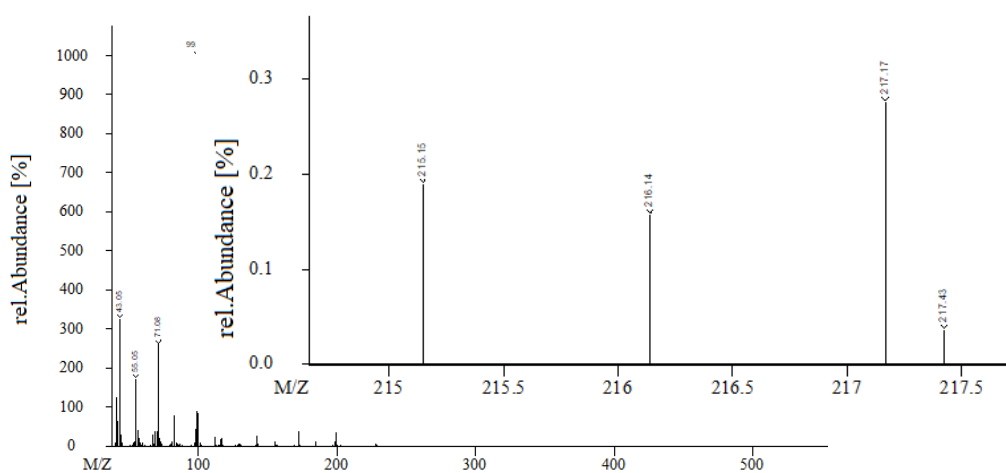
6a: IR (ATR, cm^{-1}): 3443 (OH), 2925, 2860, 1713 (C=O from ester) 1455, 1378 and

1244. **6j:** IR (ATR, cm^{-1}): 3401 (OH), 2928, 2861, 1715 (C=O from ester), 1451, 1383 and 1245.

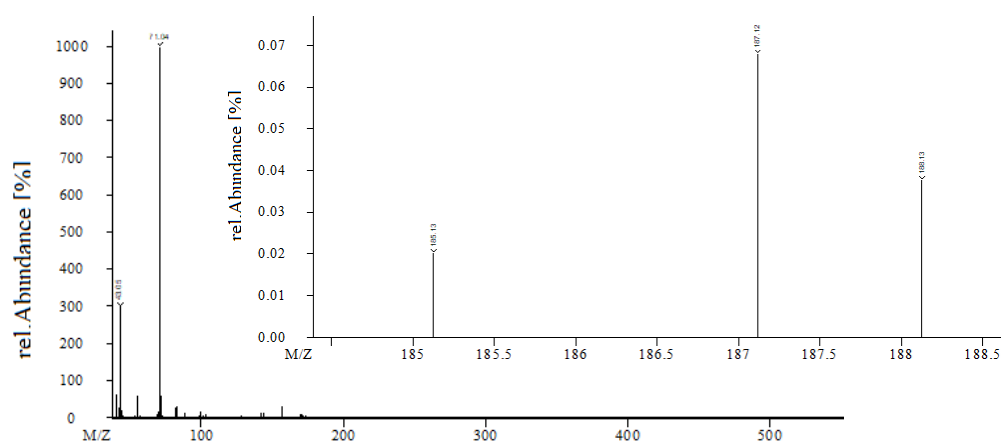
CHAPTER 4



(a)



(b)



(c)

Fig.4.6 Mass spectra obtained for a) 3a, b) 3b and c) 3c.

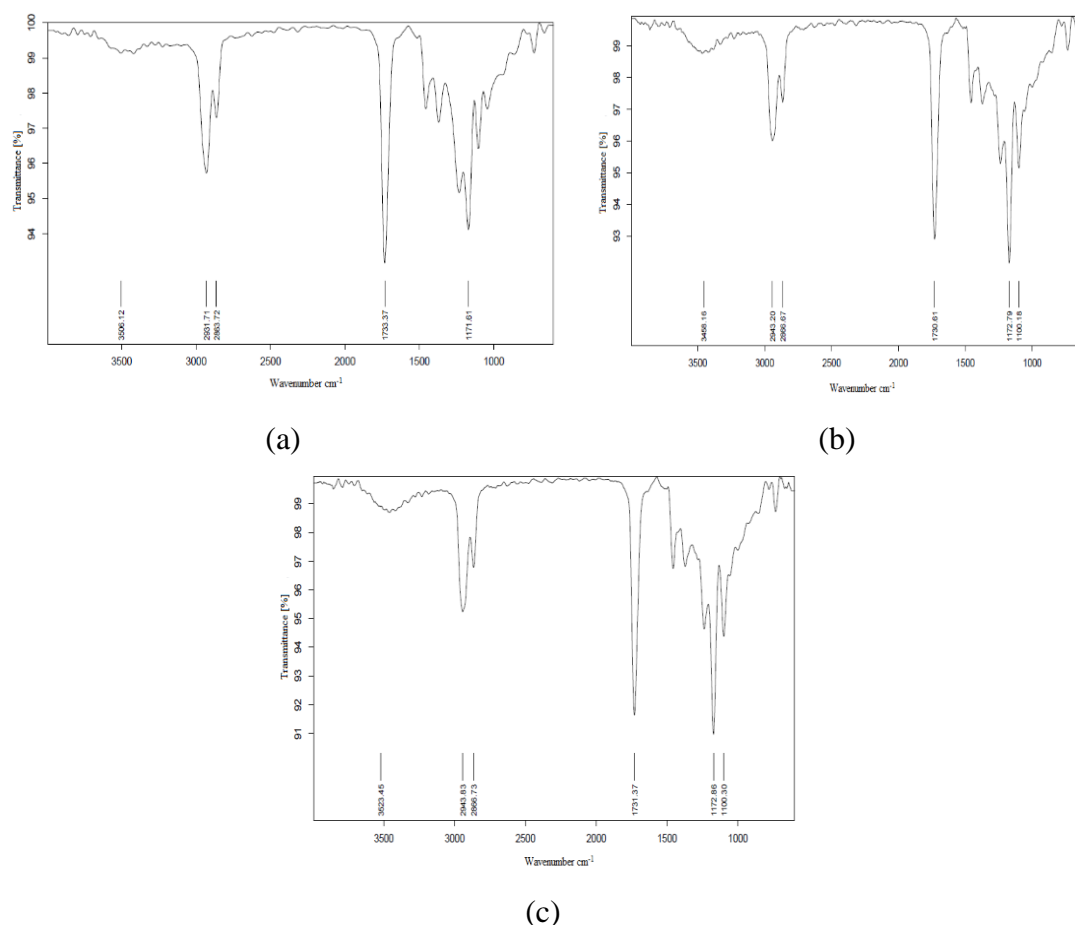


Fig.4.7 FTIR spectra of a) 3a, b) 3b and c) 3c).

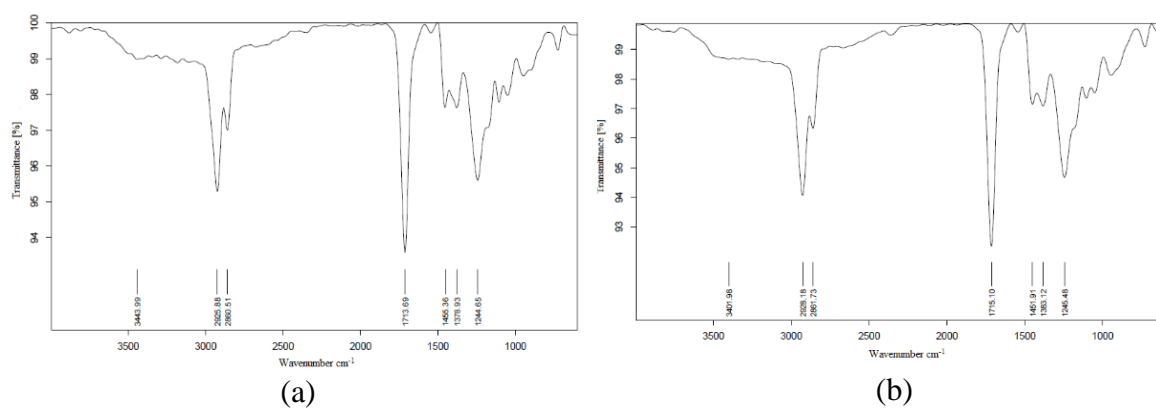


Fig.4.8 FTIR spectra of a) 6a and b) 6j.

4.3.2 Structural characterization of hexanol and corresponding esters (8a-c)

The single sharp peak observed in both 1D (Fig.4.9 a) 2D gas chromatogram (Fig.4.10a) of hexanol (HL) confirms the purity of the sample. Also, there is no unwanted signal in the density distribution spectrum which further confirms its purity. The IR spectrum of HL displayed a broad OH band at 3369 cm^{-1} (Fig.4.13a).

CHAPTER 4

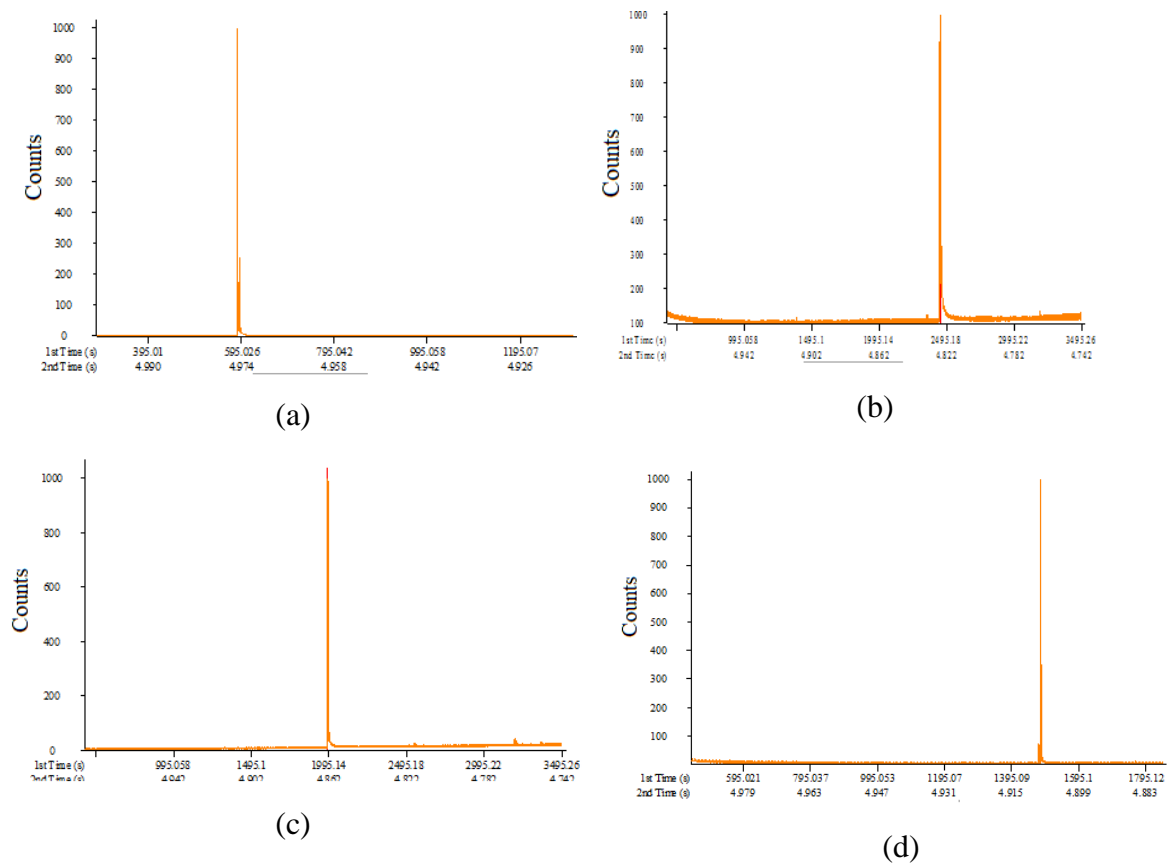
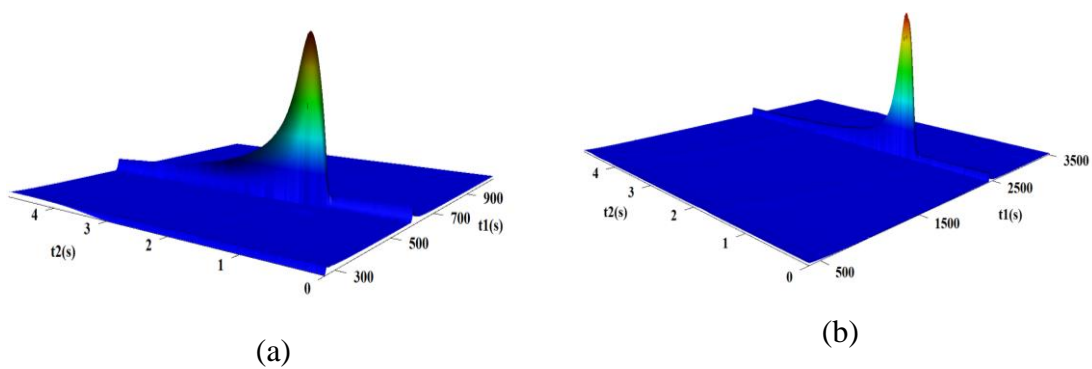


Fig.4.9 Gas chromatogram obtained for a) HL, b) 8a, c) 8b and d) 8c.



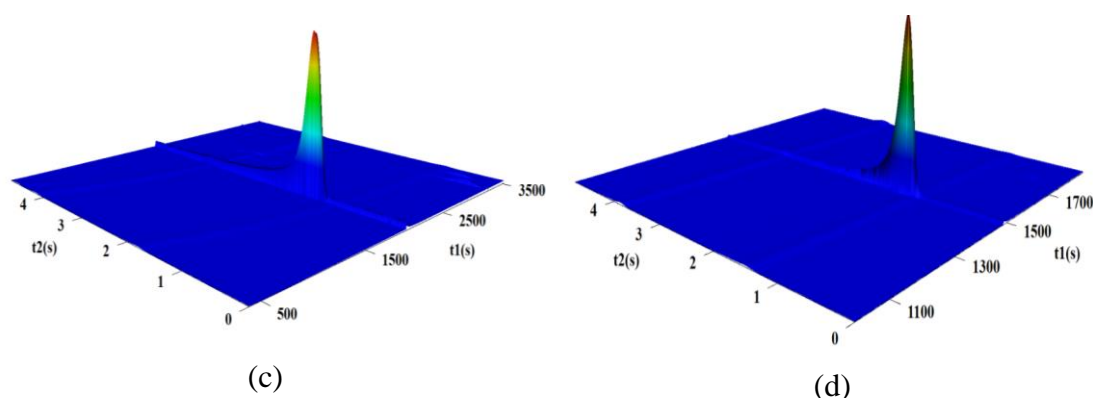
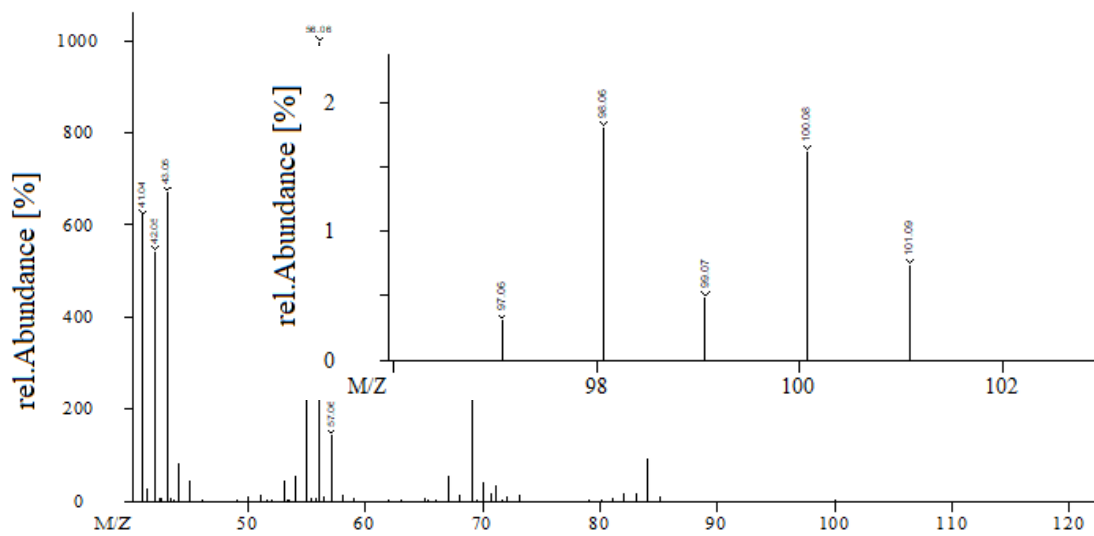


Fig.4.10 2D gas chromatogram of a) HL, b) 8a, c) 8b and d) 8c. (t_1 is the first dimensional retention, t_2 is the second dimensional retention).

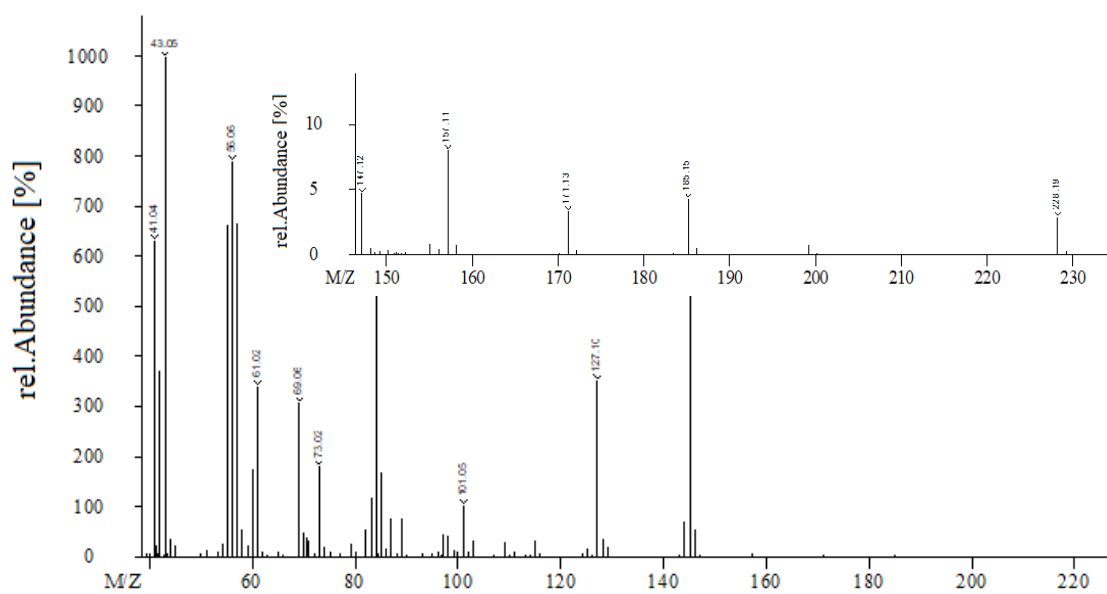
The 1D gas chromatogram (Fig.4.9 b-d), two-dimensional chromatogram (Fig.4.10b-d), mass spectra (Fig. 4.11 b-d), density distribution spectra (Fig.4.12 b-d), and IR spectra (Fig.4.13 b-d) confirm the formation of the esters (8a-c). The purity of the samples was established by the single sharp peak detected in both one and two-dimensional gas chromatogram. The mass spectra of the esters (Fig.4.11 b-c) displayed characteristic molecular ion peak corresponding to (m/z) 228.15 for 8a, 200.18 for 8b and 172.13 for 8c. With an increase in the molecular weight of the product from 8c to 8a, the corresponding density distribution spectra shifts from lower to higher period (from 1500s to 2500 s) which further confirms the efficient conversion of HL to corresponding esters (8a-c). The FTIR spectra of samples (8a-c) displayed a strong band in the range of $1733\text{--}1736\text{ cm}^{-1}$ corresponding to -C=O stretching of the ester group along with other characteristic peaks. The broad OH band and band corresponding to C=O of carboxylic acid group were absent in the spectra which further confirms the completion of the reaction and the purity of the final products. The FTIR spectral data of HL and (8a-c) are given below.

HL: IR (KBr, cm^{-1}): 3370 (OH), 2952, 2871, 1720, 1457, 1370, 1053 and 670. **8a:** IR (KBr, cm^{-1}): 2926, 2881, 1737 (C=O from ester), 1461 and 1170. **8b:** IR (KBr, cm^{-1}): 2931, 2865, 1737 (C=O from ester), 1461 and 1172. **8c:** IR (KBr, cm^{-1}): 2931, 2885, 1733 (C=O from ester), 1357 and 1178.

CHAPTER 4

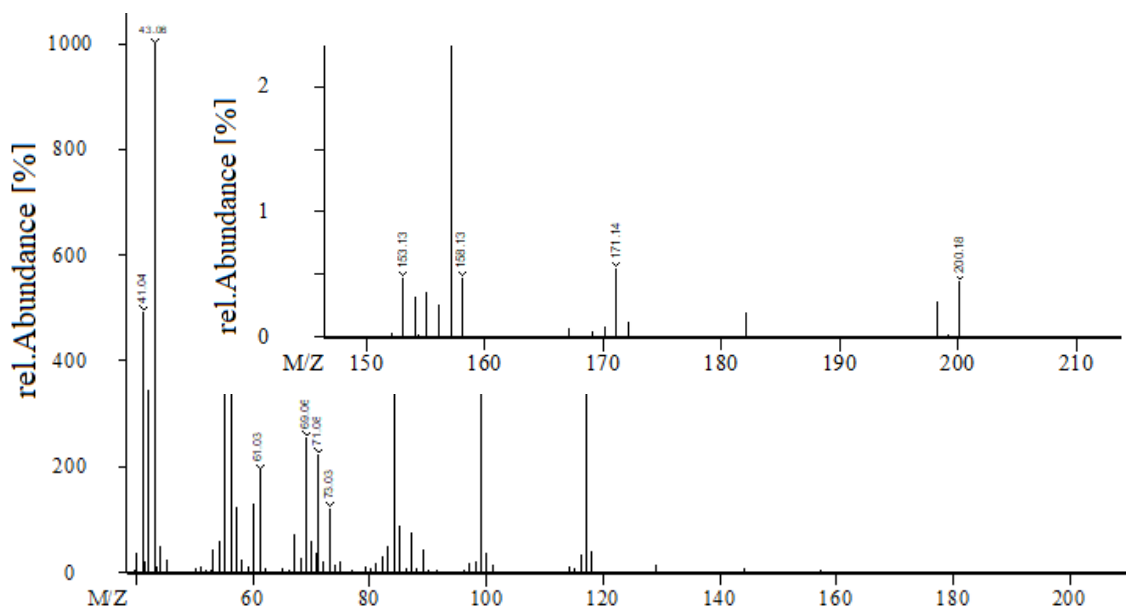


(a)

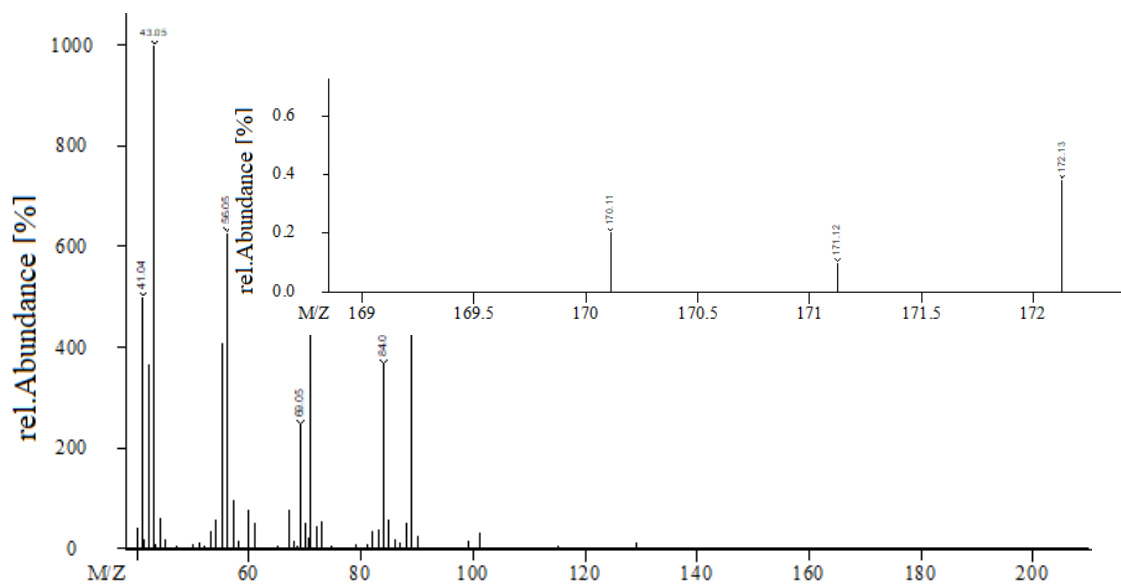


(b)

CHAPTER 4



(c)



(d)

Fig.4.11 Mass spectra obtained for a) HL, b) 8a, c) 8b and d) 8c.

CHAPTER 4

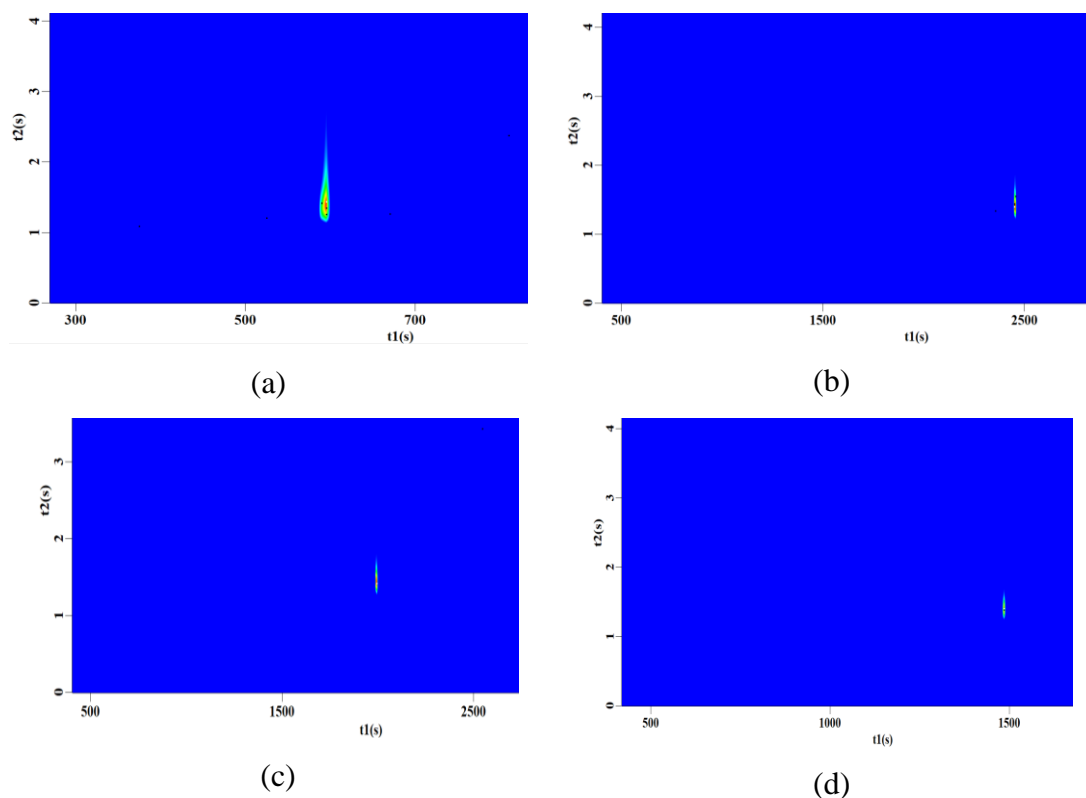
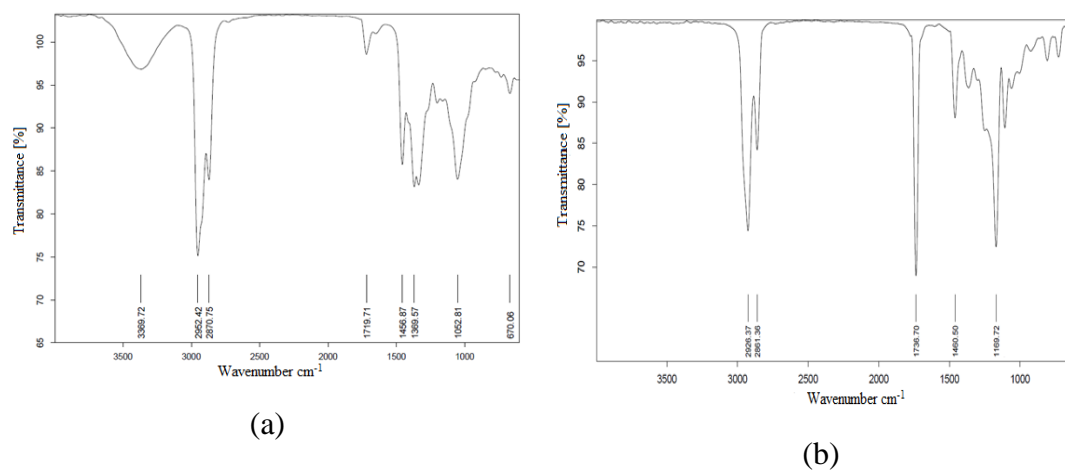


Fig.4.12 2D density distribution spectra of a) HL, b) 8a, c) 8b and d) 8c. (t₁ is the first dimensional retention, t₂ is the second dimensional retention).



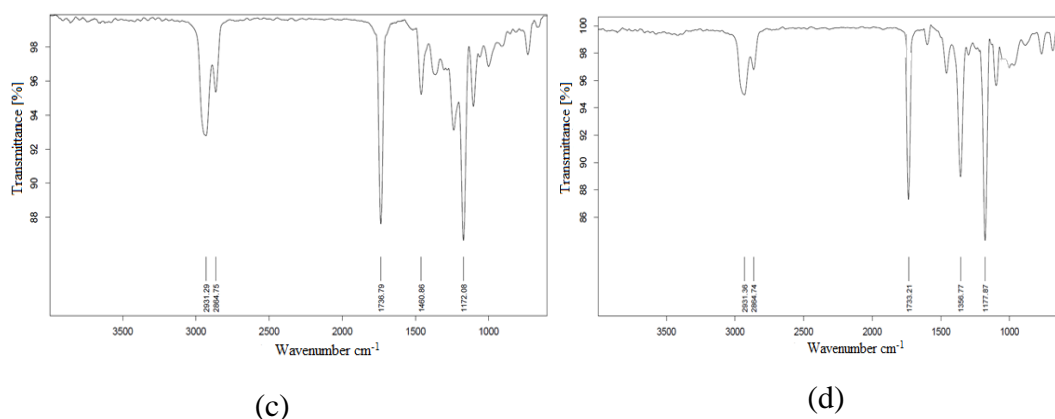


Fig.4.13 FTIR spectra of a) HL b) 8a c) 8b and d)8c.

4.3.3 Structural characterization of hydroxy LCN (HLCN) and LCN esters (ELCN) (10a-j)

The 1D and 2D gas chromatograms (Fig.4.14a and 4.15a) as well as the 2D density distribution spectrum (Fig.4.14b) of hydroxy LCN (HLCN) displayed multiple peaks indicating the presence of a mixture of LCN-based hydroxy compounds. The compounds are identified tentatively based on the GC traces and the details are given in Table 4.5. The 2D gas chromatogram of HLCN displayed peaks in the range of 415-1330s whereas for the ELCN, peaks were observed in the range of 2200-3700s (Fig. 4.15b) which confirms the successful conversion of HLCN to ELCN. The FTIR spectrum of HLCN displayed a broad OH band at 3348 cm^{-1} whereas in the case of ELCN (10e), a strong band appeared at 1734 cm^{-1} corresponding to -C=O stretching of the ester group (Fig.4.16). The mass spectrum of major component of 10e confirms the presence of molecular ion peak at m/z 257.26 (Fig.4.17).

The FTIR spectral data of HLCN and ELCN (10e) are given below.

HLCN: IR (KBr, cm^{-1}): 3349 (OH), 2948, 2876, 1455, 1386, 1047 and 669. **ELCN (10e):** IR (KBr, cm^{-1}): 2926, 2860, 1734 (C=O from ester), 1458, 1372, 1174, 1109 and 725.

Table 4.5: The composition of HLCN identified through 2D-GCMS

Alcohol	Formula	Retention time
3-Methyl-2-pentanol	$\text{C}_6\text{H}_{14}\text{O}$	415.007 s, 1.643 s
2-Methyl-1-pentanol	$\text{C}_6\text{H}_{14}\text{O}$	505.014 s, 1.858 s
2-Methylcyclopentanol	$\text{C}_6\text{H}_{12}\text{O}$	525.016 s, 2.374 s
1-Pentanol	$\text{C}_5\text{H}_{12}\text{O}$	375.004 s, 1.631 s

CHAPTER 4

Cyclopentanol	C ₅ H ₁₀ O	405.006 s, 2.180 s
2-Methyl-3-pentanol	C ₆ H ₁₄ O	380.004 s, 1.478 s
3-Hexanol	C ₆ H ₁₄ O	425.008 s, 1.635 s
2-Hexanol	C ₆ H ₁₄ O	435.008 s, 1.666 s
2,3-Dimethyl-1-butanol	C ₆ H ₁₄ O	490.013 s, 1.902 s
3-Methylcyclohexanol	C ₇ H ₁₄ O	645.025 s, 2.351 s
2-Methyl-1-hexanol	C ₇ H ₁₆ O	755.034 s, 2.124 s
1-Hexanol	C ₆ H ₁₄ O	590.021 s, 2.092 s
4-Methyl-2-pentanol	C ₆ H ₁₄ O	360.002 s, 1.383 s
3-Methyl-1-pentanol	C ₆ H ₁₄ O	535.016 s, 1.981 s
2-Ethyl-1-butanol	C ₆ H ₁₄ O	525.016 s, 1.953 s
1,3-Dimethylcyclopentanol	C ₇ H ₁₄ O	610.022 s, 2.470 s
(Z)-3-Hepten-2-ol	C ₇ H ₁₄ O	620.023 s, 2.329 s
cis-2-Methylcyclohexanol	C ₇ H ₁₄ O	760.034 s, 2.920 s
4-Heptanol	C ₇ H ₁₆ O	580.02 s, 1.833 s
3-Methyl-2-hexanol	C ₇ H ₁₆ O	625.024 s, 2.001 s
Cyclohexanol	C ₆ H ₁₂ O	625.024 s, 2.962 s
Cycloheptanol	C ₇ H ₁₄ O	775.036 s, 2.781 s
4-Methyl-3-hexanol	C ₇ H ₁₆ O	610.022 s, 1.949 s
Cyclopentanemethanol	C ₆ H ₁₂ O	675.028 s, 2.910 s
cis-4-Methylcyclohexanol	C ₇ H ₁₄ O	670.027 s, 2.454 s
trans-4-Methylcyclohexanol	C ₇ H ₁₄ O	655.026 s, 2.415 s
5-Methyl-3-Hexanol	C ₇ H ₁₆ O	655.026 s, 2.000 s
2-Pentanol	C ₅ H ₁₂ O	670.027 s, 2.013 s
4-Heptanol	C ₇ H ₁₆ O	640.025 s, 1.925 s
2,3-Dimethyl-1-pentanol	C ₇ H ₁₆ O	650.026 s, 1.986 s
1-Cyclopropylpentan-1-ol	C ₈ H ₁₆ O	980.052 s, 2.615 s
4-Methyl-3-hexanol	C ₇ H ₁₆ O	600.022 s, 1.914 s
5-Methyl-3-hexanol	C ₇ H ₁₆ O	550.018 s, 1.787 s
3-(2,2-dimethylpropoxy)-butan-2-ol	C ₉ H ₂₀ O ₂	830.04 s, 1.299 s
(Z)-3-Penten-1-ol	C ₅ H ₁₀ O	360.002 s, 1.795 s
4-Butoxy-1-butanol	C ₈ H ₁₈ O ₂	1330.08 s, 3.089 s
trans-3-Methylcyclohexanol	C ₇ H ₁₄ O	780.036 s, 2.954 s
3-Methyl-1-hexanol	C ₇ H ₁₆ O	765.035 s, 2.215 s
Cyclohexanemethanol	C ₇ H ₁₄ O	830.04 s, 2.871 s
3-Ethyl-2-pentanol	C ₇ H ₁₆ O	620.023 s, 2.116 s
3-Methyl-3-pentanol	C ₆ H ₁₄ O	350.002 s, 1.593 s
4-Methylcyclohexanol	C ₇ H ₁₄ O	800.038 s, 2.834 s
cis-2-Ethyl-2-hexen-1-ol	C ₈ H ₁₆ O	930.048 s, 2.659 s
3-Octanol	C ₈ H ₁₈ O	845.041 s, 2.051 s
2,6-Dimethylcyclohexanol	C ₈ H ₁₆ O	885.044 s, 2.649 s

CHAPTER 4

4-Ethylcyclohexanol	$C_8H_{16}O$	905.046 s, 2.622 s
11-Methyldodecanol	$C_{13}H_{28}O$	1445.09 s, 1.811 s
2,4-Dimethylcyclohexanol	$C_8H_{16}O$	800.038 s, 2.389 s

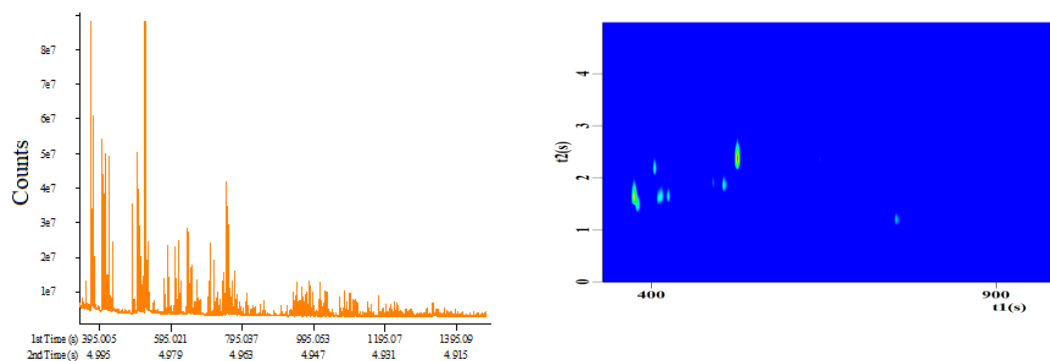


Fig.4.14 a) Gas chromatogram of HLCN and b) 2D density distribution spectrum of HLCN

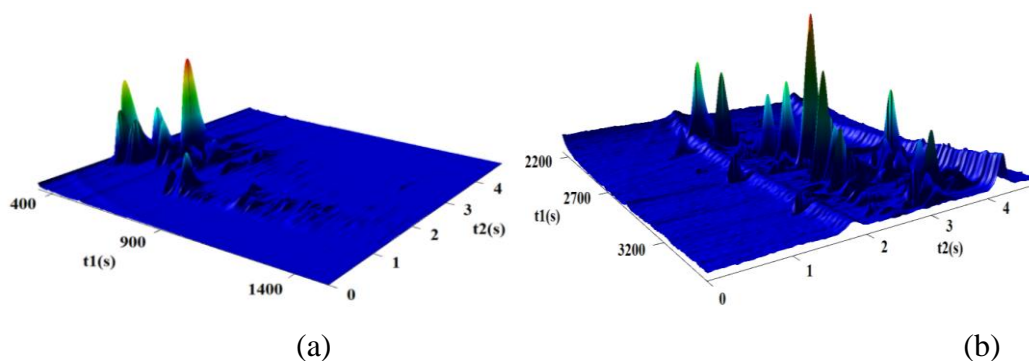


Fig.4.15 2D gas chromatogram of a) HLCN and b) ELCN (10e) (t1 is the first dimensional retention, t2 is the second dimensional retention).

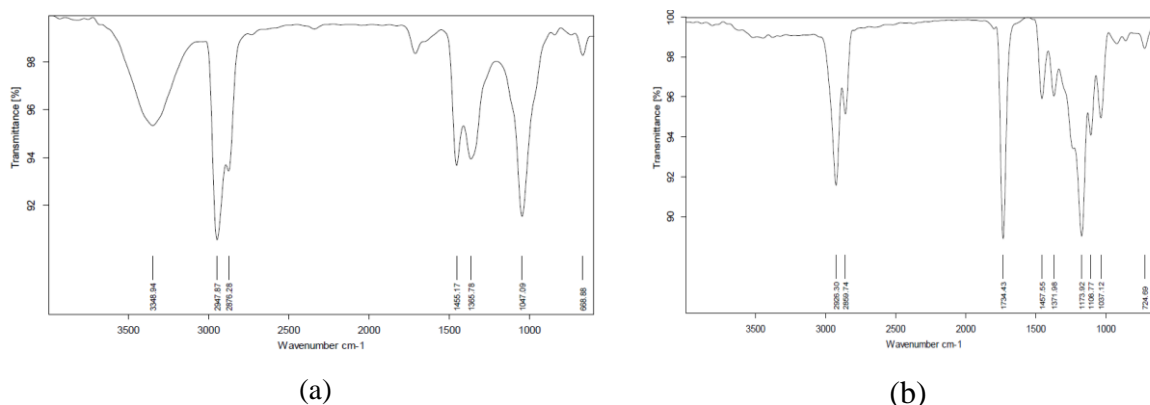


Fig.4.16 FTIR spectra of a) HLCN and b) ELCN (10e).

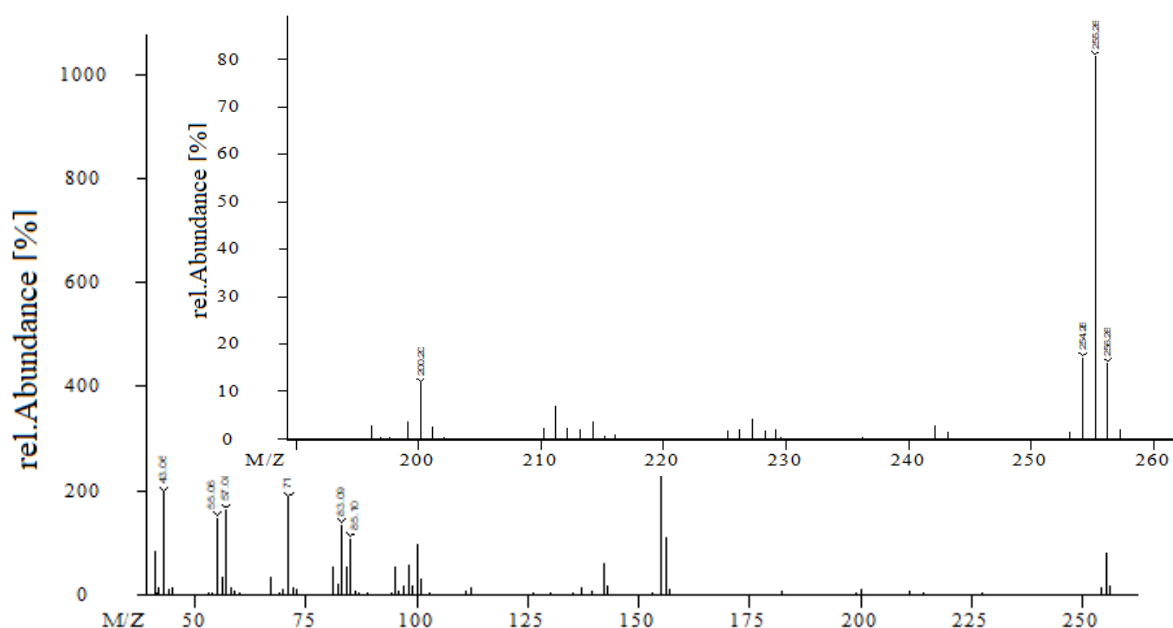


Fig.4.17 Mass spectrum of major peak identified in ELCN (10e). Inset shows the enlarged spectrum in the region m/z 190 – 260.

4.4. LUBRICITY ANALYSIS

The lubricity of (3a-c), (6a-j), (8a-c) and (10a-j) was analysed through HFRR method at 60 °C. The WSD values of neat ULSD and blended ULSD are given in Table 4.6. The graphical representation of WSD value obtained for (3a-c)- ULSD, (6a-j)- ULSD, (8a-c) ULSD and (10a-j)- ULSD blends is given in Fig.4.18.

Table 4.6: The lubricity data of neat ULSD and blended ULSD (WSD values lower than 460 μm are represented in bold)

HFRR 60°C								
Sample ID	Conc. ppm	Wear scar diameter (μm)			Conc. ppm	Wear scar diameter (μm)		
		Ball, X	Ball, Y	WSD, μm (X+Y)/2		Ball X	Ball Y	WSD, μm (X+Y)/2
Neat, ULSD	NA	535	485	510	NA	NA	NA	NA
3a		445	408	427		420	385	403
3b		472	448	460		448	415	432
3c		504	458	481		482	451	467
6a		425	396	411		405	359	382
6b		436	408	422		420	375	398

CHAPTER 4

6c	150	440	412	426	300	428	384	406
6d		462	434	448		450	402	426
6e		466	438	452		442	410	426
6f		466	440	453		449	421	435
6g		485	452	469		472	438	455
6h		508	468	488		496	452	474
6i		515	485	500		518	490	504
6j		518	485	502		510	476	493
8a	150	468	402	435	300	447	407	427
8b		468	462	465		455	415	435
8c		499	441	470		507	419	463
10a		485	355	420		439	343	391
10b		468	382	425		442	358	400
10c		435	423	429		449	365	407
10d		458	440	449		457	395	426
10e		453	447	450		475	391	433
10f		456	462	459		500	374	437
10g		475	469	472		480	432	456
10h		490	474	482		505	431	468
10i		525	471	498		541	427	484
10j	530	474	502	503	473	488		

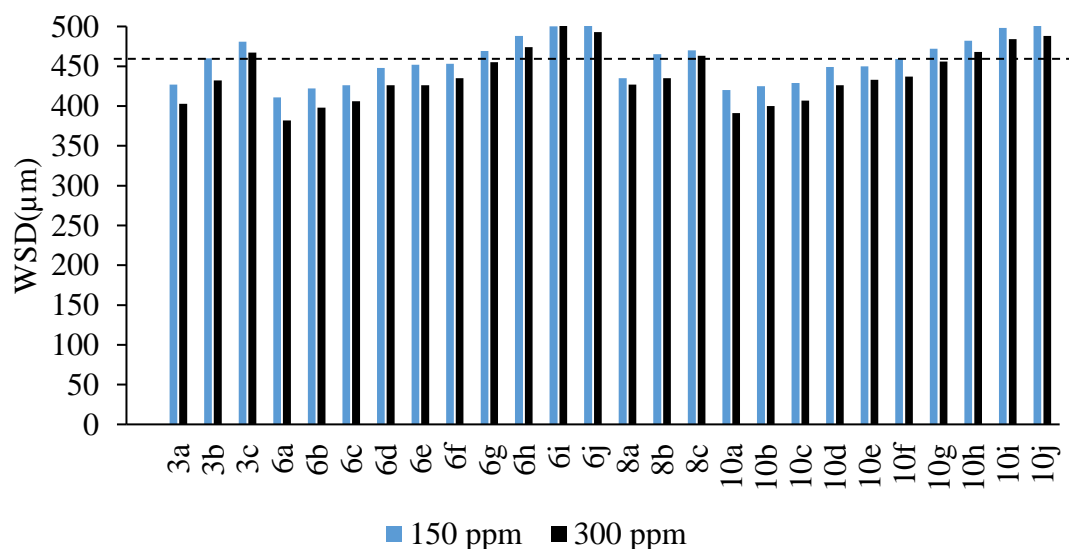
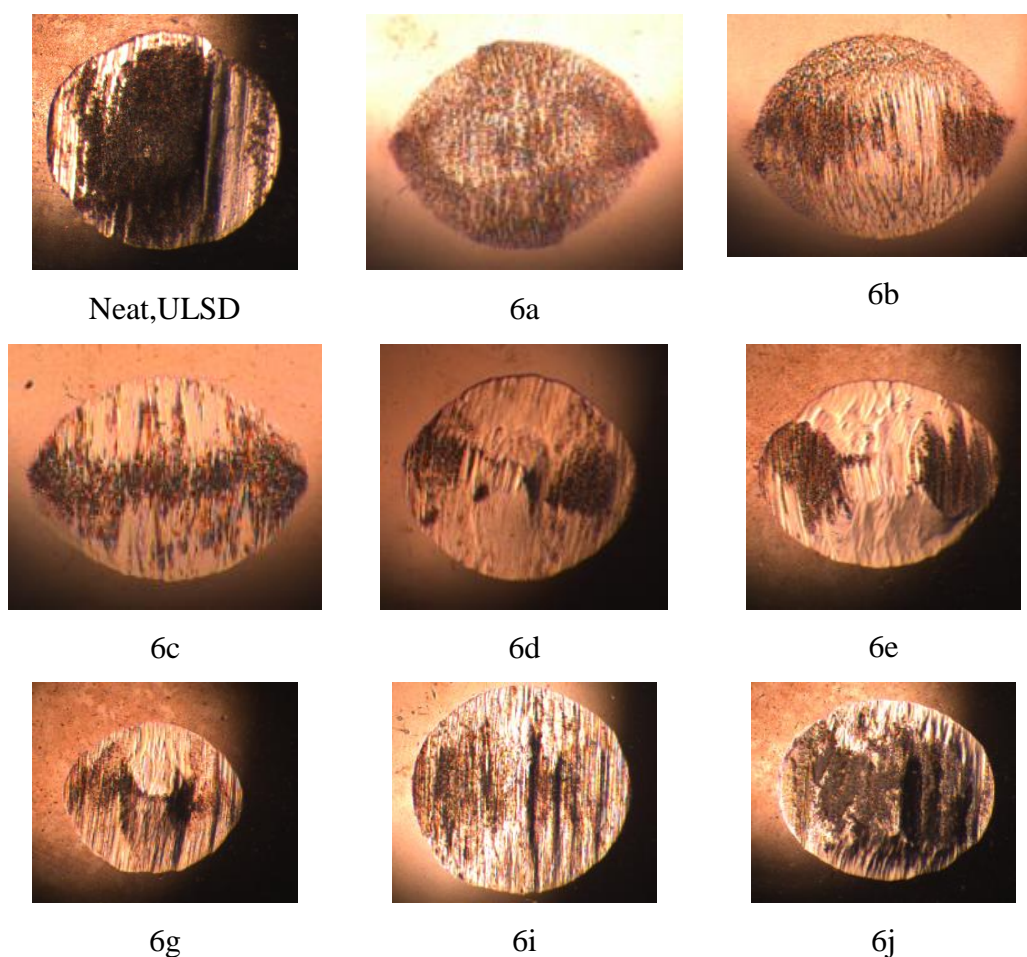


Fig.4.18 Graphical representation of WSD value obtained for (3a-c)- ULSD, (6a-j)- ULSD, (8a-c) ULSD and (10a-j)- ULSD blends (dotted line implies the accepted WSD value of 460 µm according to BS VI norms)

CHAPTER 4

Among different ULSD- ester (6a-j and 10a-j) blends, the least WSD value was observed for the blend with 6a (411 and 382 μm at 150 and 300 ppm respectively) as the additive. The optical microscopic images of the wear scars on the balls employed in lubricity measurement of neat ULSD and blended ULSD are shown in Fig.4.19. Almost all blend fuels except blends of (6h-j) and (10h-j) resulted minimum wear and scar on the surfaces. The LCN hydroxy esters (6a-j) show better lubricity than the LCN esters (10a-j), which could be due to additional polar hydroxyl group present in 6a-j. It is clear from the figure that with an increase in carbon chain length of the additives the film formation increases. As a result, the friction experienced between the metallic surfaces decreases which decreases the WSD value. These results indicate that the LCN esters are efficient lubricity improvers for ULSD.



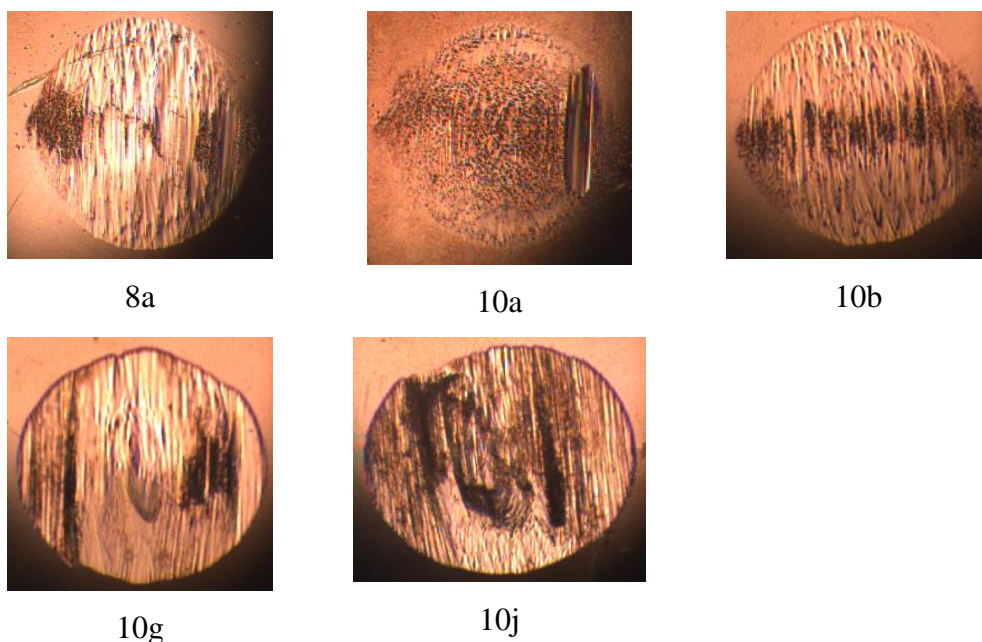


Fig.4.19 The optical microscopic images of wear and scar for neat ULSD, ULSD-additive blends (300 ppm).

4.5. PHYSIOCHEMICAL PARAMETERS STUDY

4.5.1 Evaluation of diesel property in ULSD blend

Different key parameters of the ester-ULSD blend fuels were analysed to verify the effect of the additives on diesel fuel properties. The results of the studies are tabulated in Table 4.7. It is clear from the data that there is no negative effect on key parameters of diesel fuel when it is blended with LCN based esters as lubricity improvers. In fact, the additives effectively increase the lubricity property of the blend fuel. Hence, the blended ULSD meets the Euro VI/BS VI fuel specifications.

Table 4.7 The key parameters of blended ULSD (150 ppm)

Parameter	Test method	Specification	Result	
			ULSD-6a	ULSD-10a
Acidity, Total, mg of KOH/g, <i>Max</i> *	ASTM D 974	0.2	0.048	0.041
Cetane Index, <i>Min</i> *	IP 380	46	56.2	56.0
Pour point, °C, <i>Max</i> *	ASTM D 5950	3 for winter 15 for summer	-30	-30

CHAPTER 4

Copper strip corrosion test 3 h at 50°C	ASTM D 130	Not worse than No.1	No.1	No.1
Distillation, 95% recovery, v/v, recovery, °C, <i>Max*</i>	ASTM D 86	360	343.7	340.5
Flash point, °C, <i>Min*</i>	IP 170	35	>100	>100
Kinematic viscosity, cSt at 40° C	ASTM D 445	2.0-4.5	3.069	3.053
Density @ 15° C, kg/m ³	ASTM D 4052	810-845	839.5	839.8
Total Sulphur, mg/Kg, <i>Max*</i>	ASTM D 5453	10	3.0	3.0
Lubricity, WSD at 60°C, microns, <i>Max*</i>	ASTM D 6079-18	460	411	420
Oxidation stability, g/m ³ , <i>Max*</i>	ASTM D 2274	25	9.5	9.0
Cold Filter Plugging Point (CFPP), °C	ASTM D 6371	6 for winter 18 for summer	-16	-16

4.6 MECHANISM OF TRIBOLOGICAL BEHAVIOUR OF ADDITIVES

The investigation of tribological behaviour of the lubricity improver towards metal surface was examined by analysing the metal surface morphologies of the friction couples through SEM and EDS techniques.

4.6.1 Analysis of wear scar using SEM

The SEM images of the wear scars on balls of the friction couples are shown in Fig.4.20. It is evident from the figure that scratching marks are very sharp for neat ULSD with high WSD of the metal surfaces. But for blended ULSD, the WSD of metal surface on the ball becomes smaller and the scratching marks also become thinner and shallower confirming the lubricating action of the LCN esters. The polar hydroxy and ester functional groups of the additives promote their absorption on the metal surface

CHAPTER 4

to form a lubricant protective film. The protective layer of lubricity additive minimizes the direct metal to metal contact and decreases the friction between the moving parts.

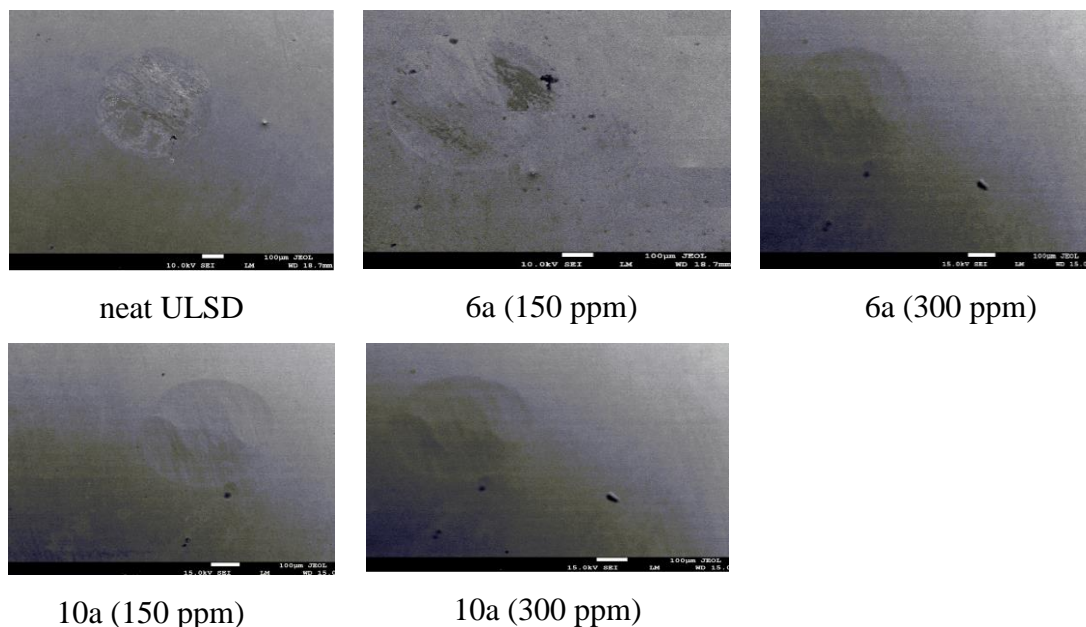


Fig.4.20 SEM images of the wear scars on balls of the friction couples with neat ULSD and blended ULSD

4.6.2 Analysis of wear scar using EDS

In order to identify the physical and chemical changes occurred during the friction process, EDS analysis of the metal surface of the balls was performed after the HFRR test. The EDS graph are shown in Fig.4.21. The spectral morphologies and the peak positions of elements C, O, Fe and Cr elements on the surfaces tested with neat ULSD and blended ULSD were compared. Higher oxygen content was observed on the metal surfaces lubricated with the blend fuel indicating the absorption of LCN esters on the metal surface through oxygen rich functional groups. With an increase in concentration of lubricity additive from 150 to 300 ppm, the oxygen percentage on metal surface increased from 5.1 to 9.1 % for 6a and 2.2 to 5.7 for 10a whereas, less oxygen content (0.8%) was found on the surfaces lubricated by the neat ULSD. Interestingly, higher oxygen content was found on the metal surface lubricated by 6a (9.1%) than 10a (5.7%), due to the presence of extra hydroxyl group in the carbon chain of 6a. These results reveal the interaction of oxygen-containing functional groups with the metal surface which assist in the formation of a protective layer of the additive

CHAPTER 4

between the metallic surfaces. Hence the friction experienced between moving metallic surfaces is reduced and the lubricative layer protects the surfaces from wear and tear.

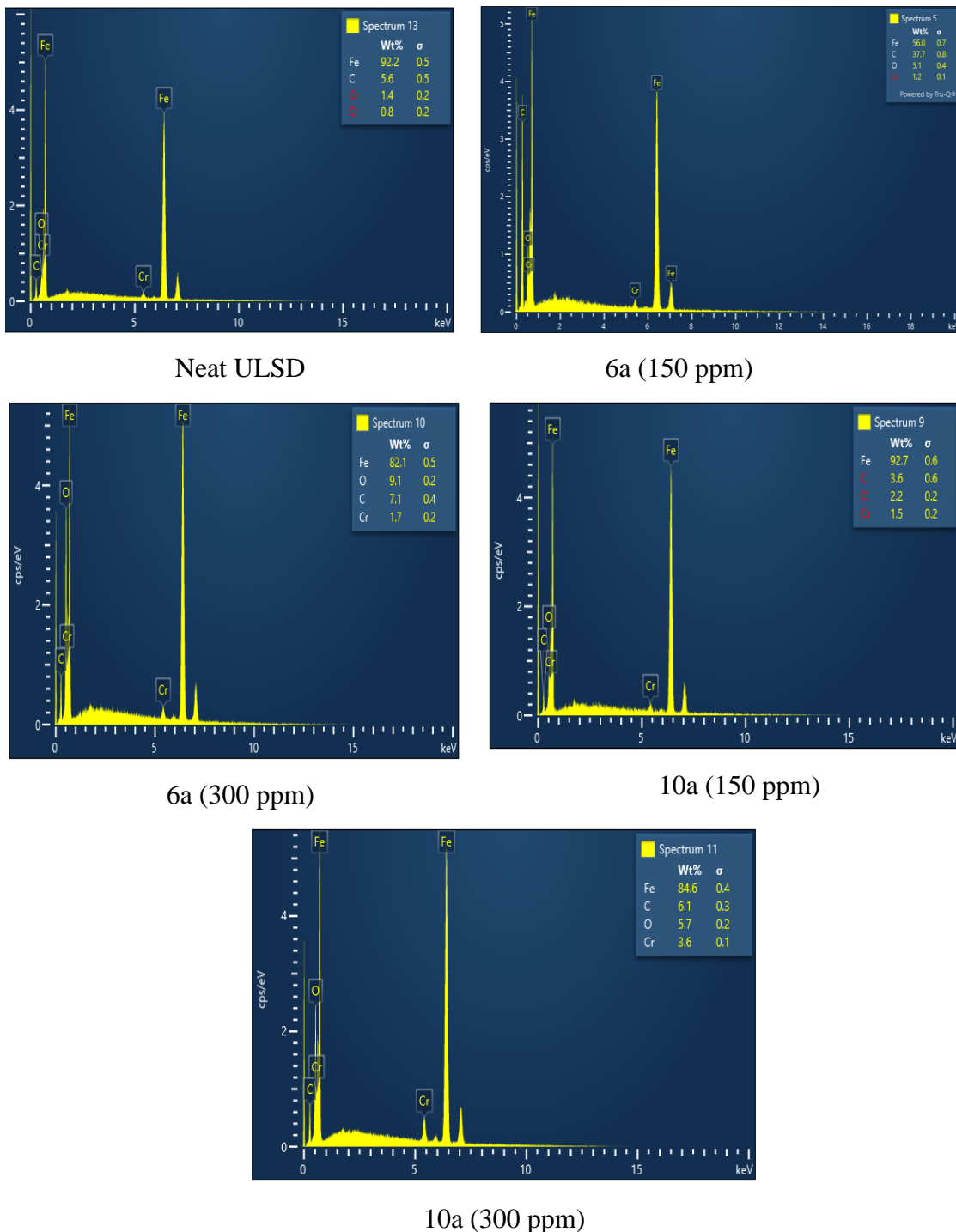


Fig.4.21 EDS graph of the metal surfaces with neat ULSD and blended ULSD

4.7 CONCLUSIONS

A novel series of LCN-based lubricity improvers (6a-j) and (10a-j) for ULSD was developed through a two-step chemical process which involved simple and cost-effective protocols such as epoxidation-esterification and hydroboration- esterification reactions. The LCN esters enhance the lubricity of ULSD significantly at a very low dosage level (150/300 ppm). The WSD of 6a is comparatively less than 10a it is due to the presence of extra hydroxy group in 6a. The studies revealed that all the lubricity improvers possess long term storage stability. Interestingly, there is no negative impact on the key physical and chemical parameters of the diesel fuel when blended with these additives. The polar hydroxy and ester functional groups of the additives favour the formation of protective lubricant film and enhance the lubricity of the blend ULSD. To conclude, the chemical process developed in the present study for ULSD additives is simple and the petroleum refineries (where the raw material LCN is available) could consider developing in-house low-cost additives as an alternative to the commercially available lubricity additives.

CHAPTER 5

CONVERSION OF LCN INTO LUBRICITY ADDITIVES FOR ULTRA-LOW SULPHUR DIESEL THROUGH A TWO-STEP PROCESS

Abstract:

This chapter comprises the synthesis of LI starting from light cracked naphtha through a maleation reaction protocol and study of lubricity property of newly synthesised LI through HFRR instrument. Also, it covers their structural characterization and lubricity mechanism on metal surfaces.

5.1 INTRODUCTION

As stated in the earlier section, LCN contains 40 - 45 vol% of olefins. Based on the promising lubricity properties of LCN esters (6a-j, 10a-j), it was planned to synthesize LCN based diesters following the maleation reaction protocol. Maleation reaction involves reaction between the maleic anhydride and olefins. The C-C double bond in the maleic anhydride generally undergoes Ene reaction with olefins at high temperatures (around 200-600°C) without the presence of any catalyst. Herein, we detailed the synthesis of diesters through simple maleation reaction of maleic anhydride with olefins of LCN followed by the esterification reaction of the adduct with different long alkyl chain alcohols.

5.2. EXPERIMENTAL PART

5.2.1 Materials and instruments

Maleic anhydride was purchased from Sigma Aldrich. A 2-liter pressure reactor was used for the maleation reaction. The details of the other instruments are given in chapter 3 (section 3.2.2).

5.2.2 Synthesis of LCN esters (15a-h)

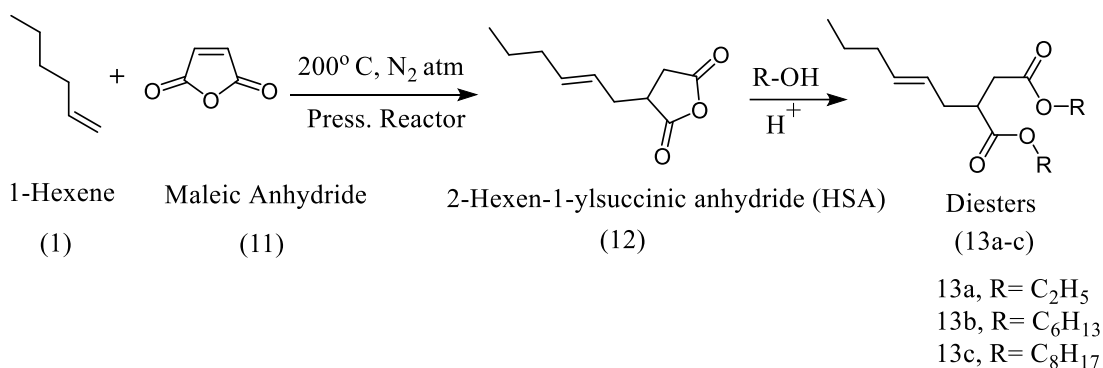
In this synthetic path, the LCN was exposed to maleation reaction to get the maleated naphtha, which was further esterified with different alcohols to get the mixture of diesters. The overall process was optimized using a neat olefin where in 1-hexene was converted to diester through maleation followed by the esterification reaction with

CHAPTER 5

different alcohols. A step-wise explanation of synthetic path for the process is given below.

5.2.2.1 Esters derived from 1-hexene

The preparation of diester from 1-hexene is shown in scheme 1.



Scheme 5.1. Synthetic route for 1-hexene based esters (13a-c)

5.2.2.2 Maleation of 1-hexene

A mixture of 1-hexene (200 g, 2.38 mol) and maleic anhydride (233 g, 2.38 mol) was taken in a pressure reactor vessel. After closing the reactor vessel, nitrogen gas was purged into it for 10 min. Then reaction mass was heated at 200 °C with continuous stirring (600 rpm) for 8h. The entire reaction mass was cooled to room temperature. Using ethyl acetate, the product was extracted, and the organic phase was thoroughly washed with excess of water. The solvent was removed under reduced pressure to get the crude product 2-hexen-1-ylsuccinic anhydride (12) as yellow liquid (yield 75%).

5.2.2.3 Esterification of 2-hexen-1-yl succinic anhydride: Synthesis of ester (13c) from n-octanol

To a mixture of 2-hexen-1-ylsuccinic anhydride (5g, 0.027 mol), PTSA (0.5g, 0.003 mol) and toluene (40 mL), octanol (7.1 g, 0.055 mol) was poured in a 100 mL round bottom flask. The flask was attached with Dean-Stark apparatus and placed in a heating mantle with a temperature controller and magnetic stirrer. The reaction mixture was refluxed at 110°C with continuous stirring. The liberated water during the reaction was removed, through the Dean-Stark apparatus. The progress of the reaction was monitored using thin layer chromatography. The entire reaction mass was cooled to

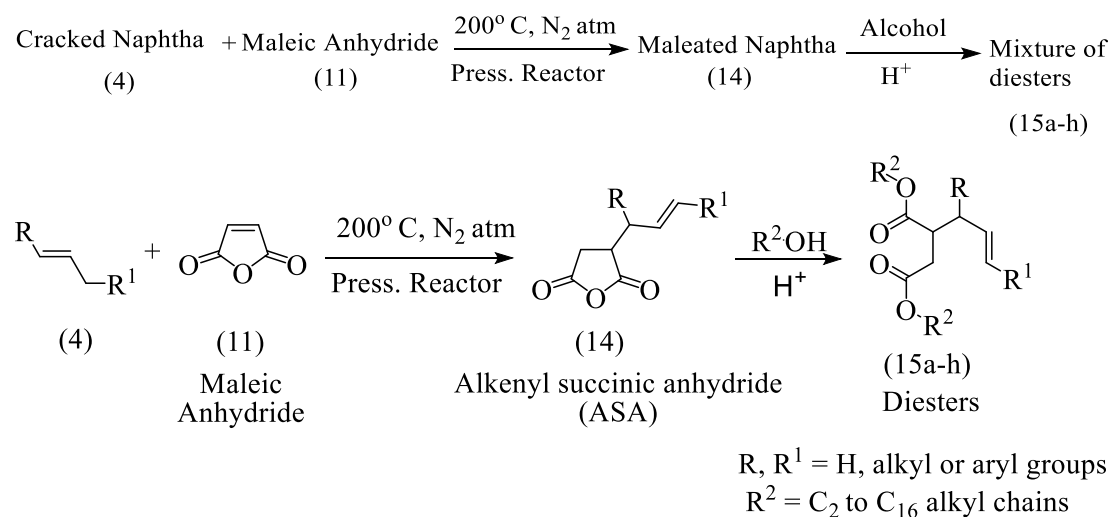
CHAPTER 5

room temperature. The product was extracted with ethyl acetate. The organic phase was thoroughly washed with excess water, dried using sodium sulphate. The solvent was removed under reduced pressure to get the product (13c) as dark yellow liquid (yield 89%).

Similarly, esters 13a (yield 85%) and 13b (yield 87%) were synthesized using the reactants ethanol and hexanol respectively.

5.2.2.4 Synthesis of diesters (15a-h) from LCN

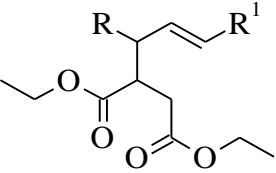
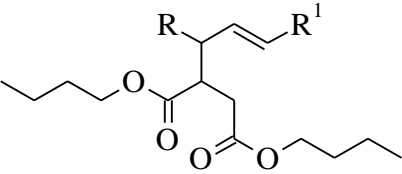
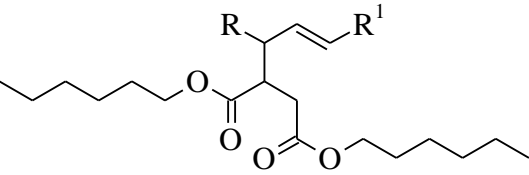
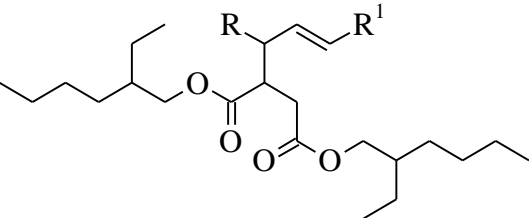
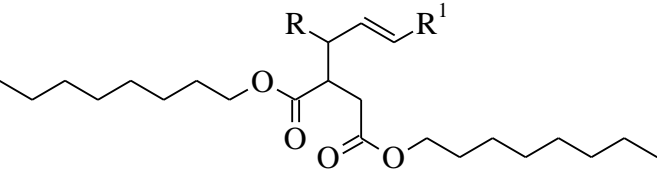
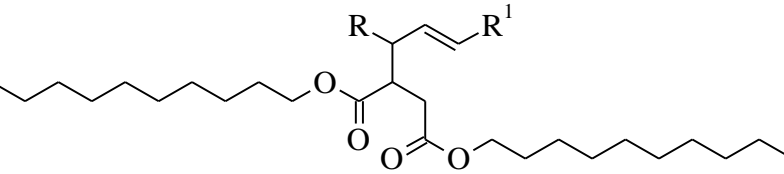
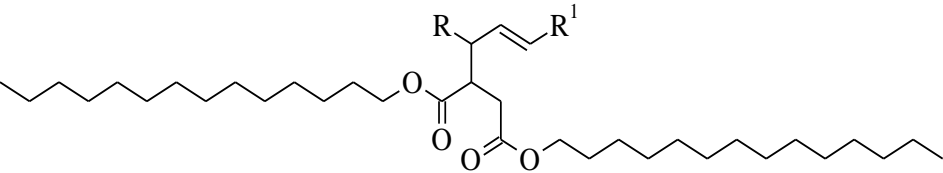
The synthesis of mixture of diesters from LCN is schematically represented in Scheme 5.2, considering a general structure (4) for the olefins present in the LCN. The maleation of LCN (200 g batch) and esterification of the maleated naphtha was performed as per the similar method described above for 1-hexene. The alcohol having C₂-C₁₆ alkyl groups are used for esterification of alkenyl succinic anhydride to get the final diesters (15a-h). The organic structures of all the diesters are described in the Table 5.1.

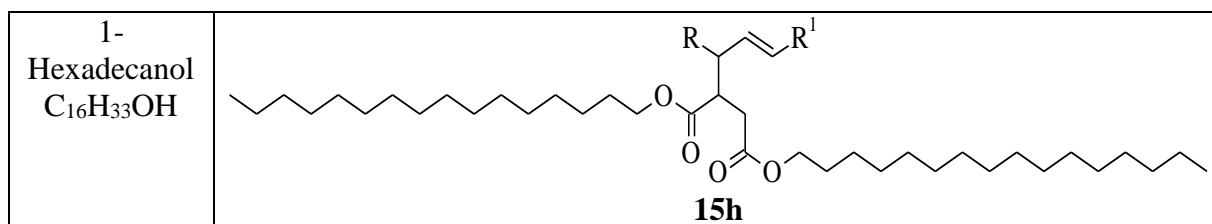


Scheme. 5.2 Synthesis of diesters (15a-h) from LCN through maleation reaction.

CHAPTER 5

Table 5.1: The chemical structures of LCN diesters (15a-h)

Alcohol	Obtained product
Ethanol C ₂ H ₅ OH	 <p style="text-align: center;">15a</p>
1-Butanol C ₄ H ₉ OH	 <p style="text-align: center;">15b</p>
1-Hexanol C ₆ H ₁₃ OH	 <p style="text-align: center;">15c</p>
2-Ethyl hexanol C ₈ H ₁₇ OH	 <p style="text-align: center;">15d</p>
1-Octanol C ₈ H ₁₇ OH	 <p style="text-align: center;">15e</p>
1-Decanol C ₁₀ H ₂₁ OH	 <p style="text-align: center;">15f</p>
1-Tetradecanol C ₁₄ H ₂₉ OH	 <p style="text-align: center;">15g</p>



Where, R, R¹ = H, alkyl or aryl groups

5.2.3 Test for friction

The lubricity study, analysis of scar and study of physical and chemical parameter of diesel fuel were carried out as described in chapter 3 (3.2.4).

5.3 RESULTS AND DISCUSSION

The n-hexene diesters (13a-c) were purified through column chromatography using ethyl acetate: hexane (40:60) as mobile phase and silica 100-200 mesh as stationary phase. The purified samples were characterised through 2D-GCMS and IR spectroscopic techniques to confirm their chemical structure.

5.3.1 Structural characterization of 2-hexen-1-ylsuccinic anhydride (HSA) and corresponding diesters (13a-c)

The 2D gas chromatogram (Fig.5.1b) of HSA exhibits single sharp peak and there is no additional signal in its density distribution spectrum (Fig.5.2a) confirming the purity of the sample. In the mass spectrum (Fig.5.1 c), the peak at (m/z) 183.13 corresponds to molecular ion of HSA. The FTIR spectrum of HSA displayed characteristic peaks of an anhydride group, a weak and a strong carbonyl stretching at 1855 and 1781 cm⁻¹ respectively (Fig.5.2b). The single sharp peak observed in both 1D (Fig.5.3) and 2D gas chromatogram (Fig.5.4) of diesters (13a-c) confirms the purity of the samples. With an increase in the molecular weight of the product from 13a to 13c, the corresponding density distribution spectrum (Fig.5.5) shifts from lower to higher period (from 2500 to 4500 s) which further confirms the efficient conversion of HSA to corresponding diesters (13a-c). The mass spectra of the esters (Fig.5.6) displayed characteristic molecular ion peaks corresponding to (m/z) at 256.16 for 13a, 368.27 for 13b and 424.45 for 13c. In the FTIR spectra of samples (13a-c), the ester peak was observed around 1730 cm⁻¹ along with other characteristic peaks (Fig.5.7). The peak intensity of C–H stretching gradually increases from 13a to 13c, apparently due to the introduction of the longer alkyl chains. The absence of peaks at 1855 and 1781 cm⁻¹

CHAPTER 5

suggests that the products are free of unreacted HSA. The broad OH band and band corresponding to C=O of carboxylic acid group also were absent in the spectra which further confirms the completion of the reaction and the purity of the final products. The FTIR spectral data of HSA and (13a-c) are given below

HSA: Yield: 75%. IR (ATR, cm^{-1}): 2975, 2633, 1855 (weak C=O from anhydride), 1781 (strong C=O from anhydride), 1722, 1441, 1233, 1074, 925 and 724. **13a:** Yield: 89 IR (ATR, cm^{-1}): 2963, 2930, 1732 (C=O from ester), 1373, 1158, 1031, 971 and 858. **13b:** Yield: 88%. IR (ATR, cm^{-1}): 2929, 2864, 1735 (C=O from ester), 1459, 1358, 1164, 975 and 901. **13c:** Yield: 88 IR (ATR, cm^{-1}): 2929, 2860, 1728 (C=O from ester), 1454, 1168, 1038, 969 and 728.

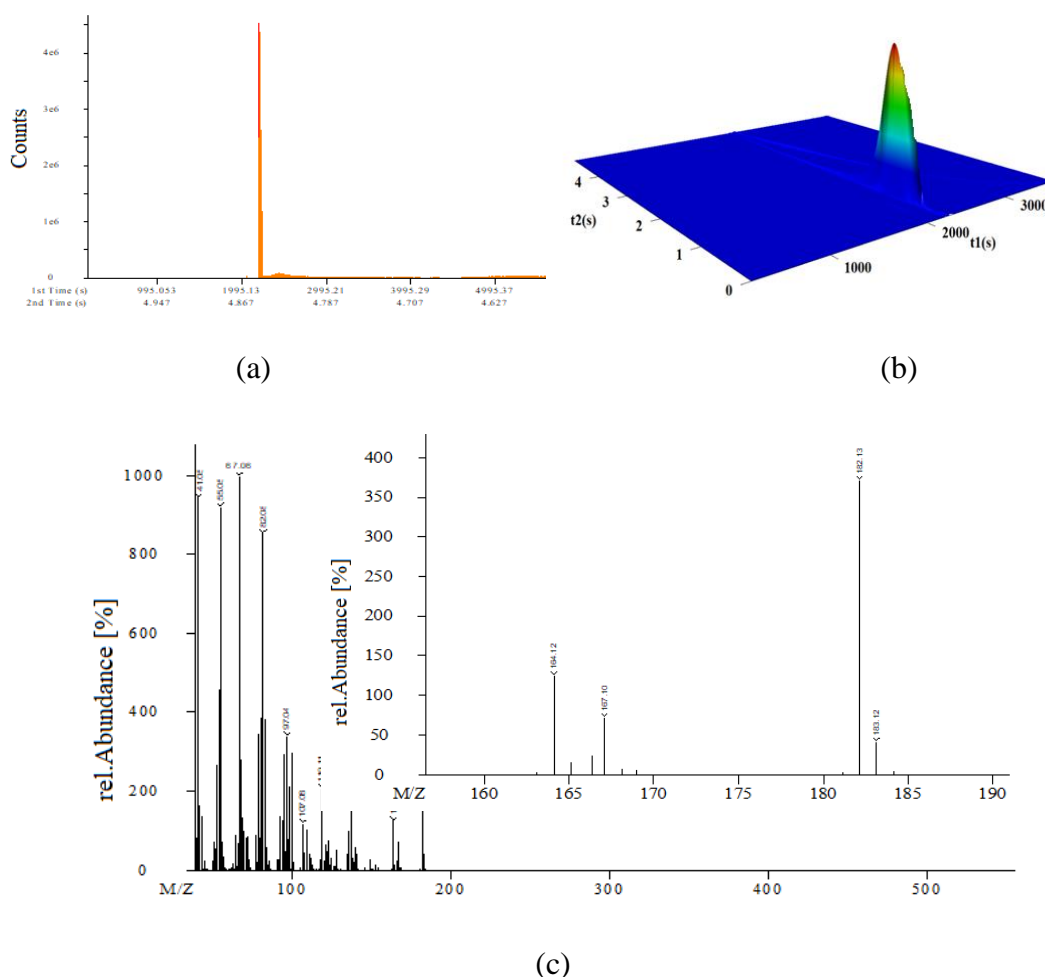


Fig.5.1 a) Gas chromatogram, b) two-dimensional chromatogram of HSA (t1 is the first dimensional retention, t2 is the second dimensional retention) and c) Mass spectrum of HSA.

CHAPTER 5

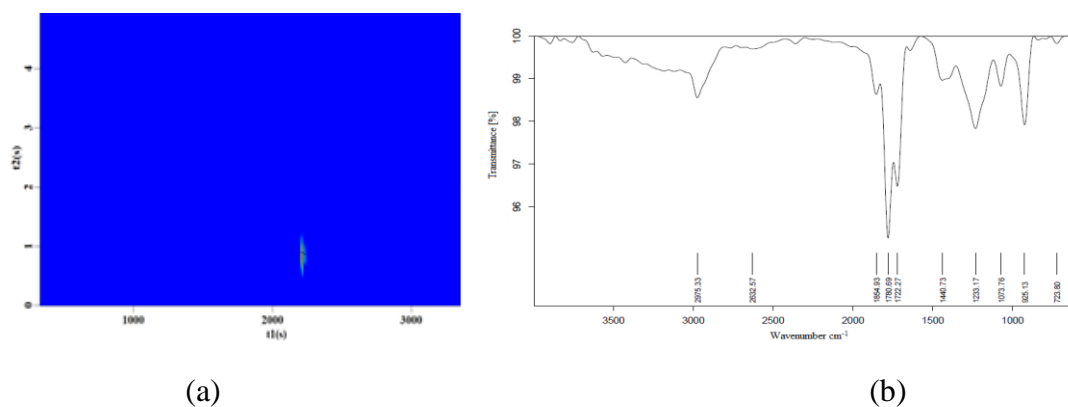


Fig.5.2 a) 2D density distribution spectrum (t1 is the first dimensional retention, t2 is the second dimensional retention) and b) FTIR spectrum of HSA. The product displays weak and strong carbonyl stretching of anhydride at 1855 and 1781 cm^{-1} respectively.

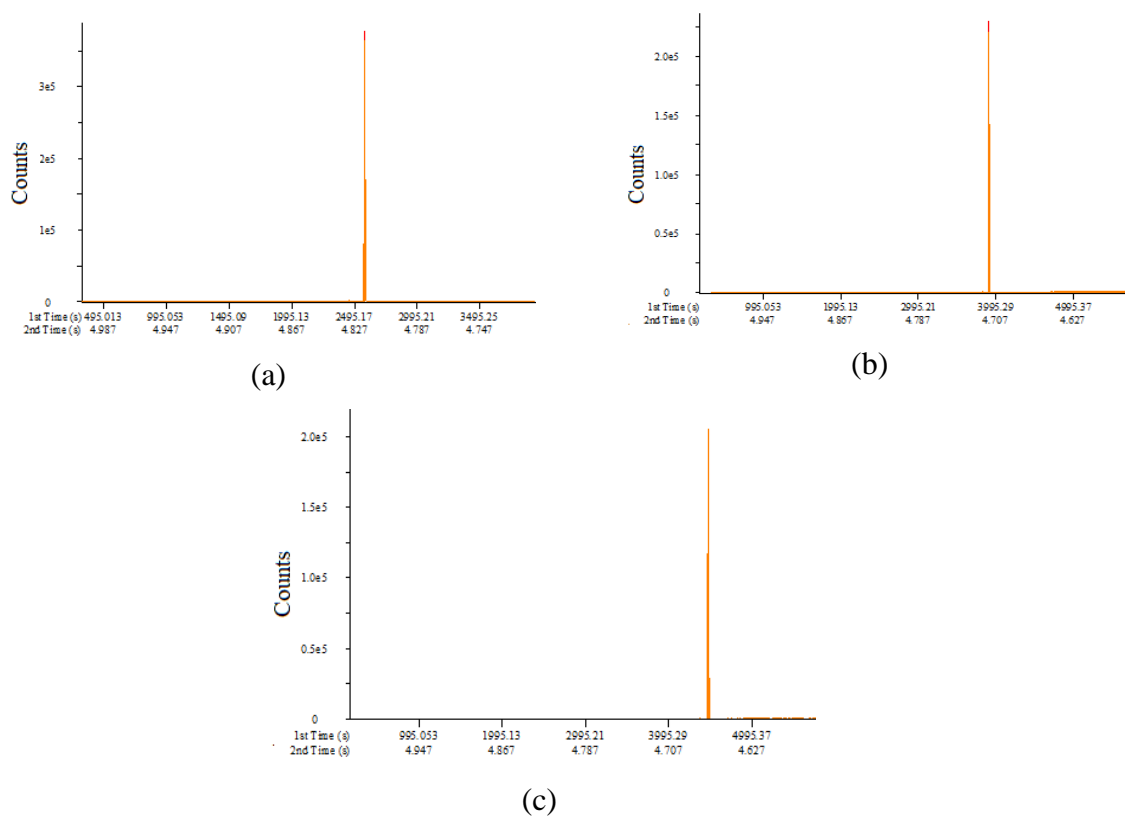


Fig.5.3 Gas chromatogram obtained for a) 13a, b) 13b and c) 13c.

CHAPTER 5

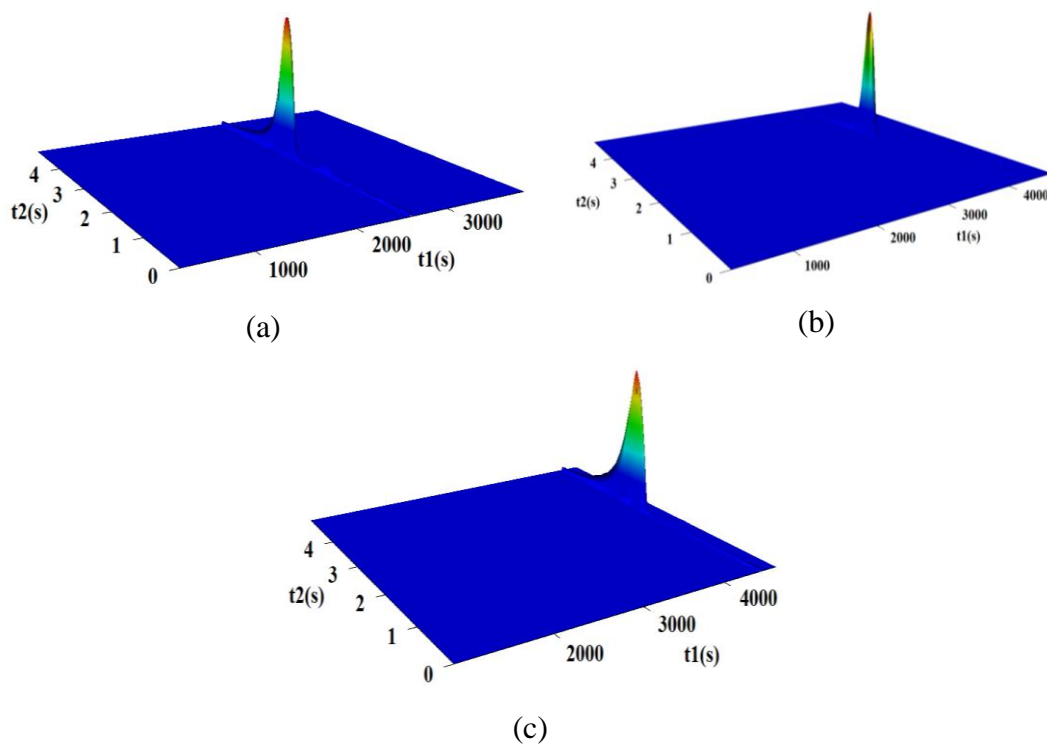


Fig.5.4 2D gas chromatogram of a)13a, b)13b and c)13c. (t_1 is the first dimensional retention, t_2 is the second dimensional retention).

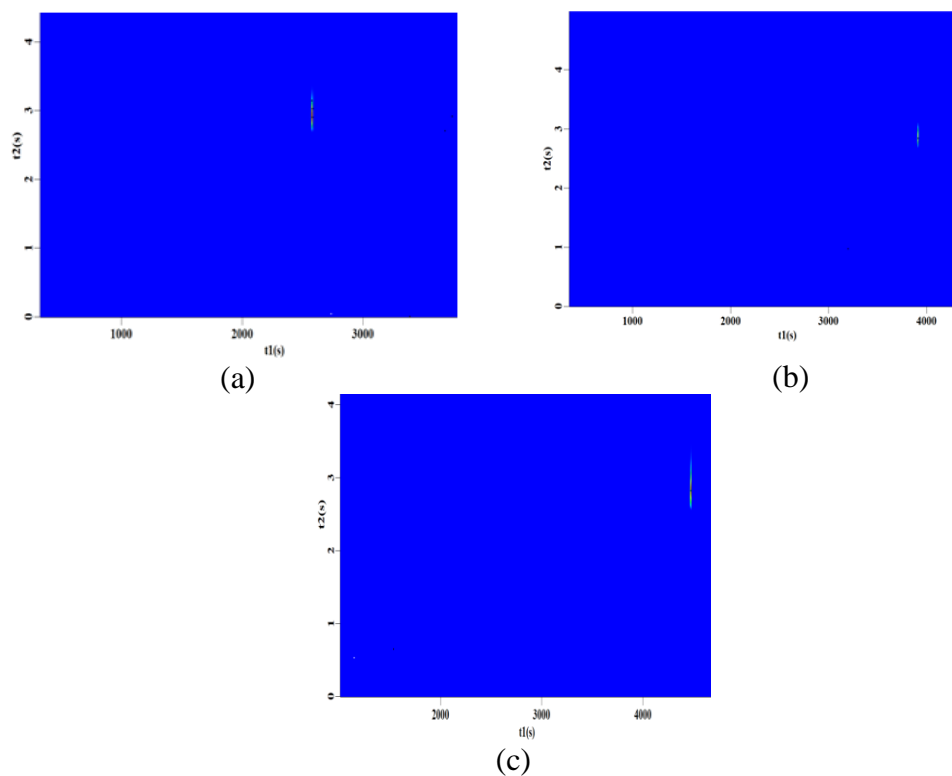
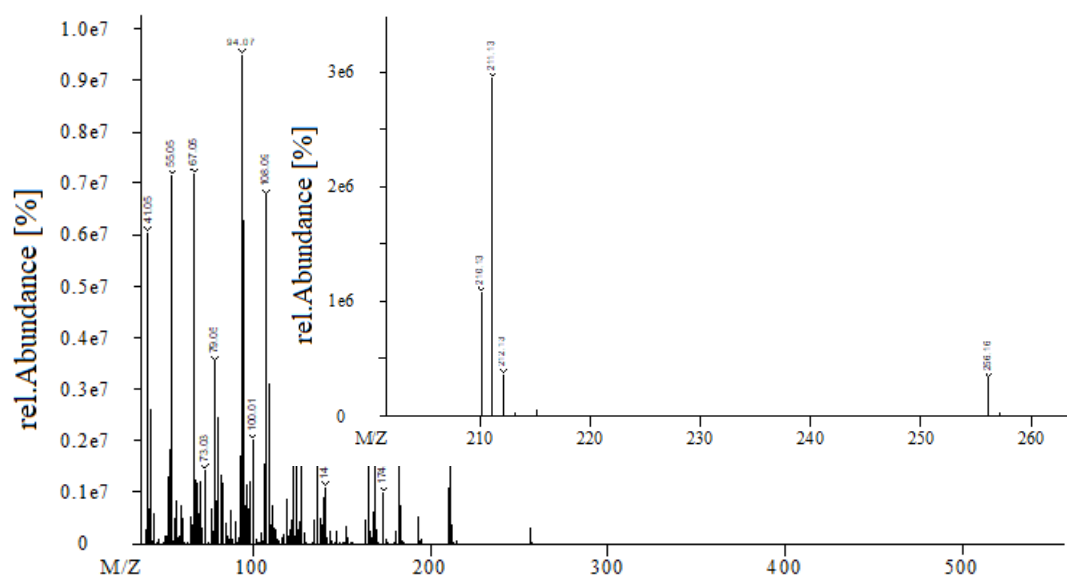
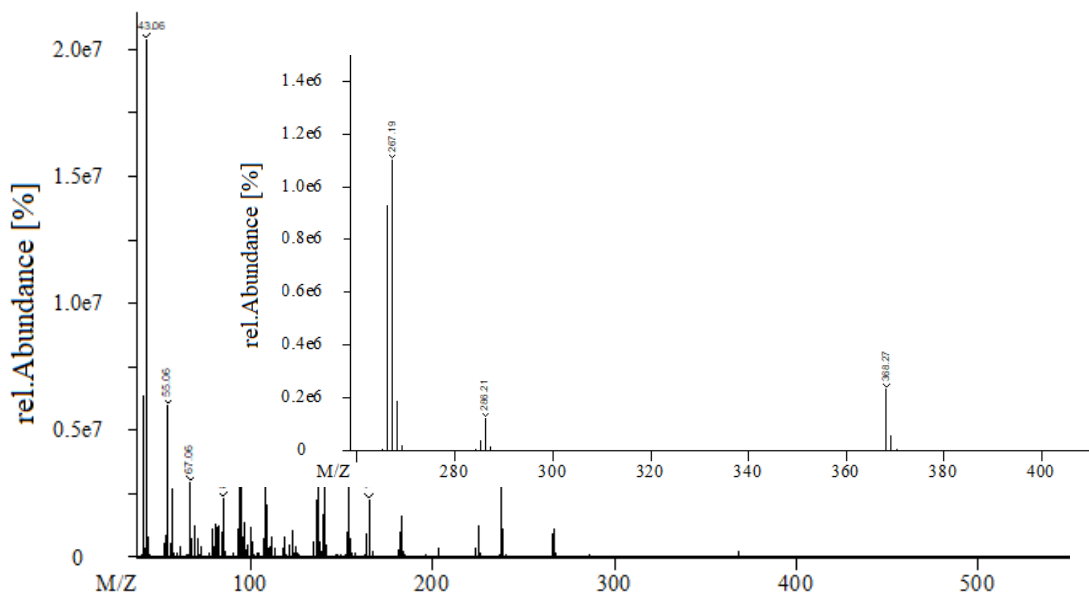


Fig.5.5 2D density distribution spectra of a)13a, b)13b and c)13c. (t_1 is the first dimensional retention, t_2 is the second dimensional retention).

CHAPTER 5



(a)



(b)

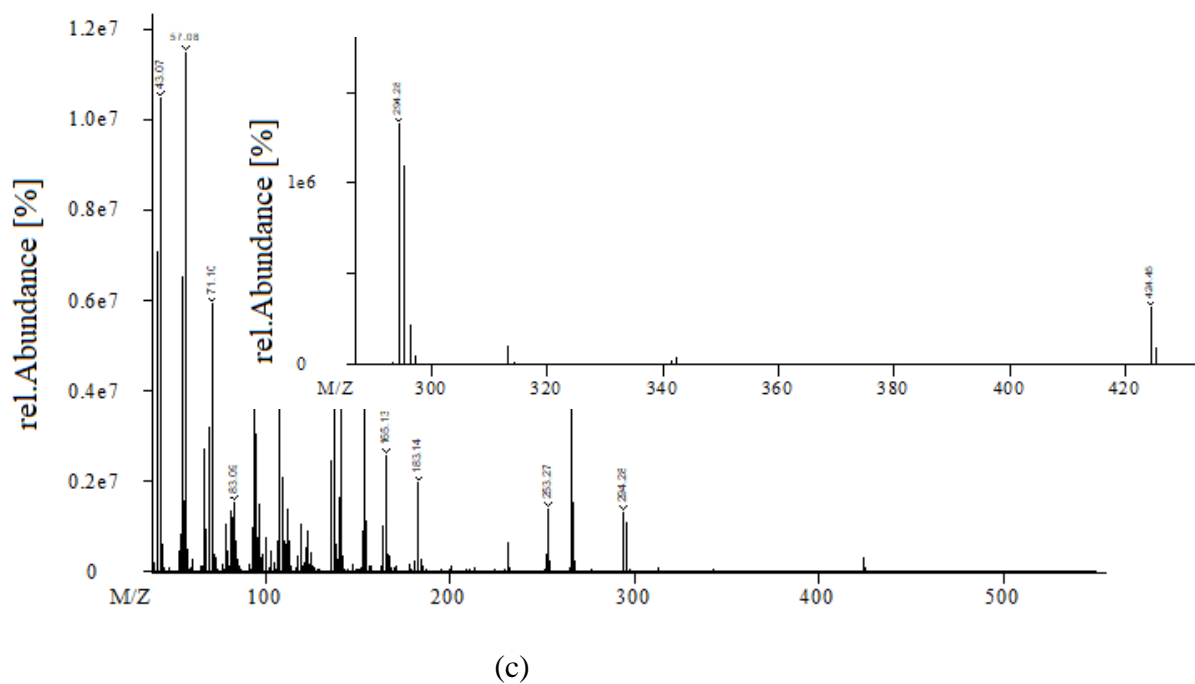


Fig.5.6 Mass spectra obtained for a)13a, b)13b and c)13c.

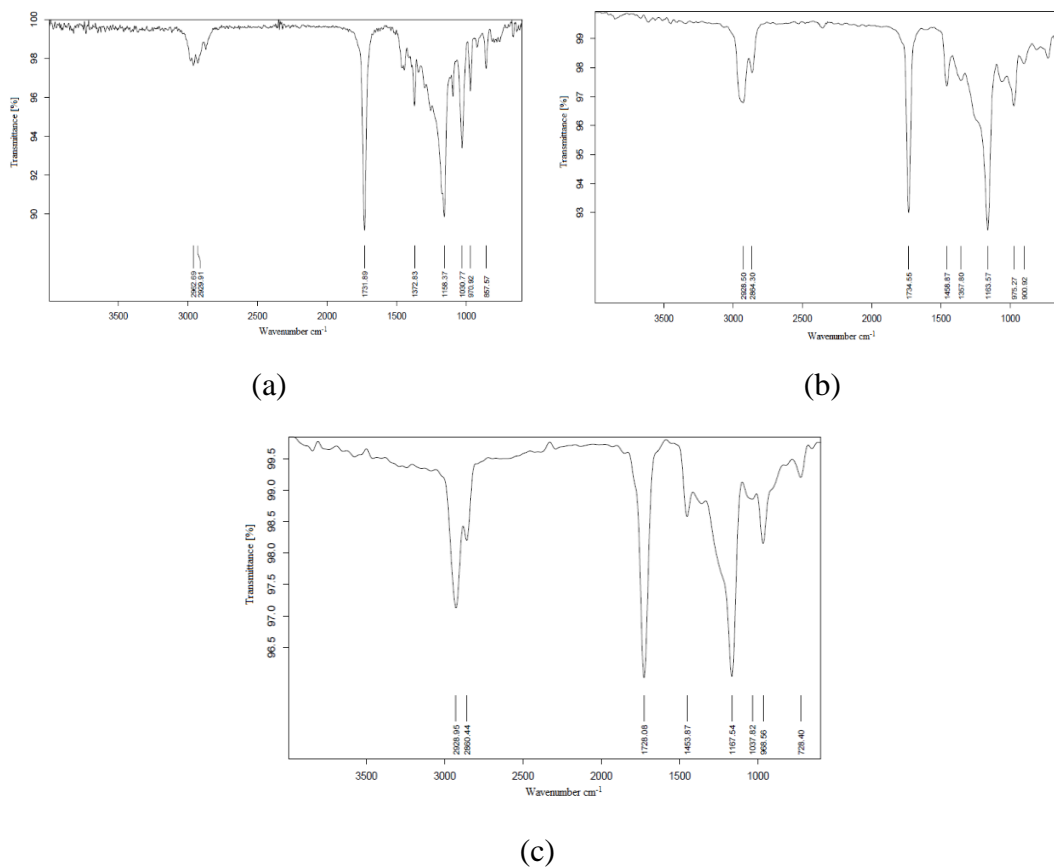


Fig.5.7 FTIR spectra of HSA diesters a) 13a, b) 13b and c) 13c. The products display a sharp carbonyl peak in the range 1728-1735 cm^{-1}

5.3.2 Structural characterization of alkenyl succinic anhydride (ASA) and LCN diesters, LCNDE (15a-h)

The 1D and 2D gas chromatograms (Fig.5.8) as well as the 2D density distribution spectrum (Fig.5.9) of ASA displayed multiple peaks indicating the formation of mixture of LCN-based alkenyl succinic anhydrides. The compounds in the mixture were identified tentatively based on the GC traces and the corresponding mass spectral data. In the mass spectra, the peaks at (m/z) 168.09 (Fig.5.10) 182.11 (Fig.5.11) and 196.12 (Fig.5.12) correspond to molecular ion of C-5, C-6 and C-7 derivatives of ASA respectively. The FTIR spectra of ASA (Fig. 5.13) displayed a weak band at 1853 cm^{-1} and a strong band at 1780 cm^{-1} corresponding to -C=O stretching of the anhydride group. The 2D gas chromatogram of ASA displayed peaks in the range of 1870-2300s whereas for the LCN diesters (LCNDE), peaks were observed in the range of 2400-2500s (Fig.5.14) which confirms the successful conversion of ASA to LCNDE. In the mass spectrum of LCNDE (15a), molecular ion peaks were observed at (m/z) 242.17 for the C-5 derivative (Fig.5.16), (m/z) 256.19 for the C-6 derivative (Fig.5.17) and (m/z) 271.17 for the C-7 derivative (Fig.5.18). The FTIR spectra of samples (15a-h) displayed ester peaks in the range of 1730-1737 cm^{-1} (Fig.5.19). The FTIR spectral data of ASA and LCNDEs are given below.

ASA: Yield: 70%. IR (ATR, cm^{-1}): 2976, 2587, 1854 (weak C=O from anhydride), 1780 (strong C=O from anhydride), 1722, 1440, 1233, 1076 and 925. **LCNDE (15a):** Yield: 88%. IR (ATR, cm^{-1}): 2954, 2877, 1732 (C=O from ester), 1458, 1381, 1169, 1062, 955 and 727. **LCNDE (15c):** Yield: 85%. IR (ATR, cm^{-1}): 2958, 2879, 1730 (C=O from ester), 1458, 1381, 1249, 1168, 1086, 956 and 737. **LCNDE (15d):** Yield: 86%. IR (ATR, cm^{-1}): 2952, 2872, 1735 (C=O from ester), 1460, 1378, 1238, 1171, 1033, 960 and 777. **LCNDE (15e):** Yield: 89%. IR (ATR, cm^{-1}): 2925, 2861, 1735 (C=O from ester), 1459, 1377, 1241, 1171, 1043, 961 and 724. **LCNDE (15f):** Yield: 88%. IR (ATR, cm^{-1}): 2927, 2860, 1732 (C=O from ester), 1456, 1380, 1171, 1058, 967 and 724. **LCNDE (15h):** Yield: 88%. IR (ATR, cm^{-1}): 2924, 2858, 1738 (C=O from ester), 1459, 1375, 1173, 1061, 952 and 723.

CHAPTER 5

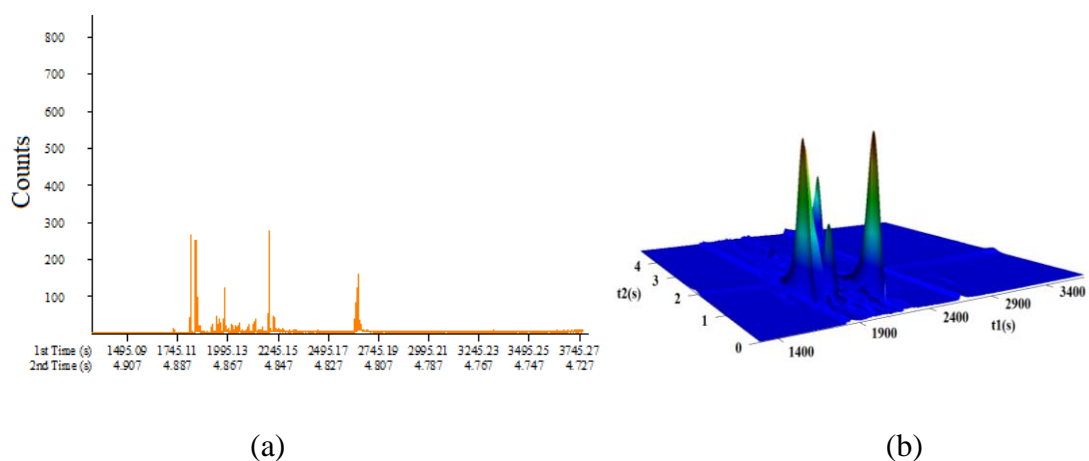


Fig.5.8 a) Gas chromatogram of ASA and b) 2D gas chromatogram of ASA (t_1 is the first dimensional retention, t_2 is the second dimensional retention).

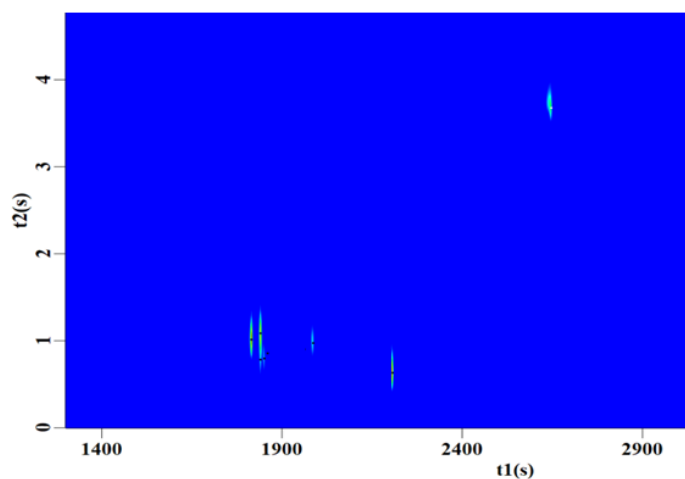


Fig.5.9 2D density distribution spectrum of ASA (t_1 is the first dimensional retention, t_2 is the second dimensional retention).

CHAPTER 5

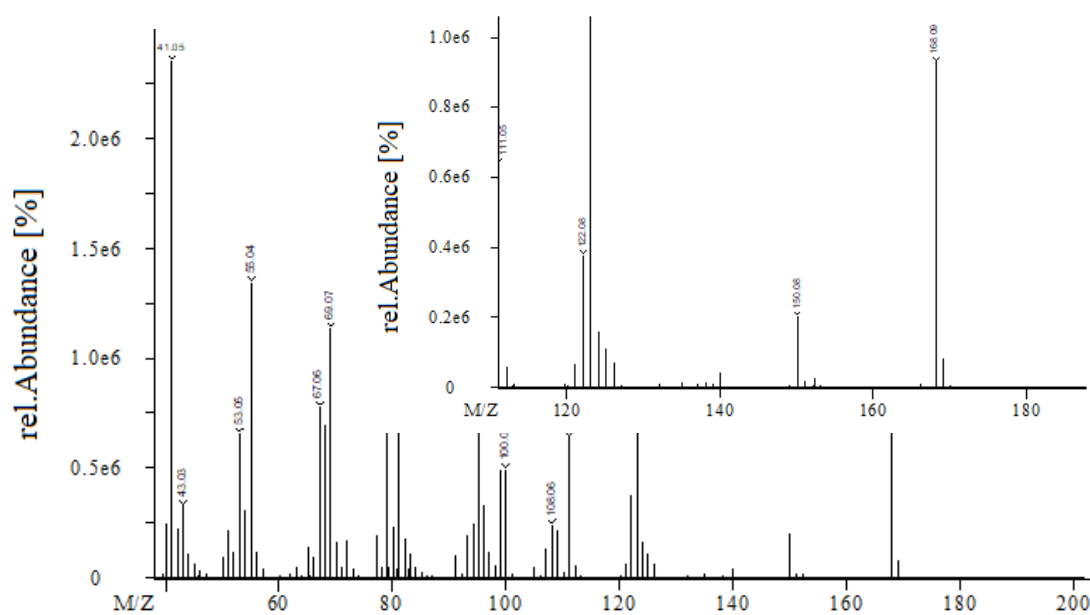


Fig.5.10 Mass spectrum of the major peak identified in ASA (C-5 derivative). Inset shows the enlarged spectrum in the region m/z 110 – 180.

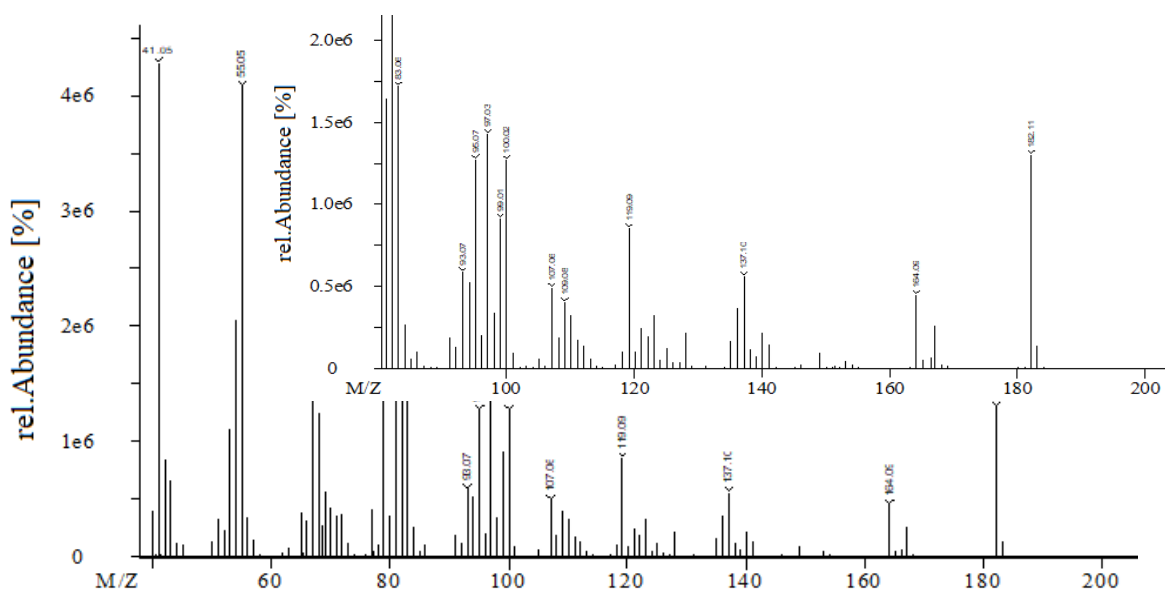


Fig.5.11 Mass spectrum of the major peak identified in ASA (C-6 derivative). Inset shows the enlarged spectrum in the region m/z 90 – 200.

CHAPTER 5

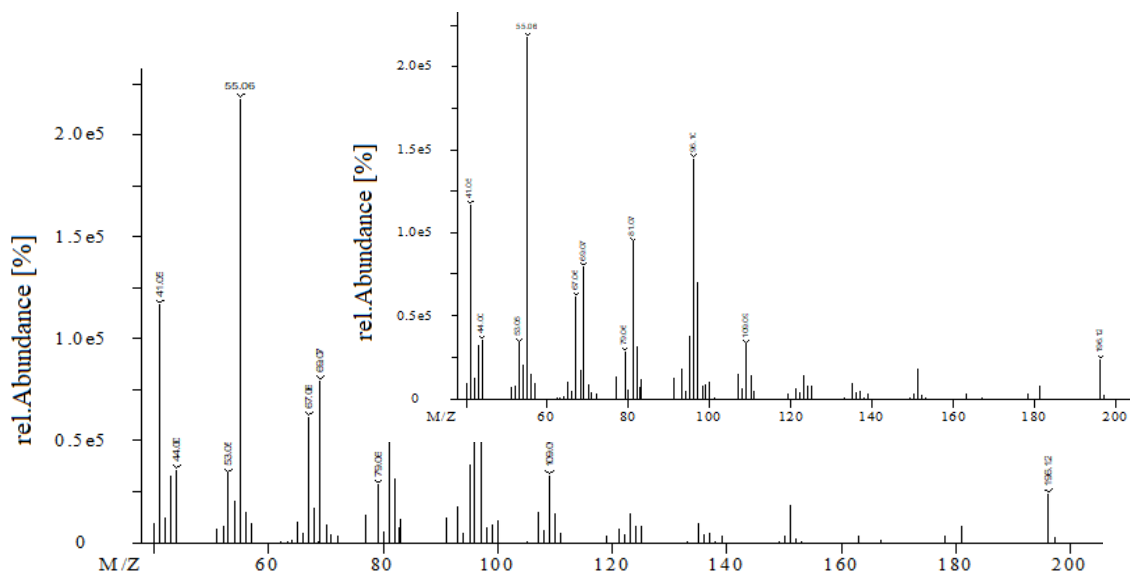


Fig.5.12 Mass spectrum of the major peak identified in ASA (C-7 derivative). Inset shows the enlarged spectrum in the region m/z 50 – 200.

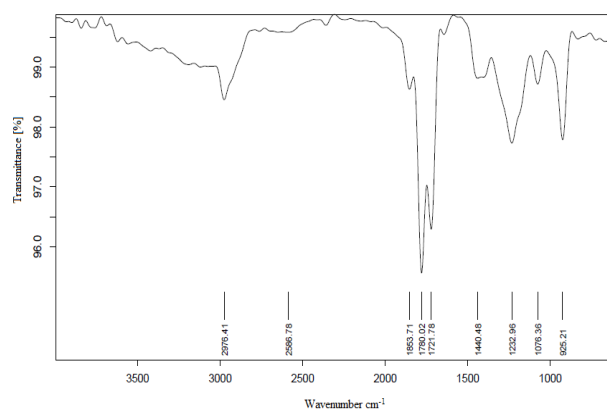


Fig.5.13 FTIR spectrum of ASA. The product displays weak and strong carbonyl peaks of anhydride at 1854 and 1780 cm^{-1} respectively.

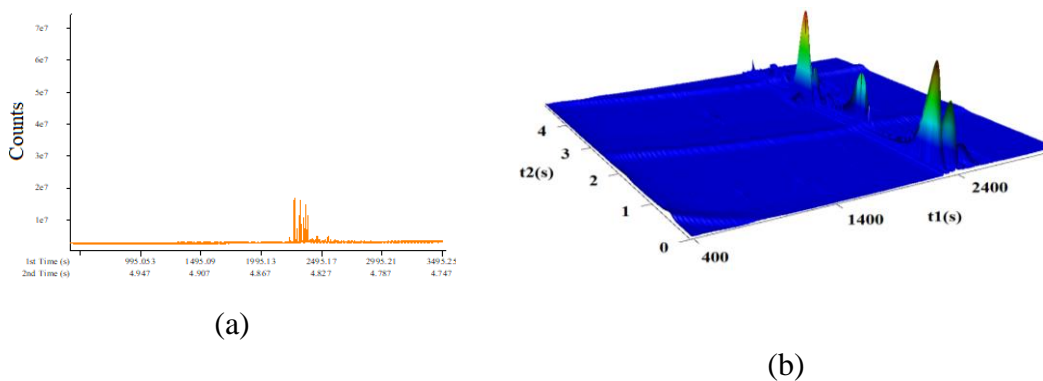


Fig.5.14 a) 1D gas chromatogram of LCNDE (15a) and b) 2D gas chromatogram of LCNFE (15a) (t_1 is the first dimensional retention, t_2 is the second dimensional retention).

CHAPTER 5

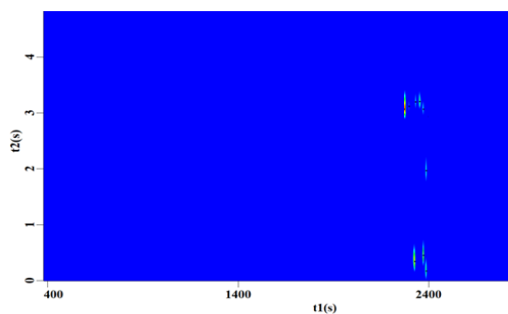


Fig.5.15 2D density distribution spectrum of LCNDE (15a) (t1 is the first dimensional retention, t2 is the second dimensional retention)

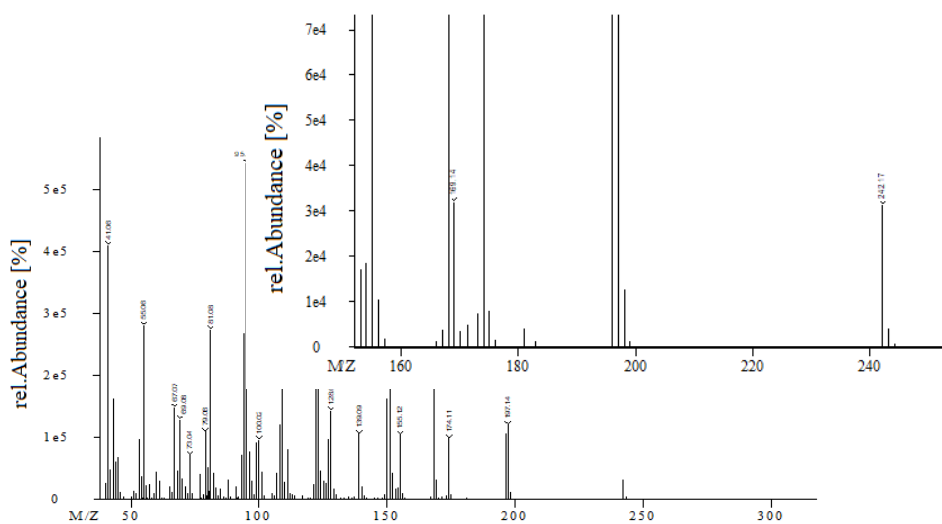


Fig.5.16 Mass spectrum of the major peak identified in LCNDE (15a) corresponding to C-5 derivative. Inset shows the enlarged spectrum in the region m/z 140 – 260.

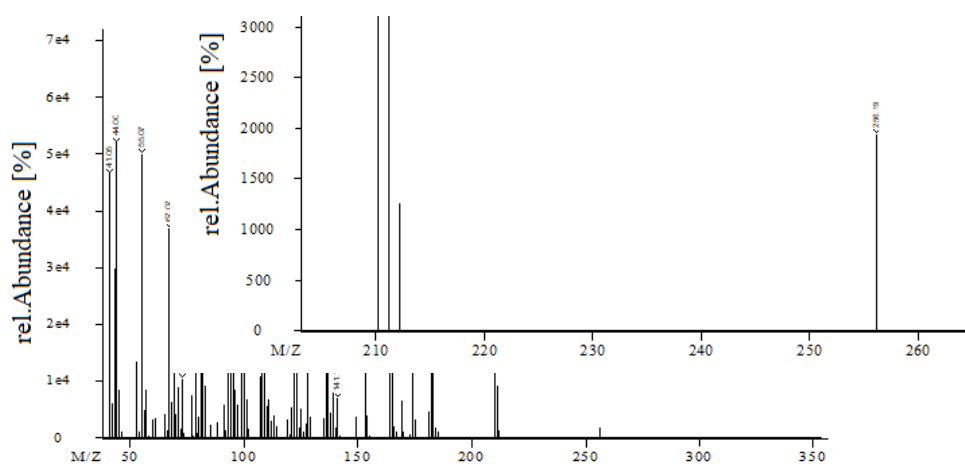


Fig.5.17 Mass spectrum of the major peak identified in LCNDE (15a) corresponding to C-6 derivative. Inset shows the enlarged spectrum in the region m/z 200 – 270.

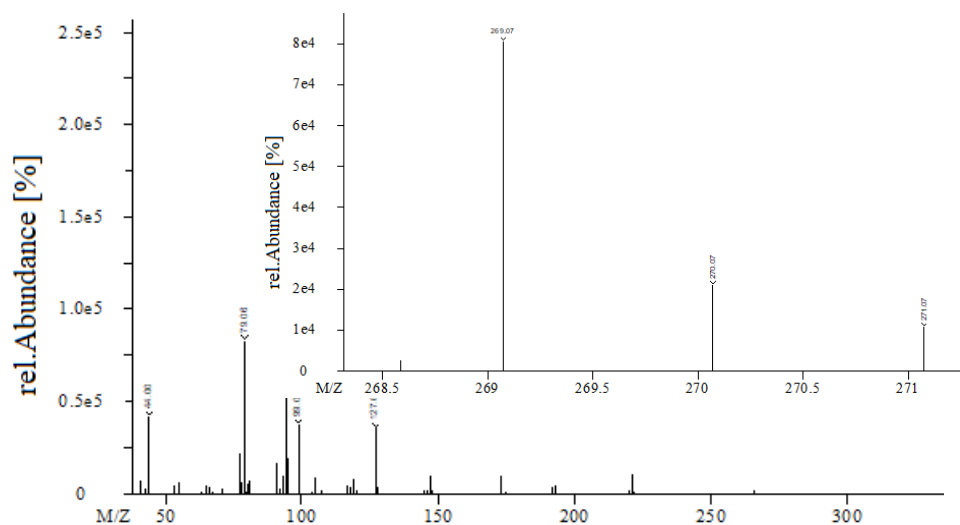
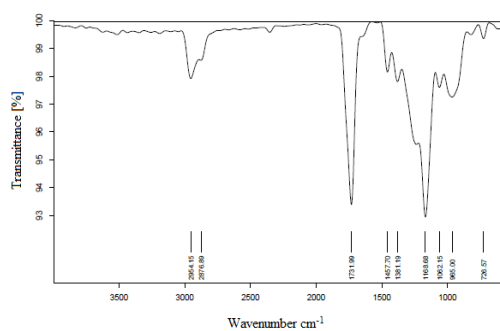
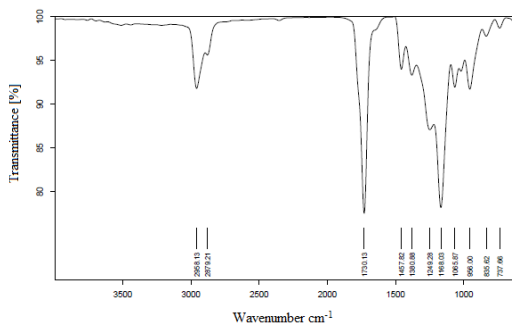


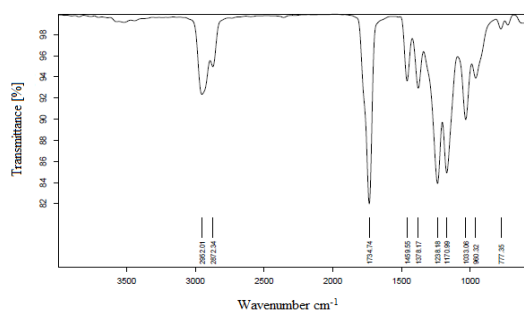
Fig.5.18 Mass spectrum of the major peak identified in LCNDE (15a) corresponding to C-7 derivative. Inset shows the enlarged spectrum in the region m/z 268 – 271.



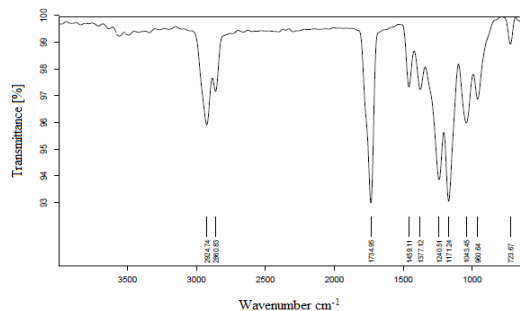
(a)



(b)



(c)



(d)

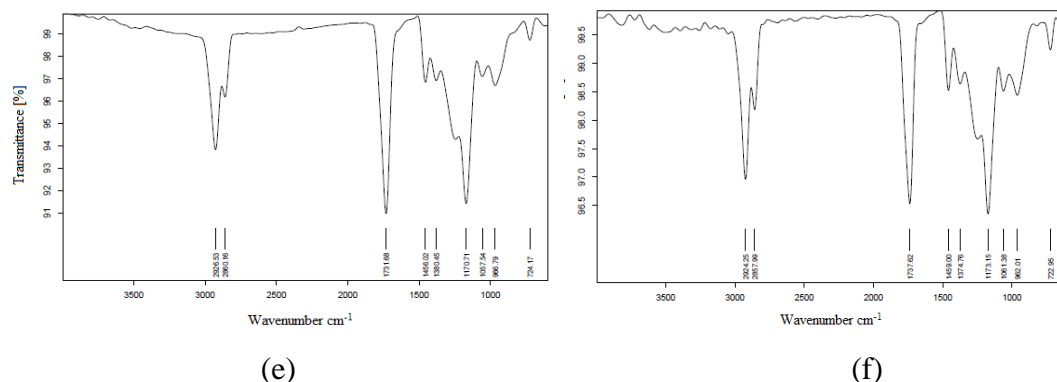


Fig.5.19 FTIR spectra of LCNDE a)15a, b)15c, c)15d, d)15e, e)15f and f)15h. The products display sharp carbonyl peaks in the range 1730-1738 cm^{-1} .

5.4. LUBRICITY MEASUREMENT

The lubricity of (13a-c) and (15a-h) was analysed through HFRR method at 60°C. Addition of the diesters lowered the WSD value of the ULSD signifying their lubricity characteristic. ULSD blends with 13c and 15d-h (at both dosage levels, 150 and 300 ppm) exhibited WSD values lower than the accepted value of 460 μm . The WSD values of neat ULSD, (13a-c)-ULSD and (15a-h) -ULSD blends are given in Table 5.2.

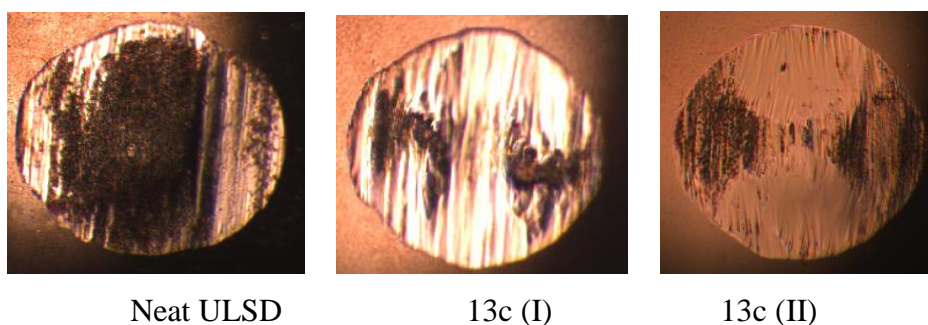
Table 5.2: The lubricity data of neat ULSD and ULSD with blend (WSD values lower than 460 μm are represented in bold)

HFRR 60 °C								
Sample ID	Conc n. ppm	Wear scar diameter (μm)			Conc n. ppm	Wear scar diameter (μm)		
		Ball X	Ball Y	WSD, (X+Y)/2		Ball X	Ball Y	WSD, (X+Y)/2
Neat, ULSD	NA	535	485	510	NA	NA	NA	NA
13a	150	521	475	498	300	515	470	493
13b		504	460	482		498	455	477
13c		457	422	440		440	410	425
15a		525	478	502		520	478	499
15b		520	470	495		504	458	481
15c		502	455	479		486	437	462
15d		477	435	456		462	428	445
15e		466	429	448		445	408	427

CHAPTER 5

15f		457	425	441		442	388	415
15g		453	383	418		441	349	395
15h		445	368	407		439	321	380

Among different ULSD- diester (15a-h) blends, the least WSD value was observed for the ULSD-15h blend sample (407 and 380 μm at 150 and 300 ppm respectively). It is evident from the table 5.2 that the lubricity of the fuel increases with the increase of carbon chain length of the diester. The WSD values of the diesters decreases from 13a to 13c and a similar trend of decrease in the WSD values was observed for diesters 15a to 15h as well. Further, the WSD values of the blend fuels decreases with an increase in the dosage level from 150 to 300 ppm. At higher blend concentration (300 ppm), a thicker protective film is formed between the metallic surfaces which reduces the friction between these surfaces. The optical microscopic images of the wear scars on the balls employed in lubricity measurement of neat ULSD, ULSD-13c and ULSD- LCNDE (15d-h) blends are shown in Fig.5.20. Interestingly, all the blend fuels resulted minimum wear and scar on the surfaces. These results indicate that the LCN-based diesters are efficient lubricity improvers for ULSD even at a low blending concentration of 150 ppm. The friction coefficient and film % graphs obtained from HFRR for neat ULSD, ULSD-15f and ULSD-15h blends (300 ppm) are given in Fig.5.21. Interestingly, the thickness of the protective film increases with the increase in length of carbon chain of the additive. The thin film minimizes the direct metal to metal contact and hence friction on the metallic surfaces decreases which improves the lubricity of the fuel. Remarkably, most of the LCN diesters, except (15a-c), imparted good lubricity with ULSD with minimum wear and scar on the surfaces. Hence, these LCN diesters could be considered as efficient lubricity enhancers for ULSD.



CHAPTER 5

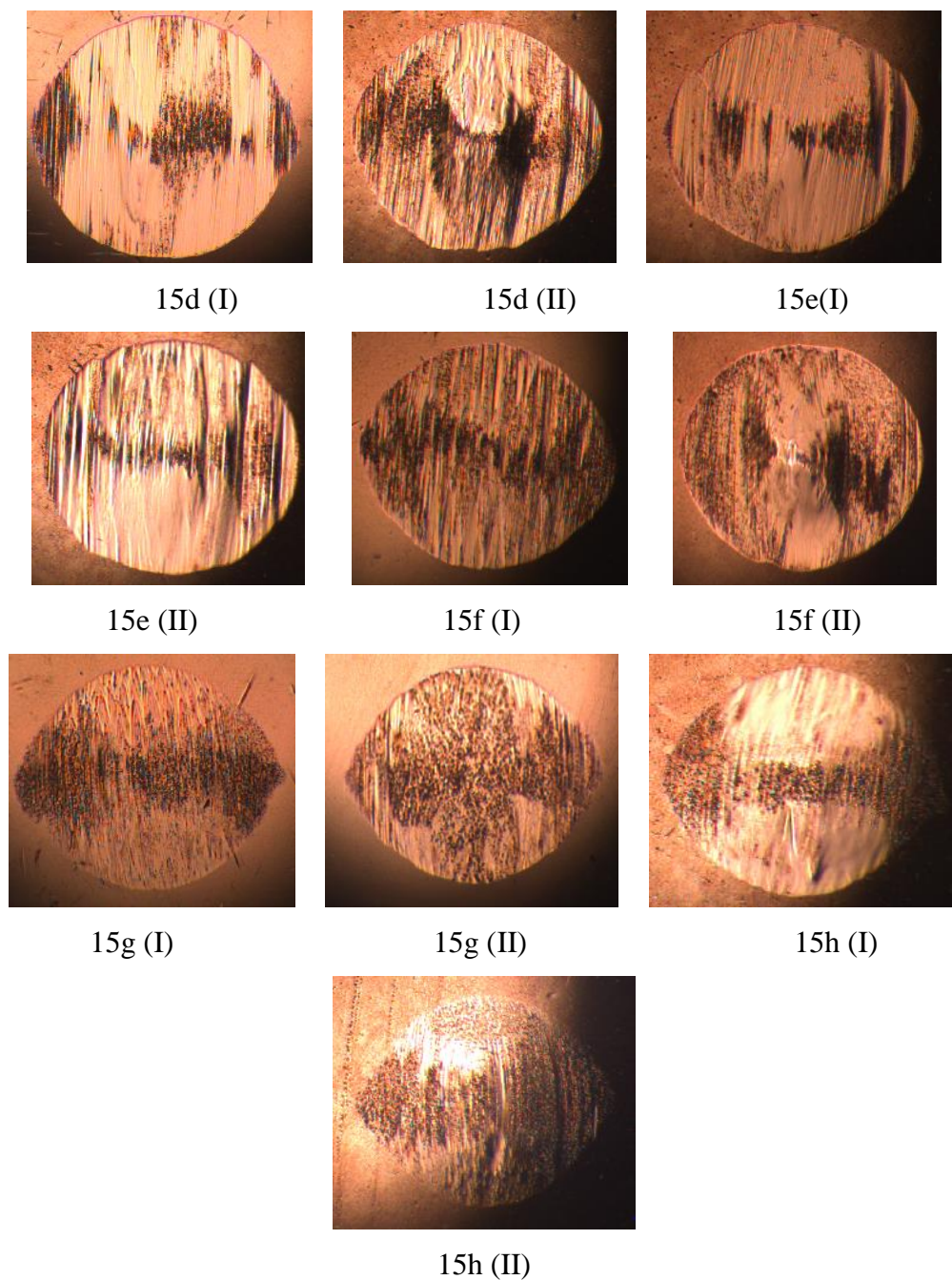


Fig.5.20 The optical microscopic images of wear and scar for neat ULSD, ULSD-13c and ULSD-(15d-h) blends. (I) and (II) corresponds dosage levels of 300 and 150 ppm respectively.

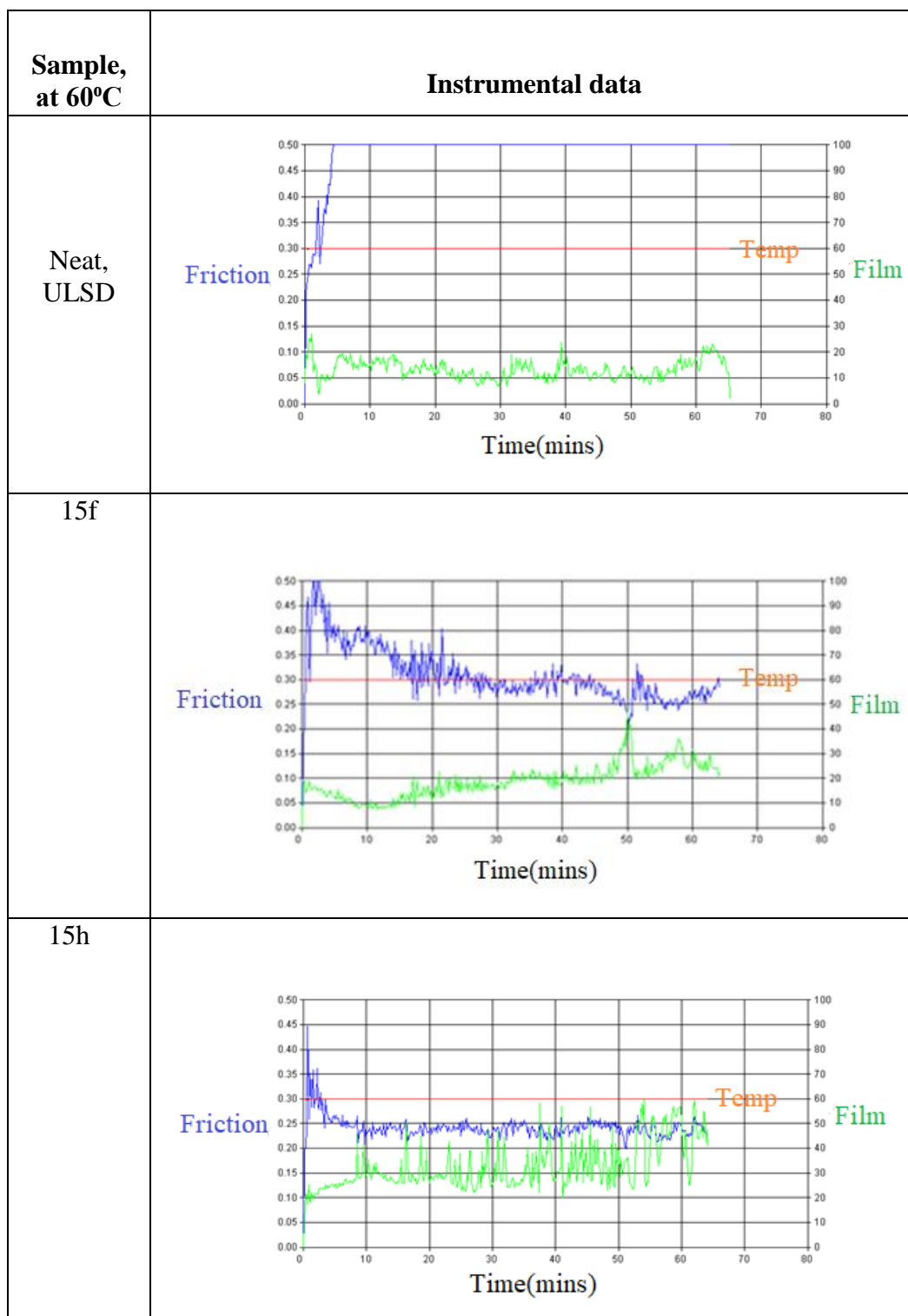


Fig.5.21 Friction coefficient and film % data obtained from HFRR for neat ULSD,15f-ULSD and 15h-ULSD blends.

5.5 PHYSIOCHEMICAL PROPERTIES OF THE BLEND FUEL

5.5.1 Impact of new lubricity enhancers on the diesel fuel's characteristics

To confirm the impact of new lubricity additive on the properties of diesel fuel, various key fuel parameters were examined for diester-ULSD blend. The results of the studies are tabulated in Table 5.3. There is no negative effect observed on diesel fuel parameters when it is blended with LCN based diesters as lubricity improvers. By lowering the wear scar diameter from 510 to 407 μm , the additives successfully improve the lubricity property of fuel. As a result, the additive ULSD blend meets the requirements for Euro 6/BS 6 fuel specification

Table 5.3. Test report summary of blended (150 ppm of 15h) ULSD

Parameter	Test method	Specification	Results
			Blend Fuel
Acidity, Total, mg of KOH/g, <i>Max</i> *	ASTM D 974	0.2	0.040
Cetane Index, <i>Min</i> *	IP 380	46	56.0
Pour point, °C, <i>Max</i> *	ASTM D 5950	3 for winter 15 for summer	-33
Copper strip corrosion test 3 h at 50°C	ASTM D 130	Not worse than No.1	No.1
Distillation, 95% recovery, v/v, recovery, °C, <i>Max</i> *	ASTM D 86	360	340.5
Flash point, °C, <i>Min</i> *	IP 170	35	>100
Kinematic viscosity, cSt at 40°C	ASTM D 445	2.0-4.5	3.051
Density @ 15°C, kg/m ³	ASTM D 4052	810-845	839.7
Total Sulphur, mg/Kg, <i>Max</i> *	ASTM D 5453	10	3.1
Lubricity, WSD at 60°C, microns, <i>Max</i> *	ASTM D 6079-18	460	407

CHAPTER 5

Oxidation stability, g/m ³ , <i>Max</i> *	ASTM D 2274	25	14.5
Cold Filter Plugging Point (CFPP), °C	ASTM D 6371	6 for winter 18 for summer	-16

5.6 MECHANISM OF LUBRICITY ACTION

The mechanism of friction reducing property of additives on the metallic surface was studied using SEM and EDS techniques by analysing the scratches on surfaces of friction couples.

5.6.1 Study of scar through SEM and EDS technique

The SEM pictures of the scars on balls of the friction couples are shown in (Fig.5.22). The dense scratches on the worn surface is clearly seen for the neat ULSD and the scar diameter of the worn surface on the ball is relatively higher for the neat ULSD than that of the ULSD-15h blend (150 and 300 ppm). Interestingly, the length of scratches on the worn surfaces becomes narrower and shallower as the lubricity enhancer concentration rises from 150 to 300 ppm. A defensive tinny protective layer forms between the metallic surfaces as a result of the polar components (diester functionality) included in the lubricity-improving agent, which speeds up the process of informal adsorption on the metal surface and shields the metallic surfaces from deterioration. The interaction of lubricity additive on metal surfaces during the rubbing process was studied using EDS technique. Mainly, three elements were detected on the worn surface: carbon from the diesel fuel, oxygen from the lubricity improver and air, and Iron from the friction medium. The energy dispersive x-ray spectra are shown in Fig.5.23. The percentage of oxygen on the surfaces tested with different blended ULSD were related with those of the surface tested with neat ULSD. As the mixture concentration increase from 150 to 300 ppm, the oxygen level on the worn surface rises from 8.2 to 10.7%, supporting the linking of the diester additive to metallic surface through oxygen rich functional group. The schematic representation of interactions between the metal surface and the LCN diester through oxygen-containing functional groups is shown in Fig.5.24.

CHAPTER 5

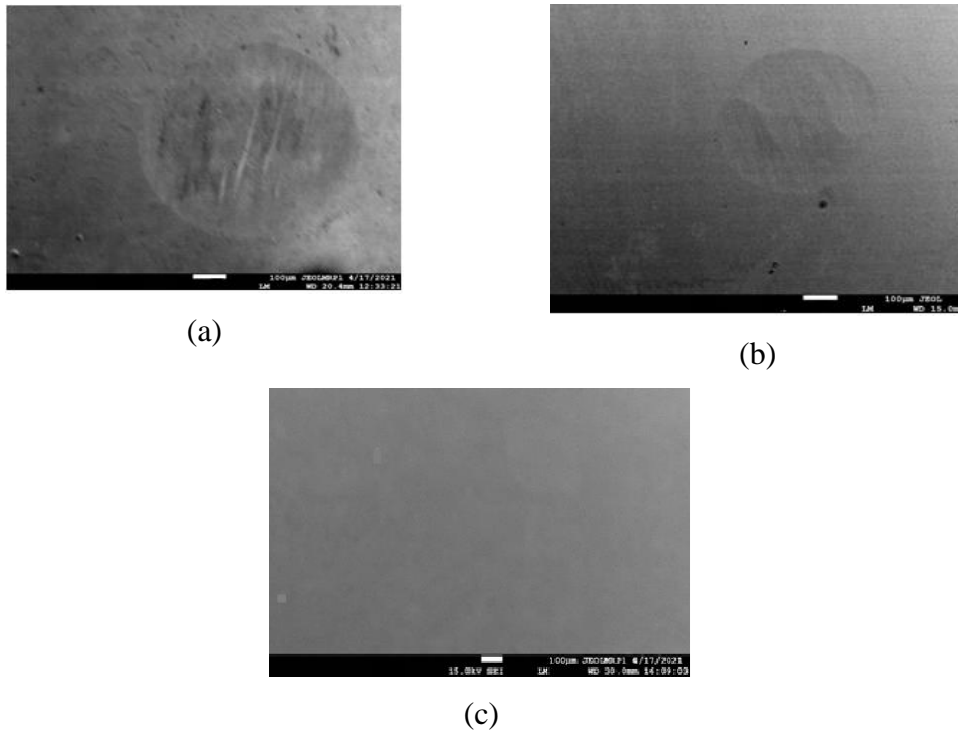
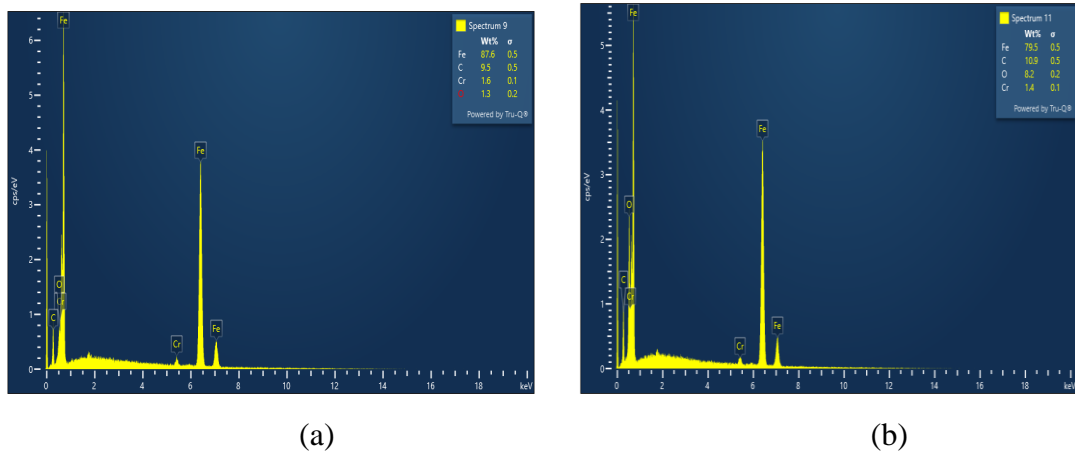
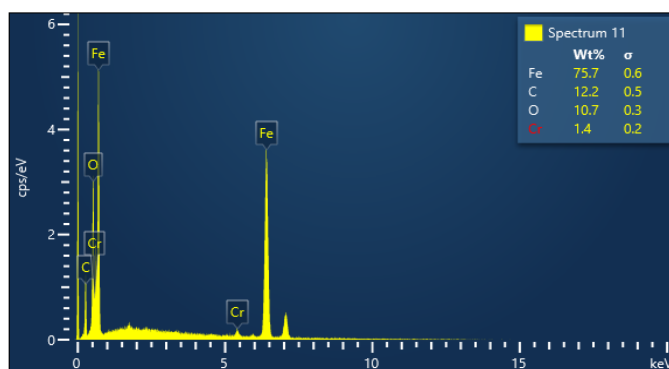


Fig.5.22 SEM images of the wear scars on balls of the friction couples with a) neat ULSD b) ULSD- 15h (150ppm) blend and c) ULSD- 15h (300ppm) blend.





(c)

Fig.5.23 Energy dispersive x-ray spectra of the metal surfaces with a) neat ULSD b) blended ULSD (15h 150 ppm) and c) blended ULSD (15h 300 ppm)

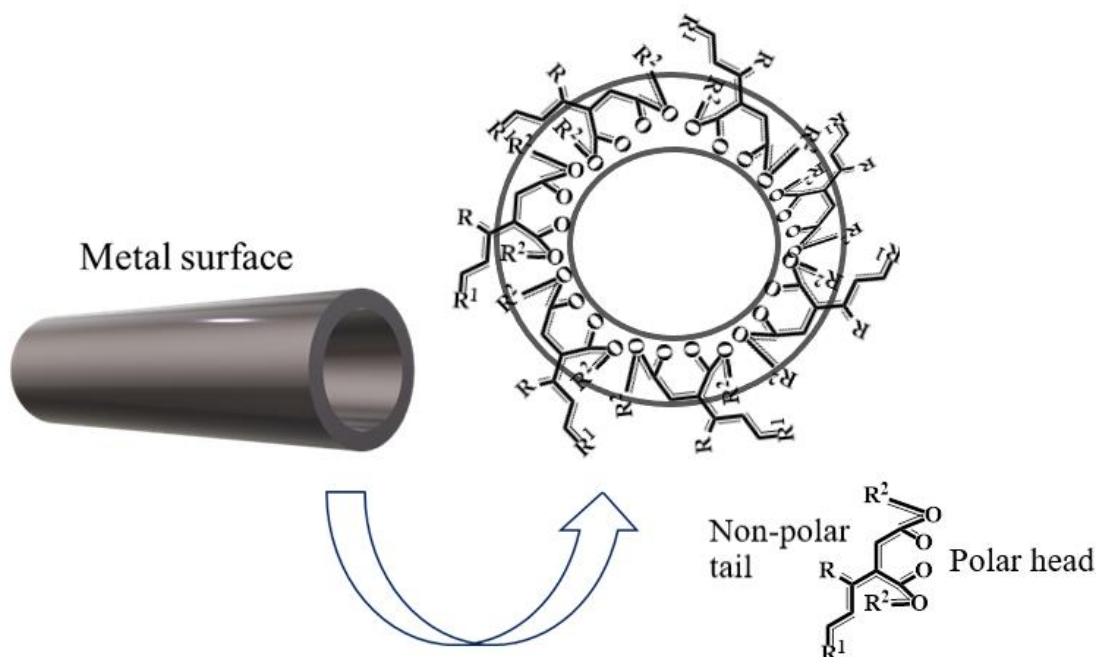


Fig.5.24 Schematic representation of interactions between the metal surface and LCN diester through oxygen-containing functional groups.

5.7 CONCLUSIONS

The refinery LCN was converted into diester-based efficient friction reducers (15a-h) for ULSD through a simple two-step process involving maleation and esterification reactions. The spectral studies revealed that C-5, C-6 and C-7 compounds are the major components in the LCN diesters. The synthesized lubricity additives possess long storage stability as revealed by the oxidation stability studies. There is no negative

CHAPTER 5

impact on the key fuel parameters of ULSD upon blending with the LCN diesters and the ULSD blends fulfil the requirements of Euro 6/BS 6 fuel specifications. Most of the synthesized LCN diesters (15d-h) enhance the lubricity of ULSD at very low blending concentrations (150/300 ppm). These results imply that the LCN-based diesters offer a good opportunity to improve diesel lubricity by decreasing friction and wear in the diesel fuel pump. A crucial point is that the two-step process described in the current study may be a cost-effective way for the refineries to create low-cost additives using basic materials (LCN) available on site.

CHAPTER 5

CHAPTER 6

GLYCIDYL METHACRYLATE, METHACRYLIC ACID AND FATTY ACID DERIVATIVES AS LUBRICITY IMPROVER FOR ULTRA- LOW SULPHUR DIESEL

Abstract

This chapter deals with the synthesis of new series of LI for ULSD starting from glycidyl methacrylate, methacrylic acid and fatty acids through a simple reaction protocol. It includes structural characterization and lubricity study and lubricity mechanism of the additives.

6.1 INTRODUCTION

In this work, lubricity enhancers are synthesized starting from simple raw materials such as glycidyl methacrylate, methacrylic acid and fatty acid. Glycidyl methacrylate contains an epoxide and acrylate groups. It is obtained by the formal condensation of the carboxy group of methacrylic acid with the hydroxy group of glycidol. It is produced in large scale by several companies worldwide, including Dow chemicals and is used in the production of polymer coatings, plastics, finishes and adhesives. Methacrylic acid is prepared from acetone cyanohydrin. It is mainly used in paints, adhesives and leather treatment. It is one of the raw materials for the manufacture of ion exchange resins. Here we discuss the conversion of glycidyl methacrylate, methacrylic acid and fatty acids into corresponding lubricity enhancers by utilizing a straightforward esterification reaction protocol and evaluated the anti-friction characteristics of these additives towards ULSD fuel.

6.2. EXPERIMENTAL PART

6.2.1 Materials

Glycidyl methacrylate (GMA) (97%, contains 100 ppm of monomethyl ether hydroquinone as inhibitor), methacrylic acid, triethylamine (TEA), organic/fatty acids, fatty alcohol, polyol, solvents and all the other chemicals were purchased from Sigma Aldrich.

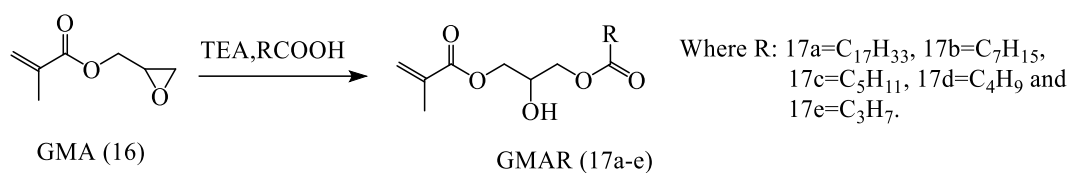
CHAPTER 6

6.2.2 Instruments

The details of instruments are given in chapter 3 (3.2.2).

6.2.3 Esterification of glycidyl methacrylate (GMA) with organic acids/fatty acids (R)

In this synthetic route, the glycidyl methacrylate was subjected to simple esterification reaction with different organic acids to get the hydroxy esters (Scheme 6.1). To a mixture of GMA (14.2 g, 0.1 mol), triethylamine (TEA) (0.1g, 0.001 mol) and toluene (10 mL), appropriate amount of the organic acid (0.1 mol) was added. The reaction mass was refluxed for 4 h. After that, the reaction mixture was left to stand for 3 h in room temperature. Then the mixture was extracted with ethyl acetate and washed with DM water (200 mL) followed by 5 % sodium bicarbonate (200 mL) solution. The organic layer was filtered and the solvent was removed under reduced pressure to yield the product. The obtained product was termed as GMAR (17a-e).

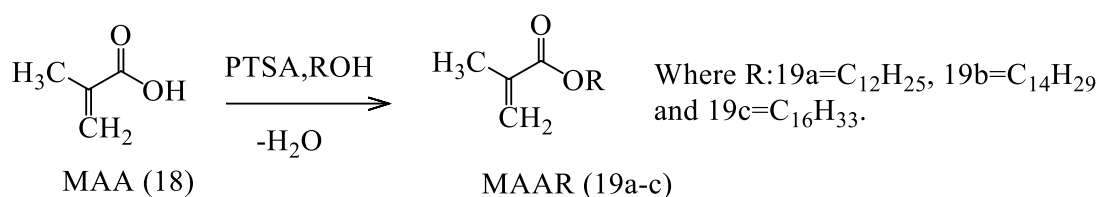


Scheme 6.1. Synthetic route of GMA-based lubricity improver for ULSD.

6.2.4 Esterification of methacrylic acid (MAA) with fatty alcohols (FAL)

Methacrylic acid (MAA) was subjected to esterification reaction with dodceanol (DDL), tetra decanol (TDL) and hexadecanol (HDL) to get the long chain esters (19a-c) (Scheme 6.2). To a mixture of MAA (8.6 g, 0.1 mol), p-toluene sulphonic acid (PTSA) (0.1g, 0.001 mol) and toluene (40 mL), appropriate amount of the alcohol (0.1 mol) was added. The flask was attached to a Dean-Stark apparatus and kept in a heating mantle with a magnetic stirrer and a temperature controller. The reaction mixture was refluxed at 110 °C with continuous stirring. The water released during the reaction was eliminated with the use of the Dean-Stark apparatus. After completion of the reaction, the whole reaction mixture was cooled to room temperature. Then organic layer was washed with DM water (200 mL) and 5% sodium bicarbonate (100 mL) solution. The product was produced as a light-yellow liquid (95% yield).

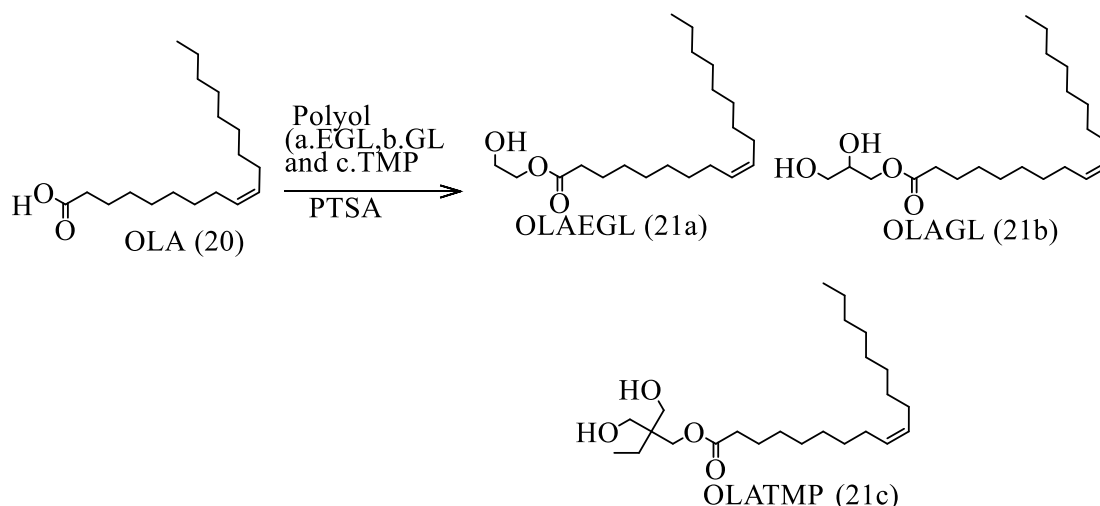
CHAPTER 6



Scheme 6.2. Synthetic route of MAA-based lubricity additive for ULSD.

6.2.5 Esterification of oleic acid (OLA) with polyols (POL).

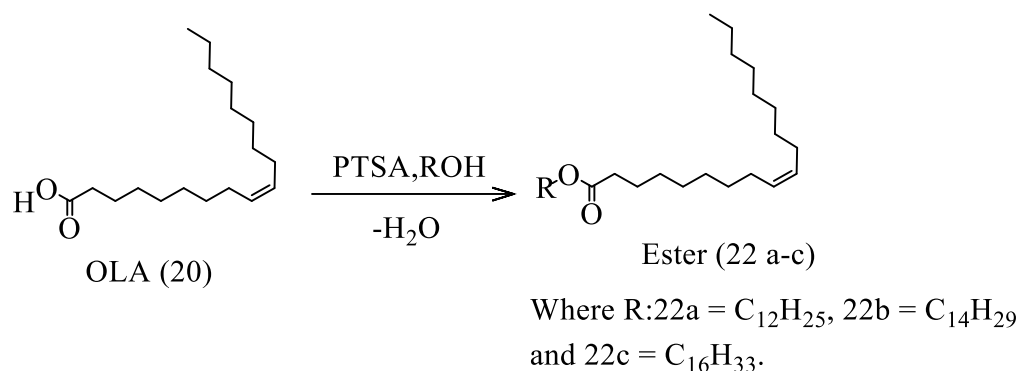
In this synthetic route, OLA was subjected to esterification reaction with three different polyols i.e., ethylene glycol (EGL), glycerol (GL) and trimethylolpropane (TMP) to get the hydroxy esters (21a-c) (Scheme 6.3). The same procedure described in the section (6.2.4) was followed for the synthesis.



Scheme 6.3. Synthetic route of OLA/POL-based lubricity improver (21a-c) for ULSD.

6.2.6 Esterification of oleic acid (OLA) with fatty alcohol (FAL).

In this synthetic route, OLA was subjected to esterification reaction with dodcanol (DDL), tetra decanol (TDL) and hexadecanol (HDL) to get the long chain esters (22a-c) (Scheme 6.4) following the above-mentioned procedure



Scheme 6.4. Synthetic route of OLA/FAL-based lubricity improver (22a-c) for ULSD.

6.3.7 Study of friction

The lubricity study, analysis of scar and study of physical and chemical parameter of diesel fuel are detailed in chapter 3 (3.2.4).

6.4. RESULTS AND DISCUSSION

6.4.1 Structural characterization of (17a-e), (19a-c) (21a-c) and (22a-c)

The conversion of glycidyl methacrylate (GMA) to corresponding ester GMAR (17a-e) was confirmed by 2D gas chromatography mass spectra (GCXGC-MS) and IR spectroscopic techniques (Fig.6.1-6.6). The mass spectra of the GMA and ester (17a) displayed characteristic molecular ion peaks corresponding to (m/z) 142.06 for GMA and 424.36 for 17a. With an increase in the molecular weight of the product from GMA to 17a, the corresponding density distribution spectrum (Fig.6.5) shifts from lower to higher period (from 1100 to 4500 s) which further confirms the efficient conversion of GMA to corresponding hydroxy ester (17a). In the FTIR spectra of samples (17a-e), the ester carbonyl peak observed in the range 1721-1725 cm⁻¹ whereas broad O-H bands appeared at 3473-3534 cm⁻¹ along with other characteristic peaks (Fig.6.6). The single sharp peak in 2D spectra of 17a indicates the purity of sample.

CHAPTER 6

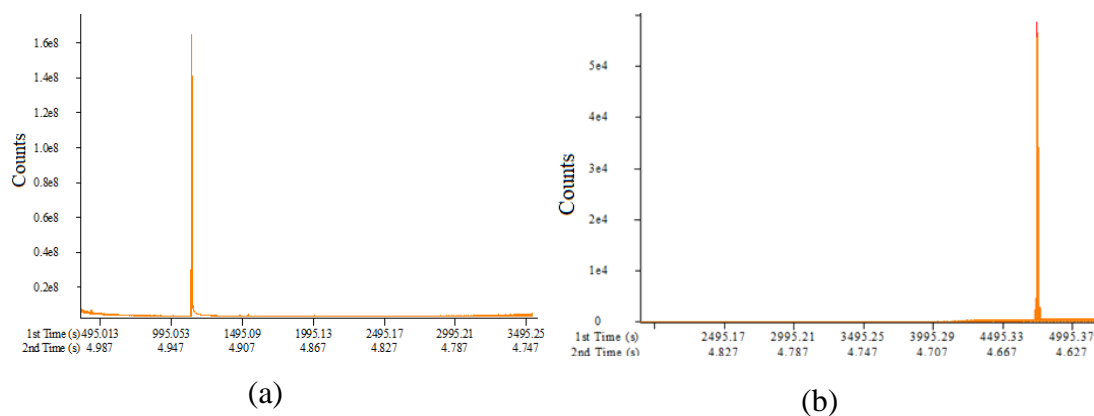


Fig.6.1 1D gas chromatogram of a) GMA and b) 17a

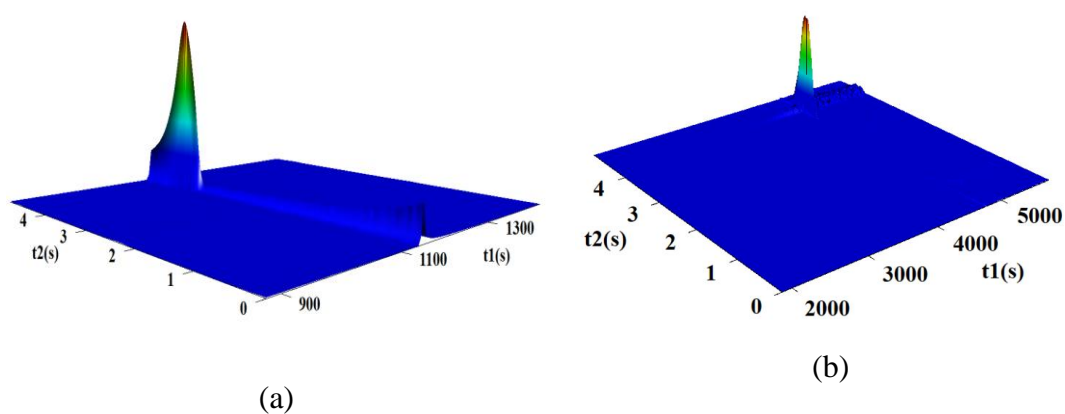


Fig.6.2 2D gas chromatogram of a) GMA and b) 17a (t_1 is the first dimensional retention, t_2 is the second dimensional retention).

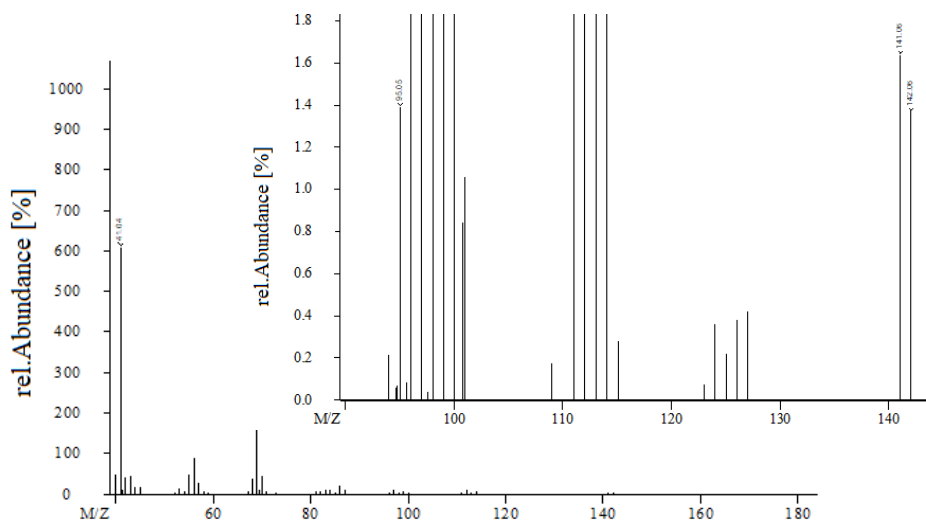


Fig.6.3 Mass spectrum of GMA. Inset shows the enlarged spectrum in the region m/z 100 – 150.

CHAPTER 6

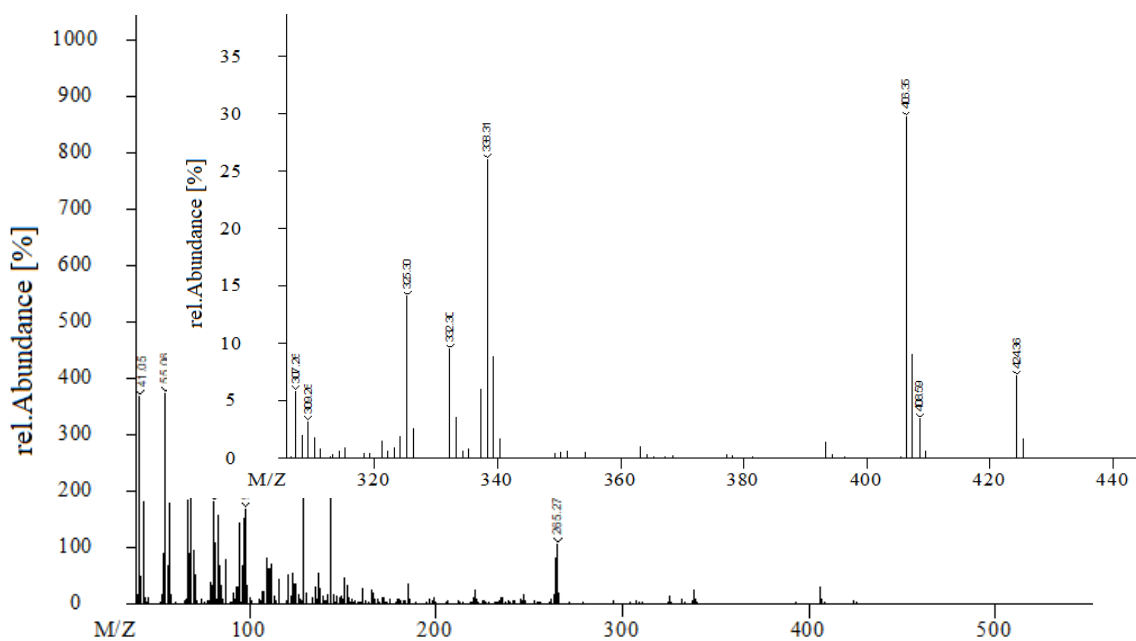


Fig.6.4 Mass spectrum of 17a. Inset shows the enlarged spectrum in the region m/z 320-440.

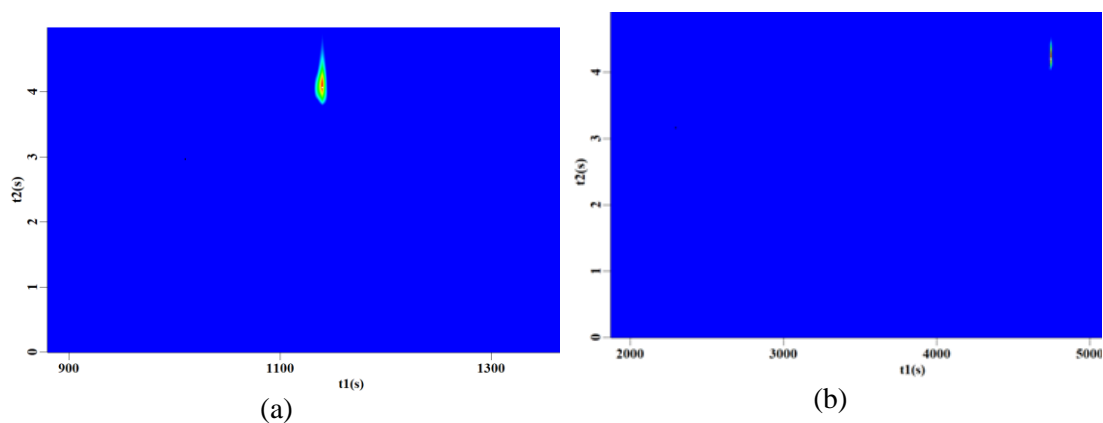


Fig.6.5 2D density distribution spectra of a) GMA and b) 17a (t1 is the first dimensional retention, t2 is the second dimensional retention).

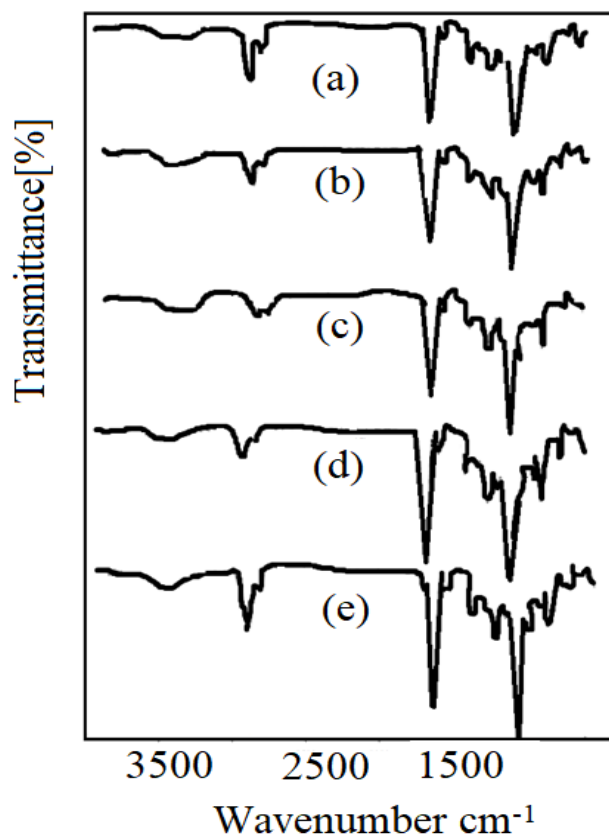
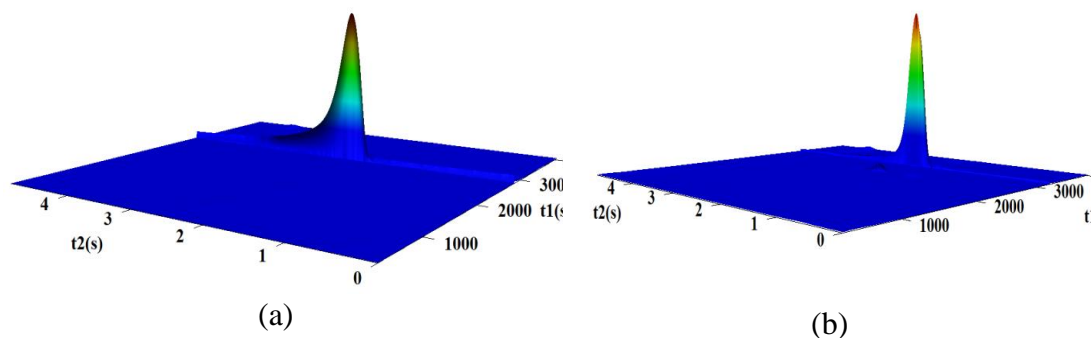
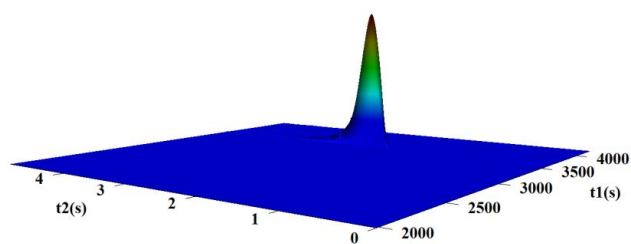


Fig.6.6 FTIR spectra of a) 17a, b) 17b, c) 17c, d) 17d and e) 17e. The all product displays a sharp carbonyl peak at 1730 cm^{-1} as well as a broad OH band at 3500 cm^{-1} .

The 2D gas chromatograms (Fig.6.7) as well as the 2D density distribution spectrum (Fig.6.8 b-c) confirms the conversion of methacrylic acid to corresponding esters MAAR (19a-c) In the mass spectra (Fig.6.9), the peaks at (m/z) 254.23, 282.24 and 311.28 correspond to molecular ion of 19a, 19b and 19c respectively. The FTIR spectra of (19a-c) (Fig.6.10) displayed a strong band at around $1693\text{-}1721\text{ cm}^{-1}$ corresponding to -C=O stretching of the α, β -unsaturated ester group along with other characteristic peaks.

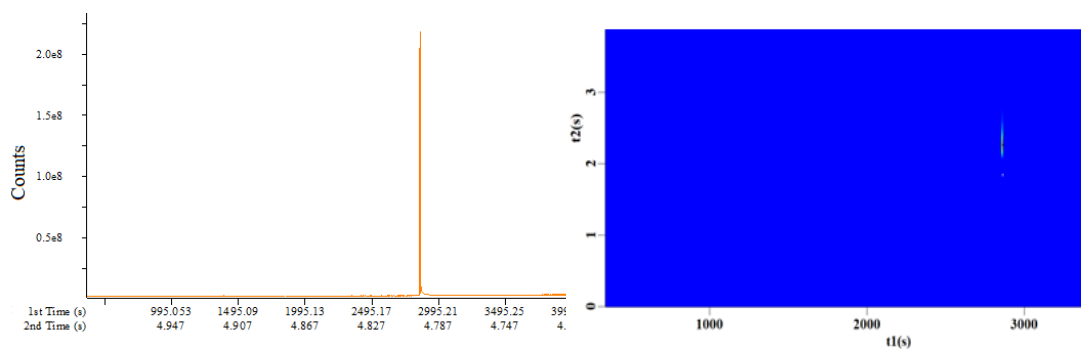


CHAPTER 6



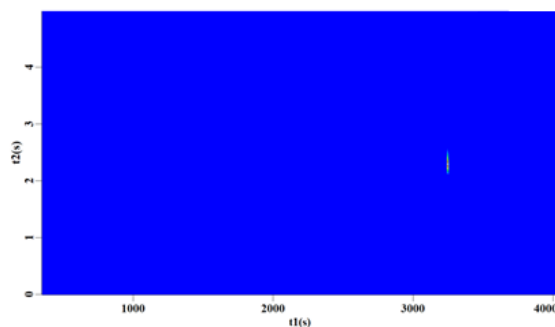
(c)

Fig.6.7 2D gas chromatogram of a) 19a, b) 19b and b) 19c (t_1 is the first dimensional retention, t_2 is the second dimensional retention).



(a)

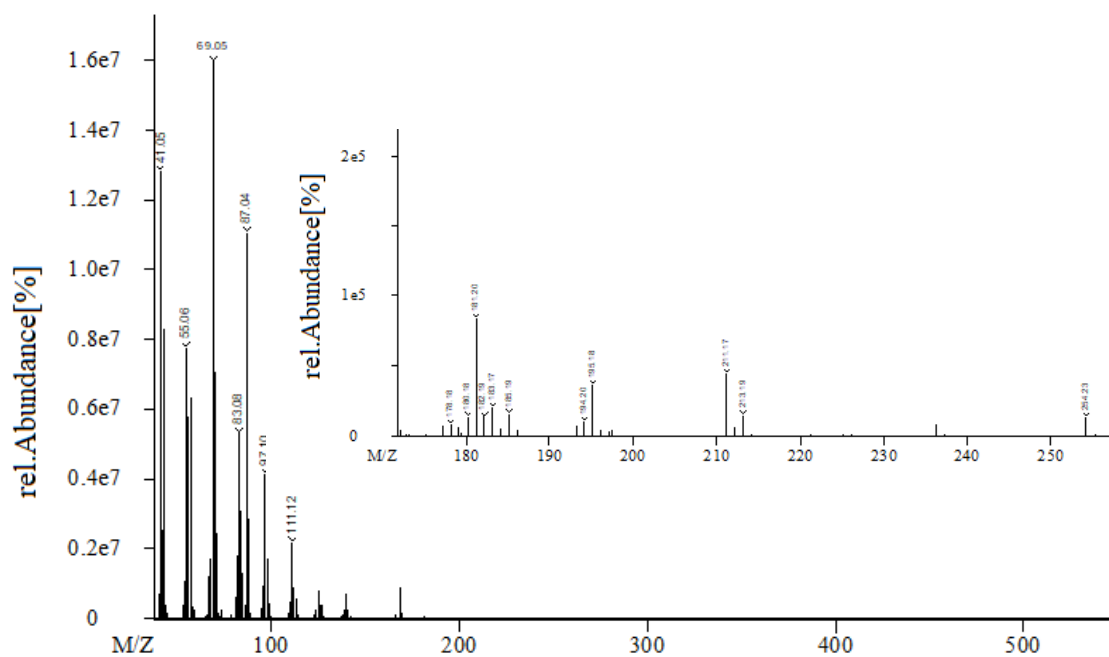
(b)



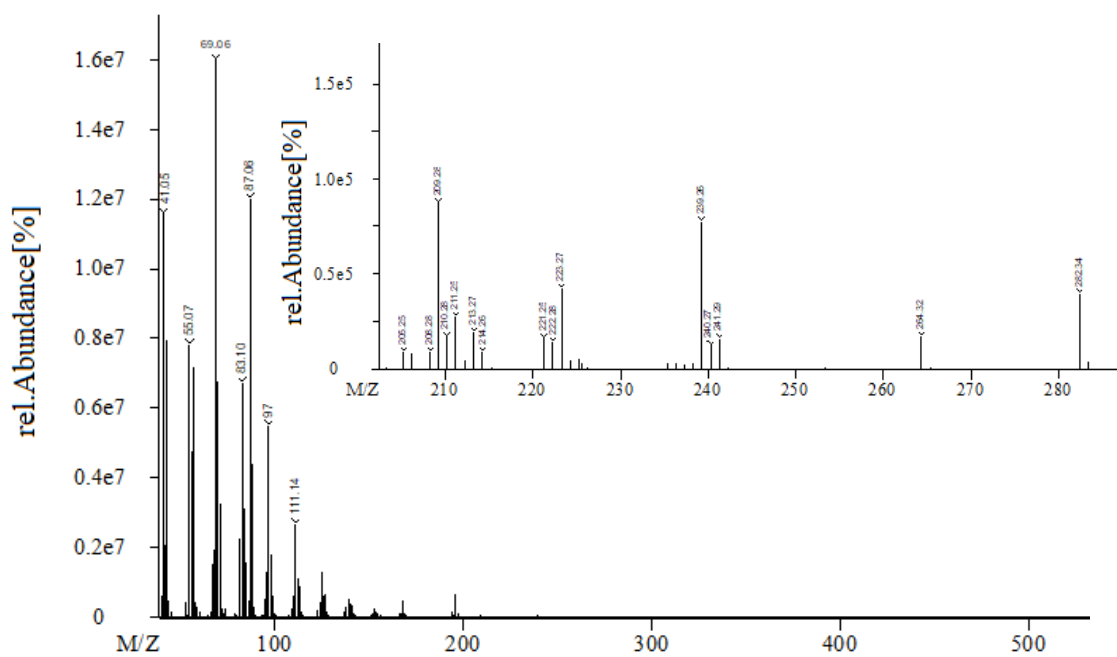
(c)

Fig.6.8 a) 1D gas chromatogram of 19a, 2D density distribution spectra of b) 19a and c) 19b (t_1 is the first dimensional retention, t_2 is the second dimensional retention).

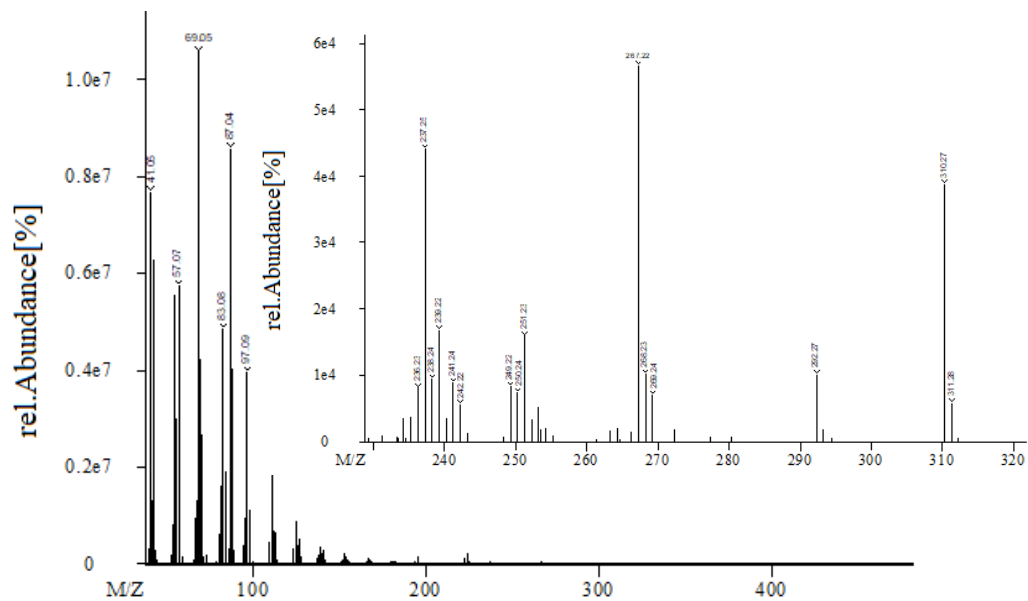
CHAPTER 6



(a)

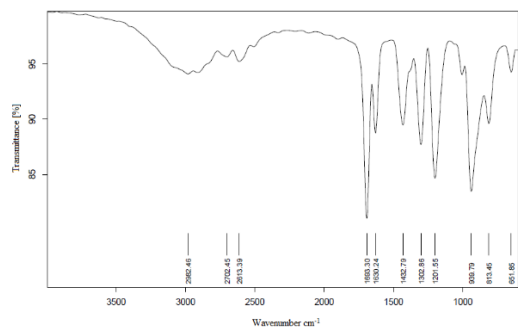


(b)

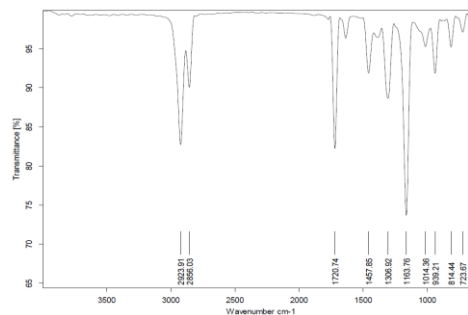


(c)

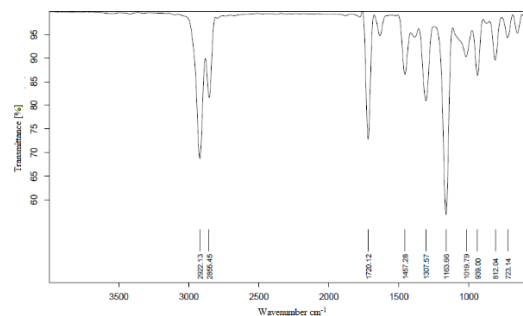
Fig.6.9 Mass spectra of a) 19a, b) 19b and c) 19c



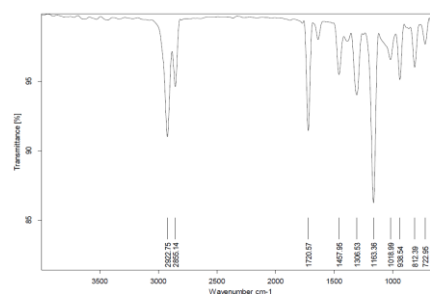
(a)



(b)



(c)



(d)

Fig.6.10 IR spectra of a) MAA, b) 19a, c) 19b and d) 19c.

CHAPTER 6

The gas chromatogram (Fig.6.11) and the mass spectra (Fig.6.12) confirm the successful conversion of oleic acid (OLA) into corresponding hydroxy esters (21a-c). The peak at (m/z) 327.29, 357.28 and 398.33 corresponds to the molecular ion of 21a, 21b and 21c respectively. The FTIR spectra (Fig.6.13) displayed a strong band at around 1730-1735 cm^{-1} corresponding to $-\text{C}=\text{O}$ stretching of the ester group as well as a broad OH band in the region 3424-3519 cm^{-1} along with other characteristic peaks. There is no absorption band observed for $\text{C}=\text{O}$ of acid group in the FTIR spectra which indicates the purity of the final product. The 2D GC (Fig.6.14), mass spectra (Fig.6.15) and IR spectra (Fig.6.16) confirms the conversion of OLA to corresponding esters (22a-c). The 2D-gas chromatogram of 22a exhibited single sharp peak which confirms the purity of sample. In the mass spectrum, the peak at (m/z) 453.45, 479.48 and 482.31 corresponds to molecular ion 22a, 22b and 22c respectively. There is no absorption band observed for $\text{C}=\text{O}$ of acid group which indicates the purity of the final product.

The FTIR spectral data of (17a-e), MAA, (19a-c), OLA, (21a-d) and (22a-c) are given below.

17a: IR (ATR, cm^{-1}): 3501(OH), 2928,2861,1721 ($\text{C}=\text{O}$ from ester), 1159 and 944

17b: IR (ATR, cm^{-1}): 3496(OH), 2923, 2856,1724 ($\text{C}=\text{O}$ from ester), 1162 and 944.

17c: IR (ATR, cm^{-1}): 3534 (OH), 2944, 2867, 1721 ($\text{C}=\text{O}$ from ester) 1158 and 941.

17d: IR (ATR, cm^{-1}): 3502 (OH), 2960, 2874, 1721 ($\text{C}=\text{O}$ from ester) 1157 and 945.

17e: IR (ATR, cm^{-1}): 3473 (OH), 2930, 2862, 1725 ($\text{C}=\text{O}$ from ester) 1163 and 946.

Methacrylic acid (MAA):IR (ATR, cm^{-1}): 2982, 2702,2613,1693 ($\text{C}=\text{O}$ from acid), 1630, 1433,1303,1202,940 and 813. **19a:** IR (ATR, cm^{-1}): 2924, 2856, 1721 ($\text{C}=\text{O}$ from ester), 1458, 1164, 1014 and 939. **19b:** IR (ATR, cm^{-1}): 2922, 2852, 1720 ($\text{C}=\text{O}$ from ester), 1457, 1307, 1164, 1019 and 939. **19c:** IR (ATR, cm^{-1}): 2923, 2855, 1721 ($\text{C}=\text{O}$ from ester), 1458, 1306 1019 and 939. **Oleic acid (OLA):**IR (ATR, cm^{-1}): 2922, 2856,1708 ($\text{C}=\text{O}$ from acid), 1448,1284,934 and 719. **21a:** IR (ATR, cm^{-1}): 3519 (OH) 2924, 2877, 1735 ($\text{C}=\text{O}$ from ester), 1454, 1169 and 722. **21b:** IR (ATR, cm^{-1}): 3445(OH) 2922, 2856, 1732 ($\text{C}=\text{O}$ from ester), 1454, 1171 and 719. **21c:** IR (ATR, cm^{-1}) 3470 (OH): 2924, 2858, 1730 ($\text{C}=\text{O}$ from ester), 1458, 1172 and 720. **22a:** IR (ATR, cm^{-1}): 2922, 2856, 1734 ($\text{C}=\text{O}$ from ester), 1458,1175 and 723. **22b:** IR (ATR, cm^{-1}):

CHAPTER 6

2922, 2855, 1736 (C=O from ester), 1457, 1174 and 722. **22c**: IR (ATR, cm^{-1}): 2921, 2855, 1737 (C=O from ester), 1458, 1173 and 721.

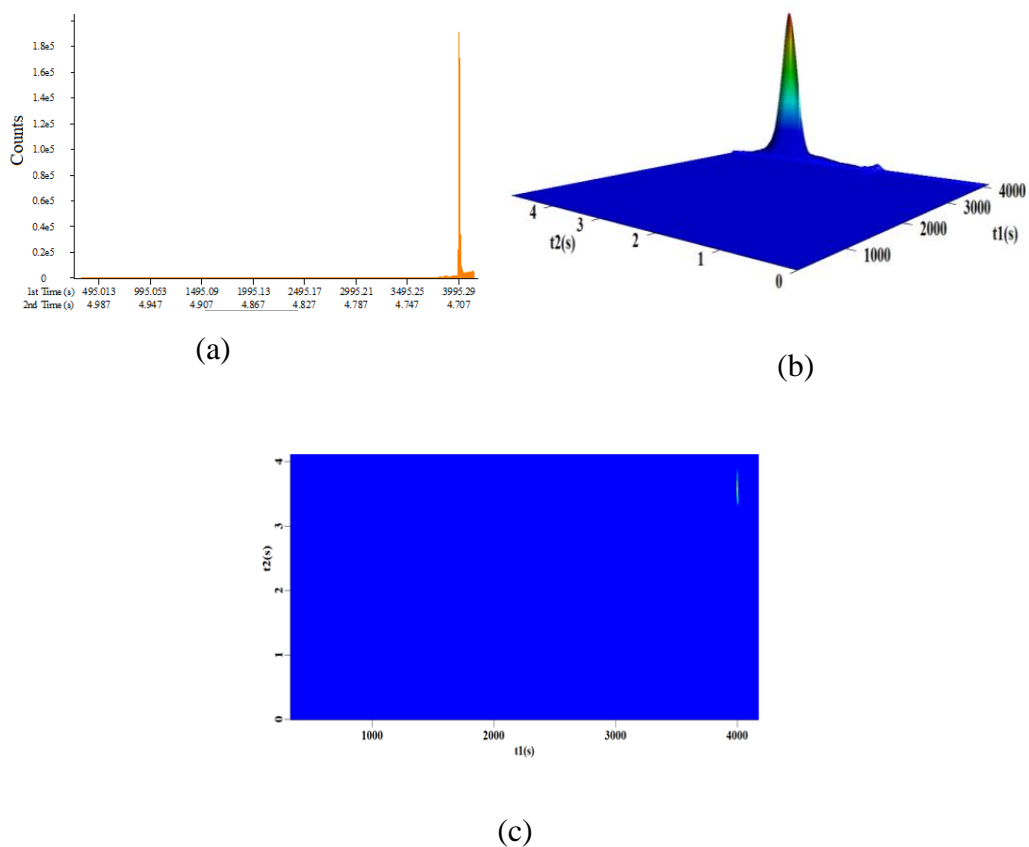
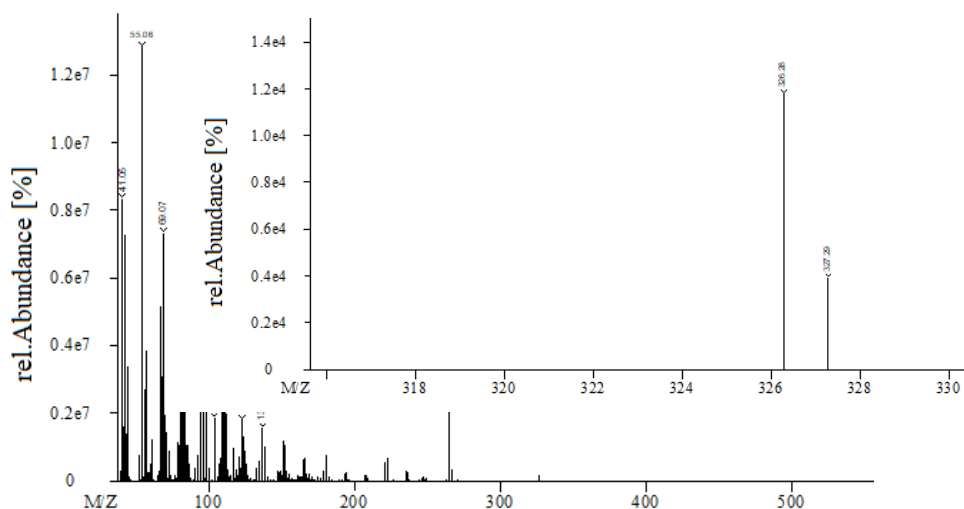


Fig.6.11 a) 1D gas chromatogram of 21a, b) 2D gas chromatogram of 21a and c) 2D density distribution spectrum of 21a (t_1 is the first dimensional retention, t_2 is the second dimensional retention).



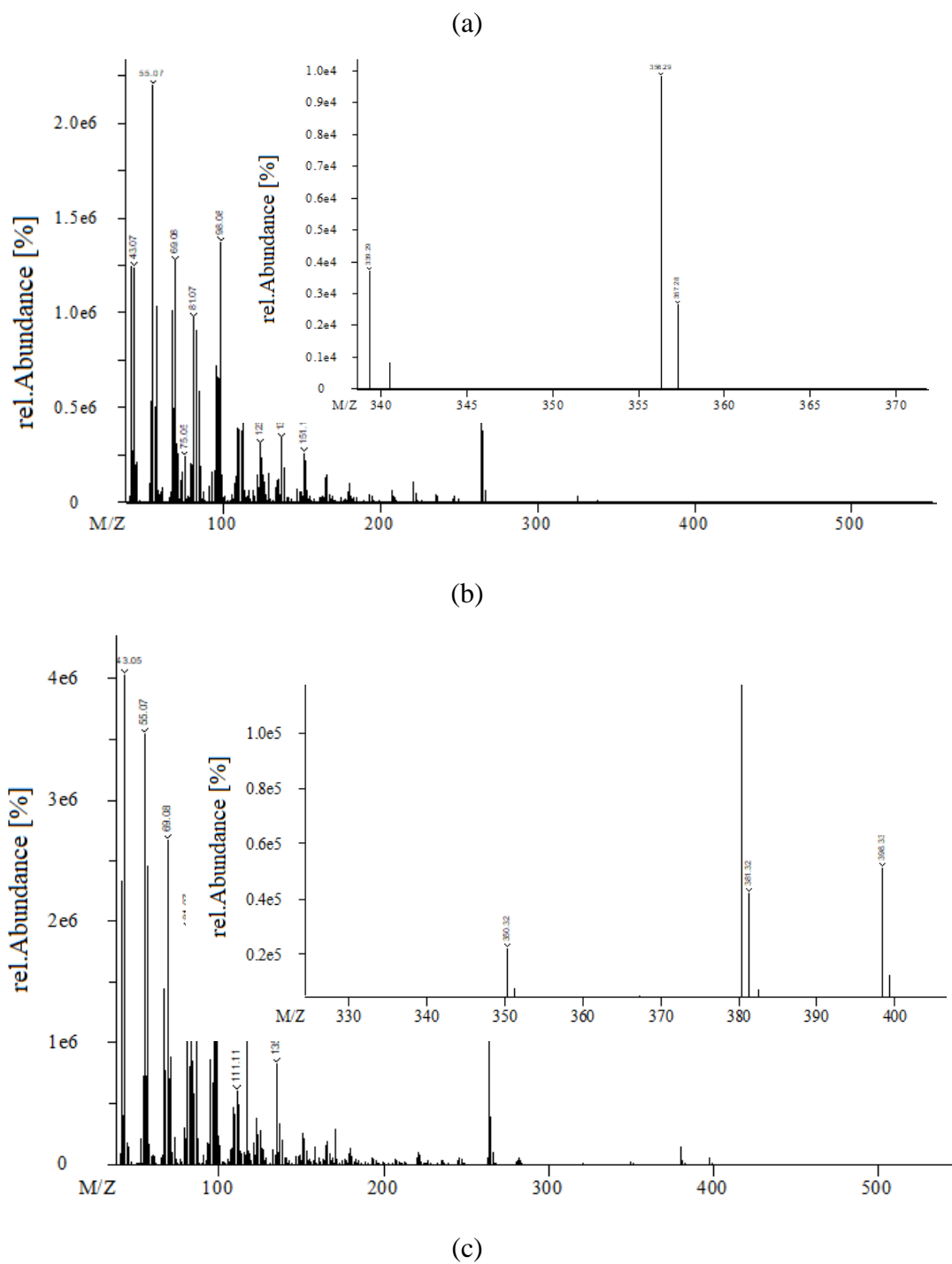


Fig.6.12 Mass spectra of a) 21a, b) 21b and c) 21c

CHAPTER 6

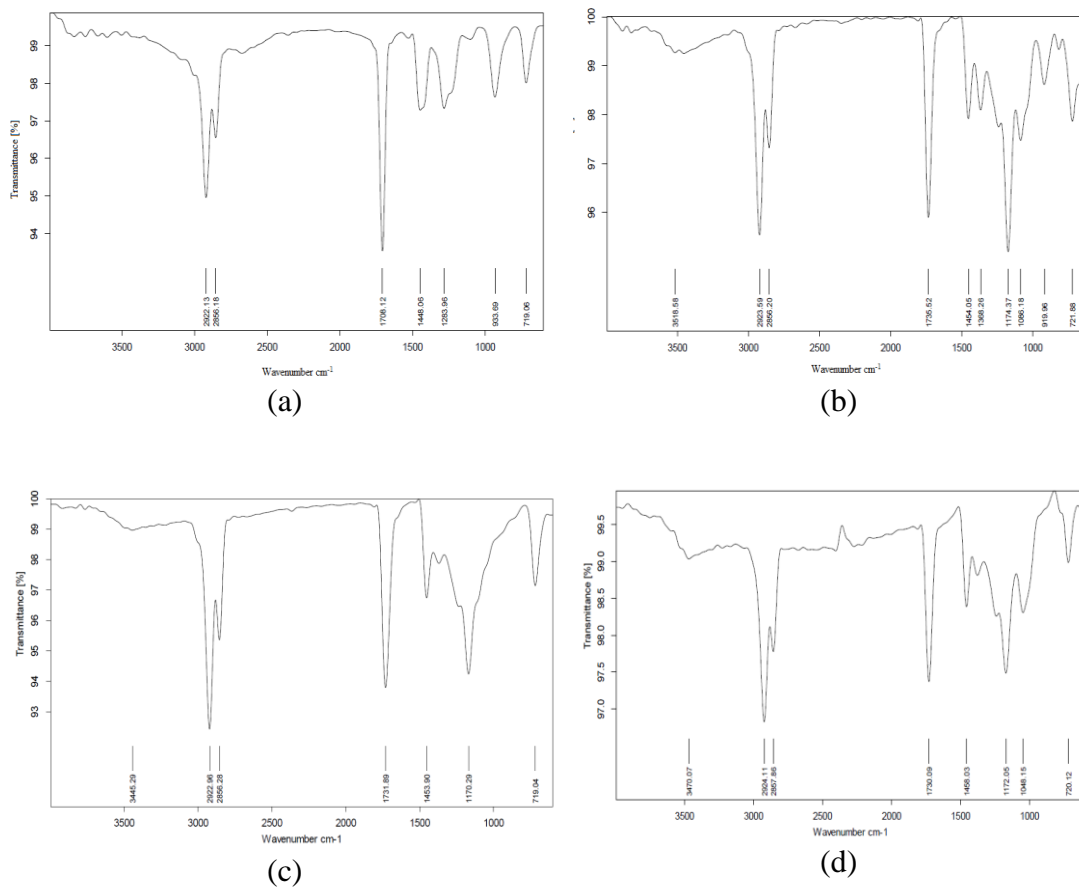


Fig.6.13 IR spectra of a) OLA, b) 21a, c) 21b and d) 21c

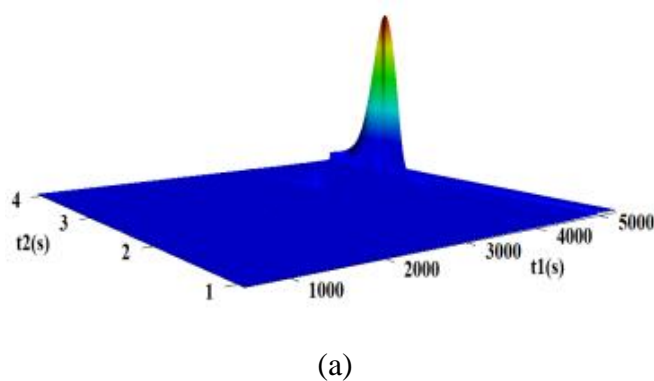
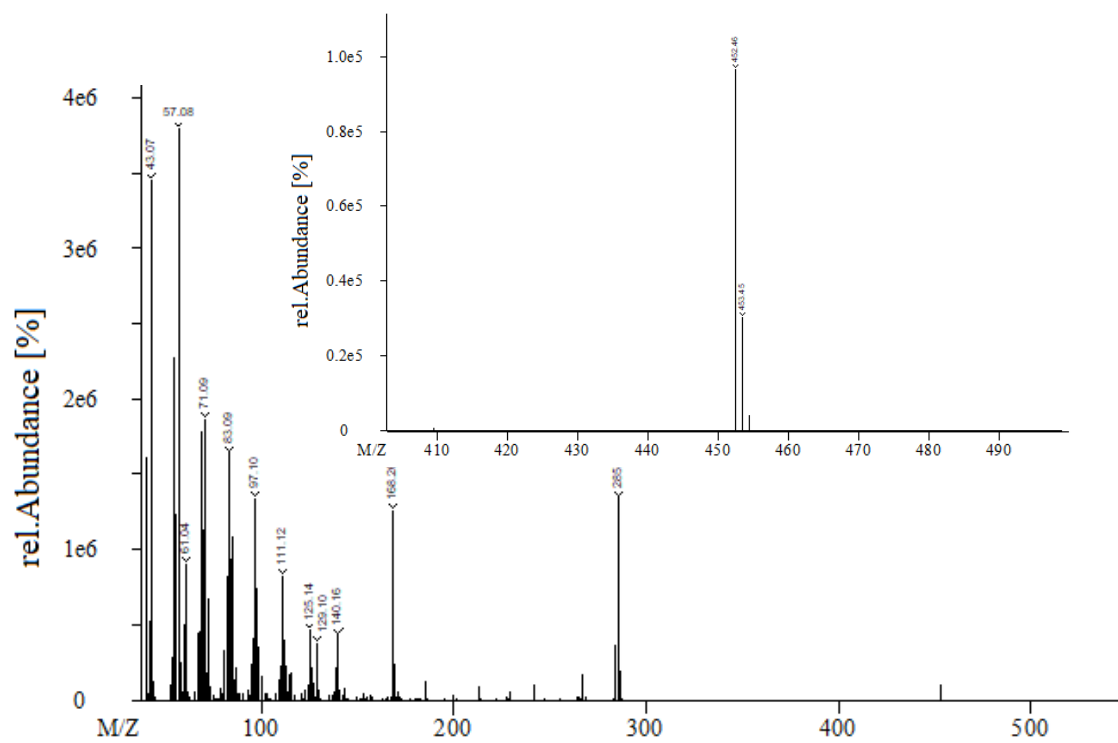
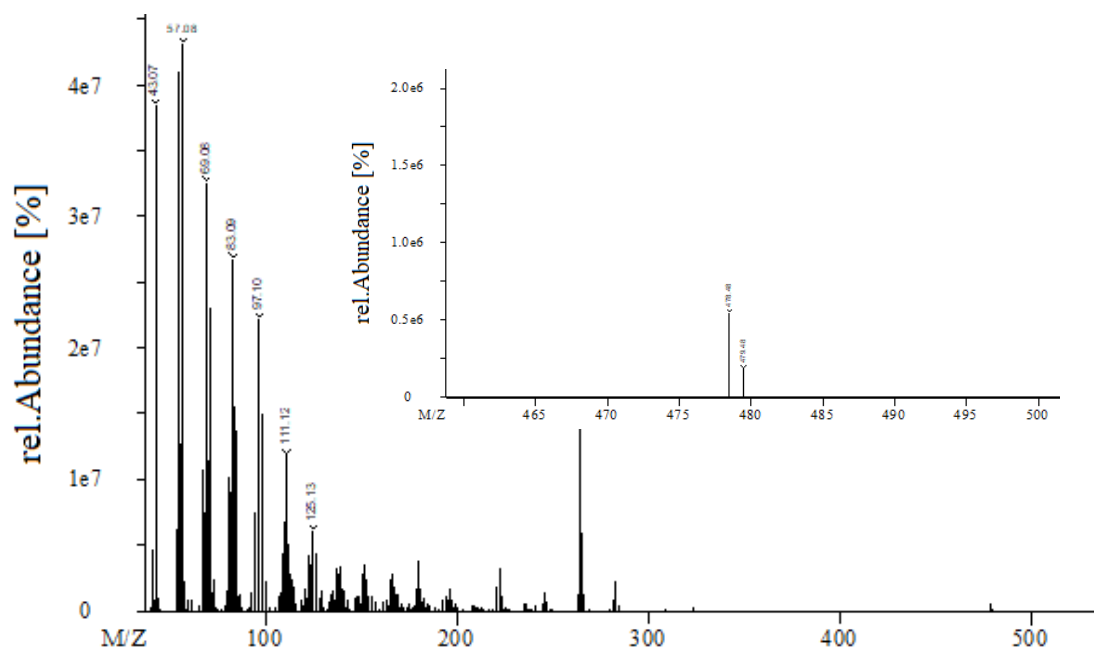


Fig.6.14 2D gas chromatogram of a) 22a (t1 is the first dimensional retention, t2 is the second dimensional retention).

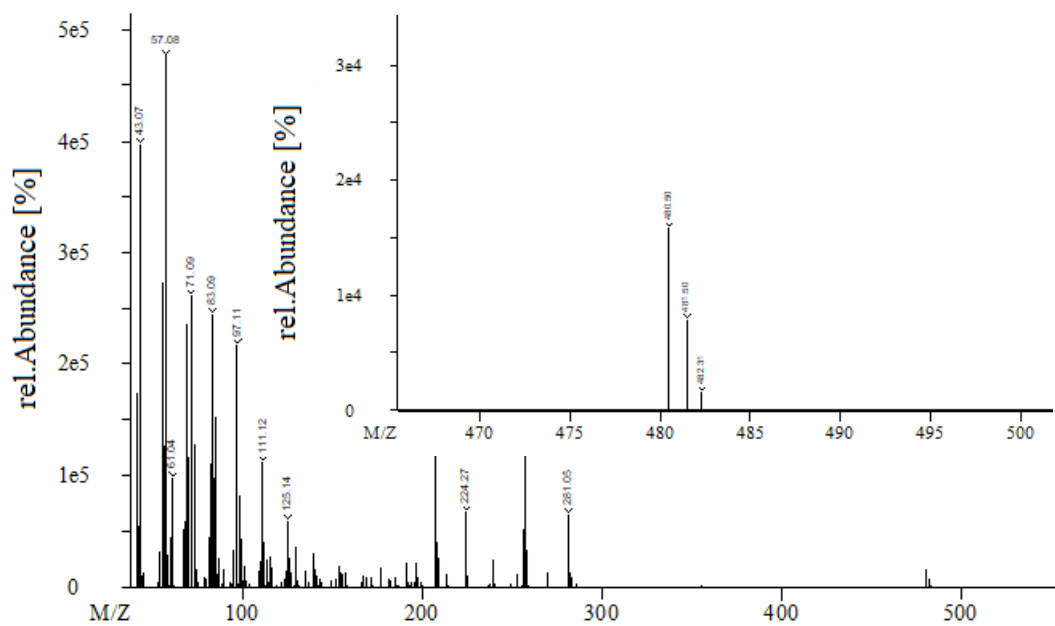
CHAPTER 6



(a)

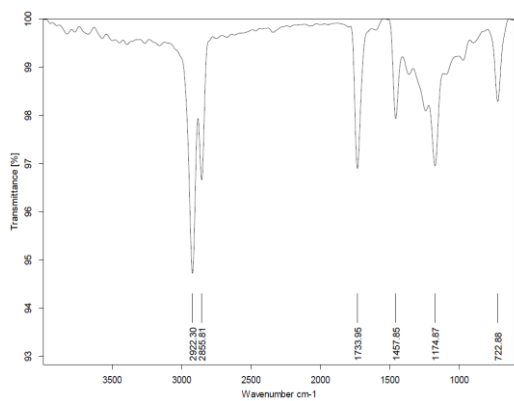


(b)

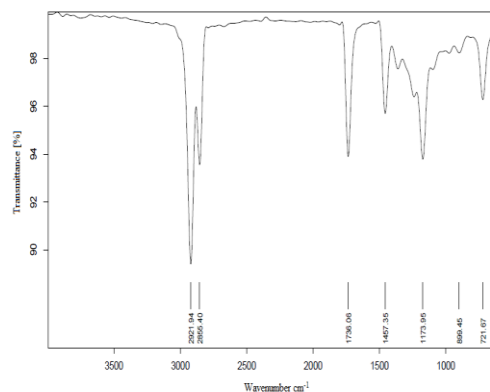


(c)

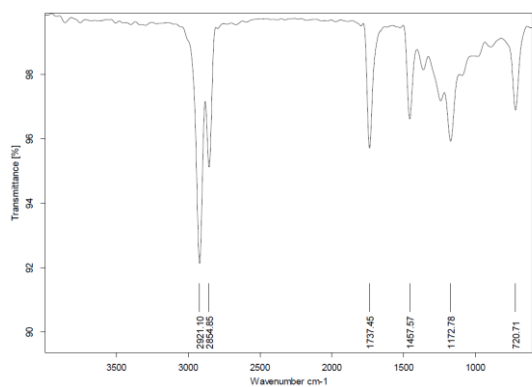
Fig.6.15 Mass spectra of a) 22a, b) 22b and c) 22c.



(a)



(b)



(c)

Fig.6.16 IR spectra of a) 22a, b) 22b and c) 22c.

CHAPTER 6

6.5 MEASUREMENT OF WEAR SCAR

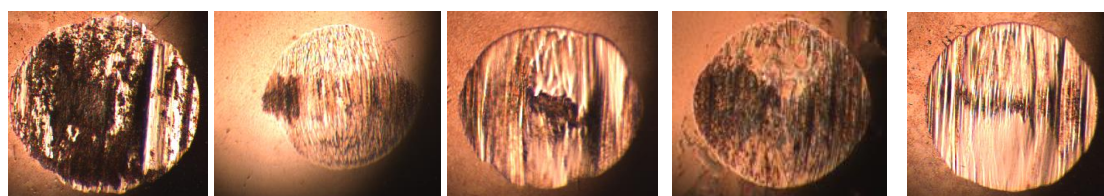
The obtained WSD, film % and friction coefficient for neat ULSD and blended ULSD (17a-e, 19a-c, 21a-c and 22a-c) are shown in Table 6.1. The optical microscopic images of scars obtained for neat ULSD and blended ULSD at different blending concentrations are given in Fig.6.17. All the derivatives exhibited good lubricity property except (19a-c). The compounds derived from oleic acid and polyol (OLA/Polyol) showed the least WSD values as compared to other derivatives. This could be due to the presence of long non-polar carbon chain with multiple polar (OH) groups on OLA/polyol derivatives (21a-c). GMA derivatives (2a-e), with only one polar (OH) group showed higher WSD values as compared with OLA/polyol derivatives. Similarly, OLA/FAL (22a-c) derivatives containing long non-polar carbon tail resulted lower WSD values than MAAR (19a-c) derivatives. The order of observed lubricant property is OLA/Polyol > OLA/FAL > GMAR > MAAR. Among different blends, the least WSD value was obtained for 21c-ULSD blend at 200 ppm. Hence 21c was chosen for further analysis wherein the lubricity was measured with different blending concentrations such as 600, 300 and 100 ppm (Table 6.1).

Table 6.1: The lubricity data of neat ULSD and blended ULSD

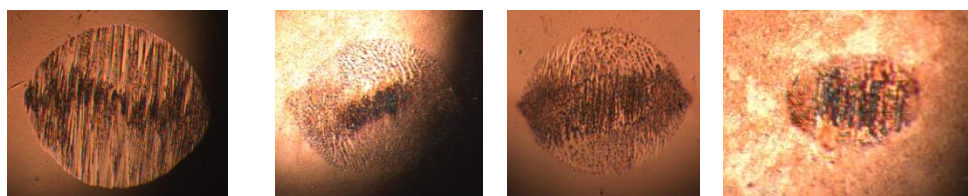
HFRR at 60 °C						
Sample ID	Blended Concentration (ppm)	Wear scar diameter (µm)			Result	
		Ball X	Ball Y	Average	Film (%)	Friction coefficient
Neat ULSD	-	511	497	504	11	0.900
17a	300	400	361	381	49	0.241
17b		438	414	426	30	0.274
17c		456	404	430	27	0.280
17d		460	416	438	22	0.298
17e		464	431	448	20	0.301
19a	300	560	520	540	6	0.699
19b		548	515	532	8	0.684
19c		533	483	508	11	0.670
17a	200	466	429	448	27	0.281
21a	200	445	385	415	37	0.253
21b		427	337	382	40	0.244
21c		353	303	328	49	0.226
22a		436	341	389	33	0.245

CHAPTER 6

22b		428	307	368	43	0.234
22c		381	318	350	47	0.229
21c	100	380	512	446	32	0.285
	300	250	194	222	86	0.201
	600	198	137	168	94	0.183

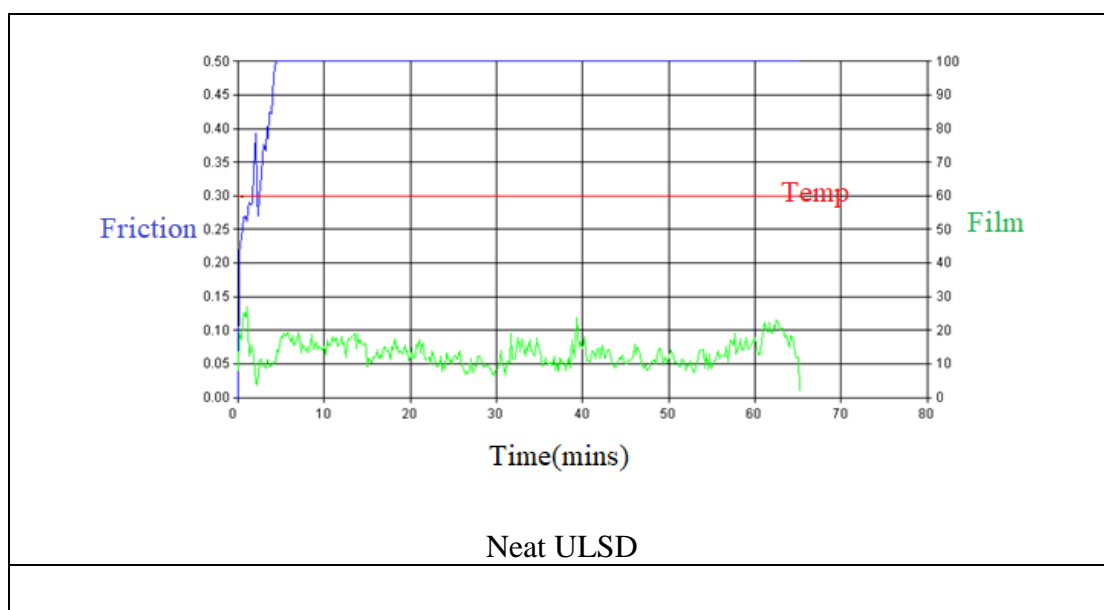


Neat ULSD 17a (A) 17d (A) 17f (A) 17a (B)



21a (B) 22a (B) 22c (B) 22c (C)

Fig.6.17 The optical microscopic images of scars obtained for neat ULSD and blended ULSD. (A), (B) and (C) corresponds blend concentration of 300, 200 and 600 ppm respectively.



CHAPTER 6

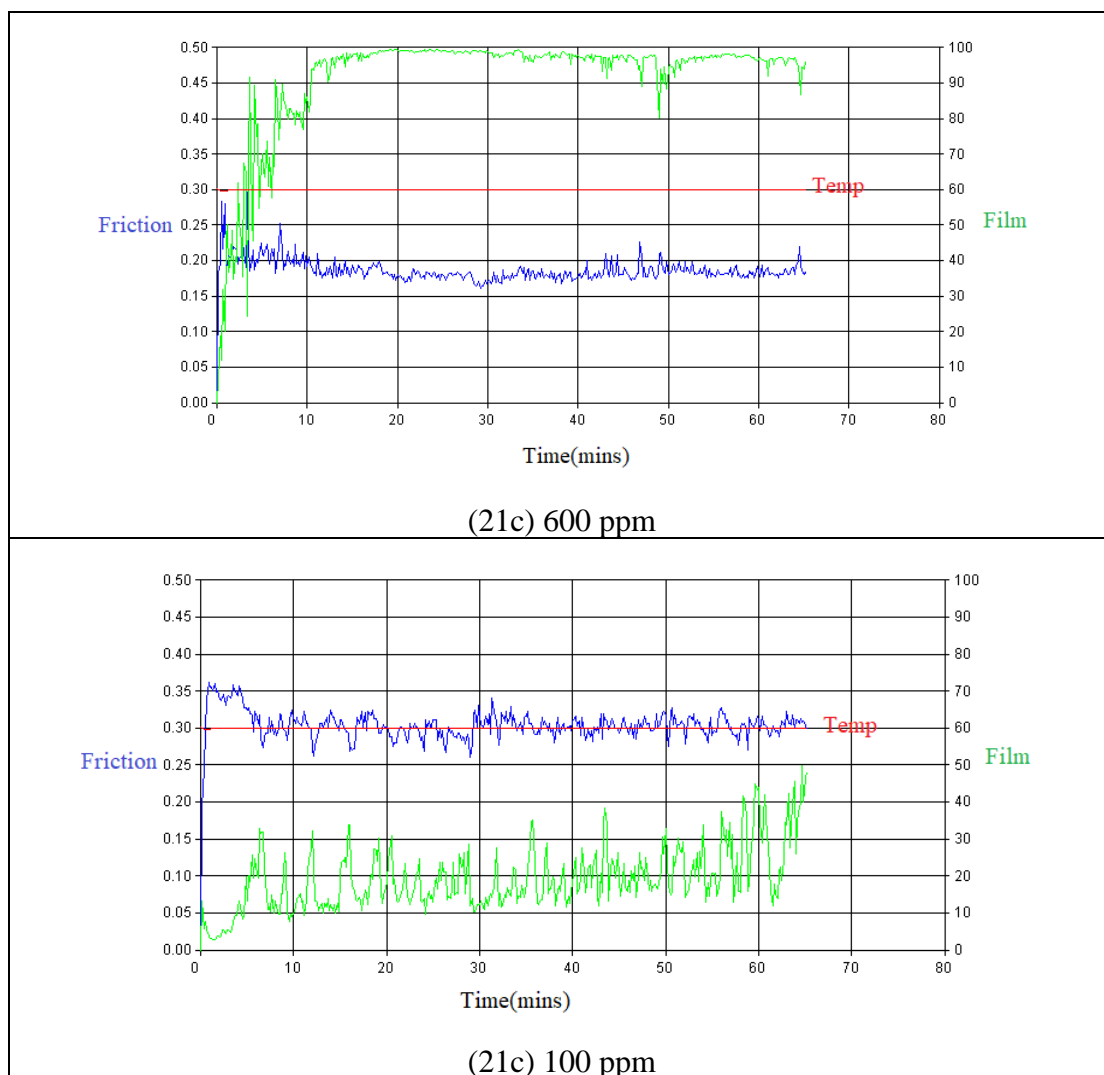


Fig.6.18 Real time graph obtained from HFRR instrument for neat ULSD, 21c-ULSD blends.

From the above data (Fig.6.18), it is clear that as the concentration of 21c increases on ULSD blend, the friction experienced between the metallic surface decreases. Due to this WSD decreases indicating that 21c is an efficient lubricity improver for ULSD. It is interesting to note that the WSD value at a low blend concentration of 100 ppm of 21c is below the accepted value of $460 \mu\text{m}$ hence lubricity additive (21c) can be used at a very low dosing concentration of 100 ppm, which makes the additives economically viable.

6.6 PHYSIOCHEMICAL PROPERTIES EVALUATION

6.6.1 Effect of new lubricity improvers on fuel properties of the diesel.

The effect of newly synthesised lubricity improvers on diesel fuel was determined by studying parameters like pour point, copper corrosion, oxidation stability etc. of the blend fuels. The test values obtained for each parameter is within permissible limit as per the IS-1460 specification. Hence the newly synthesized additive does not alter the key properties of the diesel fuel. The results of these measurements for neat ULSD and the blended fuel (100 ppm of 21c) are given in below.

Table 6.2: The test report summary of neat ULSD and blended ULSD (100 ppm of 21c)

Parameter	Test method	Specification	Results
			Blend fuel
Acidity, Total, mg of KOH/g, <i>Max</i> *	ASTM D 974	0.2	0.11
Cetane Index, <i>Min</i> *	IP 380	46	56.0
Pour point, °C, <i>Max</i> *	ASTM D 5950	3 for winter 15 for summer	-33
Copper strip corrosion test 3 h at 50°C	ASTM D 130	Not worse than No.1	No.1
Distillation, 95% recovery, v/v, recovery, °C, <i>Max</i> *	ASTM D 86	360	345.1
Flash point, °C, <i>Min</i> *	IP 170	35	>100
Kinematic viscosity, cSt at 40°C	ASTM D 445	2.0-4.5	3.058
Density @ 15°C, kg/m ³	ASTM D 4052	810-845	839.9
Total Sulphur, mg/Kg, <i>Max</i> *	ASTM D 5453	10	3.1
Lubricity, WSD at 60°C, microns, <i>Max</i> *	ASTM D 6079-18	460	446
Oxidation stability, g/m ³ , <i>Max</i> *	ASTM D 2274	25	12.5
Cold Filter Plugging Point (CFPP), °C	ASTM D 6371	6 for winter 18 for summer	-16

6.7 LUBRICITY MECHANISM

The investigation of tribological behaviour of lubricity improver towards metal surface was carried out using SEM and EDS techniques. The FESEM images of the scars on ball's surface are shown in Fig.6.19. The FESEM image of worn surface of

CHAPTER 6

blended ULSD (21c) shows fewer scratch marks than neat ULSD. The hydroxy and ester functional groups of 21c offer active oxygen sites that bind to the metal surface to form a thin layer, which can avoid the direct metal to metal contact in friction couples. Through this way ULSD-21c blend reduces the friction on the metallic surfaces. The interaction between the additive and the metal surface was studied through EDS technique. Through EDS graph (Fig.6.20) the percentage of C, O, Fe and Cr on the surfaces for neat ULSD as well as blended ULSD (21c) was estimated. The percentage of oxygen on the specimen lubricated by the blend fuel was higher than that on the surface lubricated by the neat ULSD. The higher oxygen content in the case of blend fuel could be due to the interaction of the metal surface with the oxygen containing functional groups of the additive which helps in the formation of a protective lubricating layer. The oxygen content on the worn surface increases from 9.1 to 12.1 % with an increase in the blend concentration from 300 to 600 ppm which further supports the interaction of the metal surface with the additive through oxygen containing functional groups. Hence, it can be confirmed that the presence of polar groups such as $-\text{COOR}$ and $-\text{OH}$ in the molecule helps to increase their absorptivity on the metal surface by the formation of thin defending layer. Hence fuel injection system of engine gets protection from wear and tear.

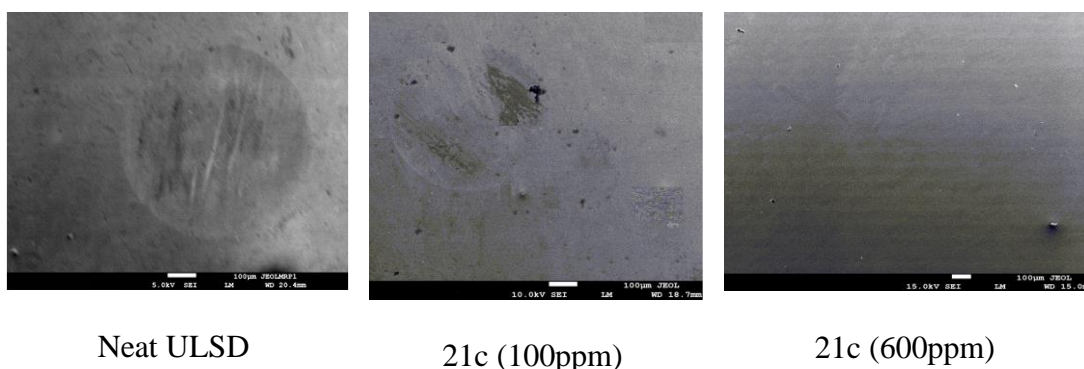


Fig.6.19 SEM images of the wear scars on balls of the friction couples with neat ULSD and ULSD-21c blends.

CHAPTER 6

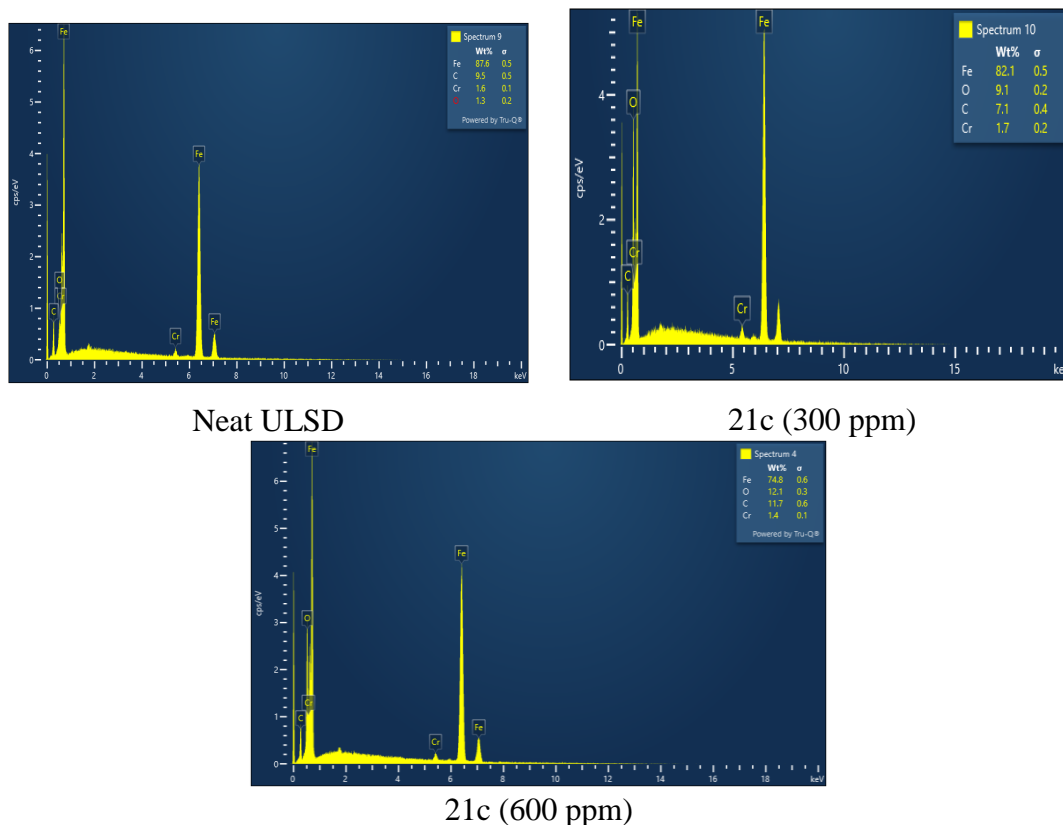


Fig.6.20 EDS graphs of the metal surfaces with neat ULSD and ULSD-21c blends

6.8 CONCLUSIONS

It can be concluded that,

- The order of friction reducing quality of different lubricity improvers is OLA/polyol > OLA/FAL > GMAR > MAAR derivatives.
- The multiple polar hydroxy groups in these additives help to enhance the lubricity properties of ULSD.
- Molecules with multiple hydroxy groups and long non-polar carbon chain favor to decrease friction between the metal surfaces.
- The lubricity action is due to the formation of shielding lubricant film of the additive between the metal surfaces. The best additive, OLA/polyol forms 98 and 55% film at dosage levels of 600 and 300 ppm respectively.
- The OLA/Polyol derivative do not affect the key properties of diesel fuel as confirmed by physical chemical studies.
- The formation of protective thin layer of LI on metal surface are confirmed by SEM and EDS techniques.

CHAPTER 7

COST EFFECTIVE LUBRICITY IMPROVER DERIVED FROM NATURALLY ABUNDANT SUBSTANCES FOR ULTRA LOW SULPHUR DIESEL

Abstract

This chapter comprises the synthesis of new series of LI for ULSD starting from naturally abundant substances like 1,2-diols, triols, an anhydride etc. through a single step reaction protocol. It includes lubricity study and mechanism of lubricity action of newly synthesised LI on metal surfaces.

7.1 INTRODUCTION

The bio and synthetic additives are the two most prevalent forms of lubricants for ULSD. The bio-based additives are directly derived from natural resources are created and blended with ULSD at specific concentrations. As opposed to this, synthetic lubricants including fatty acid esters, carbonates, and synthetic additives made by straightforward synthetic processes are highly intriguing. These substances, which are produced from naturally occurring substances that are inexpensively available, are an appealing option because of their effective lubricity-improving characteristics. Therefore, it is advised to create highly accessible synthetic materials into efficient and affordable lubricity additives. In this direction, the potential group of raw materials, such as 1,2-diols, triols, an anhydride, and a fatty acid, are transformed into inexpensive additives through a simple reaction protocol.

7.2 EXPERIMENTAL SECTION

7.2.1 Materials and Instruments

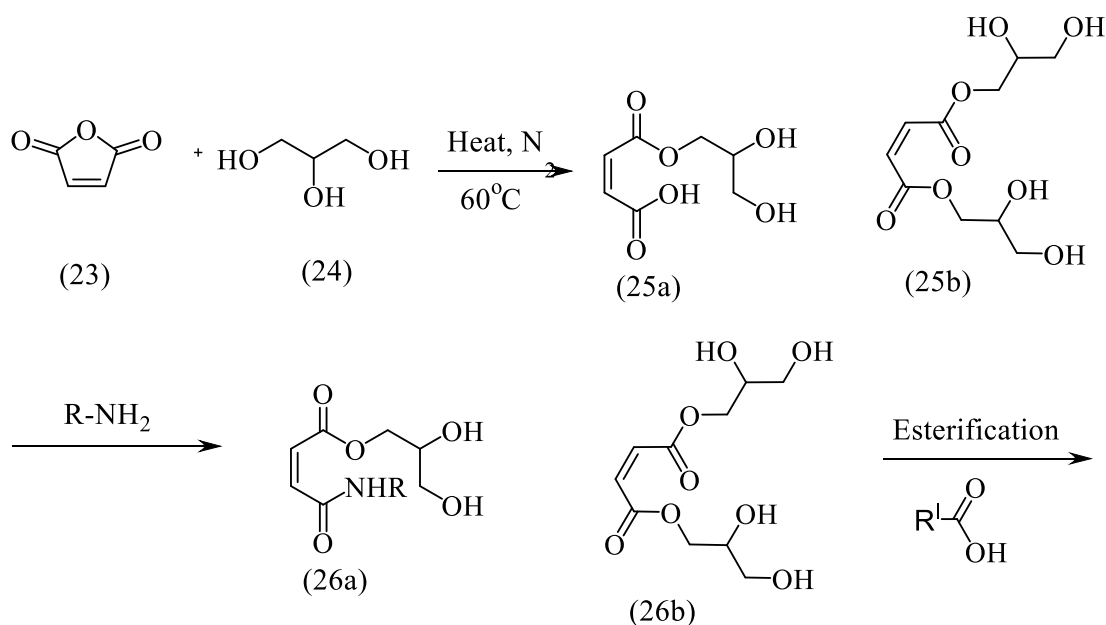
The details of all materials and instruments are discussed in chapters 3.

*[Glycerol (GL), ethylene glycol (EGL), maleic anhydride (MA), octanoic acid (OA), oleic acid (OLA), and 2-ethylhexanoic acid (2EHA), diethanolamine (DELA), diethylamine (DEA), ethanolamine (ELA), ethyl aminoethanol (EAEL), dimethylformamide (DMF), tetrahydrofuran (THF), p-toluene sulphonic acid (PTSA)

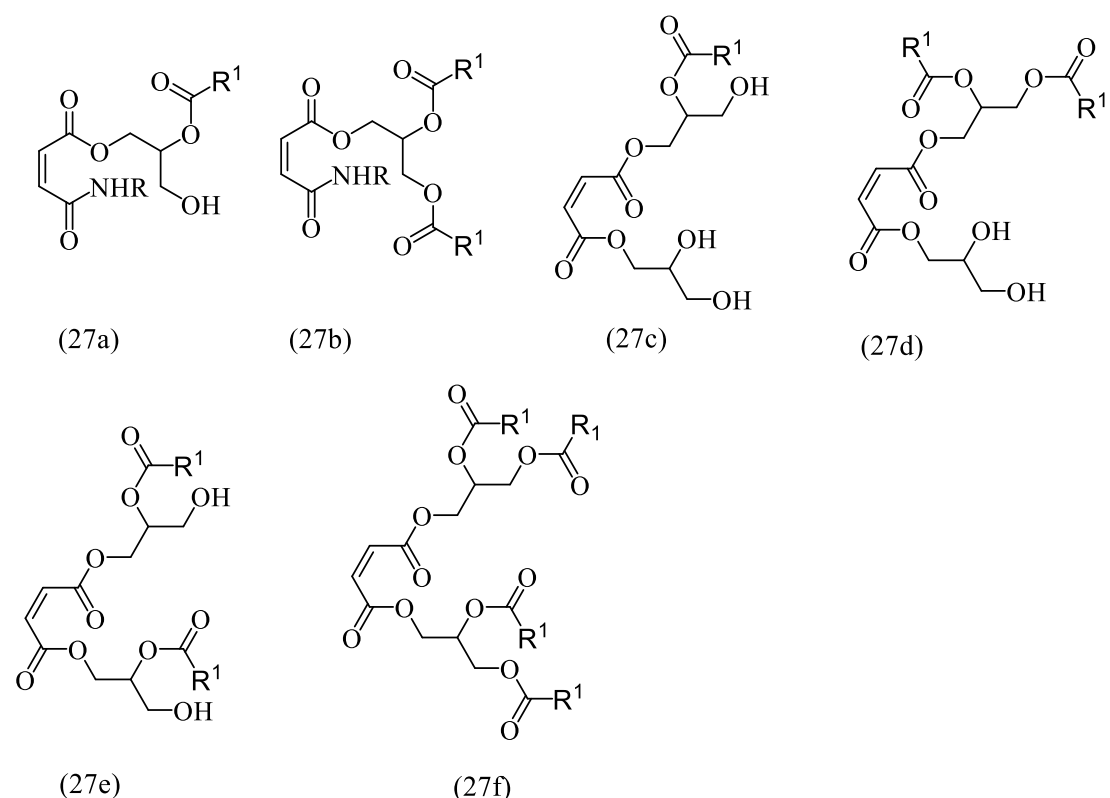
and triethylamine (TEA)]. * The abbreviations of the chemicals, reagents and catalyst are used.

7.2.2 General procedure for the synthesis of lubricity improver starting from an anhydride, triol, fatty acid and amine

To a mixture of maleic anhydride (1 mol), PTSA (0.006 mol) and THF (100 mL), appropriate amount of the triol (1 mol) was added. The reaction mixture was refluxed until the reaction mixture becomes homogeneous (scheme 7.1). Then, appropriate amount of the amine (1 mol) and organic acid (1 mol) were added. After completion of the reaction, the mixture was cooled to room temperature and left to stand for 3 h. Then the mixture was extracted with ethyl acetate and the organic layer was washed with DM water (200 mL) followed by 5% HCL (200 mL) and 5 % sodium bicarbonate (200 mL) solution. The organic layer was filtered through sodium sulphate and the solvent was evaporated using rotary evaporator to yield the product. The obtained product was termed as MAGLRR¹ (where R and R¹ corresponds to different amine and fatty acid groups respectively).



CHAPTER 7



Scheme 7.1: Typical reaction scheme for the synthesis of LI (MAGLRR¹) for ULSD.

7.2.2.1 The optimisation of reaction

To establish and optimize the reaction, different trials were carried out by varying the reactants ratio. The summary of yield (%) obtained for MAGLR¹R and MAEGLR¹R at different reactant ratios is given in Tables 7.1 - 7.7.

Table 7.1: The summary of yield (%) obtained for MAGL2EHAR at different reactant ratio (trial- 1)

Trial 1: Using DMF/PTSA				
Acid	Amine	MA:GL: R ¹ COOH: RNH ₂ Ratio	Symbol	Yield (%)
2EHA	DELA	3:1:1:1	1E	50
	DEA	3:1:1:1	2E	51
	ELA	3:1:1:1	3E	55
	2EAEL	3:1:1:1	4E	49
	DELA	1:1:1:1	5E	56
	DEA	1:1:1:1	6E	59
	ELA	1:1:1:1	7E	50

CHAPTER 7

	2EAEL	1:1:1:1	8E	52
	DELA	1:2:1:1	9E	55
		1:2:1:2	10E	60
		1:1:1:2	11E	59
	DEA	1:2:1:1	12E	55
		1:2:1:2	13E	60
		1:1:1:2	14E	62

Table 7.2: The summary of yield (%) obtained for MAGL2EHAR at different reactant ratio (trial- 2)

Trial 2: Using THF/PTSA				
Acid	Amine	MA:GL: R ¹ COOH: RNH ₂ Ratio	Symbol	Yield (%)
2EHA	DELA	3:1:1:1	15E	61
	DEA	3:1:1:1	16E	60
	ELA	3:1:1:1	17E	54
	2EAEL	3:1:1:1	18E	69
	DELA	1:1:1:1	19E	69
	DEA	1:1:1:1	20E	60
	ELA	1:1:1:1	21E	67
	2EAEL	1:1:1:1	22E	66
	DELA	1:2:1:1	23E	64
		1:2:1:2	24E	65
		1:1:1:2	25E	61
	DEA	1:2:1:1	26E	66
		1:2:1:2	27E	68
		1:1:1:2	28E	64

Table 7.3: The summary of yield (%) obtained for MAGL2EHAR at different reactant ratio (trail-3)

Trial 3: Using THF/TEA				
Acid	Amine	MA:GL: R ¹ COOH: RNH ₂ Ratio	Symbol	Yield (%)
2EHA	DELA	3:1:1:1	29E	44
	DEA	3:1:1:1	30E	40
	ELA	3:1:1:1	31E	43
	2EAEL	3:1:1:1	32E	39
	DELA	1:1:1:1	33E	49
	DEA	1:1:1:1	34E	50

CHAPTER 7

	ELA	1:1:1:1	35E	47
	2EAEL	1:1:1:1	36E	46
	DELA	1:2:1:1	37E	44
		1:2:1:2	38E	55
		1:1:1:2	39E	51
	DEA	1:2:1:1	40E	46
		1:2:1:2	41E	58
1:1:1:2		42E	54	

Table 7.4 :The summary of yield (%) obtained for MAEGL2EHAR at different reactant ratio (trail-4)

Trial 4: Using THF/PTSA				
Acid	Amine	MA:EGL: R ¹ COOH: RNH ₂ Ratio	Symbol	Yield (%)
2EHA	DELA	1:1:1:1	43E	60
	DEA	1:1:1:1	44E	65
	ELA	1:1:1:1	45E	59
	2EAEL	1:1:1:1	46E	53

Table 7.5: The summary of yield (%) obtained for MAGLROLA and MAGLROA at different reactant ratio (trail-4)

Trial 4: THF/PTSA (MA :GL ;1:1)				
Acid	Amine	RNH ₂ : R ¹ COOH Ratio	Symbol	Yield (%)
OLA	DELA	1:1	OL1	85
	DEA	1:1	OL2	90
	ELA	1:1	OL3	85
	2EAEL	1:1	OL4	86
OA	DELA	1:1	OA1	85
	DEA	1:1	OA2	90
	ELA	1:1	OA3	85
	2EAEL	1:1	OA4	86

CHAPTER 7

Table 7.6: The summary of yield (%) obtained for MAEGLROLA and MAEGLROA at different reactant ratio (trial -5)

Trial 5: Using THF/PTSA (MA: EGL; 2:1)				
Acid	Amine	RNH ₂ : R ¹ COOH Ratio	Symbol	Yield (%)
OLA	DELA	1:1	OL5	80
	DEA	1:1	OL6	83
	ELA	1:1	OL7	75
	2EAEL	1:1	OL8	76
OA	DELA	1:1	OA5	75
	DEA	1:1	OA6	80
	ELA	1:1	OA7	69
	2EAEL	1:1	OA8	70

Note* Comparing ethylene glycol derivatives, glycerol derivative shows better enhancement in lubricity and also, diethyl amine derivative show better lubricity than another amine derivative. Hence further reaction were carried out using glycerol and diethylamine as a starting material.

Trial 6: MAGLOLADEA (1:1:1:1) [1A]

To a mixture of maleic anhydride (20 g, 0.20 mol), THF (20 mL) appropriate amount of glycerol (18 g, 0.20 mol) and PTSA (1 g, 0.006 mol) was added. Then, the reaction mixture was allowed to reflux for 1 h. After 1 h, DEA (14 g, 0.20 mol) and OLA (56 g, 0.20 mol) was added to the reaction mixture, then reaction was continued with continues stirring. After completion of the reaction, the product was extracted using ethyl acetate. Organic phase was washed with excess of water and 1.0 M sodium bicarbonate solution to remove the un-reacted acid. Finally, the organic layer was dried over anhydrous sodium sulphate and the solvent was removed under vacuum to yield the mixture of esters as yellow liquid.

Same procedure was followed for the synthesis of MAGLOLADEA at different ratios (1:1:0.5:0.5) [2A], (1:1:0.25:0.25) [3A], (1:1:0.125:0.125) [4A], (1:1:1:0.5) [5A], (1:1:1:0.25) [6A], (1:1:1:0.125) [7A], (0.5:0.5:1:1) [8A], (0.5:0.5:2:1) [9A]. And also

CHAPTER 7

for (MAGLOADEA), at (1:1:1:1) [10A], (1:1:0.5:0.5) [11A], (1:1:0.25:0.25) [12A], (1:1:0.125:0.125) [13A], (1:1:1:0.5) [14A]. (1:1:1:0.25) [15A], (1:1:1:0.125) [16A], (0.5:0.5:1:1) [17A]. (0.5:0.5:2:1) [18A]. (MAGL2EHADEA) at (1:1:1:1) [19A], (1:1:0.5:0.5) [20A], (1:1:0.25:0.25) [21A], (1:1:0.125:0.125) [22A], (1:1:1:0.5) [23A]. (1:1:1:0.25) [24A], (1:1:1:0.125) [25A], (0.5:0.5:1:1) [26A]. (0.5:0.5:2:1) [27A] ratio.

Table 7.7: The summary of yield (%) obtained for MAGLDEAR¹ at different reactant ratio (trail-6).

Acid (R ¹)	Ratio (MAGLDEA R ¹)	Symbol	Reaction time	Yield (%)
OLA	1:1:1:1	1A	4 h	90
	1:1:0.5:0.5	2A		87
	1:1:0.25:0.25	3A		70
	1:1:0.125:0.125	4A		68
	1:1:0.5:1	5A		70
	1:1:0.25:1	6A		67
	1:1:0.125:1	7A		60
	0.5:0.5:1:1	8A		65
	0.5:0.5:1:2	9A		70
OA	1:1:1:1	10A		88
	1:1:0.5:0.5	11A		85
	1:1:0.25:0.25	12A		81
	1:1:0.125:0.125	13A		80
	1:1:0.5:1	14A		79
	1:1:0.25:1	18A		77
	1:1:0.125:1	16A		68
	0.5:0.5:1:1	17A		60
	0.5:0.5:1:2	18A		67
2EHA	1:1:1:1	19A	87	
	1:1:0.5:0.5	20A	77	
	1:1:0.25:0.25	21A	71	
	1:1:0.125:0.125	22A	68	

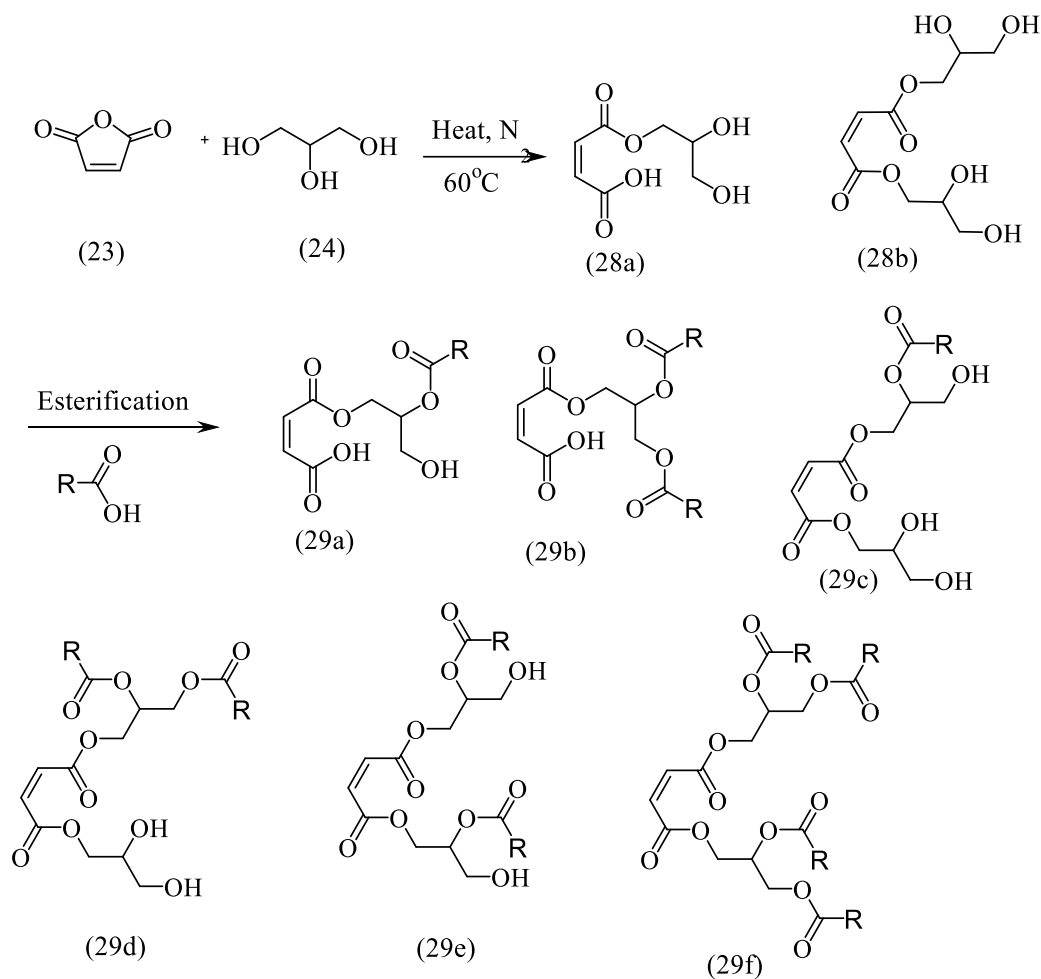
	1:1:0.5:1	23A		67
	1:1:0.25:1	24A		67
	1:1:0.125:1	25A		60
	0.5:0.5:1:1	26A		66
	0.5:0.5:1:2	27A		69

Note*: There is no much difference in lubricity enhancing properties of the additives synthesised in presence of amine, hence further reaction was carried out using MA, GL and acid (without amine)

7.2.3 General procedure for the synthesis of LI starting from an anhydride triol and fatty acid (Scheme 7.2)

To a mixture of anhydride (1 mol), PTSA (0.006 mol) and THF (100 mL), appropriate amount of the triol (1 mol) was added. The reaction mixture was refluxed until the mixture becomes homogeneous. Later, appropriate amount of the organic acid (1 mol) was added. After completion of the reaction, the mixture was cooled to room temperature and left to stand for 3 h. Then the mixture was extracted with ethyl acetate and the organic layer was washed with DM water (200 mL) followed by 5 % sodium bicarbonate (200 mL) solution. The organic layer was filtered through sodium sulphate and the solvent was evaporated using rotary evaporator to yield the product. The obtained product was termed as MAGLR (where R corresponds to different fatty acid groups).

CHAPTER 7



Scheme 7.2 Typical reaction scheme for the synthesis of LI (MAGLR) for ULSD.

Trial 7: MAGLOLA (1:1:1) [1B]

To a mixture of maleic anhydride (20 g, 0.20 mol), THF (20 mL) appropriate amount of glycerol (18 g, 0.20 mol) and PTSA (1 g, 0.006 mol) was added. Then, the reaction mixture was allowed to reflux for 1h. After 1h, OLA (56 g, 0.20 mol) was added to the reaction mixture, then reaction was continued with stirring. After completion of the reaction, the product was extracted using ethyl acetate. Organic phase was washed with excess of water and 1.0 M sodium bicarbonate solution to remove the un-reacted acid. Finally, the organic layer was dried over anhydrous sodium sulphate and the solvent was removed under vacuum to yield the mixture of esters as yellow liquid.

MAGLOLA at different ratios (1:1:0.5) [2B], (1:1:0.25) [3B], (1:1:0.125)[4B], (MAGLOA), at (1:1:1) [5B], (1:1:0.5) [6B], (1:1:0.25) [7B], (1:1:0.125) [8B],

CHAPTER 7

(MAGL2EHA) at (1:1:1) [9B], (1:1:0.5) [10B], (1:1:0.25) [11B], (1:1:0.125) [12B], were synthesised following the same procedure. The summary of yield (%) obtained for MAGLR at different reactant ratio given in Table 7.8.

Table 7.8: The summary of yield (%) obtained for MAGLR at different reactant ratio (trail-6)

Acid (R)	Ratio (MAGLR)	Symbol	Reaction time	Yield (%)
OLA	1:1:1	1B	4 h	90
	1:1:0.5	2B		87
	1:1:0.25	3B		75
	1:1:0.125	4B		67
OA	1:1:1	5B		84
	1:1:0.5	6B		80
	1:1:0.25	7B		75
	1:1:0.125	8B		65
2EHA	1:1:1	9B		80
	1:1:0.5	10B		77
	1:1:0.25	11B		71
	1:1:0.125	12B		60

7.2.4 Test for friction

The lubricity study, analysis of scar and study of physiochemical parameter of diesel fuel are detailed in chapter 3 (3.2.4).

7.3 RESULTS AND DISCUSSION

7.3.1 Measurement and analysis of wear scar

The lubricity of mixtures was analysed through HFRR method at 60°C. ULSD blends exhibited WSD values lower than the accepted value of 460 μm . The WSD values of neat ULSD and blended ULSD are given in Table 7.9 to Table 7.15.

CHAPTER 7

Table 7.9: Lubricity data of MAGL2EHARNH₂ at dosage level of 150 ppm.

Sample ID	Wear scar diameter (µm)		
	Ball, X	Ball, Y	WSD, (X+Y)/2
Neat ULSD	539	513	526
19E	396	343	371
20E	381	348	365
21E	400	368	384
22E	429	339	382

Table 7.10: Lubricity data of MAGL2EHADEA at dosage level of 150 ppm

Sample ID	Wear scar diameter (µm)		
	Ball, X	Ball, Y	WSD, (X+Y)/2
Neat ULSD	539	513	526
26E	455	423	439
27E	434	325	380
28E	391	379	385

Table 7.11: Lubricity data of MAEGL2EHA RNH₂ at dosage level of 150 ppm

Sample ID	Wear scar (µm)		
	Ball, X	Ball, Y	WSD, (X+Y)/2
Neat ULSD	539	513	526
43E	418	378	398
44E	433	335	384
45E	462	376	419
46E	487	424	456

Table 7.12: Lubricity data of MAGLOA at dosage level of 150 ppm

Sample ID	Wear scar (µm)		
	Ball, X	Ball, Y	WSD, (X+Y)/2
Neat ULSD	539	513	526
OA1	413	365	389
OA2	415	374	395

CHAPTER 7

Table 7.13: Lubricity data of MAGLOLA RNH₂ at dosage level of 150 ppm

Sample ID	Wear scar (µm)		
	Ball, X	Ball, Y	WSD, (X+Y)/2
Neat ULSD	539	513	526
OL1	460	350	405
OL2	462	376	419

Table 7.14: Lubricity data of MAEGL2EHADEA at dosage level of 150 ppm

MA	Glycerol	2EHA	DEA	Solvent /catalyst	HFRR 60°C		
					X	Y	(X+Y)/2WSD
1	1	1	1	THF/P TSA	413	362	388
0.5	0.5	1	1		381	348	365
0.5	0.5	2	1		425	333	379
1	1	-	1		521	491	506
2	1	-	2		520	470	495

Table 7.15: Lubricity data of MAGLOLA at different ratio

MA	Glycerol	OLA	Solvent/catalyst	Con. ppm	HFRR 60°C		
					X	Y	(X+Y)/2WSD
1	1	1	THF/PTSA	150	433	333	383
1	1	0.5			422	366	394
1	1	0.4			444	363	404
1	1	0.25			439	408	424
1	1	0.125			537	499	518
1	1	1		100	441	374	408
1	1	0.5			456	407	429
1	1	0.4			479	427	453
1	1	0.25			507	473	490
1	1	1		80	464	439	452
1	1	0.5			478	462	470
1	1	0.4			510	454	482
1	1	0.25			504	499	502

CHAPTER 7

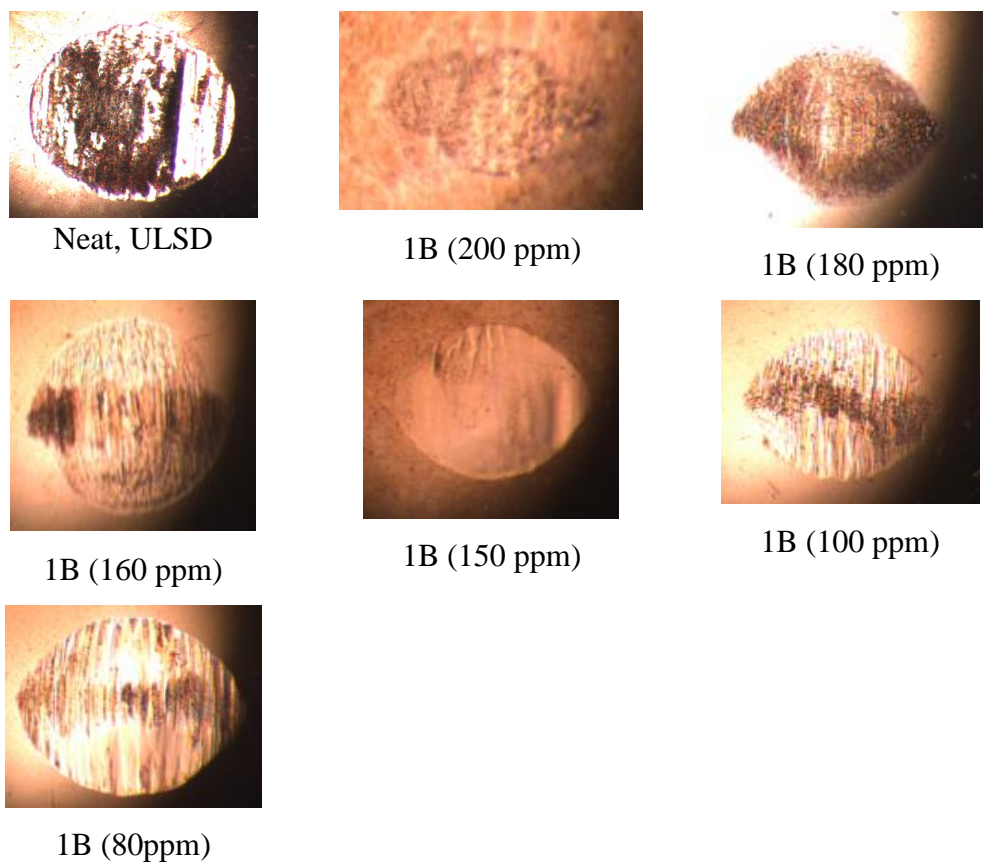
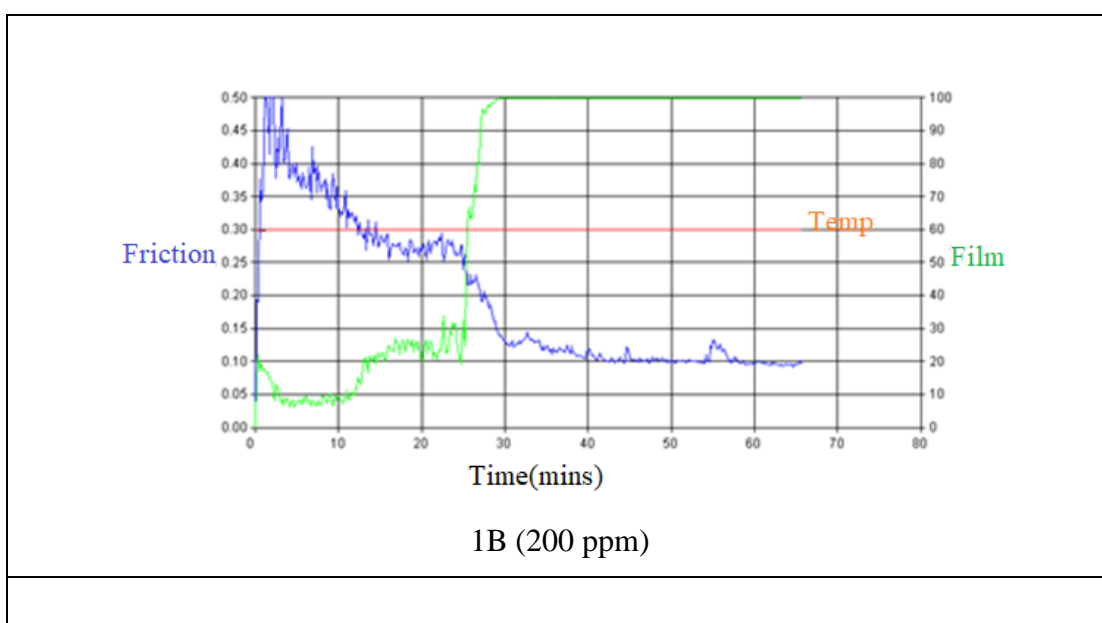
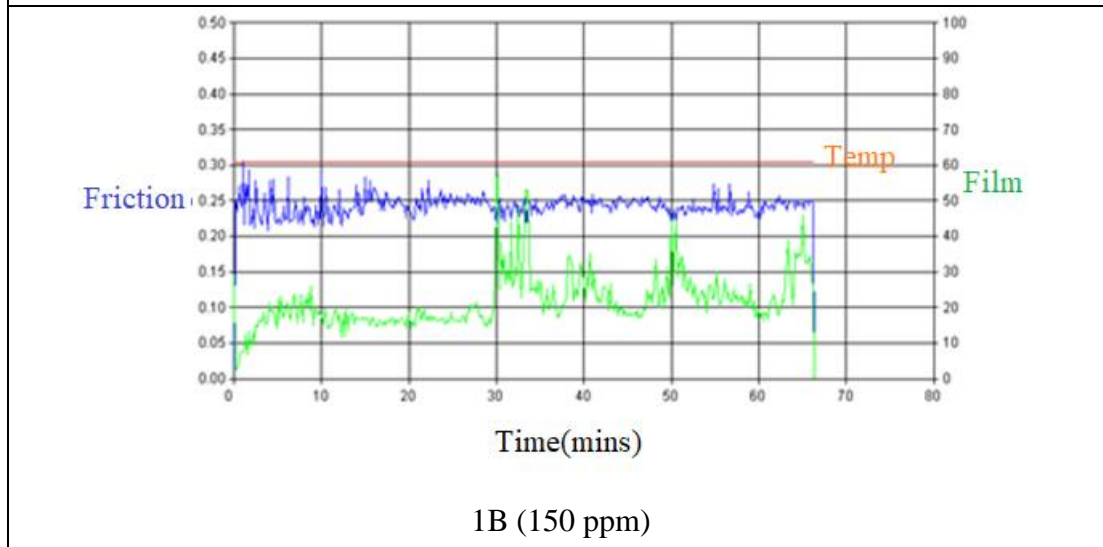
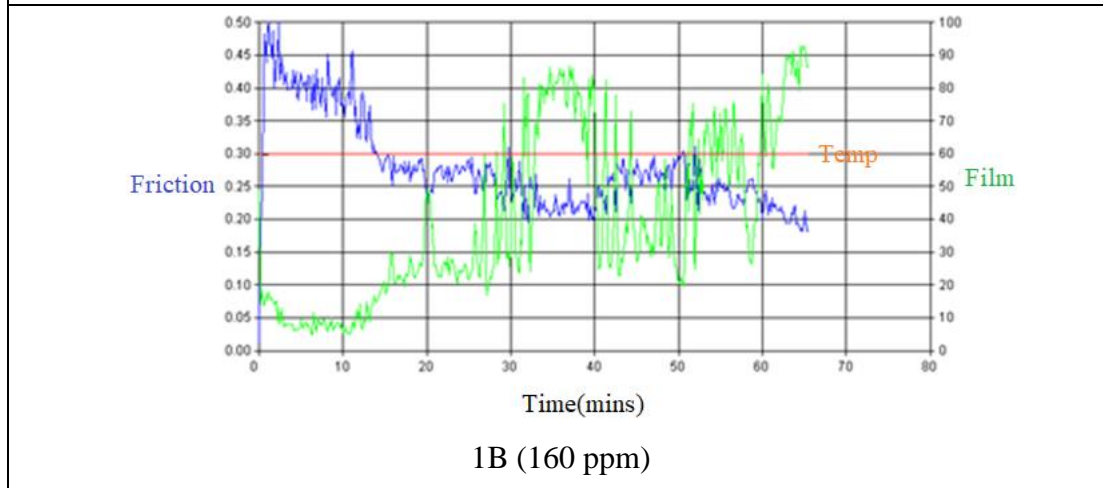
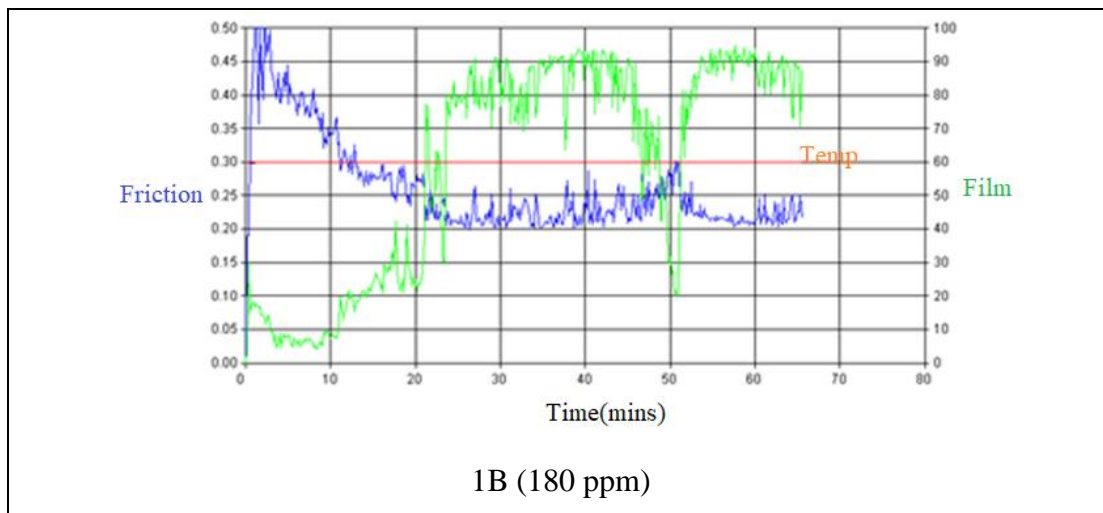


Fig.7.1 The optical microscopic images of wear and scar for samples neat ULSD and blended MAGLOLA (1B)



CHAPTER 7



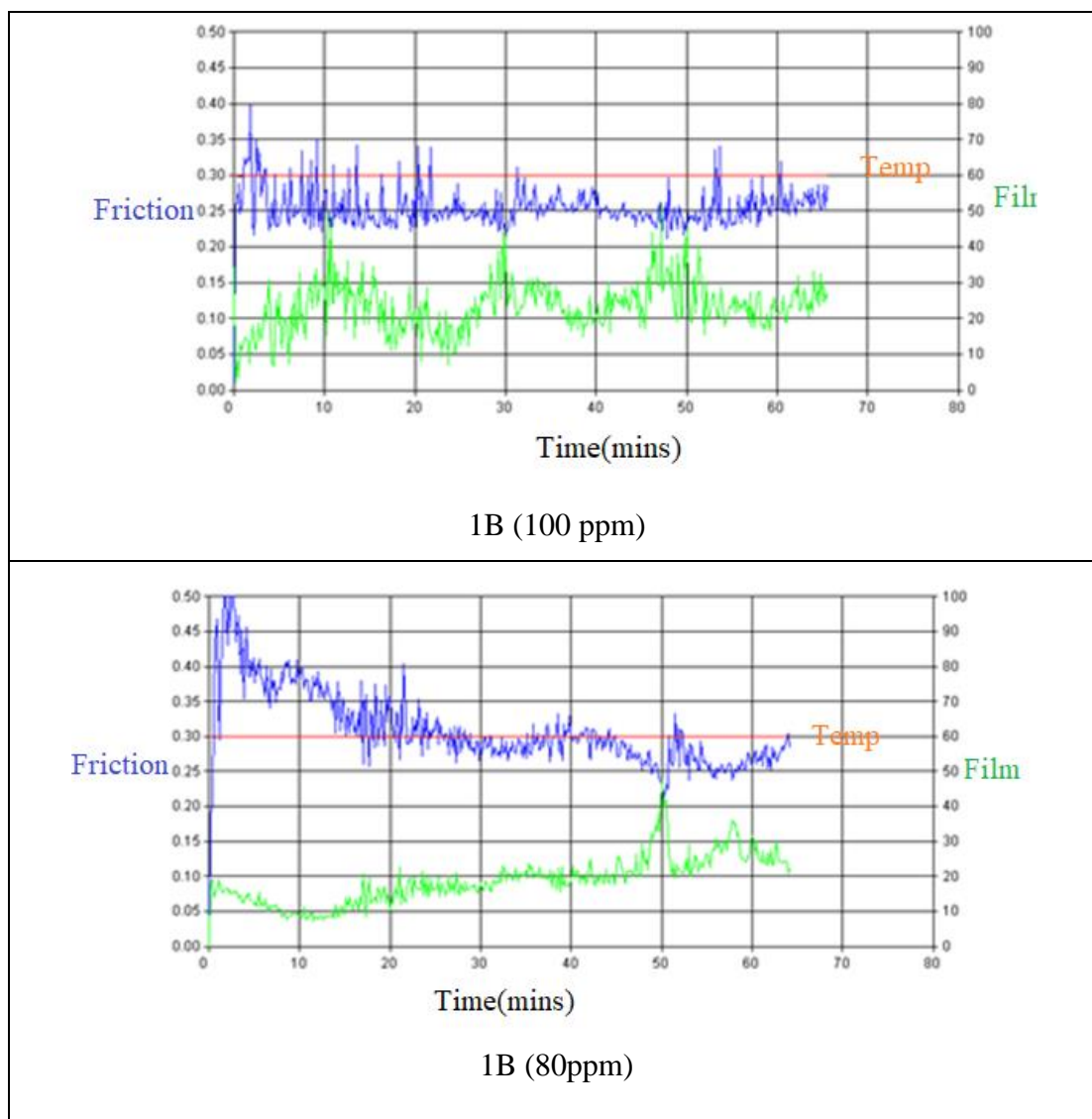


Fig.7.2 Friction coefficient and film % data obtained from HFRR and the optical microscopic images of wear and scar for ULSD blends(1B).

7.4. PHYSIOCHEMICAL PARAMETERS INVESTIGATION

7.4.1 Impact of new lubricity enhancers on the characteristics of diesel fuel

The different key parameters of the ester-ULSD blend fuels were studied to confirm the effect it's diesel fuel properties. The results of the studies are tabulated in Table 7.16. There is no negative effect observed on diesel fuel parameters when it is blended with the MAGLOLA (1B) lubricity improvers. The blended ULSD meets the Euro 6/BS6 fuel specifications.

CHAPTER 7

Table 7.16: The test report summary of blended MAGLOLA (1B) ULSD

Parameter	Test method	Specification	Result	
			Blend Fuel (100ppm)	Blend Fuel (150 ppm)
Acidity, Total, mg of KOH/g, <i>Max</i> *	ASTM D 974	0.2	0.034	0.034
Cetane Index, <i>Min</i> *	IP 380	46	56.0	56.1
Pour point, °C, <i>Max</i> *	ASTM D 5950	3 for winter 15 for summer	-30	-30
Copper strip corrosion test 3 h at 50°C	ASTM D 130	Not worse than No.1	No.1	No.1
Distillation, 95% recovery, v/v, recovery, °C, <i>Max</i> *	ASTM D 86	360	343.6	343.6
Flash point, °C, <i>Min</i> *	IP 170	35	>100	>100
Kinematic viscosity, cSt at 40°C	ASTM D 445	2.0-4.5	3.058	3.059
Density @ 15°C, kg/m ³	ASTM D 4052	810-845	839.8	839.9
Total Sulphur, mg/Kg, <i>Max</i> *	ASTM D 5453	10	3.1	3.1
Lubricity, WSD at 60°C, microns, <i>Max</i> *	ASTM D 6079-18	460	408	383
Oxidation stability, g/m ³ , <i>Max</i> *	ASTM D 2274	25	9.5	9.6
Cold Filter Plugging Point (CFPP), °C	ASTM D 6371	6 for winter 18 for summer	-16	16

7.5 MECHANISM OF LUBRICITY ACTION

The mechanism of lubricity action of lubricity enhancer on the metal surface was studied by examining the worn surfaces of friction couples using SEM and EDS techniques.

7.5.1 Study of wear scar using SEM

The SEM images of the wear scars on balls of the friction couples are shown in (Fig.7.3). It is evident from the SEM images that for neat ULSD, the scratch marks on metal surface are thick and the WSD of the worn surface on the ball is comparatively higher than that of the ULSD-1B blend (100 ppm). The presence of polar components such as hydroxy and ester groups in the lubricity improving agent accelerates the easy adsorption on the surface of the metal to form a defending thin layer between the metal surfaces, which protects the metal surfaces from wear and tear.

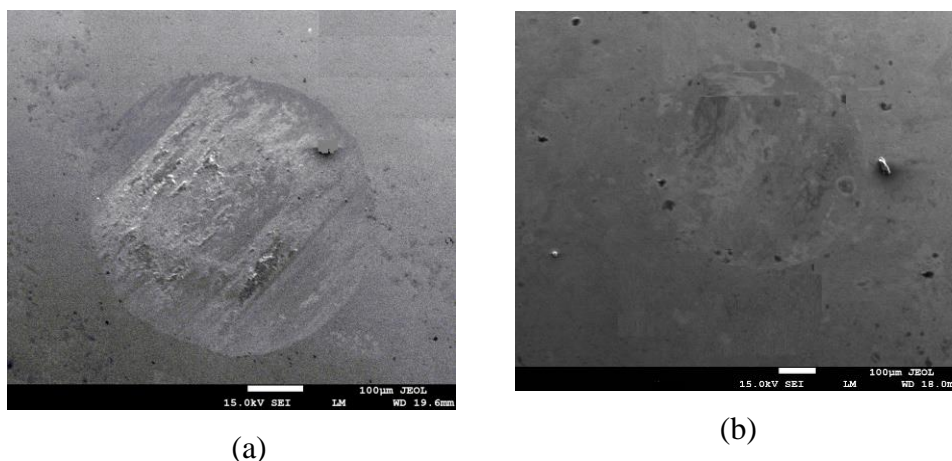


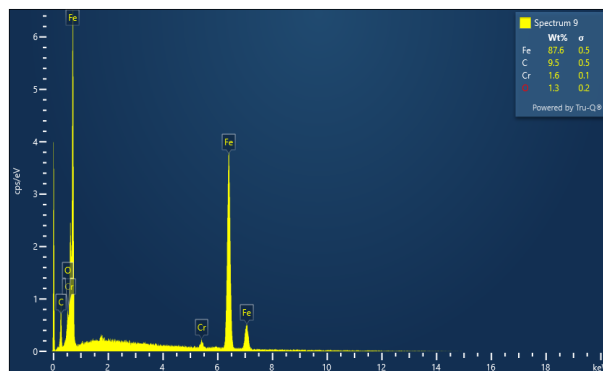
Fig.7.3 SEM images of the wear scars on balls of the friction couples with a) neat ULSD and b) ULSD- 1B (100ppm) blend

7.5.2 Study of wear scar through EDS

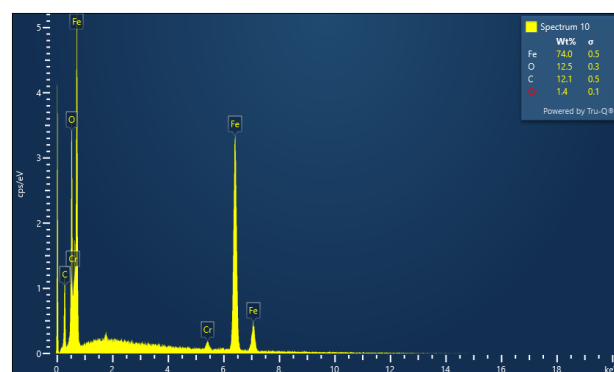
The interaction of additive on metal surfaces during the friction process was studied using EDS technique. Mainly three elements were detected on the metal surface, carbon from the diesel, oxygen from the lubricity improving agent and air, and Fe from the friction matrix. The EDS graphs are shown in Fig.7.4. The EDS spectra indicates a higher oxygen content on the metal surfaces lubricated by the blend fuel (ULSD-1B) as compared with that on the surfaces lubricated by the neat ULSD which confirms the lubrication action of the lubricity enhancer. The oxygen content on the metal surface increases from 1.3 (neat ULSD) to 12.5 % (blended ULSD (1B)), which

CHAPTER 7

further supports the interaction of the metal surface with the esters through oxygen containing functional groups.



(a)



(b)

Fig.7.4 EDS graphs of the worn surfaces with a) neat ULSD b) blended ULSD (1B150 ppm).

7.6 CONCLUSIONS

A series of cost-effective lubricity improver were successfully synthesized from naturally abundant substances following simple reaction protocols. There are no stains and precipitates detected during the oxidation stability study, which reveals that lubricity additives possess long storage stability. Also, there is no change in the diesel fuel properties upon blending with the additives and the ULSD blends fulfil the requirements of Euro VI/BS VI fuel specifications. Most of the synthesized additives enhance the lubricity of ULSD at very low blending concentrations (80-150 ppm). Hence, this method developed in the present study for the synthesis of low-cost LIs using naturally abundant substances could be a budget friendly protocol for the industries to manufacture efficient additives for ULSD.

CHAPTER 8

SUMMARY AND CONCLUSIONS

Abstract:

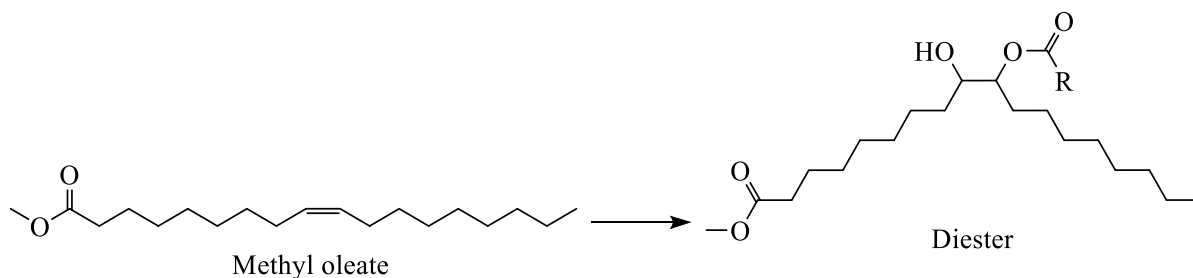
This chapter contains summary and important conclusions of the present research work. It also includes a brief account on the scope for further work.

8.1 SUMMARY

The public health problems linked to toxic diesel engine emissions accelerated efforts to create effective strategies for lowering such emissions. Consequently, it was thought of adopting stringent fuel standards for diesel, particularly to reduce sulphur and aromatics content allowed in the fuel. ULSD is a non-polluting fuel in which allowed sulphur content is 10 ppm. The direct usage of ULSD in motor vehicles causes several unwanted side effects on fuel injection part of engine. Loss of lubricity which damages the fuel injection pump of the engine is the major problem associated with ULSD. Adding a lubricity agent helps to decrease friction between the fuel injection system of engine thus minimizing the impact of these moving parts, thereby saving the engine components from wear and tear.

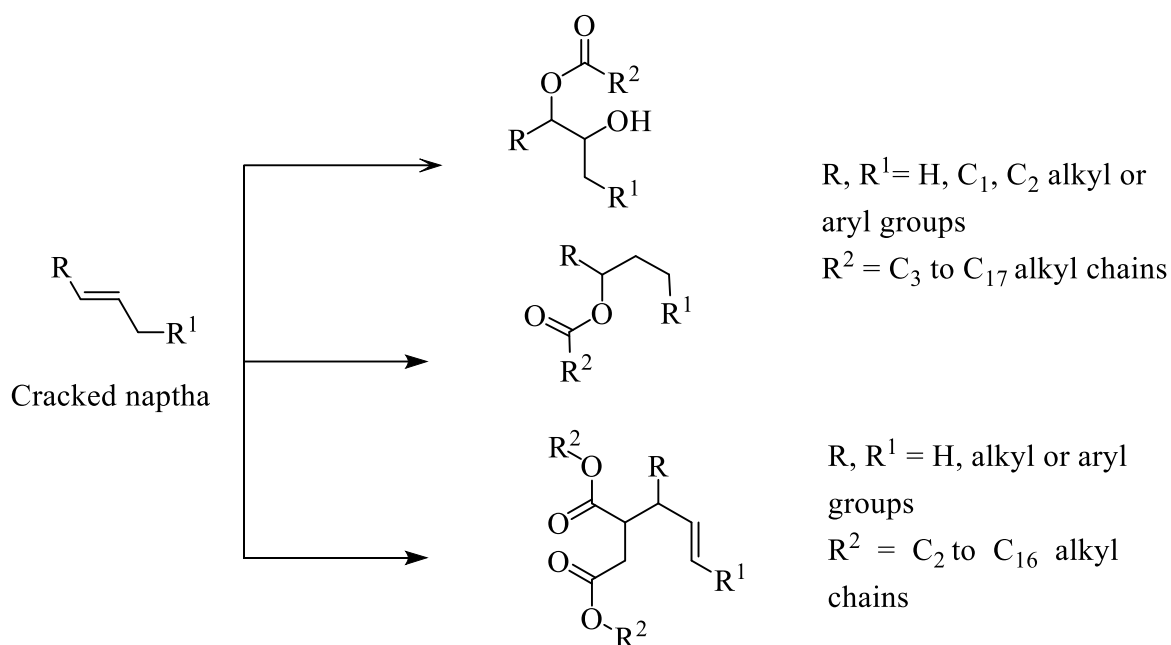
Based on a detailed literature survey, six new series of lubricity enhancers were synthesized. New additives from methyl oleate (**Series 1**), light cracked naphtha (**Series 2-4**), glycidyl methacrylate, methacrylic acid and fatty acid (**Series 5**) and maleic anhydride (**Series 6**) were synthesized successfully following simple reaction protocols. The tribological study was carried out for all the molecule using HFRR. The wear scar diameter was measured through optical microscope. Further, physical and chemical parameters of blended fuel were checked to confirm the effect of lubricity additive on diesel fuel properties. The mechanism of lubricity actions of newly synthesised materials on metal surface were studied through SEM and EDS techniques. The summary of the reaction schemes and the general structure of all the LIs synthesized in the present study is given below.

CHAPTER 8



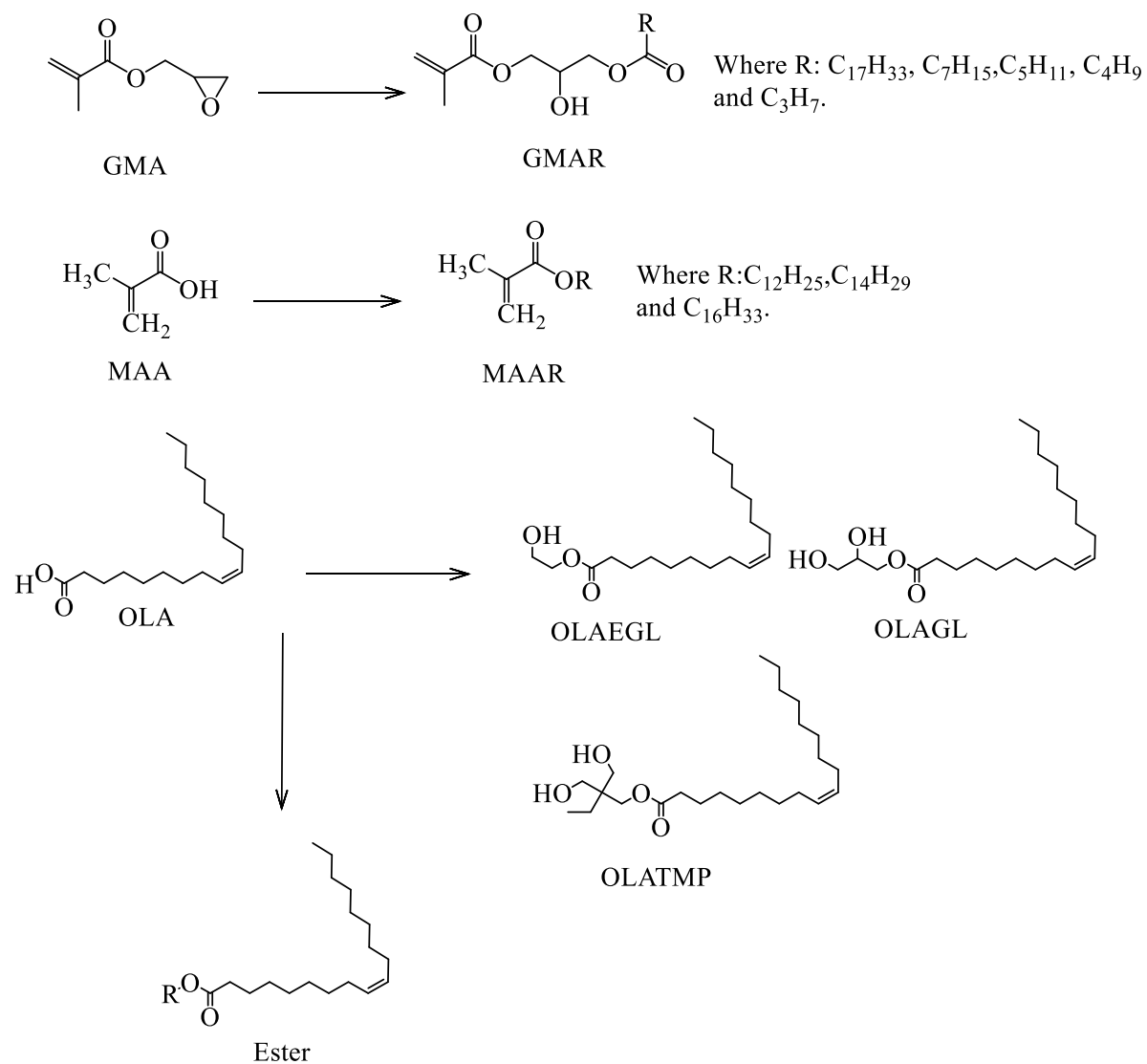
Where, R = C₁₇H₃₃, C₁₇H₃₅, C₁₅H₃₁, C₁₃H₂₇, C₁₁H₂₃, C₉H₁₉,
C₇H₁₅, C₇H₁₅, C₅H₁₁, C₄H₉ and C₃H₇

Series 1 (11 compounds)

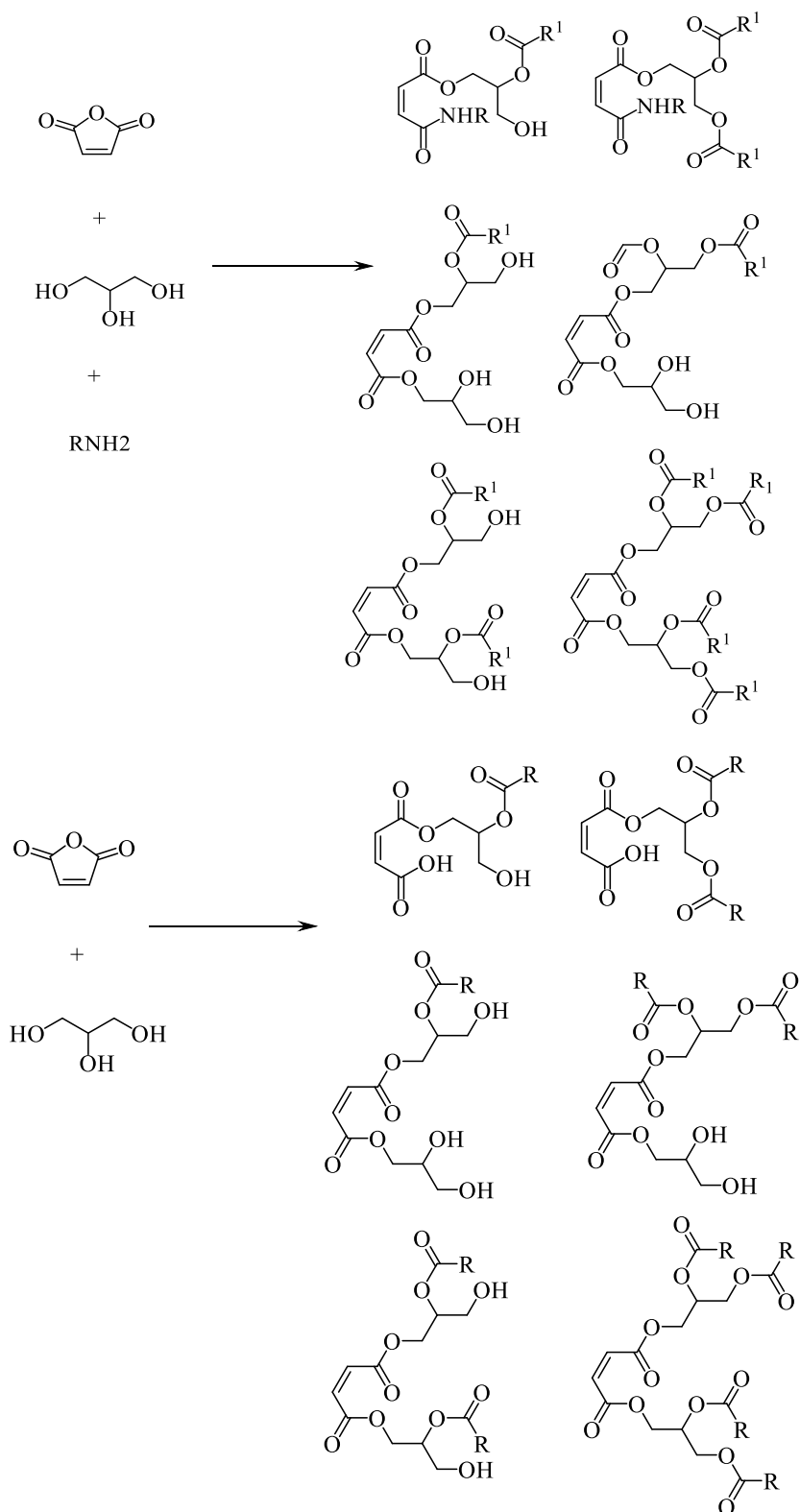


Series 2-4 (28 compounds)

CHAPTER 8



Series 5 (14 compounds)



Series 6 (101 compounds)

Fig.8.1 The summary of the reaction schemes and the general structure of all the LIs synthesized in the present study.

CHAPTER 8

8.1.1 The summary of best lubricity value obtained in each series

The summary of WSD values of LI is given in table 8.1.

Table 8.1. The comparison of WSD of LAMOSA, 10a, 6a, 15h, 21c and 1B with commercial LA

Sample ID	Blend concentration (ppm)	Wear scar diameter (μm)		
		Ball X	Ball Y	Average
LAMOSA	200	460	440	450
LCN ester (10a)	150	485	355	420
LCN hydroxy ester (6a)	150	425	396	411
LCN diester(15h)	150	445	368	407
OLA/Polyol (21c)	100	380	512	446
MAGLOLA (1:1:1) 1B	80	464	439	452
Commercial lubricity additives	150	454	445	450

8.2 CONCLUSIONS

On the basis of experimental results, following significant conclusions have been drawn from present research work.

1. Based on detailed literature survey, six new series of lubricity improver synthesised through simple reaction schemes using easily available cost-effective chemicals.
2. More than 100 new compounds were synthesized and their synthetic protocols were optimized to get a good yield of the products. The chemical structures of the additives were established by spectral techniques.
3. The new additives were synthesized using low-cost raw materials such as methyl-oleate, cracked naphtha, glycidyl methacrylate, methacrylic acid, fatty acid derivatives and maleic anhydride and hence are promising candidates for developing low-cost additive for commercialization.

CHAPTER 8

4. From their lubricity studies, it is clear that most of the esters effectively improve the lubricity of ultra-low sulphur diesel at low blending concentrations, which is an important parameter for the low-cost additives. The esters derived from oleic acid and stearic acid showed the best lubrication enhancing property at low (below 200 ppm) dosage level
5. From their physicochemical studies, it is evident that, the synthesised ester has no negative influence on key fuel properties of the diesel and the blend fuel meets the BS VI fuel specifications.
6. From their oxidation stability studies, it is concluded that, all the esters have long term anti-wear stability when blended with the diesel fuel
7. The studies on mechanism of lubricity action using SEM/EDS techniques reveal that the adsorption of lubricity improver through the oxygen atom of the polar functional groups on the surface of friction couples contributes to the formation of lubricant protective film which improves the lubricity of the blend fuel.

Conclusively, in the present work more than 100 new lubricity improvers were designed, synthesized and characterized. The synthetic methodology followed in the present study are very simple and could benefit the petroleum refineries to develop low-cost additives using the refinery raw material as well as abundantly available cost-effective materials.

8.3 SCOPE FOR FUTURE WORK

As concluded, additive derived from long chain carboxylic acid with multiple oxygen moiety shows good lubricating properties with ULSD. Hence in future, the seed oil with long fatty acid groups can be used for esterification reaction instead of pure acids as a budget friendly option.

The present study demonstrates for the first time, useage of LCN (raw material of refinery) based additives as lubricity enhancers for ULSD. Their lubricating property is highly encouraging. So, in future other cost-effective lubricity enhancer could be synthesized by employing the by-products of the petroleum refinery as raw materials which also economically benefit large scale production in petroleum refineries.

References

Abdulkadir, T., and Khalid, A. (2019). “Advanced hydrodesulfurization catalysts: A review of design and synthesis.” *Energy Fuels* ,33,2810–2838.

Anastopoulos ,G., Lois, E., Karonis, D., Zankos, F., and Kalligeros, S.(2001). “A Preliminary evaluation of esters of monocarboxylic fatty acid on the lubrication properties of diesel fuel.” *Industrial and Engineering Chemistry Research* ,40, 452-456.

Arukali, S., Korlipara V. P., Shiva, S. K., and Rachapudi, B. N. P. (2015). “Multifunctional lubricant additives derived from natural amino acids and methyl oleate.” *RSC Advances*, 5,77538-77544.

ASTM D 975-06. Standard specification for diesel fuel oils.

ASTM Standards, Designation: D6079 – 18. Standard test method for evaluating lubricity of diesel fuels by HFRR. DOI: 10.1520/D6079-18.

ASTM D6079-11. Standard test method for evaluating lubricity of diesel fuels by HFRR. West Conshohocken, PA: ASTM International,2011.

Bryan, R.M., Steven, C.C., and Terry, A.I. (2008). “Evaluation of castor and lesquerella oil derivatives as additives in biodiesel and ultralow sulphur diesel fuels.” *Energy and Fuels*, 22, 1349–1352.

Bryan, R.M., Aaron, W., Michael, J.H., and Robert, L.M. (2009). “Exhaust emissions and fuel properties of partially hydrogenated soybean oil methyl esters blended with ultra-low sulphur diesel fuel.” *Fuel Processing Technology*, 90,1122–1128

Bryan, R.M. (2014).” Preparation and evaluation of multifunctional branched diesters as fuel property enhancers for biodiesel and petroleum diesel fuels.” *Fuels* ,2,3262–3270.

Bryan, R.M., Roque, L.E., and Terry, A.I. (2016).” Preparation and fuel properties of field pennycress (*Thlaspiarvense*) seed oil ethyl esters and blends with ULSD fuel.” *Energy Fuels*,30(1), 473-479.

CEC F-06-A, The guideline for HFRR testing - Diesel fuel lubricity plates and balls specimens.

References

- Daniel, P.G., and John, W.G. (2004). "Effects of specific fatty acid methyl esters on diesel fuel lubricity." *Fuel*, 83,2351-2356.
- Danping, W., and Spikes, H.A. (1986). "The Lubricity of diesel fuels." *Wear*,1, 217-235.
- David, Claydon. (2014). "The use of lubricity additives to maintain fuel quality in low sulphur diesel fuel." *Gorivaimaziva*, 53(4),342-353.
- De-Xing, P. (2015). "The effect on diesel injector wear, and exhaust emissions by using ultralow sulphur diesel blending with biofuels." *Materials Transactions*,56, 642-647.
- Diesel fuel-assessment of lubricity using high frequency reciprocating rig.(HFRR) ISO12156
- EN 590, European diesel fuel specification
- Gerhard, K., and Kevin, R.S. (2005). "Lubricity of components of biodiesel and petrodiesel, the origin of biodiesel lubricity." *Energy and Fuels*,19,1192-1200.
- George, K., Stamoulis, S., and Evangelos B. (2009). "Effects of diesel/biodiesel blends on regulated and unregulated pollutants from a passenger vehicle operated over the European and the Athens driving cycles." *Atmospheric Environment*, 43 ,1745–1752.
- Haseeb, A.S.M.A., Sia, S.Y., Fazal, M.A., and Masjuki, H. H. (2010). "Effect of temperature on tribological properties of palm biodiesel." *Energy* ,35,1460-1464.
- Hazrat, M.A., Rasul, M.G., and Khan, M.M.K. (2015). "Lubricity Improvement of the ultra-low sulphur diesel fuel with the biodiesel." *Energy Procedia*, 75,111 – 117.
- Hazrat, M. A., Rasul, M. G., Mofijur, M., Khan, M. M. K., Djavanroodi,F., Azad, A. K., Bhuiya, M. M. K.,and Silitonga, A.S. (2020). "A Mini Review on the Cold Flow Properties of Biodiesel and its Blends." *Frontiers in Energy Research*,8,598651.
- Homa, H.B., Meisam, T., Mortaza, A., Majid, K., and Ayhan, D. (2018). "A comprehensive review on the environmental impacts of diesel/biodiesel additives." *Energy Conversion and Management*,174,579–614.

References

Hu, J., Du, Z., Li, C., and Min, E. (2005). "Study on the lubrication properties of biodiesel as fuel lubricity enhancers." *Fuel*, 84,1601-1606.

ISO 12156, Diesel fuel assessment of lubricity using the high-frequency reciprocating rig (HFRR).

IS1460, Automotive diesel fuel specification of India.

IP 450, Diesel fuel assessment of lubricity using the high-frequency reciprocating rig (HFRR).

Jack, Burgazli. (2007). ULSD-additive requirements and interaction. Proceedings of the International conference on stability, handling and use of liquid Fuels, 10th, Tucson, AZ, United States.

James, A.K., Gerhard, K., Robert, O.D., Thomas, W.R., and Andrew, M. (2005). "Physical Properties of Oleochemical Carbonates." *JAOCs*,201-205.

Jumat, S., Nadia, S., and Emad, Y. (2012). "Improvement of pour point and oxidative stability of synthetic ester base stocks for bio lubricant applications." *Arabian Journal of Chemistry*,5,193-200.

John, K., Naomi, K.F., Britt, A., and Holmen. (2019). "Fuel composition effects on carbonyls and quinones in particulate matter from a light-duty diesel engine running biodiesel blends from two feedstocks." *Energy Fuels*, 33,1133–1145.

Jose, L.G.G., Irene, P.L., Fidencio, H, P., Georgina CL., and Federico J.C. (2012). "R&D in Oxidative desulfurization of fuels technologies: from chemistry to patents." *Bentham Science publisher* 5(3),174-196.

JPI-5S-50, Standard testing method for petroleum products by Japan.

Kapila, W., Mahbuba, A., Steven, O.S., and Simon, Ng, K.Y. (2009). "Investigation of lubricity characteristics of biodiesel in petroleum and synthetic fuel." *Energy and Fuels*, 23, 2229–2234.

Keneseý, E., and Ecker, A. (2003). "Additives for improvement of lubricity in fuels." *Tribologic Schmierungstechnik*,50(2),21–26.

References

- Kenneth M. D., Brajendra K. S., and Sevim Z. E. (2007). "Synthesis of Branched Methyl Hydroxy Stearates Including an Ester from Bio-Based Levulinic Acid." *Industrial and Engineering Chemistry Research*, 46, 3513-3519.
- Kim, Y.J., Lee, Shin-ho., Kim, Y.W., and Chung, K. (2012). "Succinic acid alkyl half-ester derivatives with improved lubricity characteristics." *Abstracts of Papers, 243rd ACS National Meeting and Exposition, San Diego, CA, United States, IEC-192.*
- Knothe, G., and Razon, L. F. (2017). "Biodiesel fuels." *Progress in Energy and Combustion Science*, 58,36–59.
- Krishnarao, L., Meeta ,S., Maya, C., Ajay, K.A., Vivekanand ,K., and Sanjiv, K.M.(2019). "Ash catalyzed synthesis of long-chain dialkyl carbonates through carbonyl exchange reaction." *Catalysis letter*,1163-1175.
- Li, Jin., Chen, Guoxu., Hu, Zexiang., Zhao, Litao., and Cheng, Peng. (2015). "Research on naphthenic acids as anti-wear additive of super low sulphur diesel fuel." *Shiyou Huagong Yingyong*,83-86,99.
- Liu ,Z., Li, Jing., Gerhard, K., Brajendra, K.S., and Jiangchung, J.(2019). "Improvement of diesel lubricity by chemically modified tung-oil based fatty acid esters as additives." *Energy Fuels*,33,5110–5115.
- Madhu Sudan, R. D., and Nanthagopal, K. (2019). "Tribological aspects of biofuels – A review." *Fuel*, ,258,116066.
- Matzke, M., Jess, A., and Litzow, U. (2015). "Polar nitrogen-containing aromatic compounds as carriers of natural diesel lubricity." *Fuel*,140, 770–777.
- Michel, Roegiers., and Boris, Zhmud. (2009). "Tribological performance of ionised vegetable oils as lubricity and fatty oiliness additives in lubricants and fuels." *Lubrication Science*, 21, 169–182.
- Momin, M., and Deka, D. C. (2015). "Performance of yellow oleander methyl ester (YOME) as lubricity additive in high speed diesel fuel." *Energy Education Science and Technology, Part C: Future Energy Sources*,7,221-230.

References

Rashad, J., and Arno, de., Klerk. (2012). “Desulfurization of heavy oil.” *Applied Petrochemical Research*,1,3–19.

Rao, T.V.V.L.N., Ahmad, M.A.R., Mokhtar, A., Masri, B., and Yoshimitsu, U. (2018). “An overview of research on bio lubricants in Malaysia and Japan for tribological applications.” *Journal Tribology* ,18, 40-57.

Salete, M.A., Aline, Cristina, M.F., Valdicleide, S.M., Jose, j.O.J. (2018). “Effect of soybean biodiesel addition on tribological performance of ULSD.” *Journal of Tribology*,141-148.

Seung-Yeob, B., Young-Wun, "K., Keunwoo, Chung., Seung-Hyun, Y., Nam, K.K., and Yeong-Joon, K. (2012). “Synthesis of succinic acid alkyl half-ester derivatives with improved lubricity characteristics.” *Industrial and Engineering Chemistry Research*,51, 3564–3568.

Shen, B., Lin, B., and Zhao, J. (2009). “Study on the components of biodiesel fuel as additive to improve the lubrication performance of ultra -low sulphur diesel fuel.” *Shiyou Lianzhi Yu Huagong* ,40,39-42.

Srivastava, S.P., and Jenoo, Hancsok. (2014). “Fuels and Fuel-Additives.” *John Wiley and Sons, Inc.*

Specification for automotive diesel fuel (BS IV) (IS 1460 – 2005 with Amendment 2 March 2010).

Standard test method for evaluating lubricity of diesel fuels by the Scuffing load ball-on-cylinder lubricity evaluator (SLBOCLE). Designation: D6078 – 04 (Reapproved 2016).

Sulek, M. W., Kulczycki, A., and Malysa, A. (2010). “Assessment of lubricity of compositions of fuel oil with biocomponents derived from rape-seed.” *Wear*,268, 104–108.

Sunmin, W., Jianheng, S.,and Martin, J.T.R.(2012). “Lubricity enhancing low-temperature diesel fuel additives.” *Journal of American Oil Chemists Society*, 89,513-522.

References

Shana P. B., Richard P.W. (2002). "Synthesis and characterization of monomers and polymers for adhesives from methyl oleate." *Journal of Polymer Science: Part A: Polymer Chemistry*, 40, 451-458.

Shilpi, A., Vijay, K. C., and Ajay, K. B. (2013). "Tribological behaviour of diesel fuels and the effect of anti-wear additives." *Fuel*, 106,21-29.

Titipong, I., Dalai, A. K., and Desai, P. (2010). "Evaluating esters derived from mustard oil as potential diesel additives." *Journal of the American Chemical Society*,88,391–402.

Topaiboul, S., and Chollacoop, N. (2010). "Biodiesel as a lubricity additive for Ultra low sulfur diesel." *Songklanakarinn Journal of Science and Technology*,32,153-156.

Zhen, Hu., Li, Zhang., and Yuba, Li. (2017). "Investigation of tall oil fatty acid as antiwear agent to improve the lubricity of ultra-low Sulphur diesels." *Tribology International*, 114 ,57–64.

Zhang, Y., Zeng, X., Wu, H., Li, Z., Ren, T., and Zhao, Y. (2014). "The tribological chemistry of a novel borate ester additive and its interaction with ZDDP using XANES and XPS." *Tribology Letters*, 53,533-542.

Zinina, N.D., Timashova, A.L., Pavlovskaya, M. V., and Grishin, D.F. (2014). "An antiwear additive for ultra-low-sulphur diesel fuel." *Petroleum chemistry*, 54,392-39

LIST OF PUBLICATIONS

Paper published in international journals

Sruthi H, Udaya Kumar D, Pramod Hegde, Manjunatha M.G, Nandakumar V (2022). “A simple method for the conversion of light cracked naphtha into efficient lubricity improvers for ULSD”. *ACS Omega*.7, 27969-27979.

Sruthi H, Udaya Kumar D, Pramod Hegde, Manjunatha M.G, Karthick. R, Nandakumar V (2022). “Transformation of Refinery Cracked Naphtha Stream into Efficient Lubricity Improvers for ULSD”. *Journal of Chemical Sciences*.134 (110), 1-11.

Sruthi H, Udaya Kumar D, Pramod Hegde, Manjunatha M.G, Nandakumar V (2022). “Efficient Lubricity Improvers Derived from Simple Methyl Oleate for Ultra Low Sulphur Diesel (ULSD).” *Petroleum Chemistry*. 62, 1126–1136.

Sruthi H, Udaya Kumar D, Pramod Hegde, Manjunatha M.G (2022). “Fatty acid, fatty alcohol and acrylate derivatives as friction depressive additives for ultra-low sulphur diesel” *Materials today conference proceedings (ICRAMM 2022)*. Published on March 2023. <https://doi.org/10.1016/j.matpr.2023.03.412>.

Sruthi H, Udaya Kumar D, Pramod Hegde, Manjunatha M.G, Karthick. R (2022). “Conversion of Refinery Light Cracked Naphtha Stream into Friction Depressive Additives for Ultra-Low Sulphur Diesel through a Two-Step Process.” *Manuscript ready for Communication*.

Sruthi H, Udaya Kumar D, Pramod Hegde, Manjunatha M.G (2022). “An overview on recent developments in lubricity improvers of ultra-low sulphur diesel (ULSD).” *Manuscript under preparation*.

Patent

Hegde Pramod Kumar, Bhat Manjunatha Megur Ganesh, Ramalingam Karthick, Nandakumar Velayudhan Pillai, Huligujje Sruthi, Dalimba Udayakumar (2021). An additive composition and a process for its preparation. Final specification filed at Indian Patent Office, Application No. 202141058744

PAPERS PRESENTED IN CONFERENCE

Sruthi H, Udaya Kumar D, “Synthesis of Cost-Effective Lubricity Improvers for Ultra Low Sulphur Diesel (ULSD)” International Virtual Conference on “Creative Research in Chemical Science and Allied Applications (CRCSA-2020)” P.G Department of Chemistry, SDM College (Autonomous), Ujire, August, 18 – 19, 2020

Sruthi H, Udaya Kumar D, “Design and Development of New Lubricity Additives for Ultra Low Sulphur Diesel (ULSD)” 3rd International Oil and Gas Chemistry, Chemicals and Additives virtual Conference (IOGCA 2020)”, September,24- 26, 2020.

Sruthi H, Udaya Kumar D, “Synthesis of New Cost-Effective Lubricity Improvers for ULSD from Glycerol” 1st International Conference on Advances in Materials Science (ICAMS 2021)”, Reva university Bengaluru, September,22- 24 ,2021.

Sruthi H, Udaya Kumar D, “Synthesis of Efficient Lubricity Improvers for Ultra Low Sulphur Diesel” Sixth International Conference on Recent Advancements in Chemical Environment & Energy Engineering (RACEEE 2022)”, SSN college of engineering, Chennai, February,24- 25 ,2022.

Sruthi H, Udaya Kumar D, Pramod Hegde, Manjunatha M.G “Fatty acid, fatty alcohol and acrylate derivatives as friction depressive additives for ultra-low sulphur diesel” Fourth International Conference on Recent Advances in Materials and Manufacturing (ICRAMM 2022)”, Velalar college of engineering and technology, Erode, Tamil Nadu, December,08- 09 ,2022.

BIO DATA

BIO-DATA

Name : **Sruthi H**
Permanent address : Aramanganam House
Kalanad post, Kasaragod
Kerala- 671317, India

Contact Details:

Email:sruthih55@gmail.com

Name of Father :Purushothama H

Name of Mother : Vimalakshi H

EDUCATION:			
COURSE	UNIVERSITY	YEAR	POSITION SECURED
Ph.D. in Chemistry	National Institute of Technology Karnataka (NITK)	2018-2022	-
Post-Graduation-M.Sc. Applied Chemistry	Mangalore University, Konaje, Mangalagangothri, Karnataka	2014-2016	First rank with gold medal
Graduation-B.Sc. Chemistry	Kannur university	2011-2014	First Class

RESEARCH PUBLICATIONS/PATENT:

Paper published in international journals :03
Paper published in conference proceedings :01
Patent filed :01

SRUTHI H